



ScuDo

Scuola di Dottorato ~ Doctoral School

WHAT YOU ARE, TAKES YOU FAR

Doctoral Dissertation
Doctoral Program in Energy Engineering (30th Cycle)

Study of the long term and short term photoinhibitory processes to improve the cyanobacteria growth in photobioreactors

By

Alessandro Cordara

Supervisor(s):

Prof. Guido Saracco

Prof. Raffaele Pirone

Doctoral Examination Committee:

Prof. Antonio Marzocchella

Prof. Giuseppe Olivieri

Politecnico di Torino
2018

Declaration

I hereby declare that, the contents and organization of this dissertation constitute my own original work and does not compromise in any way the rights of third parties, including those relating to the security of personal data.

Alessandro Cordara

2018

* This dissertation is presented in partial fulfillment of the requirements for **Ph.D. degree** in the Graduate School of Politecnico di Torino (ScuDo).

Acknowledgment

Abstract

This Ph.D. Thesis deals the study of the photoinhibition in the cyanobacterial model microorganism *Synechocystis* grown within the commercial flat panel photobioreactor (PBR) FTM 150/1000 under increasing intensities of red light, showing the effects of photodamage in response to long-term and short-term light treatments. The photoinhibition occurs when a large light intensity inhibits the activity of Photosystem II (PSII). This process was studied both in vivo and in vitro systems, with the goals to: (i) optimize the growth conditions of the model cyanobacterium *Synechocystis* sp. PCC 6803 (hereafter *Synechocystis*) in PBR; (ii) better understand the effects of treatments with increasing intensities of red light on long- (24 h) and short-terms (1 h) on the main protein complexes of the photosynthetic thylakoid membranes in *Synechocystis* with particular focus on the multi-subunit enzyme PSII, that is the main target of the photoinhibition process.

The photoinhibition under long-term treatment was investigated growing *Synechocystis* within the FMT150/1000 PBR in semicontinuous mode under red light. The following light intensities were tested: 50, 200, 300, 500, 800, 950 and 1460 $\mu\text{mol photons m}^{-2} \text{s}^{-1}$, adapting cells for 24 h at each intensity. The intensity of 50 $\mu\text{mol photons m}^{-2} \text{s}^{-1}$ was taken as control light. It was found that for *Synechocystis*, the saturating red light intensity ranged between 200-500 $\mu\text{mol photons m}^{-2} \text{s}^{-1}$, and a maximum growth rate was observed at 300 $\mu\text{mol photons m}^{-2} \text{s}^{-1}$. Symptoms of photoinhibition started to appear at 800 $\mu\text{mol photons m}^{-2} \text{s}^{-1}$ and reached an apex at 1460 $\mu\text{mol photons m}^{-2} \text{s}^{-1}$. Upon reverting the light intensity to 200 $\mu\text{mol photons m}^{-2} \text{s}^{-1}$, *Synechocystis* showed a remarkable ability to recover from the state of photoinhibition. In order to evaluate the PSII activity of *Synechocystis* during the long-term treatment, the amount of oxygen evolved by PSII and dissolved in the medium was measured. The highest PSII activity was observed in the range of light between 300 and 500 $\mu\text{mol photons m}^{-2} \text{s}^{-1}$. Increasing the light intensity to 800 $\mu\text{mol photons m}^{-2} \text{s}^{-1}$ the amount of oxygen dissolved in the medium decreased reaching its minimum value at 1460 $\mu\text{mol photons m}^{-2} \text{s}^{-1}$. When the light was reverted to 200 $\mu\text{mol photons m}^{-2} \text{s}^{-1}$, *Synechocystis* showed a considerable recover of its PSII activity. In addition, these data were used to create a model of the PBR by COMSOL 5.3® platform, in order to study the influences

of the different light distribution inside the PBR from varying the incident light furnished to the system.

The long-term photoinhibition was also studied by performing quantitative proteomic analyses and comparing the thylakoids proteome extracted from cells grown under photoinhibitory (800, 950, 1460 $\mu\text{mol m}^{-2} \text{s}^{-1}$) and control (50 $\mu\text{mol m}^{-2} \text{s}^{-1}$) light intensity. This studies revealed several potential strategies adopted by *Synechocystis* to cope with photoinhibitory growth irradiance among which : 1) a lower number of phycobilisome antenna (PBS) and an accumulation of the orange carotenoids protein (OCP) to prevent the excess of light absorption and reduce the oxidative stress from the oxygen reactive species (ROS); 2) the accumulation of the PSII repair machinery and of thylakoid-associated ribosomes to increase the turnover of the photodamaged PSII core subunits; 3) an increased cyclic electron flow (CEF) capacity around PSI to either counterbalance the reduced Linear electron flow (LEF) capacity or sustain the accumulation of supplementary ATP; 4) a differential response of PSI components to sustain cells performance in high light.

Preliminary studies of the short term photoinhibition were conducted to observe the effect of the strong light irradiation on the activity of the PSII core. Since, the high conservation of the D1 protein across the oxygenic photosynthetic organisms, this study was firstly conducted in vitro on PSII core monomers isolated from pea plants. An SDS-PAGE was performed to characterize the protein profiles of the starting thylakoids used to isolate the PSII core monomers, and to compare the protein composition of the light-treated PSII core monomers with the untreated counterparts. Further western blot analysis with specific antibodies against the D1 protein, revealed that the photodamage occurs at the level of the D1 protein, whose amount was markedly reduced in PSII core monomers treated with high light intensity while, in the photoinhibited sample, the band of the D1 protein almost disappeared and concomitantly some bands at lower weight, corresponding to D1 fragments, were clearly detected. Because of the crucial role of the D1 protein for optimal PSII activity in *Synechocystis*, the effect of the short-term photoinhibition was further studied in vivo. For this purpose, as starting material we used *Synechocystis* cells grown in the same PBR used for the long-term treatments under 50 $\mu\text{mol photons m}^{-2} \text{s}^{-1}$ of red light. The photoinhibitory treatment was conducted at 1460 $\mu\text{mol photons m}^{-2} \text{s}^{-1}$ for 1 h, either in the absence or presence of the protein synthesis inhibitor lincomycin. Pulse-amplitude modulated (PAM) fluorescence measurements were performed at intervals of ten minutes during the photoinhibitory treatment to evaluate the quantum yield of PSII photochemistry (ϕII).

Contents

Summary.....	1
1. General Introduction.....	3
1.1 Environmental effect of an increased CO ₂ in atmosphere	4
1.2 Biofuels, an approach to mitigate the global climate change.....	4
1.3 Cyanobacteria.....	5
1.3.1 <i>Synechocystis</i> sp. PCC 6803	5
1.4 Oxygenic photosynthesis, light dependent reactions.....	6
1.4.1 Linear electron flow in cyanobacteria.....	6
1.4.2 Phycobilisomes	8
1.4.3 Photosystem II	9
1.4.4 Cytochrome <i>b6f</i>	10
1.4.5 Photosystem I.....	10
1.4.6 Atp-synthase	12
1.5 Photosynthesis – irradiance response curves	12
1.6 Photoinhibition	14
1.6.1 Acceptor side photoinhibition.....	15
1.6.2 Donor side photoinhibition.....	15
1.7 Photoprotection	16
1.7.1 State transition (qT).....	16
1.7.2 OCP – dependent quenching (qz)	17

1.7.3 PSI electron cycling	17
1.8 Reactors.....	18
1.9 Liquid mixing and light/dark cycle in photobioreactor	20
1.10 References	22
Aims	35
2. Analysis of the light intensity dependence of the growth of <i>Synechocystis</i> and the light distribution in a photobioreactor energized by 636 nm light .36	
Abstract.....	37
2.1 Introduction	38
2.2 Material and Methods	40
2.2.1 Strain and preculture conditions	40
2.2.2 PBR growth conditions.....	40
2.2.3 Dry weight, cell size and count measurements	42
2.2.4 Model description.....	42
2.2.4.1 Assumptions, inlet and boundary conditions	42
2.2.4.2 Mathematical models.....	43
2.2.4.3 Fluid-dynamic equations	43
2.2.4.4 Heat transfer with radiation: light transmission equations	47
2.2.4.5 Kinetic models and calculation theory: cyanobacterial growth equations.....	49
2.3 Results and discussion	50
2.3.1 Growth rate, oxygen evolution activity and dimension of cells are regulated by light intensity	50
2.3.2 Influence of local light intensity distribution on photoinhibition of microorganism.	56
2.4 Discussion	61
2.5 Conclusions	64
2.6 Nomenclature	65
2.7 References.....	68

2.8 Supplementary information.....	78
3. Response of the thylakoid proteome of <i>Synechocystis</i> sp. PCC 6803 to photoinhibitory intensities of orange-red light.....	82
Abstract.....	83
3.1 Introduction.....	84
3.2 Material and Methods.....	86
3.2.1 Precultures.....	86
3.2.2 Cell cultures.....	87
3.2.3 Thylakoid membranes extraction.....	87
3.2.4 Gel electrophoresis.....	88
3.2.5 Protein precipitation and digestion.....	88
3.2.6 Mass spectrometry analysis.....	88
3.2.7 Protein database search and identification.....	89
3.2.8 Protein quantification.....	90
3.3 Results and discussion.....	90
3.3.1 Physiological monitoring of cellular photoinhibition.....	90
3.3.2 Functional classification of differently expressed proteins in thylakoids isolated from photoinhibited cells.....	92
3.3.3 Quantitation of the changes in the proteome of the thylakoid membrane of photoinhibited cells.....	94
3.3.3.1 Photosystem II.....	94
3.3.3.2 Photosystem I.....	100
3.3.3.3 Electron transport chain and ATP synthase.....	101
3.3.3.4 Light harvesting, photoprotection and pigments biosynthesis...	102
3.3.3.5 Ribosomes and associated proteins.....	104
3.4 Conclusions.....	106
3.5 References.....	108
3.6Supplementary.....	131
4. Short term photoinhibition.....	142

4.1 Introduction	143
4.2 Material and Methods	144
4.2.1 Isolation and photoinhibition of PSII monomer	144
4.2.2 <i>Synechocystis</i> growth condition	145
4.2.3 SDS-page and Western blot.....	145
4.2.4 Mass spectrometry analysis	145
4.2.5 PSI activity in short term photoinhibition assay by mini-PAM....	147
4.3 Result and discussion.....	148
4.3.1 Short term photoinhibition in vitro (PSII monomer)	148
4.3.2 Proteomic analysis of the PSII photoinhibited	150
4.3.3 Short term photoinhibition <i>in vivo</i> (<i>Synechocystis</i>)	152
4.4 Conclusions	156
4.6 References	157
4.7 Supporting information.....	160
5. Conclusions	161
5.1 Future plan.....	164
6. Acknowledgment.....	167

List of Figures

Fig 1.1 Representation of the linear electron flow and the mechanisms of photoprotection in Cyanobacteria.

Fig 1.2 Sideview of the structure of photosystem II and OEC complex.

Fig 1.3. PSI crystal structures.

Fig 1.4 Photosynthesis–irradiance response curve.

Fig 1.5. Different types of reactors.

Fig 2.1. Photobioreactor schematic representation.

Fig 2.2. Challenging *Synechocystis* by high light intensity revealed its adaptive capacity.

Fig 2.3. Recovery of growth of *Synechocystis* after high light treatment.

Fig 2.4. Relationship of the cell size and growth rate of *Synechocystis* set at different light intensities.

Fig 2.5. 3D trend of normalized light intensity along YZ slice of the model PBR.

Fig 2.6. 2D trend of normalized light intensity along XZ slice of the model PBR.

Fig 3.1. Growth of *Synechocystis* sp. PCC 6803 under increasing intensities of orange-red light.

Fig 3.2. Protein composition of thylakoid membranes of *Synechocystis* grown under photoinhibitory intensities of orange-red light.

Fig 3.3. Functional classification of the proteins that represent the thylakoid proteome of *Synechocystis* which are significantly different in all the three photoinhibitory conditions with respect to the low light intensity.

Fig 4.1 Pulse-amplitude modulated (PAM) and filtration system .

Fig 4.2 Photo-degradation of D1 protein and identification of its degradation products in PSII monomer extracted by thylakoid isolated from control light treated plants.

Fig 4.3 Measurement of fluorescence yield in short term photoinhibition experiment with a pulse-amplitude modulated (PAM) fluorescence in wild type *Synechocystis* sp. PCC 6803.

Fig 4.4 Measurement of PSII fluorescence yield in short-term photoinhibition experiment, after the addition of lincomycin, with a pulse-amplitude modulated (PAM) fluorescence in wild type *Synechocystis*

List of Tables

Table 2.1. Cell size and dry cell weight of *Synechocystis* grown under increasing light intensities.

Table 3.1. Relative quantification of the differentially abundant photosynthetic structural proteins of thylakoid membranes isolated from *Synechocystis* grown under photoinhibitory conditions.

Table 3.2. Relative quantification of the differentially abundant adjuvant proteins of thylakoid membranes isolated from *Synechocystis* grown under photoinhibitory conditions.

Table 3.3. Relative quantification of the differentially abundant ribosomal proteins associated with thylakoid membranes isolated from *Synechocystis* grown under photoinhibitory conditions.

Table 4.1 Relative quantification of PSII monomer proteins isolated from pea plants.

Summary

The work in this thesis is aimed to wide our knowledge of the oxygenic photosynthes and the photoinhibition in order to optimize the growth and the exploitation of the photosynthetic model organism *Synechocystis*. The phoinhibitory process was studied at different levels. We started out with a deep investigation of the photoinhibition *in vivo* by growing *Synechocystis* in fully controlled PBR. The experimental data were then used to perform a Modelling simulations of *Synechocystis* growth depending on the different distribution of the light inside the PBR. The work then continued by studying the modulation of the thylakoids proteins composition in response of the increased light intensity by mass spectrometry analysis. In the end an initial characterization of the PSII photo-damage in both *in vitro* and *in vivo* was performed

Chapter 1 is a general introduction on the present knowledge of the society on the possible exploitation of the photosynthetic organisms for recovering CO₂ and produce high value products. In this chapter is also explored the effective acquaintance of the photosynthetic processes, beside the photoinhibitory and the photoprotective mechanisms that occur in Synrchocystis. In the end it was summarized a short overview of the different typologies of reactors used for growing photosynthetic microorganisms

In **Chapter 2** the cells were grown in turbidostat-controlled lab-scale cultivation system and the influence of varying orange-red light intensities on *Synechocystis* growth rate, and morphology was tested. From the experimental data we applied a modelling approach to simulate how the local light distribution within the vessel was affected by varying the incident light intensity provided to the photobioreactor.

Chapter 3 goes into the study of the long term photoinhibition growing *Synechocystis* in PBR for 24 h at increased light intensities. The growth rate was the main parameter used to assess the photoinhibitory process. The photoinhibition was investigated with the quantitative mass spectrometry analysis. Thylakoids proteins extracted from cells grown under light stress and light control condition

were compared to better understand the different strategies adopted by *Synechocystis* to protect the photosynthetic apparatus from the photooxidation.

In **Chapter 4** a preliminary study on the effect of the short term photoinhibition (1h) on the PSII activity and the damage of the D1 protein was performed. This process was initially explored *in vitro* on the PSII monomer extracted from pea thylakoids. The estimation of the PSII impairment and the D1 photodegradation was performed by western blot and mass spectrometry analysis. The study was then conducted *in vivo* on the model organism *Synechocystis* by monitoring the quantum yield of PSII photochemistry (ϕ_{II}) in order to define the D1 turnover.

Finally, the **Chapter 5** is a review of the main results obtained in the PhD work project

Chapter 1

General Introduction

1.1 Environmental effect of an increased CO₂ in atmosphere

The Carbon cycle is a biogeochemical cycle in which the carbon is exchanged among the biosphere, hydrosphere and atmosphere of the Earth. It involves a sequence of reactions and events that make the Earth adapt to the life. On the Earth's atmosphere carbon exist mainly as carbon dioxide (CO₂) gas and its amount is balanced in function of the CO₂ emission and absorption. The increment of population observed in the last decades was accompanied by an increased emission of fossil fuel, energy consumption and land area deforested with a consequent increment of the amount of CO₂ in the atmosphere and exacerbation of the greenhouses effect(Sherbinin et al., 2007).

In the last fifty years , a constant raising of the surface temperature of the planet was observed(UNFCCC. Conference of the Parties (COP), 2015) Researchers have estimated that an increase of 3° C can be reach in 2050 leading to an augmented risk and frequency of the natural disaster (Berz, 1997);(Matthews et al., 2012). From the 2015 Paris UN Climate Conference (UNFCCC. Conference of the Parties (COP), 2015) the international communities started to cope the increased world temperature trying to relieve emission of CO₂. According to the 4th IPCC assessment a stabilization of the greenhouses between 445 and 536 ppm, is needed to avoid the dangerous climate changes and , estimating that these stabilization may cost less than 3% of the global gross domestic product (GDP) (IPCC, 2007).

1.2 Biofuels, an approach to mitigate the global climate change

In order to alleviate the dramatic increase of the CO₂ in the atmosphere and the greenhouse emission, the governments have incentivized the developing of methods finalized to the sustainable production of high value products. One of the main proposal to reach this aim was the exploitation of some microorganism to use the light energy for making organic the CO₂ by the process known as photosynthesis. Thus, in the last decades, widely proposal on the exploitation of algae and cyanobacteria as most promising microbial factories were developed (Wijffels et al., 2013). The several advantage in the use of Cyanobacteria (the high photosynthetic efficiency, high growth rate and a well-know metabolism) made them the best candidate for the production of carbon based product via photosynthetic process.

1.3 Cyanobacteria

Cyanobacteria are photoautotrophs prokaryotes, which contains a set of pigment that allow them to perform the oxygenic photosynthesis. They are considered the oldest photosynthetic organisms on the Earth (Hedges et al., 2001) and, there is a strong evidence that their oxygenic photosynthetic activities has played an important role in raising the oxygen level in the atmosphere (Schopf, 2000) The Cyanobacteria could have different shapes as unicellular, filamentous form, or grouped in colonies (Whitton and Potts, 2012) and, since their ability to change rapidly their metabolisms, Cyanobacteria are able to grown in different ecological habitat, from oceans to fresh water. They are characterized by a highly organized system of photosynthetic lamellae. In the Cyanobacterial thylakoids is present the chlorophyll *a* (Chl *a*) but, differently from the higher plant and the algae lack chlorophyll *b* or *c*. The main pigments responsible of the energy transfer from the solar light to the photosystems are the phycobilisomes. This are structures composed of phycoerythrin, phycocyanin and allophycocyanin connected by linker peptides and in association with the Chl *a* give them a peculiar blue-green colour (Sukenik et al., 2009) In the last decades this photosynthetic organisms were deeply studied since their great potential to be used in different biotechnological systems.

1.3.1 *Synechocystis* sp. PCC 6803

Synechocystis is a genus of freshwater cyanobacteria mainly represented by *Synechocystis* sp. PCC 6803 strain (here after *Synechocystis*) (Yu et al., 2013a). This strain was isolated for the first time from a fresh water lake in 1968 and now it is part of the Pastour culture collection (Grugger, Biological Resources Center of Institute Pastour, 2011). *Synechocystis* is an unicellular non-nitrogen(N₂) fixing prokaryotes defined by a spherical shape and lacking of vesicles. The replication of this microorganism is carried on by binary fission on two or three successive planes. In their cytoplasm are present approximately 12 copies of a single chromosome and it was deduced that one circular genome is formed by 3573470 bp (Ikeuchi and Tabata, 2001) . The complete sequencing of its genome, included four endogenous plasmids, was achieved in 1996 (Kaneko et al., 1996), making *Synechocystis* the first photoautotrophic organism fully sequenced. Since its ability to be spontaneously transformable (homolog recombination at high frequency) *Synechocystis* was widely investigate for the production of high value product derived from the genetic manipulation of its metabolic pathway (Al-Haj et al., 2016). Moreover, the fully sequenced genome of *Synechocystis* has made this

photosynthetic microorganism the best candidate for studying its adaptation at different stress condition (Los et al., 2010). Among them the light stress environment resulted one of the most attractive topic studied in the last decades.

1.4 Oxygenic photosynthesis, light dependent reactions

The photosynthesis is a process performed by photosynthetic organisms where the solar light is adsorbed and converted into chemical bond, forming organic molecules and fixing the carbon dioxide (Ort et al., 2011); (Nelson, 2011). The oxygenic photosynthesis is composed of two stages: the light dependent reaction and the light independent reaction. The light dependent reactions occur in the thylakoids of the photosynthetic organisms. During this process, the light energy is adsorbed by the antenna systems of the photosynthetic organism. The absorption of a photon by the antenna complex frees an electron by a process called photoinduced charge separation. The freed electron is subsequently transmitted through and electron transport in a process called z scheme (Peretó, 2011) .

There are four major protein complexes involved in the z scheme process: the Photosystem II (PSII), the cytochrome b6f, the Photosystem I and the ATP-synthase. The freed electron formed by the oxidation of H₂O in the PSII is transmitted to the PSI through the multi-enzymatic complex cytochrome b6f and different metabolic intermediates (linear electron flow). During this process the trans-electrochemical gradient generate through the thylakoids, is used by ATP-synthetase enzyme for the synthesis of ATP molecule (Hill and Bendall, 1960);(Hasan et al., 2013); (L. N. Liu, 2016). On the base of the reactions catalysed , the PSII can be defined as water-plastocyanin oxidoreductase, the cyt-b6f as plastoquinone-plastocyanin oxidoreductase and the PSI as plastocyanin – ferredoxin oxidoreductase (Saroussi et al., 2016).

1.4.1 Linear electron flow in cyanobacteria

The PSII can be directly excited from the light or adsorb energy ptychobilisome auxiliaries pigments. In this last cases the energy is transferred to the Chla by inductive resonance (Gantt, 1980). The energy trapped by the PSII lead to the excitation of one electron from the Chla(P680) to a higher level (P680*). This excited electron is subsequently transferred to the Pheophytin acceptor (Pheo) located in the proximity of the D1 protein, generating a charge separation (Cardona et al., 2012). The electron is then transferred to the Plastoquinone (P-QA), second electron carrier situated in the PSII core, which is subsequently reduced to plastoquinol (P-QH₂) from a second electron (Seibert et al., 1992). On the luminal

side of the thylakoids, the OEC inorganic cluster (Mn_4O_5Ca), connected to the PSII, oxidize the H_2O in proton H^+ and oxygen (Fig 2.1). This reaction release 4 electrons which are used to replace the electron hole present in the ($P680^*$). The electron transfer is mediated by the redox active Tyr side chain (Tyr-z) present in D1 (Porankiewicz et al., 1998); (De Las Rivas et al., 2004). The second multicomplex enzymes involved in the z scheme is the cytochrome b6f (Fig 1.1) .

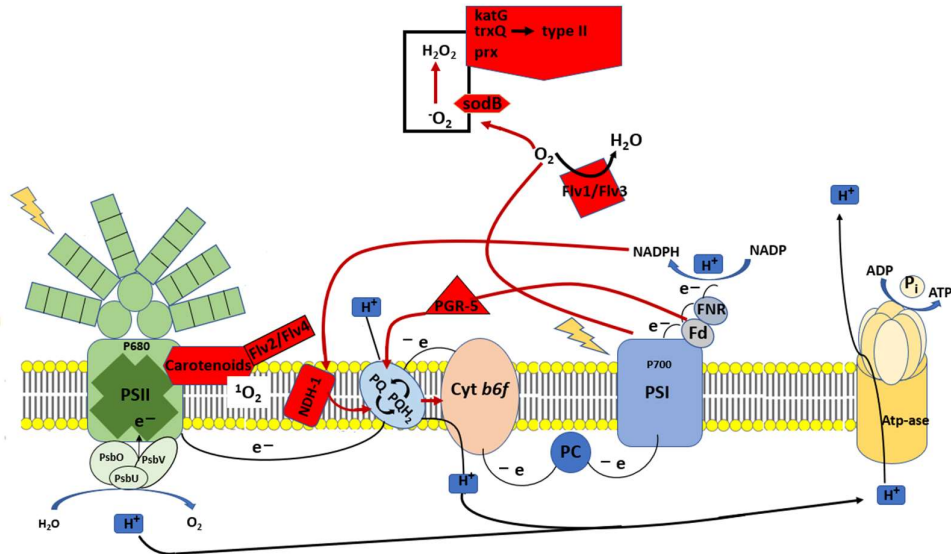


Fig 1.1 Representation of the linear electron flow and the mechanisms of photoprotection in Cyanobacteria.

Photosynthetic electron transport complexes include phycobilisome, PSII and PSI, *cyt b6f* and electron transports PQ and PC. The black arrows represent the linear electron flux. In red the stress-induced defence under photoinhibitory condition to protect the PSII and PSI. The carotenoids and Flv2/4 are the main mechanisms involved for dissipating the excess of energy from PSII to PSII. The red arrows represent the alternative pathway activated on the PSI side under HL condition: Mehler reaction and Cyclic electron fluxes. In the Mehler reaction the O_2 can be directly reduced to H_2O from Flv1 and Flv3 preventing the ROS formation while, when the excess of electron lead to the formation of oxide anion radical (O_2^-), SOD's work with different catalase disabling the ROS. In the first way of the cyclic electron flow PQ is reduced from Fd by the PGR5 protein. The alternative way of the cyclic electron flow involve the NDH1 enzyme which is reduced by the NADPH transferring the electrons to PQ.

The cytochrome *b6f* works as connector between the two photosystems transferring the electrons from the PSII to the PSI and, coupling an activity of proton translocation from the stromal side of the thylakoids membranes to the luminal generating a proton force needed for the synthesis of the ATP. The oxidation of the plastoquinol take place at the Q₀ site situated in the subunits IV of the cytochrome *b6f*. One electron is transferred from the Q₀ site to the Rieske iron- sulfur centre where is subsequently moved to the cytochrome *f* for reducing one of the electron carrier between the plastocyanin or the cytochrome C6 (Allen, 2004); (Merchant and Sawaya, 2005). The PSI is the third super complex present in the electron transport chain, which is involved in the oxidation of the plastocyanin or cytochrome C6 for transferring the electrons to the ferredoxin (Fd) (Fig2.1). The Chl(P700) is the first acceptor in the PSI that is excited upon adsorption of a photons to Chl(P700*). One electron is subsequently transferred to the special Chl_a (A₀) that works as intermediate for the reduction of the phylloquinone molecule A₁. The electron is then transferred to the immobile iron-sulfur proteins FeS_x, FeS_A and FeS_B before to reduce the Ferredoxin (Fd). The ferredoxin NADP oxidoreductase (FNR) is the final acceptor of the of the electron chain.

This electron carrier exploits the electrons from Fd for promoting the NADPH production from NADP⁺. The proton motive forces generated during the electron flux from the PSII to NADP is subsequently used by the ATP synthase for cycling back the electron in the lumen and synthesized the ATP (Merchant and Sawaya, 2005). Both the energy carriers NADPH and ATP are then used in the light independent reaction to fix the inorganic CO₂ in organic molecules.

1.4.2 Phycobilisomes

The phycobilisomes are super-molecular structures which work as accessory pigments in cyanobacteria and red algae (Mimuro et al., 1999). They are located on the stromal side of the thylakoids membranes and are tightly related to the PSII. The phycobilisomes have a adsorption range between 500 and 660 nm and, working in association with the Chl *a*, they are essential for optimizing the light harvesting in the Cyanobacteria photosynthetic process (Gantt, 1980). The four different classes of biliproteins forming the phycobilisomes differ for the type of chromophores covalently bounded (Toole et al., 1998). The allophycocyanin (APC) characterize the core of the multicomplex, the phycoerythrin (PE) and the phycoerythrocyanin (PEC) are mainly present in the distal end of the rods and the phycocyanin (PC) is present in the rods structure close to the core (Chang et al.,

2015). Besides the billiproteins, also the linker polypeptides (which do not bind any chromophores) are fundamental not only for organizing the different units forming phycobilisomes in ordered arrays, but also for connecting the phycobilisome complexes to the thylakoids membranes (Liu et al., 2013). The linker can be classified in four groups: Group I (Lr) are the polypeptides involved in the assembling of the peripheral rod structures, in the Group II (Lrc) are present the linker responsible of the attachment of the peripheral rods to the APC, in the Group III (Lc) the linker proteins connects the units forming the cores while the linker of the Group IV (Lcm) are involved in the connection between the phycobilisomes and the thylakoids membrane (Glazer et al., 1994).

1.4.3 Photosystem II

The PSII is the multi-subunits complex in the thylakoids membranes from which start the electron flow of the z scheme. In the photosynthetic organism the PSII is a heterodimer complex and, in cyanobacteria it consists in approximately 20 proteins surrounded by several cofactors (Fig1.2).

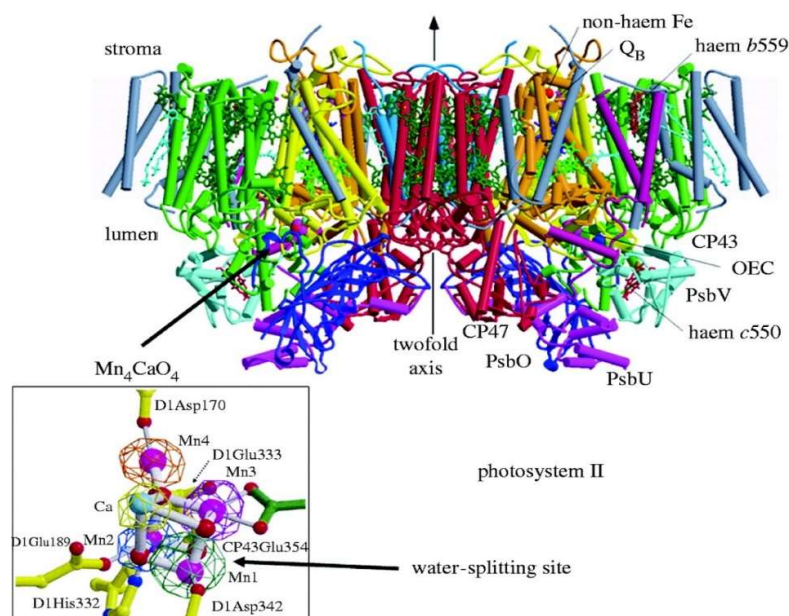


Fig 1.2 Sideview of the structure of photosystem II and OEC complex. View of the PSII dimer perpendicular to the membrane normal. Helices are shown as cylinders: D1 (yellow); D2 (orange); CP47 (red); CP43 (green); cyt *b559* (red); PsbL, PsbM, and PsbT (light blue); PsbH, PsbI, PsbJ, PsbK, PsbX, PsbZ, and the putative PsbN (gray). The proteins forming the OEC complex are: PsbO (blue), PsbU (magenta), and PsbV (cyan).

The oxygen-evolving center (OEC) is shown in the red (oxygen atoms), magenta (Mn ions), and cyan (Ca^{2+}) balls. Structure determined by X-ray crystallography, (Ferreira et al., 2004)

The core centre of the PSII monomer is composed of two trans-membrane proteins PsbA and PsbD (D1 and D2) which are connected to the chlorophyll binding proteins PsbC and PsbB (CP43 and CP47) (Heinz et al., 2016) and the two subunits forming the Cyt b559 PsbE and PsbF. The light harvesting proteins PSbC and PbbB are respectively bonded to 14 and 16 molecules of Chlorophyll a (Chl a), while two special pigment chlorophyll (P680) are joined to PsbA and PsbD (Nelson and Ben-Shem, 2004). Associated to the PSII core the Oxygen evolving complex (OEC) works as an active centre for the water oxidation (Fig 1.1). The OEC is composed of an inorganic $\text{Mn}_4\text{O}_5\text{Ca}$ cluster which is linked to PsbA, PsbD and PsbC by amino acid residues and protected from the luminal extrinsic proteins PsbO, PsbU and PsbV (Barber, 2016). Among the small sub-units in PSII, the very hydrophobic proteins PsbL, PsbM, PsbT are located in the interface the in the monomer-monomer interface, while the function of majority of them PsbH, PsbI, PsbJ, PsbK, PsbX, PsbY, PsbZ, Psb30 is still unknown.

1.4.4 Cytochrome *b6f*

The cytochrome *b6f* is a multi-proteins complex situated in the thylakoids bilayer between the PSII and the PSI. It is formed by eight polypeptides tightly linked to each other and it plays an essential role in the electron transport process from the PSII to PSI, (Peschek 1987, (Scherer, 1990). The four main subunits forming the cytochrome *b6f* are represented by the cytochrome *f*, the cytochrome *b6*, the Rieske protein and the subunits IV. Conversely, the further low molecular weight proteins (less than 10 kDa) present in the Cyt *b6f* are the products of the genes *petG*, *petL*, *petM* and *petN* (Baniulis et al., 2009). Among the eight subunits only *cyt b6*, *cyt f*, SuIV and Rieske ISP, *petG*, and *petN* resulted essential for the function of the multicomplex (Baniulis et al., 2009). Surprisingly, in different studies on photosynthetic organisms, including cyanobacteria, the presence of a single molecule of Chl_a per multicomplex was observed (Kallas, 1994).

1.4.5 Photosystem I

In Cyanobacteria the PSI complex can exist in both monomeric and trimeric forms (Fig 1.3). This last conformation is the form more adopted when cyanobacteria grown under low light intensity, resulting in the most abundant complex present in

the cyanobacterial thylakoids membranes (Fromme et al., 2003). The monomeric unit is from by 12 proteins, 96 chlorophylls, 22 carotenoids, and approximately 127 cofactor non-covalently (Grotjohann and Fromme, 2005).

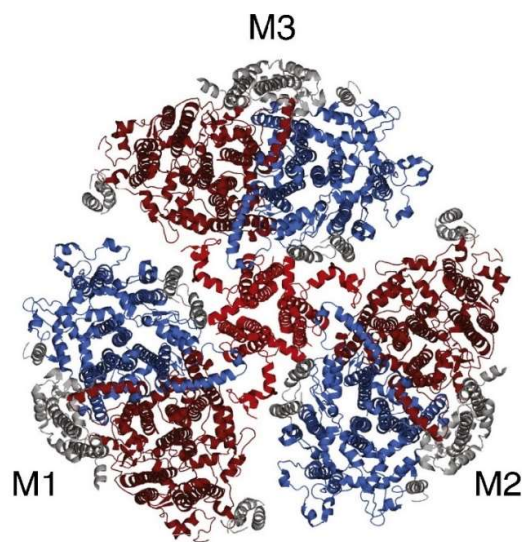


Fig 1.3. PSI crystal structures. Crystall structure of the PSI from cyanobacteria (*Thermosynechococcus elongatus*). M1-3 represent the individual monomers including the native trimer. The major helices are represented in burgundy (PsaA), in blue (PsaB), in red (PsaL), while the other subunits in (gray). Adapted from (Nguyen and Bruce, 2014)

The core centre of the PSI monomer is composed by the two large subunits PsaA and PsaB which host the special Chla (P700) and most of the cofactors needed for the electron transport in the electrochemical chain included. At the interfaces between the different monomers are located the highly hydrophobic proteins PsaI, PsaL and PsaM, with the subunits PsaL which works as structural and functional connectors. On the more distal part of the PSI core, in contact with the thylakoids bilayer, are situated the subunits PsaF, PsaJ, PsaK and PsaX. Their presence is considered important for stabilizing the antenna system present in the core of the PSI (Jordan et al., 2001). The group of the extrinsic subunits bonded to the PSI are composed of the subunits PsaC, PsaD and PsaE, They are situated on the stromal side of the thylakoids and play a key role in for the docking with the electron carriers ferredoxin/ flavodoxin (Grotjohann and Fromme, 2005).

1.4.6 Atp-synthase

The Atp-synthase is an enzyme complex present in both eukaryotic and prokaryotic organisms, where it is responsible for the ATP synthesis by exploiting of the electrochemical proton gradient formed between the two side of the thylakoid bilayer. It is composed of two major units called F_0 and F_1 . The thylakoid integrated complex F_0 allows the translocation of the proton H^+ through the membrane inducing a rotation needed to F_1 for the ATP synthesis (Boyer, 1997). In the F_0 are present the sub units a, b and c, common in the different organisms, and the sub-units b' characteristic of the photosynthetic organisms (Walker and Tybulewicz, 1985), The subunits c form the proton channel inside the thylakoids bilayer, and it is considered extremely conserved among the different organisms. Conversely, the sub-units a and b seems participate in the linkage between F_0 and F_1 (Curtis, 1988) The subunits forming the F_1 complex are called with the Greek letters α , β , γ , δ and ϵ . The active site of the complex is shielded by the units α and β , while the polypeptide δ is needed for the functional connection between F_0 and F_1 . The subunit γ and ϵ is not still clear the function but, in the photosynthetic organisms seems they are involved in the regulation of the multi enzymatic complex activity (McCarty and Hammes, 1987).

1.5 Photosynthesis – irradiance response curves

The irradiance response curves compare the photosynthetic rate (**P**) and the irradiance (**E**) in order to describe the different steps which taking part in the photosynthetic process in response to the light intensity. The Michaelis–Menten formulation is usually suitable to show the correlation between light intensity and photosynthetic rate:

$$P_E = \frac{P_{max} E_1}{K_m + E_1}$$

Eq. 1.1

where P_E represent the photosynthetic rate at different irradiance E , E_1 define the spectral irradiance (in $\mu\text{mol m}^{-2}\text{sec}^{-1}$) and K_m is the half saturation constant when $P_E = P_{max}/2$ (Barsanti and Gualtieri, 2006).

The Photosynthesis – irradiance response curve (PI-curve) describe three different regions (Fig. 1.4): a light-limited region, a light-saturated region, and a light-inhibited region.

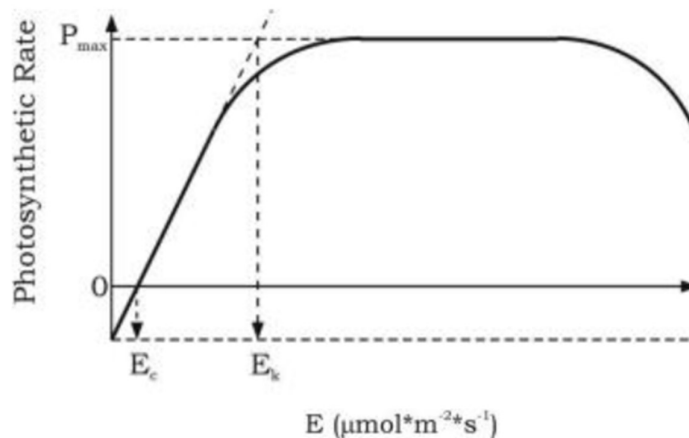
In the light-limited region the state of electron transport from the H₂O to the CO₂ is determinates from the rate of photon adsorption. In this region we can described the rate of photosynthesis (P_E) as:

$$P_E = E_\lambda * \alpha$$

Eq.1.2

where E_λ represent the spectral irradiance and α is a measure of the photosynthetic efficiency. Therefore, at low light intensity, the photosynthetic efficiency and the consequent production of energy carriers (ATP, NADH) is proportional to the amount of light provided to the cells (Barsanti and Gualtieri, 2006).

The light compensation point (E_c) represent the light intensity where the rate of photosynthesis balances the rate of cellular respiration (Fig.1.4).



(Barsanti and Gualtieri, 2006)

Fig. 1.4 Photosynthesis–irradiance response curve. E_c , irradiance compensation point; E_k , saturating irradiance; and P_{max} : maximum photosynthetic rate

With the progressive increase of the light intensity, the linearity among the photons adsorbed the photosynthetic rate is increasingly lost, and it reach its saturation level

P_{max} . in the Fig. 1.4 E_k represent the point at which the extrapolated initial slope meets P_{max} .

Above E_k the light dependent reaction lead to the production of more ATP and NADH of which is consumed from the light independent reaction for fixing the CO_2 . Hence, in the light-saturated region, the increasing of the light is not followed by the increase of the photosynthetic efficiency anymore.

Further increase of the light intensity over the light suturing regime for a prolonged period of time result in the process called photoinhibition.

1.6 Photoinhibition

The photoinhibitory process is define by a constant decrease in the capacity of light energy conversion into photosynthesis because of the damage of the proteins forming the photosynthetic apparatus. Photosystem II is the protein complex most sensible to the light in the photosynthetic machinery so that concept of photoinhibition is usually similar to PSII photoinactivation (Chow and Aro, 2005). The process of photoinhibition can be induced from both visible (400-700 nm) and ultraviolet light (220-400 nm), with the last more efficient to induce photodamage (RENGER et al., 1989); (Jung and Kim, 1990). The extra-production of Oxygen reactive species (ROS) and the formation of a long-live radicals $P680^{+\bullet}$ is considered the main event that lead to the photodamage of the PSII with the subsequent decrease of the photosynthetic efficiency. On the other hand, the photosynthetic organisms can promptly active a PSII repair cycle which allows them to survive under light stress condition. The photoinhitory process became evident and extremely dangerous for the organisms survive when the impairment of the PSII exceed the rate on repair (Andersson and Aro, 2001); (Tyystjärvi, 2008). The main target of the photoinhibitory process is the protein D1 situated in the PSII core. After the photodamage of the D1 protein the PSII complex is disassembled, the impaired D1 is replaced by a new copy and the PSII is again reassembled in the functional PSII dimer (Campbell et al., 1996). In different studies was highlighted how the ROSs not only induce the photodamage of the PSII but, they can also inhibit the repair process of the photodamaged PSII, preventing the synthesis of the novo D1 protein (Nishiyama et al., 2001); (Takahashi and Murata, 2005); (Nishiyama et al., 2006); (Takahashi and Murata, 2008). Different photoinhibitory mechanisms has been suggested: acceptor side photoinhibition, donor side photoinhibition, manganese mechanism, singlet oxygen mechanism. Among them

the acceptor side photoinhibition and the donor side photoinhibition are the process more studied in the last decades (Aro et al., 1993a); (Napiwotzki et al., 1997).

1.6.1 Acceptor side photoinhibition

The acceptor-side photoinhibition occurs when the prolonged strong illumination induce an extended reduction of the PQ pool resulting in the double reduction of the electron acceptor Q_A (Styring et al., 1990);(Vass et al., 1992a). The resulting incapacity of Q_A to work as an electron carrier and the resulting stoppage of the electron transport leads to a charge recombination of the primary radical pair $P680^+Pheo^-$ with the formation of the triplet excitate state of the 3Chla (P680) (Vass et al., 1992). The subsequent interaction of the triplet Chlorophyll with the molecular oxygen result in the production of harmful singlet oxygen (1O_2) which induce the damage of the proteins surrounding its production site (Krieger-Liszkay et al., 2008).

1.6.2 Donor side photoinhibition

The acceptor side photoinhibition, discussed in the previous section, is considered the main mechanism for the photoinactivation of the PSII and the damage of the protein D1. Nevertheless, a further PSII inactivation process take place when the electron transport between the manganese cluster in the OEC and chlorophyll P680 in the PSII is impaired (Blubaugh and Cheniae, 1990); (Blubaugh et al., 1991); (Jegerschöld et al., 1990) ; (Eckert et al., 1991). Conversely to the acceptor side photoinhibition process, which occurs only under high light condition, the donor side photodamage mechanism can be induced under either low or high light intensities. During the donor side photoinhibition , the damage of the electron transport from OEC to the PSII result in the formation of a long lived $P680^+$ (and/or $TyrZ^+$) which have a high oxidizing power and result in the damage of the protein surrounding them (Callahan et al., 1986); (Chen et al., 1992); (Anderson et al., 1998). Moreover, the Mn_4Ca cluster is sensitive to the structural change at the PSII donor side. The impairment of the protein forming the OEC complex can result in a not optimal function of the cluster. Under such condition the electron transfer between the Tyr-Z and P680 lead to the formation of H_2O_2 . The light -dissociation of the H_2O_2 to the highly reactive $OH\cdot$, concur to the PSII proteins damage (Schröder and Åkerlund, 1986).

1.7 Photoprotection

To cope the light environmental fluctuation, plant, algae and cyanobacteria have enhanced different strategies which result in the reduction of the light excitation from the light harvesting complex to the photosynthetic reaction centres. In accordance with extensive literature the dissipation of the excess of energy, absorbed by the chlorophyll pigment, in heat or fluorescence are the main mechanisms used from the photosynthetic organisms to prevent the PSII photodamage in a process called non-photochemical quenching (NPQ)(Schreiber, 2004) ;(Bailey and Grossman, 2008); (Derks et al., 2015) The different NPQ can be classify in base of : i) how fast they are induced , ii)the type of mechanisms involved. The energy- state quenching process (qE) is mediated by the presence of a ΔpH gradient (second time scale). The state of transition process (qT), is involved in the balancing of the excitation energy distribution between PSII and PSI (minutes time scale). The carotenoids (OCP) mediated photoprotective mechanism(qZ) is quickly induced but prolonged during the time (Horton, 2012); (Derks et al., 2015). In addition, during the process of photoinhibition , also the electron cycling around the PSI plays an important role for both prevent the PSI photoinhibition and drive the formation of a trans-thylakoid proton gradient needed to generate ATP needed for major energy request from the cells grown under light stress condition (Thomas et al., 2001), (Bailey and Grossman, 2008).

Although, for many year cyanobacteria were considered lacking of the NPQ photoprotective processes, recently is was proved that they can use the NPQ- qT and NPQ- qZ mechanisms as photoprotective strategies .

1.7.1 State transition (qT)

The illumination of the PSII antenna under high light or a specific illumination with orange or green light of the PBS can lead to an over reduction of the intersystem electron carriers which may result dangerous when react with the molecular oxygen(Kirilovsky, 2015). The state transition mechanism promotes the redistribution of the excited energy between PSII and PSI in response to the imbalanced excitation of the two photosystems. In cyanobacteria there are two possible processes involved in the redistribution of the excited energy :1) the PBS translocation from the PSII to the PSI is (mobile PBS mechanism), 2) the energy transfer from PSII to PSI favourite by the proximity between the two photosystems (spillover mechanisms) (Mullineaux et al., 2014); (Li et al., 2006). In the PBS translocation mechanism two different state are defined: the **state I**, where the

pigments arrangement promote the excitation of the PSII and the **state II**, where the excitation of the PSI is favoured. The state of transition in cyanobacteria cause the detachment of the PBS from the PSII and their subsequent migration to the PSI (Roach and Krieger-Liszkay, 2014).

Moreover, in *Synechocystis* is studied that a strong illumination resulted in a detachment of the PBS from the thylakoids and their subsequent disassembling. Indeed, the surplus of energy absorbed by the PBS can be converted in heat resulting in a deformation of the thermos-sensible L_{cm} linker, giving to the state of transition also a role of long-term photoprotection (Tamary et al., 2012a).

1.7.2 OCP – dependent quenching (qz)

In Cyanobacteria, carotenoids (OCP) molecules are soluble pigments which bind the keto-carotenoid 3'-hydroxyechinenone (hECN). Beside their importance in the light harvesting mechanisms, the OCP play a key role in the photoprotective processes (Kusama et al., 2014);(Tóth et al., 2015);(Zakar et al., 2016). The strong light induces conformational changes in the OCP pigment that result essentially for their photoprotective role (Wilson et al., 2008). In darkness or under low light regimes the OCP is orange in its closed conformation (OCP^0) while the exposition of OCP to high light resulted in a structural change of hECN. Under such light condition OCP^0 is converted to a more opened red coloured conformation (OCP^R) (Zhang et al., 2016). Only the OCP^R forms can binds the PBSs, promoting its function of quencher by the thermal dissipation of the excess of energy adsorbed by APC bilin and decreasing the energy addressed to the PSII (Fig 1.1). Moreover, in cyanobacteria growth under light stress condition, an over expression of the flavodiiron proteins flv2 and flv4 was observed. Despite their function in the photoprotective mechanism is still not clear, in (Zhang et al., 2012); (Montgomery, 2014) was suggested their role as alternative acceptor of the OCP in the photoprotective process.

1.7.3 PSI electron cycling

The cycling electron flow around the PSI (CEF) is proposed as further mechanism for protecting the PSII from the photoinhibition (Fork and Herbert, 1993);(Herbert et al., 1995) and driving a major production of ATP needed to support the PSII repair cycle (Huang et al., 2018). In cyanobacteria are present two CEF mechanisms: i) mediated by the ferredoxin- quinone reductase (FQR), ii) mediated by the NDH-1 complex (Fig 1.1). In the FQR cycle the electrons are moved from the ferredoxin present on the PSI donor side to PQ via PGR5 protein, which works

as ferredoxin- plastoquinone activity enzymes (Munekage et al., 2002) .The cycle is then closed by the electron transfer back to the PSI passing by the *Cytb6f* and one between the electron carriers PC or cytochrome C6. Conversely, in the second PSI cycling pathway, the NDH-1 complex, oxidizes the NADPH driving the electron to the PQ. From PQ the electron are then cycled back to PSI via *Cytb6f* and the electron carriers PC or cytochrome C6 (Battchikova et al., 2011) Furthermore, in accordance with (Zhang et al., 2012), the photoinhibitory regime induce to the overexpression of the flavodiiron proteins Flv1 and Flv3 involved in the Mehler reaction , where the molecular O₂ is directly covered in H₂O, specific enzymes as catalases and Superoxide dismutase (SOD) which prevent the PSI damage inactivating the ROS (Helman,et al., 2003).

1.8 Reactors

In the last decades a lot of efforts has been focused to improve the growth conditions of the photosynthetic microorganism in order to maximizing the final mass cultivation and making more efficient the production of valuable products (Kim and Lee, 2005); (Kim Z.-H. et al., 2006). The cultivation of cyanobacteria and algae can be carried on in both open system as pound, or in closed controlled systems called photobioreactors (PBR).

In the first case the cultivation of photosynthetic microorganisms is carried on in open systems which employ raceway pounds. This can be composed of long channels arranged in a single or multiple loop, coupled with a paddle-wheels system to ensure an efficient biomass recycling (Chisti, 2016) ; (Chaumont, 1993). Despite the open pound is considered the most easy and cheap system for growing Cyanobacteria and micro algae, it shows different disadvantages which affect the cells biomass productivity. Indeed, the high risk of contamination, the little light penetration and the limited opportunity to control the growth condition make this system not suitable the production of specific strains or products(Guedes et al., 2013).

In the PBR system the microorganisms are not exposed to the to the external environment, reducing the contamination event and making the work condition more controlled (Tredici, 2004). In the last decades different shapes of photobioreactors were developed to optimize the growth conditions of the photosynthetic microorganisms. In Fig 1.5 are shown the three basic types of photobioreactor include : tubular PBR(Lee et al., 1995)(Hai et al., 2000), flat panel PBR(Richmond and Cheng-Wu, 2001) and fermenter PBR (Pohl et al., 1988).

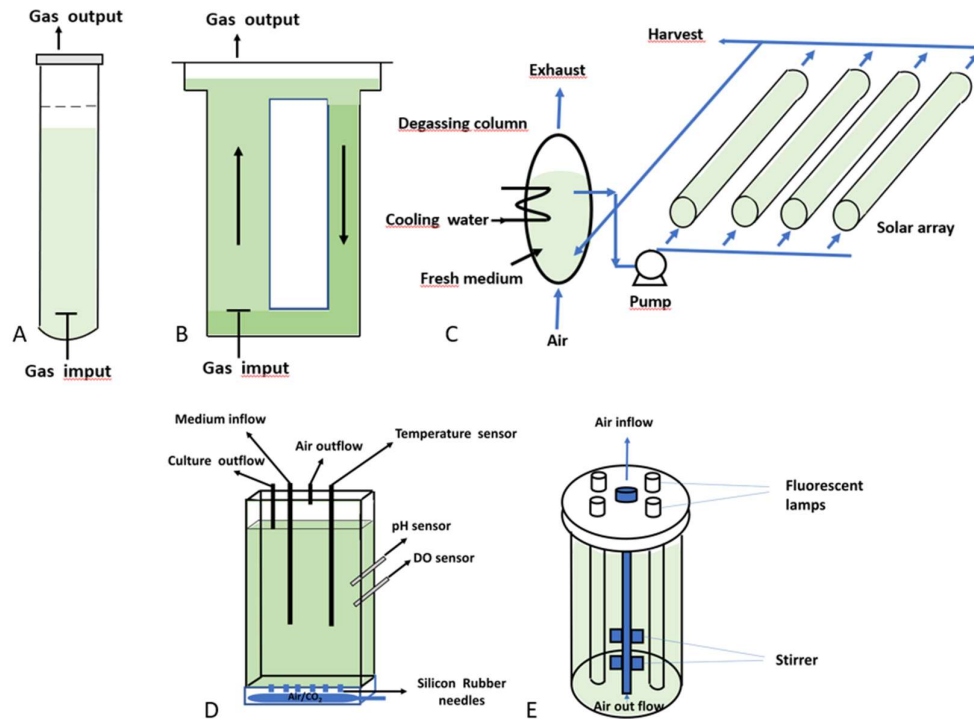


Fig 1.5 Different types of reactors. A: Bubble columns , **B:** Airlift, **C:** Horizontal tubular reactor, **D:** Flat panel, **E:** Fermenter type reactor.

The tubular PBR can be roughly classified in vertical and horizontal reactor. Among the vertical reactor the Bubble column and the Airlift are the more widely used and studied. The main differences between these two vertical tubular systems lies in the geometry of the system. Indeed, the bubble column reactor (Fig. 1.5 A) is composed of a simple vertical tubular vessel where the gas is injected on the bottom and the culture mixing is due to the bubble rising (Sánchez *et al.*, 2000); (Sánchez *et al.*, 2002). Conversely, in the Airlift reactor (Fig 1.5 B), the recirculation of the culture is definite by the design of the PBR which has two different channels linked at the bottom and at the top forming a closed loop. In one channel, called raiser area, the gas mixture is bubbled in the culture while in the downcomer channel the media and the cells not receive gas (Singh and Sharma, 2012).

The horizontal reactors, as the vertical reactors, are composed of a transparent tubing system. Beside they can be present in different shape variants (i.e inclined tubular shapes, horizontal, or parallel set of tubes) (Singh and Sharma, 2012) all of them are characterized by a high surface exposed towards the sun light a large volume of work (Fig 1.5C). This feature make the horizontal reactor extremely indicate for outdoor culture with high volume of work (Carvalho et al., 2006).

The flat panel PBR can be made by glass, plexiglass or polycarbonate and they are characterized by a short light path between the two panels forming the vessel (Fig 1.5D). Since their shape this reactor are characterized by a high area to volume ratio and an efficient use of the light. The CO₂ mixing is sparged by a sparger placed on the bottom of the vessel and the mixing of the culture is provided from both air bubbling and mechanic rotation through motor.

In the end the fermenter PBR (Fig 1.5E) is constituted by the most conventional fermenter bioreactor adapted to grow photosynthetic microorganisms by the implementation of an illuminating system (Singh and Sharma, 2012). It is composed of a tank where the culture is mechanically stirred by an appropriate rotor. In the tank are present baffles to decrease vortex. the CO₂ mixture is usually bubbled from the bottom.

1.9 Liquid mixing and light/dark cycle in photobioreactor

The light intensity distribution inside the PBR's is not uniform because of the light scattering and absorption phenomena (Quan et al., 2004). Different factors can influence the attenuation of the radiation inside the PBR as the cell concentration, light sources distance, shape of the reactors.

In base on the cell growth rate, the PBR's can be split in three main zones: the heavy illumination zone, that is extended from the illuminated wall to the point where the light intensity provided induce the cells to growth at their maximum rate; the low intensity zones, where the energy of the light is just sufficient for satisfying the cells energy requirement and the dark zones, where the light is extremely low and do not allow the cells growth. When the cells stay for a prolonged period in a too strong illumination region the photosynthetic rate decrease, inducing the cells in the state of photoinhibition. This implies that a good hydrodynamics and the mixing system of the culture result markedly influent on the performance of the PBR. As show in paragraph 1.8, the mixing inside the reactor usually is induced by gas bubbling or mechanical agitation. It is largely accepted that an enhanced phothosynthetic process can be reached by optimizing the mixing

system inside the reactors (García-Camacho et al., 2012). Indeed, an efficient recirculation of the microbial cells from high light to dark reactor zone promote a flashing -light effect which lead to a quick reduction of the electron acceptors Q_A and Q_B associated to the PSII in the light region , and their subsequent oxidation in the dark period, reducing the extra-production of ROS (Abu-Ghosh et al., 2016) .

1.10 References

- Abu-Ghosh S., Fixler D., Dubinsky Z., Iluz D. 2016. Flashing light in microalgae biotechnology. *Bioresource Technology* 203:357–363. DOI: 10.1016/J.BIORTECH.2015.12.057.
- Al-Haj, L., Lui, Y., Abed, R., Gomaa, M., Purton, S., 2016. Cyanobacteria as Chassis for Industrial Biotechnology: Progress and Prospects. *Life* 6, 42. <https://doi.org/10.3390/life6040042>
- Allen, J.F., 2004. Cytochrome b6f: structure for signalling and vectorial metabolism. *Trends Plant Sci.* 9, 130–137. <https://doi.org/10.1016/j.tplants.2004.01.009>
- Anderson, J.M., Park, Y.-I., Chow, W.S., 1998. Unifying model for the photoinactivation of Photosystem II in vivo under steady-state photosynthesis. *Photosynth. Res.* 56, 1–13. <https://doi.org/10.1023/A:1005946808488>
- Andersson, B., Aro, E.-M., 2001. Photodamage and D1 Protein Turnover in Photosystem II, in: *Regulation of Photosynthesis*. Kluwer Academic Publishers, Dordrecht, pp. 377–393. https://doi.org/10.1007/0-306-48148-0_22
- Anupama, Ravindra, P., 2000. Value-added food: single cell protein. *Biotechnol. Adv.* 18, 459–79.
- Aro, E.M., Virgin, I., Andersson, B., 1993. Photoinhibition of Photosystem II. Inactivation, protein damage and turnover. *BBA - Bioenerg.* 1143, 113–134. [https://doi.org/10.1016/0005-2728\(93\)90134-2](https://doi.org/10.1016/0005-2728(93)90134-2)
- Bailey, S., Grossman, A., 2008. Photoprotection in cyanobacteria: Regulation of light harvesting. *Photochem. Photobiol.* 84, 1410–1420. <https://doi.org/10.1111/j.1751-1097.2008.00453.x>
- Baniulis, D., Yamashita, E., Whitelegge, J.P., Zatsman, A.I., Hendrich, M.P., Hasan, S.S., Ryan, C.M., Cramer, W.A., 2009. Structure-Function, Stability, and Chemical Modification of the Cyanobacterial Cytochrome b6f Complex from *Nostoc* sp. PCC 7120. *J. Biol. Chem.* 284, 9861–9. <https://doi.org/10.1074/jbc.M809196200>

-
- Barsanti L., Gualtieri P. 2006. *Algae, Anatomy, Biochemistry, and Biotechnology*. DOI: 10.1017/CBO9781107415324.004.
- Barber, J., 2016. "Photosystem II: the water splitting enzyme of photosynthesis and the origin of oxygen in our atmosphere." *Q. Rev. Biophys.* 49, e14. <https://doi.org/10.1017/S0033583516000093>
- Battchikova, N., Eisenhut, M., Aro, E.M., 2011. Cyanobacterial NDH-1 complexes: Novel insights and remaining puzzles. *Biochim. Biophys. Acta - Bioenerg.* 1807, 935–944. <https://doi.org/10.1016/j.bbabi.2010.10.017>
- Berz, G.A., 1997. Natural Disasters and the Greenhouse Effect: Impact on the Insurance Industry and Possible Countermeasures. *Geneva Pap. Risk Insur. - Issues Pract.* 22, 501–514. <https://doi.org/10.1057/gpp.1997.35>
- Blubaugh, D.J., Atamian, M., Babcock, G.T., Golbeck, J.H., Cheniae, G.M., 1991. Photoinhibition of hydroxylamine-extracted photosystem II membranes: identification of the sites of photodamage. *Biochemistry* 30, 7586–97.
- Blubaugh, D.J., Cheniae, G.M., 1990. Kinetics of photoinhibition in hydroxylamine-extracted photosystem II membranes: relevance to photoactivation and sites of electron donation. *Biochemistry* 29, 5109–18.
- Boyer, P.D., 1997. THE ATP SYNTHASE—A SPLENDID MOLECULAR MACHINE. *Annu. Rev. Biochem.* 66, 717–749. <https://doi.org/10.1146/annurev.biochem.66.1.717>
- Callahan, F.E., Becker, D.W., Cheniae, G.M., 1986. Studies on the Photoactivation of the Water-Oxidizing Enzyme: II. Characterization of Weak Light Photoinhibition of PSII and Its Light-Induced Recovery. *Plant Physiol.* 82, 261–9. <https://doi.org/10.1104/PP.82.1.261>
- Campbell, D., Clarke, A.K., Gustafsson, P., Oquist, G., 1996. DI exchange and the Photosystem II repair cycle in the cyanobacterium *Synechococcus*. *iENCE ELSEVIER Plant Sci. IS* 183–190.
- Cardona, T., Sedoud, A., Cox, N., Rutherford, A.W., 2012. Charge separation in Photosystem II: A comparative and evolutionary overview. *Biochim. Biophys. Acta - Bioenerg.* 1817, 26–43. <https://doi.org/10.1016/j.bbabi.2011.07.012>
- Carvalho, A.P., Meireles, L.A., Malcata, F.X., 2006. Microalgal reactors: A review of enclosed system designs and performances. *Biotechnol. Prog.* 22, 1490–1506. <https://doi.org/10.1021/bp060065r>

- Chang, L., Liu, X., Li, Y., Liu, C.-C., Yang, F., Zhao, J., Sui, S.-F., 2015. Structural organization of an intact phycobilisome and its association with photosystem II. *Cell Res.* 25, 726–737. <https://doi.org/10.1038/cr.2015.59>
- Chaumont, D., 1993. Biotechnology of algal biomass production: a review of systems for outdoor mass culture. *J. Appl. Phycol.* 5, 593–604. <https://doi.org/10.1007/BF02184638>
- Chen, G.X., Kazimir, J., Cheniae, G.M., 1992. Photoinhibition of hydroxylamine-extracted photosystem II membranes: studies of the mechanism. *Biochemistry* 31, 11072–11083. <https://doi.org/10.1021/bi00160a017>
- Chini Zittelli, G., Lavista, F., Bastianini, A., Rodolfi, L., Vincenzini, M., Tredici, M.R., 1999. Production of eicosapentaenoic acid by *Nannochloropsis* sp. cultures in outdoor tubular photobioreactors. *J. Biotechnol.* 70, 299–312. [https://doi.org/10.1016/S0168-1656\(99\)00082-6](https://doi.org/10.1016/S0168-1656(99)00082-6)
- Chisti, Y., 2016. Algae Biotechnology. <https://doi.org/10.1007/978-3-319-12334-9>
- Chisti, Y., 2007. Biodiesel from microalgae. *Biotechnol. Adv.* 25, 294–306. <https://doi.org/10.1016/J.BIOTECHADV.2007.02.001>
- Chow, W.S., Aro, E.-M., 2005. Photoinactivation and Mechanisms of Recovery, in: *Photosystem II*. Springer-Verlag, Berlin/Heidelberg, pp. 627–648. https://doi.org/10.1007/1-4020-4254-X_28
- Curtis, S.E., 1988. Structure, organization and expression of cyanobacterial ATP synthase genes. *Photosynth Res* 18, 223–244.
- De Las Rivas, J., Balsera, M., Barber, J., 2004. Evolution of oxygenic photosynthesis: Genome-wide analysis of the OEC extrinsic proteins. *Trends Plant Sci.* 9, 18–25. <https://doi.org/10.1016/j.tplants.2003.11.007>
- Derks, A., Schaven, K., Bruce, D., 2015. *Biochimica et Biophysica Acta* Diverse mechanisms for photoprotection in photosynthesis . Dynamic regulation of photosystem II excitation in response to rapid environmental change. *BBA - Bioenerg.* 1847, 468–485. <https://doi.org/10.1016/j.bbabi.2015.02.008>
- Eckert, H.-J., Geiken, B., Bernarding, J., Napiwotzki, A., Eichler, H.-J., Renger, G., 1991. Two sites of photoinhibition of the electron transfer in oxygen evolving and Tris-treated PS II membrane fragments from spinach. *Photosynth. Res.* 27, 97–108. <https://doi.org/10.1007/BF00033249>

-
- Ferreira, K.N., Iverson, T.M., Maghlaoui, K., Barber, J., Iwata, S., 2004. Architecture of the photosynthetic oxygen-evolving center. *Science* 303, 1831–8. <https://doi.org/10.1126/science.1093087>
- Fork, D.C., Herbert, S.K., 1993. Electron transport and photophosphorylation by Photosystem I in vivo in plants and cyanobacteria. *Photosynth. Res.* 36, 149–168. <https://doi.org/10.1007/BF00033035>
- Fromme, P., Melkozernov, A., Jordan, P., Krauss, N., 2003. Structure and function of photosystem I: Interaction with its soluble electron carriers and external antenna systems. *FEBS Lett.* 555, 40–44. [https://doi.org/10.1016/S0014-5793\(03\)01124-4](https://doi.org/10.1016/S0014-5793(03)01124-4)
- García-Camacho, F., Sánchez-Mirón, A., Molina-Grima, E., Camacho-Rubio, F., Merchuck, J.C., 2012. A mechanistic model of photosynthesis in microalgae including photoacclimation dynamics. *J. Theor. Biol.* 304, 1–15. <https://doi.org/10.1016/j.jtbi.2012.03.021>
- Gantt, E., 1980. Structure and Function of Phycobilisomes: Light Harvesting Pigment Complexes in Red and Blue-Green Algae, *International Review of Cytology*. [https://doi.org/10.1016/S0074-7696\(08\)61971-3](https://doi.org/10.1016/S0074-7696(08)61971-3)
- Glazer, A.N., Gindt, Y.M., Chan, C.F., Sauer, K., 1994. Selective disruption of energy flow from phycobilisomes to Photosystem I. *Photosynth. Res.* 40, 167–173. <https://doi.org/10.1007/BF00019333>
- Grotjohann, I., Fromme, P., 2005. Structure of cyanobacterial Photosystem I. *Photosynth. Res.* 85, 51–72. <https://doi.org/10.1007/s11120-005-1440-4>
- Guedes, A.C., Katkam, N.G., Varela, J., Malcata, F.X., 2013. Photobioreactors for cyanobacterial culturing. *Cyanobacteria An Econ. Perspect.* 270–292. <https://doi.org/10.1002/9781118402238.ch17>
- Hai, T., Ahlers, H., Gorenflo, V., Steinbüchel, A., 2000. Axenic cultivation of anoxygenic phototrophic bacteria, cyanobacteria, and microalgae in a new closed tubular glass photobioreactor. *Appl. Microbiol. Biotechnol.* 53, 383–9.
- Hasan, S.S., Yamashita, E., Baniulis, D., Cramer, W.A., 2013. Quinone-dependent proton transfer pathways in the photosynthetic cytochrome b6f complex. *Proc. Natl. Acad. Sci.* 110, 4297–4302. <https://doi.org/10.1073/pnas.1222248110>
- Hedges, S.B., Chen, H., Kumar, S., Wang, D.Y., Thompson, A.S., Watanabe, H.,

2001. A genomic timescale for the origin of eukaryotes. *BMC Evol. Biol.* 1, 4. <https://doi.org/10.1186/1471-2148-1-4>
- Heinz, S., Liauw, P., Nickelsen, J., Nowaczyk, M., 2016. Analysis of photosystem II biogenesis in cyanobacteria. *Biochim. Biophys. Acta - Bioenerg.* 1857, 274–287. <https://doi.org/10.1016/j.bbabi.2015.11.007>
- Herbert, S.K., Martin, R.E., Fork, D.C., 1995. Light adaptation of cyclic electron transport through Photosystem I in the cyanobacterium *Synechococcus* sp. PCC 7942. *Photosynth. Res.* 46, 277–285. <https://doi.org/10.1007/BF00020441>
- Hernández-Calderón, O.M., González-Llanes, M.D., Rios-Iribe, E.Y., Jiménez-Lam, S.A., Chavez-Parga, M. de. C., Escamilla-Silva, E.M., 2017. Hydrodynamics and Mass Transfer Simulation in Airlift Bioreactor with Settler using Computational Fluid Dynamics. *Int. J. Chem. React. Eng.* 15. <https://doi.org/10.1515/ijcre-2016-0173>
- HILL, R., BENDALL, F., 1960. Function of the Two Cytochrome Components in Chloroplasts: A Working Hypothesis. *Nature* 186, 136–137. <https://doi.org/10.1038/186136a0>
- Horton, P., 2012. Optimization of light harvesting and photoprotection: molecular mechanisms and physiological consequences. *Philos. Trans. R. Soc. Lond. B. Biol. Sci.* 367, 3455–65. <https://doi.org/10.1098/rstb.2012.0069>
- Huang, W., Yang, Y.-J., Zhang, S.-B., Liu, T., 2018. Cyclic Electron Flow around Photosystem I Promotes ATP Synthesis Possibly Helping the Rapid Repair of Photodamaged Photosystem II at Low Light. *Front. Plant Sci.* 9, 239. <https://doi.org/10.3389/fpls.2018.00239>
- Ikeuchi, M., Tabata, S., 2001. *Synechocystis* sp. PCC 6803 - a useful tool in the study of the genetics of cyanobacteria. *Photosynth. Res.* 70, 73–83. <https://doi.org/10.1023/A:1013887908680>
- IPCC, 2007. Climate Change 2007 Synthesis Report. Intergov. Panel Clim. Chang. [Core Writ. Team IPCC 104. <https://doi.org/10.1256/004316502320517344>
- Iqbal, M., Grey, D., Stepan-Sarkissian, F., Fowler, M.W., 1993. A flat-sided photobioreactor for culturing microalgae. *Aquac. Eng.* 12, 183–190. [https://doi.org/10.1016/0144-8609\(93\)90010-9](https://doi.org/10.1016/0144-8609(93)90010-9)
- Jegerschöld, C., Virgin, I., Styring, S., 1990. Light-dependent degradation of the D1

protein in photosystem II is accelerated after inhibition of the water splitting reaction. *Biochemistry* 29, 6179–86.

Jordan, P., Fromme, P., Witt, H.T., Klukas, O., Saenger, W., Krauß, N., 2001. Three-dimensional structure of cyanobacterial photosystem I at 2.5 Å resolution. *Nature* 411, 909–917. <https://doi.org/10.1038/35082000>

Jung, J., Kim, H.-S., 1990. THE CHROMOPHORES AS ENDOGENOUS SENSITIZERS INVOLVED IN THE PHOTOGENERATION OF SINGLET OXYGEN IN SPINACH THYLAKOIDS. *Photochem. Photobiol.* 52, 1003–1009. <https://doi.org/10.1111/j.1751-1097.1990.tb01817.x>

Kallas, T., 1994. The Cytochrome b6f Complex, in: *The Molecular Biology of Cyanobacteria*. Springer Netherlands, Dordrecht, pp. 259–317. https://doi.org/10.1007/978-94-011-0227-8_9

Kaneko, T., Sato, S., Kotani, H., Tanaka, A., Asamizu, E., Nakamura, Y., Miyajima, N., Hirosawa, M., Sugiura, M., Sasamoto, S., Kimura, T., Hosouchi, T., Matsuno, A., Muraki, A., Nakazaki, N., Naruo, K., Okumura, S., Shimpo, S., Takeuchi, C., Wada, T., Watanabe, A., Yamada, M., Yasuda, M., Tabata, S., 1996. Sequence analysis of the genome of the unicellular cyanobacterium *Synechocystis* sp. strain PCC6803. II. Sequence determination of the entire genome and assignment of potential protein-coding regions. *DNA Res.* 3, 109–36.

Kim, J.-D., Lee, C.-G., 2005. Systemic optimization of microalgae for bioactive compound production. *Biotechnol. Bioprocess Eng.* 10, 418–424. <https://doi.org/10.1007/BF02989824>

Kirilovsky, D., 2015. Modulating energy arriving at photochemical reaction centers: Orange carotenoid protein-related photoprotection and state transitions. *Photosynth. Res.* 126, 3–17. <https://doi.org/10.1007/s11120-014-0031-7>

Krieger-Liszkay, A., Fufezan, C., Trebst, A., 2008. Singlet oxygen production in photosystem II and related protection mechanism. *Photosynth. Res.* 98, 551–564. <https://doi.org/10.1007/s11120-008-9349-3>

Kusama, Y., Inoue, S., Jimbo, H., Takaichi, S., Sonoike, K., Hihara, Y., Nishiyama, Y., 2014. Zeaxanthin and echinenone protect the repair of Photosystem II from inhibition by singlet oxygen in *synechocystis* sp. PCC 6803. *Plant Cell Physiol.* 56, 906–916. <https://doi.org/10.1093/pcp/pcv018>

- Lee, K.-S., Lo, Y.-S., Lo, Y.-C., Lin, P.-J., Chang, J.-S., 2004. Operation strategies for biohydrogen production with a high-rate anaerobic granular sludge bed bioreactor. *Enzyme Microb. Technol.* 35, 605–612. <https://doi.org/10.1016/J.ENZMICTEC.2004.08.013>
- Lee, Y.-K., Ding, S.-Y., Low, C.-S., Chang, Y.-C., Forday, W.L., Chew, P.-C., 1995. Design and performance of an α -type tubular photobioreactor for mass cultivation of microalgae. *J. Appl. Phycol.* 7, 47–51. <https://doi.org/10.1007/BF00003549>
- Li, H., Li, D., Yang, S., Xie, J., Zhao, J., 2006. The state transition mechanism—simply depending on light-on and -off in *Spirulina platensis*. <https://doi.org/10.1016/j.bbabi.2006.08.009>
- Liu, H., Zhang, H., Niedzwiedzki, D.M., Prado, M., He, G., Gross, M.L., Blankenship, R.E., 2013. Phycobilisomes Supply Excitations to Both Photosystems in a Megacomplex in Cyanobacteria. *Science* (80-.). 342, 1104–1107. <https://doi.org/10.1126/science.1242321>
- Liu, L.-N., 2016. Distribution and dynamics of electron transport complexes in cyanobacterial thylakoid membranes. *Biochim. Biophys. Acta* 1857, 256–65. <https://doi.org/10.1016/j.bbabi.2015.11.010>
- Los, D.A., Zorina, A., Sinetova, M., Kryazhov, S., Mironov, K., Zinchenko, V. V., 2010. Stress sensors and signal transducers in cyanobacteria. *Sensors* 10, 2386–2415. <https://doi.org/10.3390/s100302386>
- Luo, L., Yan, Y., Xu, Y., Xie, P., Sun, J., Guo, W., Yuan, J., 2013. Study of pressure fluctuations in an internal loop airlift bioreactor. *Can. J. Chem. Eng.* 91, 212–222. <https://doi.org/10.1002/cjce.21624>
- Matthews, H.D., Solomon, S., Pierrehumbert, R., 2012. Cumulative carbon as a policy framework for achieving climate stabilization. *Philos. Trans. A. Math. Phys. Eng. Sci.* 370, 4365–79. <https://doi.org/10.1098/rsta.2012.0064>
- McCarty, R.E., Hammes, G.G., 1987. Molecular architecture of chloroplast coupling factor 1. *Trends Biochem. Sci.* 12, 234–237. [https://doi.org/10.1016/0968-0004\(87\)90116-2](https://doi.org/10.1016/0968-0004(87)90116-2)
- Merchant, S., Sawaya, M.R., 2005. The light reactions: a guide to recent acquisitions for the picture gallery. *Plant Cell* 17, 648–63. <https://doi.org/10.1105/tpc.105.030676>

-
- Mimuro, M., Kikuchi, H., Murakami, A., 1999. Structure and function of phycobilisomes. *Photosynth. Photomorphogenes.* 104–135.
- Montgomery, B.L., 2014. The Regulation of Light Sensing and Light-Harvesting Impacts the Use of Cyanobacteria as Biotechnology Platforms. *Front. Bioeng. Biotechnol.* 2, 22. <https://doi.org/10.3389/fbioe.2014.00022>
- Mullineaux, C.W., Kirchhoff, H., Schneider, D., 2014. Electron transport and light-harvesting switches in cyanobacteria THE ENVIRONMENT IN AND AROUND CYANOBACTERIAL THYLAKOID MEMBRANES 18, 44–1. <https://doi.org/10.3389/fpls.2014.00007>
- Munekage, Y., Hojo, M., Meurer, J., Endo, T., Tasaka, M., Shikanai, T., 2002. PGR5 Is Involved in Cyclic Electron Flow around Photosystem I and Is Essential for Photoprotection in Arabidopsis. *Cell* 110, 361–371. [https://doi.org/10.1016/S0092-8674\(02\)00867-X](https://doi.org/10.1016/S0092-8674(02)00867-X)
- Napiwotzki, A., Bergmann, A., Decker, K., Legall, H., Eckert, H.-J., Eichle, H.-J., Renger, G., 1997. Acceptor side photoinhibition in PS II: On the possible effects of the functional integrity of the PS II donor side on photoinhibition of stable charge separation. *Photosynth. Res.* 52, 199–213. <https://doi.org/10.1023/A:1005897503276>
- Nelson, N., 2011. Photosystems and global effects of oxygenic photosynthesis. *Biochim. Biophys. Acta - Bioenerg.* 1807, 856–863. <https://doi.org/10.1016/j.bbabi.2010.10.011>
- Nelson, N., Ben-Shem, A., 2004. The complex architecture of oxygenic photosynthesis. *Nat. Rev. Mol. Cell Biol.* 5, 971–982. <https://doi.org/10.1038/nrm1525>
- Nguyen, K., Bruce, B.D., 2014. Growing green electricity: Progress and strategies for use of Photosystem I for sustainable photovoltaic energy conversion. *Biochim. Biophys. Acta - Bioenerg.* 1837, 1553–1566. <https://doi.org/10.1016/j.BBABIO.2013.12.013>
- Nishiyama, Y., Allakhverdiev, S.I., Murata, N., 2006. A new paradigm for the action of reactive oxygen species in the photoinhibition of photosystem II. *Biochim. Biophys. Acta - Bioenerg.* <https://doi.org/10.1016/j.bbabi.2006.05.013>
- Nishiyama, Y., Yamamoto, H., Allakhverdiev, S.I., Inaba, M., Yokota, A., Murata, N., 2001. Oxidative stress inhibits the repair of photodamage to the photosynthetic machinery. *EMBO J.* 20, 5587–94.

<https://doi.org/10.1093/emboj/20.20.5587>

- Ort, D.R., Melis, A., Melis, A., 2011. Optimizing antenna size to maximize photosynthetic efficiency. *Plant Physiol.* 155, 79–85. <https://doi.org/10.1104/pp.110.165886>
- Peretó, J., 2011. Oxygenic Photosynthesis, in: *Encyclopedia of Astrobiology*. Springer Berlin Heidelberg, Berlin, Heidelberg, pp. 1209–1209. https://doi.org/10.1007/978-3-642-11274-4_1721
- Pohl, P., Kohlhase, M., Martin, M., 1988. Photobioreactors for the axenic mass cultivation of microalgae. *Algal Biotechnol.* / Ed. by T. Stadler ... [et al.].
- Porankiewicz, J., Schelin, J., Clarke, A.K., 1998. The ATP-dependent Clp protease is essential for acclimation to UV-B and low temperature in the cyanobacterium *Synechococcus*. *Mol. Microbiol.* 29, 275–83.
- RENGER, G., VÖLKER, M., ECKERT, H.J., FROMME, R., HOHM-VEIT, S., GRÄBER, P., 1989. ON THE MECHANISM OF PHOTOSYSTEM II DETERIORATION BY UV-B IRRADIATION. *Photochem. Photobiol.* 49, 97–105. <https://doi.org/10.1111/j.1751-1097.1989.tb04083.x>
- Rg Degen, J., Uebele, A., Retze, A., Schmid-Staiger, U., Trö Sch, W., 2001. A novel airlift photobioreactor with baffles for improved light utilization through the flashing light effect. *J. Biotechnol.* 92, 89–94.
- Richmond, A., Cheng-Wu, Z., 2001. Optimization of a flat plate glass reactor for mass production of *Nannochloropsis* sp. outdoors. *J. Biotechnol.* 85, 259–69.
- Roach, T., Krieger-Liszkay, A., 2014. Regulation of photosynthetic electron transport and photoinhibition. *Curr. Protein Pept. Sci.* 15, 351–362. <https://doi.org/10.2174/1389203715666140327105143>
- Sánchez Mirón, A., Cerón García, M.-C., García Camacho, F., Molina Grima, E., Chisti, Y., 2002. Growth and biochemical characterization of microalgal biomass produced in bubble column and airlift photobioreactors: studies in fed-batch culture. *Enzyme Microb. Technol.* 31, 1015–1023. [https://doi.org/10.1016/S0141-0229\(02\)00229-6](https://doi.org/10.1016/S0141-0229(02)00229-6)
- Sánchez Mirón, A., García Camacho, F., Contreras Gómez, A., Grima, E.M., Chisti, Y., 2000. Bubble-column and airlift photobioreactors for algal culture. *AIChE J.* 46, 1872–1887. <https://doi.org/10.1002/aic.690460915>

- Saroussi, S.I., Wittkopp, T.M., Grossman, A.R., 2016. The Type II NADPH Dehydrogenase Facilitates Cyclic Electron Flow, Energy-Dependent Quenching, and Chlororespiratory Metabolism during Acclimation of *Chlamydomonas reinhardtii* to Nitrogen Deprivation. *Plant Physiol.* 170, 1975–1988. <https://doi.org/10.1104/pp.15.02014>
- Scherer, S., 1990. Do photosynthetic and respiratory electron transport chains share redox proteins? *Trends Biochem. Sci.* 15, 458–462. [https://doi.org/10.1016/0968-0004\(90\)90296-N](https://doi.org/10.1016/0968-0004(90)90296-N)
- Schopf, J.W., 2000. The Fossil Record: Tracing the Roots of the Cyanobacterial Lineage, in: *The Ecology of Cyanobacteria*. Kluwer Academic Publishers, Dordrecht, pp. 13–35. https://doi.org/10.1007/0-306-46855-7_2
- Schreiber, U., 2004. Pulse-Amplitude-Modulation (PAM) Fluorometry and Saturation Pulse Method: An Overview, in: *Chlorophyll a Fluorescence*. Springer Netherlands, Dordrecht, pp. 279–319. https://doi.org/10.1007/978-1-4020-3218-9_11
- Schröder, W.P., Åkerlund, H.-E., 1986. H₂O₂ accessibility to the Photosystem II donor side in protein-depleted inside-out thylakoids measured as flash-induced oxygen production. *Biochim. Biophys. Acta - Bioenerg.* 848, 359–363. [https://doi.org/10.1016/0005-2728\(86\)90211-2](https://doi.org/10.1016/0005-2728(86)90211-2)
- Seibert, M., Toon, S., Govindjee, O'Neil, M.P., Wasielewski, M.R., 1992. Primary charge separation in isolated photosystem II reaction centers. *Res. Photosynth.* II 41–44.
- Sherbinin, A. de, Carr, D., Cassels, S., Jiang, L., 2007. Population and Environment. *Annu. Rev. Environ. Resour.* 32, 345–373. <https://doi.org/10.1146/annurev.energy.32.041306.100243>
- Sims, R., Taylor, M., Jack, S., Mabee, W., 2008. From 1st to 2nd Generation Bio Fuel Technologies: An overview of current industry and RD&D activities. *IEA Bioenergy* 1–124. <https://doi.org/10.1128/AAC.03728-14>
- Singh, R.N., Sharma, S., 2012. Development of suitable photobioreactor for algae production – A review. *Renew. Sustain. Energy Rev.* 16, 2347–2353. <https://doi.org/10.1016/j.rser.2012.01.026>
- Styring, S., Virgin, I., Ehrenberg, A., Andersson, B., 1990. Strong light photoinhibition of electrontransport in Photosystem II. Impairment of the function of the first quinone acceptor, QA. *Biochim. Biophys. Acta - Bioenerg.*

1015, 269–278. [https://doi.org/10.1016/0005-2728\(90\)90031-X](https://doi.org/10.1016/0005-2728(90)90031-X)

Sukenik, A., Zohary, T., Padisák, J., 2009. Cyanoprokaryota and Other Prokaryotic Algae, in: *Encyclopedia of Inland Waters*. Elsevier, pp. 138–148. <https://doi.org/10.1016/B978-012370626-3.00133-2>

Takahashi, S., Murata, N., 2008. How do environmental stresses accelerate photoinhibition? *Trends Plant Sci.* 13, 178–182. <https://doi.org/10.1016/j.tplants.2008.01.005>

Takahashi, S., Murata, N., 2005. Interruption of the Calvin cycle inhibits the repair of Photosystem II from photodamage. *Biochim. Biophys. Acta - Bioenerg.* 1708, 352–361. <https://doi.org/10.1016/j.bbabi.2005.04.003>

Tamary, E., Kiss, V., Nevo, R., Adam, Z., Bernát, G., Rexroth, S., Rögner, M., Reich, Z., 2012. Structural and functional alterations of cyanobacterial phycobilisomes induced by high-light stress. *BBA - Bioenerg.* 1817, 319–327. <https://doi.org/10.1016/j.bbabi.2011.11.008>

Thomas, D.J., Thomas, J., Youderian, P.A., Herbert, S.K., 2001. Photoinhibition and Light-Induced Cyclic Electron Transport in *ndhB*– and *psaE*– Mutants of *Synechocystis* sp. PCC 6803. *Plant Cell Physiol.* 42, 803–812. <https://doi.org/10.1093/pcp/pce104>

Toole, C.M., Plank, T.L., Grossman, A.R., Anderson, L.K., 1998. Bilin deletions and subunit stability in cyanobacterial light-harvesting proteins. *Mol. Microbiol.* 30, 475–486. <https://doi.org/10.1046/j.1365-2958.1998.01082.x>

Torzillo, G., Chini Zittelli, G., 2015. Tubular Photobioreactors, in: *Algal Biorefineries*. Springer International Publishing, Cham, pp. 187–212. https://doi.org/10.1007/978-3-319-20200-6_5

Tóth, T.N., Chukhutsina, V., Domonkos, I., Knoppová, J., Komenda, J., Kis, M., Lénárt, Z., Garab, G., Kovács, L., Gombos, Z., Van Amerongen, H., 2015. Carotenoids are essential for the assembly of cyanobacterial photosynthetic complexes. *Biochim. Biophys. Acta - Bioenerg.* 1847, 1153–1165. <https://doi.org/10.1016/j.bbabi.2015.05.020>

Tredici, M.R., n.d. Mass Production of Microalgae: Photobioreactors, in: *Handbook of Microalgal Culture*. Blackwell Publishing Ltd, Oxford, UK, pp. 178–214. <https://doi.org/10.1002/9780470995280.ch9>

Tredici, Zittelli, 1998. Efficiency of sunlight utilization: tubular versus flat

photobioreactors. *Biotechnol. Bioeng.* 57, 187–97.

Tyystjärvi, E., 2008. Photoinhibition of Photosystem II and photodamage of the oxygen evolving manganese cluster. *Coord. Chem. Rev.* 252, 361–376. <https://doi.org/10.1016/j.ccr.2007.08.021>

UNFCCC. Conference of the Parties (COP), 2015. Paris Climate Change Conference- November 2015, COP 21. Adopt. Paris Agreement. Propos. by Pres. 21932, 32. <https://doi.org/FCCC/CP/2015/L.9/Rev.1>

Vass, I., Styring, S., Hundal, T., Koivuniemi, a, Aro, E., Andersson, B., 1992. Reversible and irreversible intermediates during photoinhibition of photosystem II: stable reduced QA species promote chlorophyll triplet formation. *Proc. Natl. Acad. Sci. U. S. A.* 89, 1408–1412. <https://doi.org/10.1073/pnas.89.4.1408>

Walker, J.E., Tybulewicz, V.L.J., 1985. Comparative genetics and biochemistry of light-driven ATP synthases.

Whitton, B.A., Potts, M., 2012. Introduction to the cyanobacteria, in: *Ecology of Cyanobacteria II: Their Diversity in Space and Time*. Kluwer Academic Publishers, Dordrecht, pp. 1–13. https://doi.org/10.1007/978-94-007-3855-3_1

Wilson, A., Punginelli, C., Gall, A., Bonetti, C., Alexandre, M., Routaboul, J.-M., Kerfeld, C.A., van Grondelle, R., Robert, B., Kennis, J.T.M., Kirilovsky, D., 2008. A photoactive carotenoid protein acting as light intensity sensor. *Proc. Natl. Acad. Sci.* 105, 12075–12080. <https://doi.org/10.1073/pnas.0804636105>

Yang Quan, Simo O. Pehkonen, and, Ray*, M.B., 2004. Evaluation of Three Different Lamp Emission Models Using Novel Application of Potassium Ferrioxalate Actinometry. <https://doi.org/10.1021/IE0304210>

Yoon, J.H., Sim, S.J., Kim, M.-S., Park, T.H., 2002. High cell density culture of *Anabaena variabilis* using repeated injections of carbon dioxide for the production of hydrogen. *Int. J. Hydrogen Energy* 27, 1265–1270. [https://doi.org/10.1016/S0360-3199\(02\)00109-X](https://doi.org/10.1016/S0360-3199(02)00109-X)

Yoon, J.J., Kim, Y.J., Kim, S.H., Ryu, H.J., Choi, J.Y., Kim, G.S., Shin, M.K., 2010. Production of Polysaccharides and Corresponding Sugars from Red Seaweed. *Adv. Mater. Res.* 93–94, 463–466. <https://doi.org/10.4028/www.scientific.net/AMR.93-94.463>

- Yoon, M., Choi, J., Lee, J.-W., Park, D.-H., 2012. Improvement of saccharification process for bioethanol production from *Undaria* sp. by gamma irradiation. *Radiat. Phys. Chem.* 81, 999–1002. <https://doi.org/10.1016/j.radphyschem.2011.11.035>
- Zakar, T., Laczko-Dobos, H., Toth, T.N., Gombos, Z., 2016. Carotenoids Assist in Cyanobacterial Photosystem II Assembly and Function. *Front. Plant Sci.* 7, 1–7. <https://doi.org/10.3389/fpls.2016.00295>
- Zhang, H., Liu, H., Blankenship, R.E., Gross, M.L., 2016. Isotope-Encoded Carboxyl Group Footprinting for Mass Spectrometry-Based Protein Conformational Studies. *J. Am. Soc. Mass Spectrom.* 27, 178–81. <https://doi.org/10.1007/s13361-015-1260-5>
- Zhang, P., Eisenhut, M., Brandt, A.-M., Carmel, D., Silén, H.M., Vass, I., Allahverdiyeva, Y., Salminen, T.A., Aro, E.-M., 2012. Operon *flv4-flv2* provides cyanobacterial photosystem II with flexibility of electron transfer. *Plant Cell* 24, 1952–71. <https://doi.org/10.1105/tpc.111.094417>

Aims

In this work I have studied the influence of varying light intensities on *Synechocystis* growth and its photosynthetic process by focusing my the attention on the photoinhibitory phenomena process.

- I have performed an analysis of the light intensity dependence of the growth of *Synechocystis* and the light distribution in a photobioreactor energized by 636 nm light.
- I have studied the response of the thylakoid proteome of *Synechocystis* to photoinhibitory intensities of orange-red light by performing mass spectrometry analysis.
- I performed a preliminary analysis on the photoinhibition of the Photosystem II and the turnover of the protein D1

Chapter 2

Analysis of the light intensity dependence of the growth of *Synechocystis* and the light distribution in a photobioreactor energized by 636 nm light

This chapter is based on joint work with Nivolò Vasile of the Istituto Italiano di Tecnologia of Turin

This chapter has been published as:

Alessandro Cordara, Angela Re, Cristina Pagliano, Pascal van Alphen, Raffaele Pirone, Guido Saracco, Filipe Branco dos Santos, Klaas J. Hellingwerf, Nicolò Vasile. (2018). Analysis of the light intensity dependence of the growth of *Synechocystis* and of the light distribution in a photobioreactor energized by 636 nm light. PeerJ,

Abstract

Synechocystis gathered momentum in modelling studies and biotechnological applications owing to multiple factors like fast growth, ability to fix carbon dioxide into valuable products, and the relative ease of genetic manipulation. *Synechocystis* physiology and metabolism, and consequently, the productivity of *Synechocystis* - based photobioreactors, are heavily light modulated. Here, we set up a turbidostat-controlled lab-scale cultivation system in order to study the influence of varying orange-red light intensities on *Synechocystis* growth characteristics and photosynthetic activity. *Synechocystis* growth and photosynthetic activity were found to raise as supplied light intensity increased up to 500 $\mu\text{mol photons m}^{-2} \text{s}^{-1}$ and to enter the photoinhibition state only at 800 $\mu\text{mol photons m}^{-2} \text{s}^{-1}$. Interestingly, reverting the light to a non-photo-inhibiting intensity unveiled *Synechocystis* to be able to promptly recover. Furthermore, our characterization displayed a clear correlation between variations in growth rate and cell size, extending a phenomenon previously observed in other cyanobacteria. Further, we applied a modelling approach to simulate the effects produced by varying the incident light intensity on its local distribution within the photobioreactor vessel. Our model simulations suggested that the photosynthetic activity of *Synechocystis* could be enhanced by finely regulating the intensity of the light incident on the photobioreactor in order to prevent cells from experiencing light-induced stress and induce their exploitation of areas of different local light intensity formed in the vessel. In the latter case, the heterogeneous distribution of the local light intensity would allow *Synechocystis* for an optimized usage of light.

2.1 Introduction

Synechocystis was the first photosynthetic organism to have its genome fully sequenced (Kaneko et al., 1996). A wealth of transcriptomic (Anfelt et al., 2013; Beck et al., 2014; Angermayr et al., 2016), proteomic (Fang et al., 2016) and metabolomic (Yang, Hua & Shimizu, 2002; Yoshikawa et al., 2013), studies allowed to investigate *Synechocystis* regulatory, signalling and metabolic pathways in finer details than in any other cyanobacterium. *Synechocystis* has attracted much interest as model organism in product-oriented industrial biotechnology due to the ability to effortlessly recycle carbon dioxide (CO₂) into valuable fuels and chemicals, the simplicity of its culture conditions, the ease of genetic manipulation and its relatively fast cell growth compared to higher plants (Janssen et al., 2003; Angermayr, Hellingwerf & Teixeira de Mattos, 2009). Genetic engineering of cyanobacteria has demonstrated the opportunity to channel solar energy into the formation of various commodity products (Angermayr, Gorchs Rovira & Hellingwerf, 2015; Zhou et al., 2016). In the last decades, *Synechocystis* has served in many genetic engineering studies as biofactory for the production of a variety of products (Yu et al., 2013a; Singh et al., 2017), such as ethanol (Gao et al., 2012), isobutanol (Varman et al., 2013), lactate (Angermayr, Paszota & Hellingwerf, 2012; Joseph et al.) and polyhydroxyalkanoate (Luengo et al., 2003), which can be widely utilized in biotechnology and industrial fields. The intensive exploitation of this microorganism for industrial uses strongly depends on the choice of optimal growth conditions, main operational parameters including culture density (Esteves-Ferreira et al., 2017; Straka & Rittmann, 2018), pH (Touloupakis et al., 2016), temperature (Panda et al., 2006), mixing rate and light environment (Touloupakis et al., 2016; Singh et al., 2009a). Even though extensive investigation showed that *Synechocystis* productivity is sensitive to most of the aforementioned operational parameters (Yu et al., 2013; Burrows & Wong, 2009; Nanjo et al., 2010; Chaves, Kirst & Melis, 2015), it is undoubted that productivity is tightly coupled with the light absorption efficiency of optical energy conversion systems. Therefore, light management during *Synechocystis* cultivation in photobioreactors (PBRs) is by far the most remarkable factor to account for in order to boost the practical exploitation of this microorganism. *Synechocystis* is able to absorb energy across the visible spectrum, mainly through three classes of pigments: bilins (Gan and Bryant, 2015), chlorophyll a (Chl a), which is associated with Photosystem II (PSII) and Photosystem I (PSI) reaction centre cores (Vermaas, 1996), and carotenoids (Glazer, 1977; Colyer et al., 2005). Achieving high performance in PBRs requires high intensity light, which nonetheless can cause light associated damages. A

number of studies sought to dilute the supplied light intensity by optimizing the light spectra distribution. These attempts were encouraged by the integration of light emitting diodes (LEDs) within indoor PBRs (Ooms et al., 2017). Tailoring light wavelength spectrum affords improved growth conditions stability and reproducibility and has been shown to lead to concrete achievements in biomass productivity and ultimately in the accumulation of useful products. For example, a perfect fit of the red light with the absorption peak of the Chl a and phycocyanobilin was observed to lead to an increased growth in cyanobacteria during cultivation (Wyman & Fay, 1986; Wang, Fu & Liu, 2007; Pcc & Alphen, 2018). In other cases, dynamic adjustments of light wavelength during cultivation of *Chlorella vulgaris* and *Haematococcus pluvialis* allowed to increase the microorganism productivity (Katsuda et al., 2004). It is well known that the exposure of photosynthetic organisms to strong solar irradiation results in inhibition of the electron transfer activity of PSII, referred to as photoinhibition responses (Powles, 1984). This phenomenon derives from an imbalance between the photodamage brought to PSII and the repair mechanisms for such damage (Murata et al., 2007). Despite the numerous studies conducted on this topic highlight that the main target of photoinhibition is the D1 protein of PSII reaction centre (Tyystjärvi, 2013), the molecular mechanisms of PSII photoinhibition are not yet completely understood. Upon exposure of photosynthetic organisms to strong irradiation, two mechanisms contribute to the photodamage of PSII, which are called acceptor-side and donor-side photoinhibition. In the acceptor-side mechanism, strong illumination causes the over-reduction of PSII, due to the double reduction of the primary quinone acceptor (QA) that, in such condition, can no longer serve as an electron carrier. The recombination between the doubled reduced form of QA and the primary radical pair P680⁺ and Pheo⁻ leads to the formation of the triplet state of the P680, which can react with molecular oxygen leading to generation of the reactive form of oxygen (ROS) singlet oxygen (¹O₂) (Mulo et al., 1998; Vass et al., 1992b). Due to the extremely short lifetime of this ROS, ¹O₂ is thought to impair mainly the proteins and lipids nearby its production site (Triantaphylidès and Havaux, 2009). Conversely, the donor-side photoinhibition is not mediated by ROS and occurs when the reduction of the PSII is slower than its oxidation, due to inactivation of the oxygen evolving system. This leads to an extended lifetime of the radicals TyrZ⁺ and P680⁺ that act as strong oxidants against the surrounding proteins and lipids, resulting in a damage to the PSII (Bumann and Oesterhelt, 1995a). In this work, we investigated the effect of increasing intensities (in the range 50-1460 $\mu\text{mol photons m}^{-2} \text{s}^{-1}$) of orange-red light on the autotrophic growth of *Synechocystis* in a turbidostat-controlled lab scale PBR. Monitoring *Synechocystis* physiological

state under varying light regimes, we found that growth rate, cell size and PSII activity were influenced by light intensity, albeit in slightly different ways. *Synechocystis* cells proved to be resilient to high light stress conditions, suffering photoinhibition only above 800 $\mu\text{mol photons m}^{-2} \text{ s}^{-1}$, and showed a remarkable ability to recover from the complete state of photoinhibition experienced at 1460 $\mu\text{mol photons m}^{-2} \text{ s}^{-1}$ when reverting light to 200 $\mu\text{mol photons m}^{-2} \text{ s}^{-1}$. Further, we combined the experimental analyses with system modelling and the related multi-physics analysis to investigate the influence of local light intensity distribution on photoinhibition of microorganism.

2.2 Material and Methods

2.2.1 Strain and preculture conditions

For all experiments, we used wild-type *Synechocystis* sp. PCC 6803, a glucose-tolerant derivative kindly provided by Devaki Bhaya (Department of Plant Biology, Carnegie Institution for Science, Stanford, California, USA). The cells were grown in flasks in 25 ml of BG11 medium (Stanier et al., 1971) with a modified protocol as described in (Van Alphen and Hellingwerf, 2015). Precultures were grown for 4 days at 30°C in a shaking incubator at 120 rpm (New Brunswick Innova 44) under constant illumination of orange-red (632 nm) and blue (451 nm) light (10:1 photon ratio) at 30 $\mu\text{mol photons m}^{-2} \text{ s}^{-1}$, measured with a LI-250 quantum sensor (LI-COR, USA).

2.2.2 PBR growth conditions

A *Synechocystis* preculture was used to seed the PBR. The culture was grown in a flat panel PBR model FMT150.2/400 Photon System Instruments (Nedbal et al., 2008) in a final volume of approximately 380 ml in the BG-11 medium modified as described above, supplemented with 10 mM of NaHCO_3 . The cyanobacterial suspension was illuminated from one side with orange-red light (636 nm) by high-power LEDs. The light regimes applied by the LED board provided cells with the following light intensities as measured outside the PBR, opposite of and at the centre of the light panel: 50, 200, 300, 500, 800, 950 and 1460 $\mu\text{mol photons m}^{-2} \text{ s}^{-1}$. The cells were subjected to increasing light intensity every 24 h. The 24 h period of light acclimation was sufficient for establishing stable (variance < 1%) growth rate and dissolved oxygen in the culture medium for each light intensity except for

the light regime of $1460 \mu\text{mol photons m}^{-2} \text{s}^{-1}$, where stable values were not obtained. The temperature and pH were kept constant at 30°C and 8.0, respectively, by automatically adjusting pCO_2 using a gas mixing system GMS150 (Photon Systems Instruments). CO_2 was provided in a mixture with N_2 with a gas flow of 150 ml min^{-1} controlled by a mass flow controller (Smart Mass Flow Model 5850S, Brooks Instruments). The PBR was run in turbidostat mode with the OD_{720} , measured by the integrated densitometer, calibrated to the bench-top spectrophotometer OD_{730} to maintain the OD_{730} at approximately 0.4 (turbidostat set to a maximum deviation of 3%) at $50 \mu\text{mol photons m}^{-2} \text{s}^{-1}$. The turbidostat mode allowed the culture to hold cell density constant and to remain in exponential phase under all tested light conditions. Dissolved molecular oxygen was normalized to the values obtained at $50 \mu\text{mol photons m}^{-2} \text{s}^{-1}$.

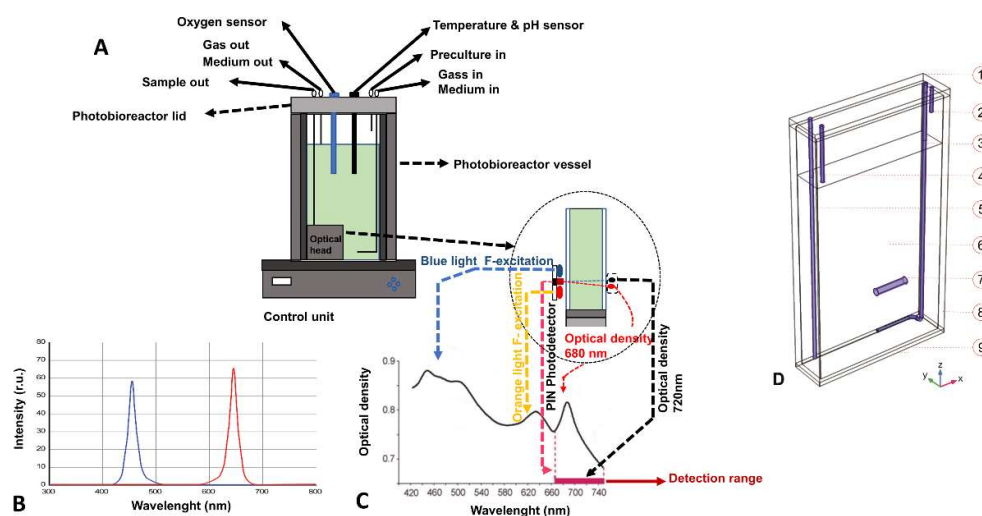


Figure 2.1. Photobioreactor schematic representation. **A:** Body of the flat panel PBR FTM150 composed of a 390 ml transparent removable flat vessel. On top of the vessel, a stainless lid accommodates different tubes, connectors and sensors. The base of the instrument contains a control unit with analogic and digital electronic circuits. Enlarged the details of the red and blue LEDs installed in the light panel of the reactor, the densitometer and the fluorometer. **B:** Red and blue LED spectra of PBR FMT150. **C:** Transmission spectrum of cyanobacterial culture affected by light absorptions, light scattering. The lines and arrows indicate wavelength of the light sources present in the flat panel reactor and the detection range of the detector filter. **D:** 3D modelled geometry of PBR with modelled domains selection: 1-closing, 2-inoculum, 3-sparger, 4-air, 5-sampling, 6-culture, 7-stirring bar, 8-wall of vessel, 9-base of vessel.

2.2.3 Dry weight, cell size and count measurements

At the end of each 24 h step of light increment, 22 ml of culture were harvested to perform in parallel dry weight measurements and cell size analysis. For the determination of dry cell weight, cellulose acetate membranes (0.2 μm , Whatman) were washed with milli-Q water (Merck Millipore Reference), left to dry for 24 h at 90°C in a stove (Electrolux) and weighted with an analytical balance (AB204, Mettler Toledo). Subsequently, the membranes were used for filtering 20 ml of sampled culture. After washing once with milli-Q water to remove salts, the membrane filter was left to dry overnight in the stove at 90°C and finally weighted again. In parallel, the OD₇₃₀ of the sampled cells was measured with a spectrophotometer (Lightwave II, Biochrom) and used to normalize the dry cell weight per OD₇₃₀. The average cell size and cell number were measured with the CASY counter instrument (Roche Applied Science). A volume of 20 μl of harvested culture was diluted with 10 ml of CASY ton solution. The average cell size was measured working in a range of calibration between 0-5 μm with a capillary of 60 μm .

2.2.4 Model description

The 3D multi-physics model of the PBR was developed on the COMSOL 5.3® platform and allowed us to simulate different phenomena such as fluid dynamic, light transmission in different media, cyanobacterial growth kinetics and mass transfer by formulating the corresponding equations. **Fig. 1D** shows the design of the 3D model based on the reactor geometry. Free tetrahedral meshing was applied to the created model prior to analysis. Meshing size was selected in order to prevent inaccuracy and imprecision of modelling resulting from model meshing.

2.2.4.1 Assumptions, inlet and boundary conditions

To solve the different mass balances and kinetic equations, it is necessary to state the initial and boundary conditions, which include inlet, outlet and wall conditions, and also to discuss the different assumptions, which clarify the limitations of the created model:

- i. the inlet velocity of recycling gas was measured experimentally. As there is no liquid exchanging during experiments, the liquid velocity in the inlet/outlet area is equal to 0;

-
- ii. the mass transfer between liquid culture and gas is considered;
 - iii. all conditions in the model of the PBR, where both liquid and gas phases are present, were formulated by assuming the gas flux at the reactor boundaries negligible and by setting the liquid velocity at the reactor surface wall different from zero. Slip conditions were applied to all PBR walls;
 - iv. since only CO₂/N₂ gas mixture flows through the sparger, its fluid-dynamic model assumed a single phase to be present. Therefore, the wall conditions used for gas flow were slip conditions, which assume that the gas velocity at the sparger solid surface is calculated by the mathematical model;
 - v. the working conditions have to be furnished to the model: temperature, inlet gas velocity (or flow rate), initial, inlet and outlet pressure, amount of initial microorganisms and nutrients;
 - vi. the influence of nutrient concentration, temperature and light intensity on cyanobacterial growth rate are all considered.

2.2.4.2 Mathematical models

The mathematical model is described in the following sections. All the variables and parameters employed in the equations are listed and described in the Nomenclature as well as in Table S1. To estimate the necessary parameters, we relied on experimentally determined values or on an inference procedure by fitting model simulations to observed data. Specifically, we compared simulated and experimental data using a statistical analysis of errors based on the Levenberg-Marquardt method, coupled with the second least-squares analysis. Since the method implements a constrained search procedure, it requires specifying lower and upper bounds on the unknown parameters, which were selected within the ranges of values most frequently observed in literature. The parameter space exploration stopped when the model simulation best fit the experimental data.

2.2.4.3 Fluid-dynamic equations

We generally need to model different domains inside the bioreactor: a gas-liquid mixture inside the vessel, and a single gas phase inside the sparger domain. Therefore, the continuity equations and the momentum balance equations need to be adapted depending on the modelled domain.

The general double-phase fluid dynamic continuity equations are formulated through Eqs. (1-3) and allow to account for the coexistence of the bubble gas phase

(dispersed phase, named by “d” as subscript) and the liquid phase (continuous phase, named by “c” as subscript):

$$(\rho_c - \rho_d) \left[\nabla \cdot (\Phi_d(1 - c_d)\mathbf{u}_{slip} - D_{md}\nabla \cdot \Phi_d) + \frac{m_{dc}}{\rho_d} \right] + \rho_c(\nabla \cdot \mathbf{u}) = 0 \quad (1)$$

$$\mathbf{u} = \frac{\phi_c \rho_c \mathbf{u}_c + \phi_d \rho_d \mathbf{u}_d}{\rho} \quad (2)$$

$$\phi_c + \phi_d = 1 \quad (3)$$

where **Eq. (1)** is the continuity equation, **Eq. (2)** expresses the velocity vector \mathbf{u} , Φ_c and Φ_d are the volume fractions corresponding to liquid and gas phases respectively, and ρ is the pseudo-continuous phase density. **Eq. (3)** describes the relation between the volume fractions for the continuous Φ_c and dispersed Φ_d phases.

As to the sparger, since a single gas phase exists, we modelled the fluid dynamic variables trends accounting only for the terms of the (**Eq. 1**) related to the gas phase, which is expressed by the following equation:

$$\frac{\partial \rho_g}{\partial t} + \nabla \cdot (\rho \mathbf{u})_g = 0 \quad (4)$$

Regarding the momentum balance equations, we adopted the Navier–Stokes model for the liquid–gas multiphase system, by using the following formulation (Li et al., 2014)

$$\frac{\partial(\rho \mathbf{u})}{\partial t} + \nabla \cdot (\rho \mathbf{u} \mathbf{u}) = -\nabla p - \nabla \cdot \boldsymbol{\tau} + \rho \mathbf{g} + \mathbf{F} \quad (5)$$

$$\boldsymbol{\tau} = -\mu \left[(\nabla \mathbf{u} + (\nabla \mathbf{u})^T) - \frac{2}{3} (\nabla \cdot \mathbf{u}) \mathbf{I} \right] \quad (6)$$

where p is the pressure, g is the gravity acceleration vector, $\boldsymbol{\tau}$ is the stress tensor and μ is the effective viscosity. For the single-phase sparger model, the momentum balance equations are similar to **Eq.(5)**, where we replaced the effective viscosity with the gas viscosity.

In **Eq.(5)**, the effective viscosity includes not only the molecular viscosity μ_i but also turbulent viscosity $\mu_{i,T}$ (Luo and Al-Dahhan, 2011), which accounts for the influence exerted by the turbulent flow **Eq.(7)**.

Among the several models introduced to handle the turbulent viscosity, we adopted the standard $k-\varepsilon$ model to simulate the turbulent flow of the fluid entrained with cyanobacteria in the mechanically stirred PBR. The standard $k-\varepsilon$ turbulent model is computationally stable, even in the presence of complex physics, and is applicable to a wide variety of turbulent flows.

The equations to calculate the effective viscosity within the $k-\varepsilon$ model are listed below:

$$\mu_{eff} = \mu_i + \mu_{i,T} \quad (7)$$

$$\mu_T = \rho C_\mu \frac{k^2}{\varepsilon} \quad (8)$$

where C_μ is a model constant equals to 0.09 and k is the turbulence kinetic energy which can be calculated by the transport equations (Ali, 2014)

$$\rho \frac{\partial k}{\partial t} + \rho \mathbf{u} \cdot \nabla k = \nabla \cdot \left(\left(\mu + \frac{\mu_T}{\sigma_k} \right) \nabla k \right) + \mathbf{P}_k - \rho \varepsilon \quad (9)$$

Where σ_k is a model constant equals to 1.0, derived from (Wilcox, 1993). To obtain the P_k values we used **Eq.(10)**

$$\mathbf{P}_k = \mu_T \left(\nabla \mathbf{u} (\nabla \mathbf{u} + (\nabla \mathbf{u})^T) - \frac{2}{3} (\nabla \cdot \mathbf{u})^2 \right) - \frac{2}{3} \rho k \nabla \cdot \mathbf{u} \quad (10)$$

where the value of turbulent energy dissipation rate ε was calculated by **Eq.(11)**:

$$\rho \frac{\partial \varepsilon}{\partial t} + \rho \mathbf{u} \cdot \nabla \varepsilon = \nabla \cdot \left(\left(\mu + \frac{\mu_T}{\sigma_\varepsilon} \right) \nabla \varepsilon \right) + C_{\varepsilon 1} \frac{\varepsilon}{k} \mathbf{P}_k - C_{\varepsilon 2} \rho \frac{\varepsilon^2}{k} \quad (11)$$

In this equation, $C_{\varepsilon 1}$ and $C_{\varepsilon 2}$ are constants equal to 1.44 and 1.92, respectively. Finally, in a turbulent bubbly flow model, the difference between gas velocity and liquid velocity consists of two terms: slip velocity and drift velocity (**Eq. (12)**):

$$\mathbf{u}_d - \mathbf{u}_c = \mathbf{u}_{slip} - \frac{D_{md}}{(1-c_d)\Phi_d} \quad (12)$$

The slip velocity \mathbf{u}_{slip} represents the relative velocity of the phases and the drift velocity is the additional velocity appearing when turbulence is taken into account. The drift velocity can be calculated by **Eq.(13)**, whereas the slip velocity can be calculated by using a pressure–drag balance (**Eq.(14)**):

$$u_{drift} = - \frac{D_{md}}{(1-c_d)} \nabla \Phi_d$$

(13)

$$\frac{3C_{drag}}{4d_b} |u_{slip}| u_{slip} \rho_l = -\nabla p$$

(14)

where the drag coefficient C_{drag} can be computed by different formulas (Hartmann et al., 2013). In our case, C_d was computed by **Eq.(15)**:

$$C_d = \frac{0.622}{\frac{\xi}{g\rho_l d_b^2} + 0.235}$$

(15)

where ζ is the surface tension coefficient and d_b is the average bubble diameter which was measured as 3 mm through video imaging ($d_b = 3$ mm).

2.2.4.4 Heat transfer with radiation: light transmission equations

The balance of the radiative intensity, including contributions regarding propagation, emission, absorption and scattering is formulated through the general radiative transfer equation (Modest, 2003) and can be written as follows:

$$\Omega \cdot \nabla I(\Omega) = \kappa I_b(T) - \beta I(\Omega) + \frac{\sigma_S}{4\pi} \int_{4\pi} I(\Omega') \Phi(\Omega', \Omega) d\Omega'$$

(16)

To account for the effect mediated by the bubble volume fraction and cyanobacterial cell concentration, we adapted the Lambert-Beer's law:

$$\frac{I}{I_0} = \exp(-\beta z) \quad (17)$$

where I is the local light intensity and I_0 represents the incident light intensity, β is the extinction coefficient and z represents the path-length of the light through the material. Eq. (17) does not account either for the light scattering by bubbles, which change the direction of light transmission, either for the light absorption by cyanobacteria [51]. Therefore, we modified Eq. 17 as follows:

$$\frac{I}{I_0} = \exp\left(-\left(\frac{\beta S}{4} + K_a\right)z\right) \quad (18)$$

Eq. (18) accounts for light absorption by *Synechocystis* cells by means of K_a , which is the absorption coefficient associated with cyanobacteria, and for the scattering associated with the bubble volume fraction through S , the interfacial area per unit volume which is a function of bubble size and bubble number density. By replacing the interfacial area with the bubble volume fraction ϕ_d and the bubble diameter, d_b , **Eq. (18)** is converted in the equation **Eq. (19)**:

$$\frac{I}{I_0} = \exp\left(-\frac{3\phi_d z}{d_b} - K_a z\right) \quad (19)$$

The difference between **Eq. (17)** and **Eq. (19)** is the effect of cyanobacteria light absorption on local light intensity distribution. The average diameter of bubbles was calculated by using the video imaging technique and performing the procedure described in (Ali, 2014; Zhang, Dechatiwongse & Hellgardt, 2015). **Eq. (19)** was then used in the general radiative transfer equation.

Calculating the radiative heat source requires information on the temperature regime throughout the entire vessel domain, which is obtained solving the general heat transfer balance equation. The general heat transfer balance (Bird et al., 2006), which takes into account the radiation in participating media, is expressed in **Eq.(20)**

$$\rho C_p \frac{\partial T}{\partial t} + \rho C_p \mathbf{u} \cdot \nabla T + \nabla \cdot \mathbf{q} = Q + Q_r$$

(20)

where Q_r is the radiative heat source expressed as **Eq.(21)**

$$Q_r = \kappa(G - 4\pi I_b)$$

(21)

2.2.4.5 Kinetic models and calculation theory: cyanobacterial growth equations

Generally, cyanobacterial growth rate is strongly influenced by various factors such as temperature, light intensity and nutrient concentration. Temperature usually affects the activity of enzymes involved in the cellular duplication, whereas light intensity determines the energy that cells can absorb for their maintenance and growth. Nutrient elements including sulphur, carbon, phosphorus and nitrogen are necessary for cyanobacteria to compose their biomass (Dechatiwongse et al., 2014).

The kinetics of cyanobacterial growth is usually defined by the Monod model, **Eq.(22)**, which only considers the effect of nutrient concentration (Vatcheva et al., 2006), because additional environmental parameters such as temperature and light intensity are always kept constant during experiments (Solimeno et al., 2015). In the Monod model, as shown in **Eq.(22)**, the maximum specific growth rate μ_{max} is treated as a constant, but in reality it is a function of light intensity and temperature. When nutrients are in excess, the growth rate is independent of nutrient concentration and expressed as:

$$\mu_{gr} = \mu_{max} \frac{C}{k_s + C}$$

(22)

where C is the concentration of the limiting substrate for growth. In order to take into account also the effects exerted by nutrients and local light intensity on

cyanobacterial growth kinetics, we decided to evaluate a modified Monod equation: the Aiba model (Aiba, 1982).

The Aiba model, shown in **Eq.(23)**, is usually employed to simulate the effect of light intensity on cyanobacterial growth rate: it is capable of modelling the photo-limitation regime under low light intensity, the photo-saturation regime under optimal light intensity, and the photo-inhibition regime under intense light intensity (D. Zhang et al., 2015). Similarly, the model can also be applied to describe the photo-dependence of the oxygen production rate.

In this equation:

$$\mu_{gr} = \frac{\mu_{max} \cdot I}{I + k_s + \frac{I^2}{k_i}} \quad (23)$$

μ_{max} is the maximum growth rate, and k_s and k_i refer to the light saturation and photo-inhibition, respectively. These parameters are only dependent on cyanobacterial properties and were fitted from experimental observations. All the variables and parameters used in the mathematical models are listed and explained in the nomenclature and in Table S1 of Supporting Information.

2.3 Results and discussion

2.3.1 Growth rate, oxygen evolution activity and dimension of cells are regulated by light intensity

During cultivation, orange-red light was used since it resulted in an optimal light regime for growing *Synechocystis* in our PBRs system. Conversely, light with wavelengths lower than 580 nm (green-blue) or higher than 670 nm (far-red) proved to be not efficient for its growth (Singh et al., 2009a). This knowledge served as a prerequisite to set up experiments aiming to quantitatively evaluate the effects of increasing intensities, ranging between 50-1460 $\mu\text{mol photons m}^{-2} \text{ s}^{-1}$, of red-orange light on the adjustments of the physiological state in *Synechocystis*. We studied the long-term photoinhibition in *Synechocystis* grown at increasing light intensities by

analysing changes in the growth rate, the physiological parameter of oxygen evolution activity and the cell size at each incremental step of light intensity. By running the PBR in turbidostat mode, *Synechocystis* was grown in a semi-continuous regime so that cells were constantly maintained in the exponential growth phase. The absence of a change in growth rate between successive measurements of less than 2 % was used as actual criterion for evaluating the achievement of the steady state. In Fig.2.2 it is possible to observe that, for each light changes , the steady state was reached in less than 24h.

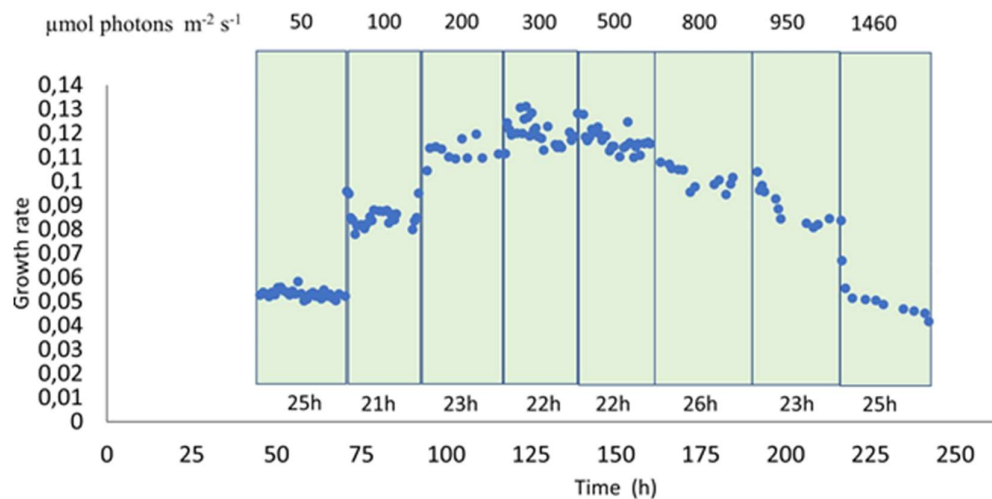


Fig. 2.2 Shown is the growth rate as a function of time. For each light intensity (top side) the growth rate (blue dots) reached the steady state within the 24 h. The time between 0 and 50 h was needed for the culture, after inoculation at low cell density, to reach the right turbidity in order to be able to activate the turbidostat regime.

Firstly, we measured *Synechocystis* growth rate to evaluate its generation time, and the amount of oxygen dissolved in the medium (dO_2), which provides an indication of the PSII activity within cell (Schuurmans et al., 2015). Both the growth rate of *Synechocystis* (Fig. 2.3A) and the dissolved oxygen produced by the cells (Fig. 2.3B) were clearly affected by increasing light intensity.

The dynamics of both variables could be broadly partitioned into four phases: an initial phase at $50 \mu\text{mol photons m}^{-2} \text{s}^{-1}$ where cells were not photoinhibited, a second phase up to $500 \mu\text{mol photons m}^{-2} \text{s}^{-1}$, where *Synechocystis* cells doubling time and PSII activity attained their maximum values, a third photoinhibitory phase up to $1460 \mu\text{mol photons m}^{-2} \text{s}^{-1}$ where both parameters dropped off, and a final

recovery phase at $200 \mu\text{mol photons m}^{-2} \text{s}^{-1}$. Hereafter, the photon irradiance of $50 \mu\text{mol photons m}^{-2} \text{s}^{-1}$, was considered the control photon irradiance. At this light condition, cells featured a relatively slow metabolism, as evidenced by the modest growth rate of $0.054 \pm 0.003 \text{ h}^{-1}$ (corresponding to a doubling time of $\approx 13 \text{ h}$) and a limited level of oxygen dissolved in the medium (roughly $35 \mu\text{M}$).

This dissolved oxygen concentration at this photon irradiance was used as reference to normalize the measurements at all sampled points (normalized reference value at one). At a photon irradiance of $200 \mu\text{mol photons m}^{-2} \text{s}^{-1}$ *Synechocystis* grew two times faster than in the control light condition, showing a growth rate of $0.114 \pm 0.005 \text{ h}^{-1}$ (corresponding to a doubling time of $\approx 6 \text{ h}$), as shown in Fig. 2.3A.

When photon irradiance was increased up to 300 and 500 $\mu\text{mol photons m}^{-2} \text{s}^{-1}$, the growth rate remained constant yielding values of $0.117 \pm 0.006 \text{ h}^{-1}$ and $0.114 \pm 0.005 \text{ h}^{-1}$, respectively. Switching photon irradiance from 50 to 200 $\mu\text{mol photons m}^{-2} \text{s}^{-1}$ led to a higher than two-fold increase in the relative amount of oxygen dissolved in the medium (from 1.00 ± 0.02 to 2.22 ± 0.07 , as shown in Fig. 2.3B), similarly to the trend displayed by growth rate.

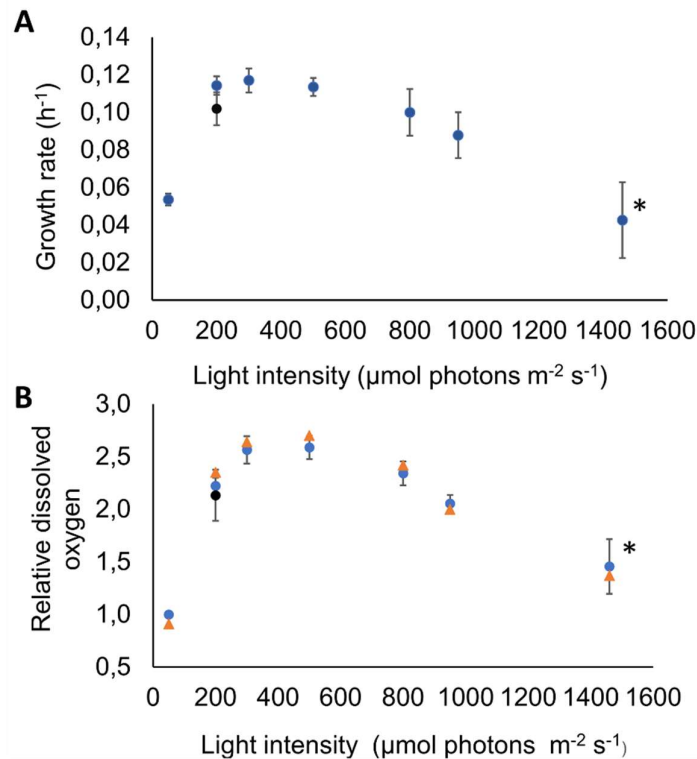


Fig 2.3. Challenging *Synechocystis* by high light intensity revealed its adaptive capacity. *Synechocystis* behaviour was assessed by quantifying the growth rate and the

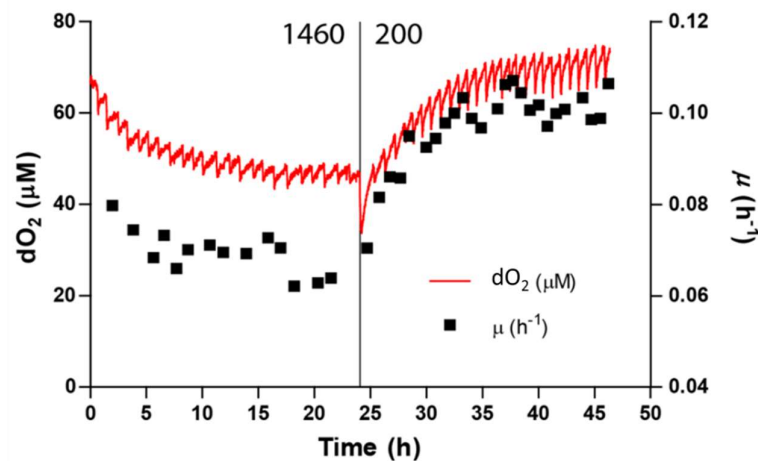
relative concentration of dissolved oxygen in the medium under increasing photon irradiance. The turbidostat-controlled cultures were grown at constant temperature (30°C) and pH (8.0) under orange-red light and acclimated for 24 h at each light intensity. The figure shows *Synechocystis* ability to fully recover after passing through a complete state of photoinhibition at 1460 $\mu\text{mol photons m}^{-2} \text{s}^{-1}$. **A:** Growth rate of *Synechocystis* evaluated at each light intensity. **B:** Oxygen released in the medium of the PBR by *Synechocystis*. The blue dots show the mean values derived from three biological replicates and are accompanied by their respective standard deviation bars. Data were normalized to the values obtained at 50 $\mu\text{mol photons m}^{-2} \text{s}^{-1}$. The orange triangles show the simulated values according to our PBR model. (•) stands for point of recovery which was set at 200 $\mu\text{mol photons m}^{-2} \text{s}^{-1}$. The recovery point is coloured in black in both panels. The asterisk indicates no steady state could be reached in 24 h at this condition, as shown by the large error bars.

However, differently from the *Synechocystis* growth rate, when we increased photon irradiance to 300 $\mu\text{mol photons m}^{-2} \text{s}^{-1}$, the relative concentration of oxygen kept increasing up to 2.56 ± 0.12 . Such difference in growth rate and dO_2 within the photon irradiance range from 200 and 300 $\mu\text{mol photons m}^{-2} \text{s}^{-1}$ suggests that light could exert different effects on the PSII functionality and the doubling time of the microorganism. In particular, the increase in dO_2 concentration measured in the cultivation medium could indicate a fine tuning of the light/energy conversion by PSII, whereas the unvaried growth rate observed could result from a limited utilization of the light energy absorbed (Kramer and Evans, 2011).

At a photon irradiance of 800 $\mu\text{mol photons m}^{-2} \text{s}^{-1}$ a substantial decrease was observed for both growth rate ($0.1 \pm 0.012 \text{ h}^{-1}$ corresponding to a doubling time of $\approx 7 \text{ h}$) and relative amount of dO_2 (2.34 ± 0.11), denoting a light intensity where *Synechocystis* cells started to get photoinhibited. Further increasing the photon irradiance up to 1460 $\mu\text{mol photons m}^{-2} \text{s}^{-1}$, *Synechocystis* growth rate dropped off to $0.043 \pm 0.020 \text{ h}^{-1}$ (corresponding to a doubling time of $\approx 16 \text{ h}$), representing roughly half of the maximum growth rate observed in our experimental set up. Furthermore, over the 24 hours acclimation period at this extreme light treatment, the growth rate was found to be constantly decreasing thus highlighting a severe state of growth inhibition. Together with the growth rate, the relative dO_2 reached its minimum of 1.45 ± 0.23 at 1460 $\mu\text{mol photons m}^{-2} \text{s}^{-1}$.

These results evidenced severe PSII photodamage caused in *Synechocystis* by its exposure to high light intensity, in accordance with extensive literature available for cyanobacteria (see review (Murata et al., 2007) and references therein). To test whether, upon photoinhibition, lowering light intensity could recover the growth rate of *Synechocystis*, a point of recovery was set to the lowest light irradiance at

which the maximal growth rate was observed (i.e. $200 \mu\text{mol photons m}^{-2} \text{s}^{-1}$). Upon reverting the photon irradiance to $200 \mu\text{mol photons m}^{-2} \text{s}^{-1}$, cells showed a remarkable ability to recover completely from the state of photoinhibition, as attested by the increased growth rate up to $0.102 \pm 0.009 \text{ h}^{-1}$ (corresponding to a doubling time of $\approx 7 \text{ h}$), which is similar to the maximum growth rate previously measured under the same light condition (Fig. 2.3A (black dot) and Fig. 2.4).



Fig

2.4. Recovery of growth of *Synechocystis* after high light treatment. *Synechocystis* quickly recovers from high light ($1460 \mu\text{mol photons m}^{-2} \text{s}^{-1}$, left side) after reducing light intensity to a non-photoinhibiting intensity ($200 \mu\text{mol photons m}^{-2} \text{s}^{-1}$, right side). Dissolved oxygen concentration (red line) and growth rate (black squares, calculated per turbidostat cycle) are shown. The half-life of this recovery is 3 h.

Similarly, the relative concentration of dO_2 in the medium was found to increase up to 2.13 ± 0.24 , attesting a full recovery of the PSII activity as well (Fig. 2.3B (black dot) and Fig. 2.4). We found that the recovery half-time is approximately 3 h and that both growth rate and dO_2 remain stable after recovery during the 24 h. As aforementioned, our phenotypic characterization included *Synechocystis* cell size, which was found to vary across the experimentally tested conditions. Even though the bacterial life cycle is usually the major determinant of morphological traits, including cell size, several studies reported that cyanobacteria modify their morphology to optimize their functionality to exogenous factors in natural contexts (Montgomery, 2015). However, the mechanisms by which light conditions, including light intensity, influence cell morphology, including cell size, are understudied (Pattanaik et al., 2011). Table 2.1 shows *Synechocystis* cell size changes in response to increasing light intensities.

Light intensity ($\mu\text{mol photons m}^{-2} \text{s}^{-1}$)	Cell size (μm)	Dry cell weight ($\text{g OD}_{730}^{-1} \text{L}^{-1}$)
50	2.11 ± 0.06	0.145 ± 0.001
200	3.02 ± 0.13	0.140 ± 0.021
300	3.22 ± 0.18	0.145 ± 0.005
500	3.29 ± 0.13	0.147 ± 0.003
800	3.09 ± 0.23	0.152 ± 0.004
950	2.94 ± 0.26	0.153 ± 0.000
1460	2.69 ± 0.21	0.158 ± 0.021
200*	3.03 ± 0.01	0.150 ± 0.003

Table 2.1. Cell size and dry cell weight of *Synechocystis* grown under increasing light intensities. The turbidostat-controlled cultures were grown at constant temperature (30°C) and pH (8.0) under orange-red light and acclimated for 24 h at each light intensity. The values are mean and standard deviation derived from three biological replicates. (*) Point of recovery at 200 $\mu\text{mol photons m}^{-2} \text{s}^{-1}$.

At 50 $\mu\text{mol photons m}^{-2} \text{s}^{-1}$ the cell size was $2.11 \pm 0.06 \mu\text{m}$. This size is commonly observed in *Synechocystis* cells cultivated under non-stressful conditions (Du et al., 2016). At a photon irradiance of 500 $\mu\text{mol photons m}^{-2} \text{s}^{-1}$ *Synechocystis* cells reached the maximum size of $3.29 \pm 0.13 \mu\text{m}$ while, at the photon irradiance of 800 $\mu\text{mol photons m}^{-2} \text{s}^{-1}$, which was found to induce photoinhibition, *Synechocystis* cell size decreased to $3.09 \pm 0.23 \mu\text{m}$ and then gradually to $2.69 \pm 0.21 \mu\text{m}$ at the maximal photoinhibitory photon irradiance of 1460 $\mu\text{mol photons m}^{-2} \text{s}^{-1}$. Notably, at the recovery light regime of 200 $\mu\text{mol photons m}^{-2} \text{s}^{-1}$, *Synechocystis* cells recovered the dimension previously observed under the control photon irradiance ($3.02 \pm 0.13 \mu\text{m}$). Altogether, cell size, growth rate and PSII functionality behaved similarly under increasing intensities of orange-red light, by reaching their maximal

values at intensities up to 500 $\mu\text{mol photons m}^{-2} \text{ s}^{-1}$ and rapidly decreasing at photoinhibiting light conditions.

We then examined the effect of long-term acclimation to increasing intensities of orange-red light by estimating the Chl *a* content in *Synechocystis* through the measurement of the OD₆₈₀/OD₇₂₀ ratio (Table S2.2). Our measurements revealed the highest content of Chl *a* at 50 $\mu\text{mol photons m}^{-2}\text{s}^{-1}$ compared to the other photon irradiances tested (Table S2.2). These data show that at limited light intensity *Synechocystis* sustains its growth by accumulating a high amount of Chl *a* to maximize light absorption. Increasing the photon irradiance to 200 $\mu\text{mol photons m}^{-2}\text{s}^{-1}$, the amount of Chl *a* decreased by around 13%, which reached the minimum at 800 $\mu\text{mol photons}^{-2} \text{ s}^{-1}$. Chl *a* reduction could be provoked by its synthesis inhibition in order to limit the absorption of harmfully excessive light (Kada et al., 2003; Xu et al., 2004). Unexpectedly, we observed Chl *a* increased also at 950 and 1460 $\mu\text{mol photons m}^{-2}\text{s}^{-1}$, which were shown to induce severe cell photoinhibition (Fig. 2.3).

2.3.2 Influence of local light intensity distribution on photoinhibition of microorganism.

Our multi-physics analysis focused on the spread of incident light within the *Synechocystis* cultivation apparatus and on the relationships between local light intensity and *Synechocystis* photosynthetic activity, which expectedly influence PBR productivity. The PBR used for culturing *Synechocystis*, the illumination setup and real-time monitoring are extensively described in Fig. 2.1, Table S2.3, Table S2.4 and Fig. S2.1. The *in silico* simulations have been developed under identical operational conditions as employed during the experiments, and are aimed at exploring the distribution of local light intensity within the cultivation apparatus as a function of the incident light intensity. As thoroughly described in the Methods section, current knowledge on mass transfer, fluid dynamics, heat transfer from radiation, and growth kinetics were entirely incorporated to frame the modelling equations (Table S2.1), and the resulting model was implemented within the COMSOL 5.3® computing platform. To obtain suitable estimates for the parameters necessary to our mathematical representation, we relied either on experimentally determined values or on an inference procedure by fitting model simulations to observed data. The observed agreement between model estimates and experimental measurements for growth rate and dissolved oxygen (Figs. 2.3 and 2.4) demonstrated that our model is built on solid foundations. Moreover, we

employed the light intensities recorded in our model simulations to estimate the light-dependent photosynthetic efficiency of the PBR in terms of moles of photons absorbed in the PBR per gram of biomass production, as shown in Table 2.2 and Table S2.5. The observed agreement between model estimates and experimental measurements for growth rate and dissolved oxygen (Figs. 2.3 and 2.4) demonstrated that our model is built on solid foundations. Moreover, we employed the light intensities recorded in our model simulations to estimate the light-dependent photosynthetic efficiency of the PBR in terms of moles of photons absorbed in the PBR per gram of biomass production, as shown in Table 2.2.

I_{in} ($\mu\text{mol photons m}^{-2}\text{s}^{-1}$)	Vol L	$\mu \text{ h}^{-1}$	gDW L ⁻¹	mol photons g DW ⁻¹	efficiency
50	0,377	0,054	0,145	0,37	2,70
200	0,377	0,110	0,140	0,61	1,64
300	0,377	0,117	0,145	0,75	1,33
500	0,377	0,110	0,147	1,11	0,90
800	0,377	0,104	0,152	1,68	0,60
950	0,377	0,088	0,153	2,10	0,48

Table 2.2 Comparison of the efficiency of photosynthesis in terms of moles of photons required for biomass production in *Synechocystis* calculated from growth simulations in a 380 ml vessel of the PBR upon acclimation for 24 h at 50, 200, 300, 500, 800 and 950 $\mu\text{mol photons m}^{-2}\text{s}^{-1}$ of orange-red light. Shown are: I_{in} ($\mu\text{mol photons m}^{-2}\text{s}^{-1}$), light intensity available to the PBR domains; $\mu \text{ h}^{-1}$, growth rate per hour; g DW L⁻¹, biomass density in gram dry weight per liter; g DW /mol photons, growth yield in mol photons absorbed per gram biomass.

These simulation results fully agree with experimental data acquired in previous studies (Schuurmans et al., 2015), and corroborated the plausibility of our modelling framework. The photosynthetic efficiency of *Synechocystis* turned out to decrease from the highest value, observed at 50 $\mu\text{mol photons m}^{-2}\text{s}^{-1}$ where 2.70 g of biomass are produced per mol of photons, to the lowest value observed at 950 $\mu\text{mol photons m}^{-2}\text{s}^{-1}$ where 0.48 g of biomass are produced per mol of photons. Moreover, the estimates of photosynthetic efficiency obtained by our model simulations confirmed that efficiency starts to drop fastest in the initial increase in intensity, which is expected at low OD batch cultures. Model simulations were then used to get insights into the local light intensity distribution along different combinations of directional axes within the cultivation apparatus. To ensure comparability of the results shown throughout our analysis, we normalized the light

intensity values corresponding to the PBR internal space and resulting from our model simulations with respect to the initial incident intensity on the PBR surface, and we plotted the ratio between the calculated light intensity and the initial incident intensity

$$R_I = \frac{I_{calc}}{I_{inc}}$$

To analyse the distribution of light along all the directions, the trends of R_I were developed by the YZ and XZ planes (Fig. 2.1D and Fig. S2.2). The light intensity distribution inside the liquid mixture on six YZ slices for three different incident light intensities, 50, 300 and 950 $\mu\text{mol photons m}^{-2}\text{s}^{-1}$, shown in Fig. 2.5, confirms the ability of our modelling approach to capture a number of features of radiation spreading within a cultivation system.

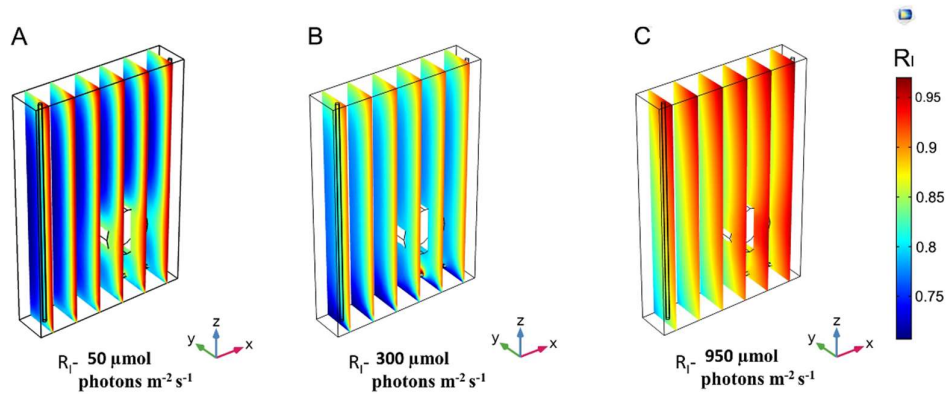


Fig 2.5. 3D trend of normalized light intensity along YZ slice of the model PBR. The calculated light intensity was normalized with respect to the initial incident intensity and the R_I trend is performed along six YZ planes for three different incident light intensities, I_{inc} . **A:** 50 $\mu\text{mol photons m}^{-2}\text{s}^{-1}$. **B:** 300 $\mu\text{mol photons m}^{-2}\text{s}^{-1}$. **C:** 950 $\mu\text{mol photons m}^{-2}\text{s}^{-1}$.

Boundary conditions and the coexistence of an upper gas phase and a lower liquid phase are expected to influence the light intensity distribution. Our modelling approach foresaw that the incident light gets reduced where the culture and glass of the vessel interface closest to the side where light is supplied. This reduction amounted to about 3-5%, and was more evident at lower intensities (Fig. 2.5). Moreover, in the area at the interface between the liquid and gas phases light

intensity was found to display an eyelet-like pattern where the upper region shows higher intensity than the lower one. Additionally, this pattern was more remarkable for lower values of the incident light intensity. Another source of variation in the spatial distribution of light is identifiable in the rotating domain created by the stirring bar (Fig. S2.1). The local liquid movement propelled by the stirring bar rotation is expected to favour the light transmission process (Dongda Zhang et al., 2015). Our model simulations consistently predicted the increase of light intensity in the stirring bar neighbourhood, which amounted to around 3-5% for low I_{inc} and around 1-2% for high I_{inc} (Fig. 2.5C).

In the interface area between the liquid phase and the bottom steel base, our model predicts a reduction in light intensity owing to the large difference between the absorption and emissivity values of these two domains.

Beyond these effects, light intensity generally decreased with the distance from the light source, as shown by the plots at equally spaced slices along the YZ axis (Fig. 2.5) and further confirmed by the plots acquired at three XZ sections (Fig. 2.6, Fig. S2.2). The light intensity decay along the path inside the cultivation apparatus was expected since it can be attributed to the compound effect of photon absorption by *Synechocystis* cells and of scattering phenomena (Grima et al., 1994). When varying the incident light intensity, our model simulations showed the extent of light decay to get lower at progressively higher incident light intensity. Decrease in light decay along the path amounting about 18% for I_{inc} of 50 $\mu\text{mol photons m}^{-2}\text{s}^{-1}$, 12% for I_{inc} of 300 $\mu\text{mol photons m}^{-2}\text{s}^{-1}$ and 7% for I_{inc} of 950 $\mu\text{mol photons m}^{-2}\text{s}^{-1}$ were calculated.

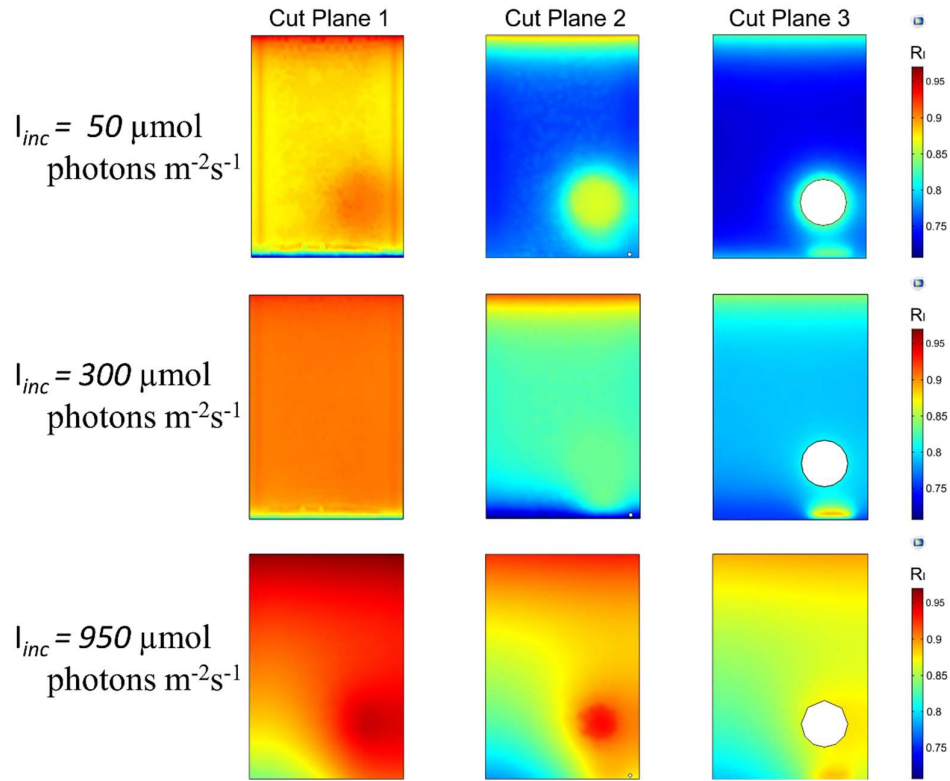


Fig 2.6. 2D trend of normalized light intensity along XZ slice of the model PBR. The calculated light intensity was normalized with respect to the initial incident intensity and the R_I trend is performed along three XZ planes for three different incident light intensities, I_{inc} **A:** $50 \mu\text{mol photons m}^{-2} \text{s}^{-1}$. **B:** $300 \mu\text{mol photons m}^{-2} \text{s}^{-1}$. **C:** $950 \mu\text{mol photons m}^{-2} \text{s}^{-1}$.

Our modelling framework was primed to afford the exploration of the relationship between the heterogeneity in local light distribution, which originates from the aforementioned sources, and the *Synechocystis* behaviour in the artificially lit cultivation system. More precisely, we expected the light environment created by the coexistence of regions of higher and lower local light intensity could favour *Synechocystis* functionalities, as gauged by the experimental measurements shown in Fig. 2.3.

From our model simulation results, it was evident that at $50 \mu\text{mol photon m}^{-2} \text{s}^{-1}$ the light penetration inside the culture was extremely low (Fig. 2.5A), suggesting that the cells were exposed to a period of lower intensity considerably longer than the expected light phase set experimentally. Under this light condition *Synechocystis* showed low growth rate, limited amount of oxygen dissolved in the medium (Fig. 2.3), and a higher Chl *a* amount than in the other tested conditions (Table S2.1),

which is likely due to the need of optimizing light absorption in a scarcely lit environment. Our simulations showed that, upon increasing the irradiance to 300 $\mu\text{mol photon m}^{-2} \text{s}^{-1}$, light managed to diffuse more deeply within the PBR interior (Fig. 2.5B and Fig 2.6). The overall increased light availability and the coexistence of regions of different local light intensities created the most favourable light environment for *Synechocystis* which indeed reached its maximal growth rate and oxygen dissolved in the medium (Fig. 2.3). Conversely, the further rise of light intensity up to 950 $\mu\text{mol photons m}^{-2} \text{s}^{-1}$, and the subsequent suppression of low local light intensity experienced by the cells (Figs. 2.5C and 2.6), led *Synechocystis* to suffer high light stress reflected in a noticeable decrease in its growth rate and oxygen evolution activity (Fig. 2.3). Under such light conditions, cells were no longer able to dissipate the excess of supplied light and entered a photoinhibition state (Chiang et al., 2011).

2.4 Discussion

The experiments conducted were particularly informative for studying the effects of increasing intensities, ranging between 50-1460 $\mu\text{mol photons m}^{-2} \text{s}^{-1}$, of red-orange light on the adjustments of the physiological state in *Synechocystis*. Although the PSII photodamage effect caused by the exposure to high (white) light intensity is well-established in plants (Theis and Schroda, 2016), corresponding quantitative data on photoinhibition by red light in cyanobacteria are scarce. Furthermore, experimental evidence of the recovery potential in *Synechocystis* from this light stress has so far been lacking. Importantly, our results evidenced the adaptive capacity of *Synechocystis* to completely recover from the harmful condition of photoinhibition under subsequent exposure to an optimal light intensity for growth. It is already well known that under photoinhibitory conditions, loss of oxygen evolution capacity of PSII activates the PSII repair cycle and that the rate of the repair reaction depends on the extent of the PSII damaged centres (Tyystjärvi, 2013). Since the D1 protein is the main target of photoinhibition and its lack within the PSII centre speeds up its synthesis, an increase of the amount of *psbA* transcript in *Synechocystis* occurs in high light (Mohamed et al., 1993) and this high level is maintained for several hours in darkness (He & Vermaas, 1998). Here the quick recovery of PSII activity observed at 200 $\mu\text{mol photons m}^{-2} \text{s}^{-1}$ suggests that the high levels of D1 transcript maintained within the surviving cells at 1460 $\mu\text{mol photons m}^{-2} \text{s}^{-1}$ allows the acceleration of D1 synthesis to reactivate the PSII activity, once cells have been reverted to the optimal growth irradiance. An

exceptional capacity to cope with fluctuations in a wide range of lights differing for spectral quality and quantity, as well as pH and temperature, was previously observed in this microorganism by (Constant et al., 2000) and (Zavřel et al., 2015). Indeed, the ability to readily adapt the metabolism to different environmental conditions allowed *Synechocystis*, and more in general cyanobacteria, to proliferate even in extreme environments on Earth (Hernández-Prieto et al., 2016). Furthermore, growth rate was found to positively correlate with cell size independently of light intensity (Fig. 2.7).

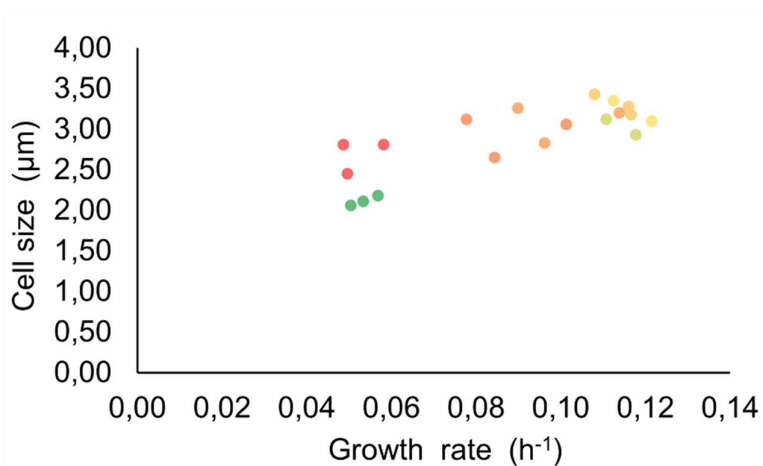


Fig 2.7. Relationship of the cell size and growth rate of *Synechocystis* set at different light intensities. The figure displays the relationship between growth rate and cell size at varying light intensities. Dot colours reflect the incident light intensity, with the green and red colours corresponding to low values and high values respectively

This trend has been previously observed in *Synechocystis* acclimated to lower intensities of light (Du et al., 2016) and in *Synechococcus* grown under limited nutrient supply of phosphate and nitrate (Garcia, Bonachela & Martiny, 2015), and hints at a tight coordination of growth rate with cell size. It has been reported that cyanobacteria can respond to different abiotic stresses by increasing the cell size, accumulating granules of different nature, e.g. glycogen, upon exposure to high light intensity (Kopečna et al., 2012) and polyhydroxybutyrate in case of high temperatures (Červený et al., 2015). Even though the mechanisms that associate cellular growth rate with cell size are still unclear (Amir, 2014), here we suggest that the increase of light intensity could accelerate both the metabolism and growth

rate of *Synechocystis*, favouring the accumulation of higher amounts of biomass that need to be properly stored, leading the cells to increase their size (Amir, 2014; Ferrezuelo et al., 2012). In general, the variation in cell size observed at incremental steps of light intensity was accompanied by the maintenance of a relatively constant dry cell weight per OD730 (Table 1), which suggests that the fluctuations observed in cell size exposed to increasing light intensities were counterbalanced by opposite fluctuations in the number of cells per volume.

The highest content of Chl *a* at 50 $\mu\text{mol photons m}^{-2}\text{s}^{-1}$ along with its decrease at increasing orange-red light intensities which we observed upon increasing the orange-red light intensity are expected since inhibition of Chl *a* synthesis could serve to limit the absorption of harmfully excessive light. Conversely, the Chl *a* increase observed at 950 and 1460 $\mu\text{mol photons m}^{-2}\text{s}^{-1}$, which were shown to induce severe cell photoinhibition (Fig. 2.3), is unexpected. This observation warrants further investigation but it is plausible to hypothesize that the observed increase in Chl *a* amount could be partially due to the accumulation of this pigment in dead cells, which likely reflects the much longer lifetime of Chl molecules with respect to that of other pigments (Steiger, Schäfer & Sandmann, 1999; Vavilin, Brune & Vermaas, 2005; Vavilin & Vermaas, 2007; Yao et al., 2011; Yao, Brune & Vermaas, 2012; Trautmann, Beyer & Al-Babili, 2013; Havaux, 2014). Finally, the recovery of pigment biosynthesis observed upon acclimation of photoinhibited cells over 24 h at 200 $\mu\text{mol photons m}^{-2}\text{s}^{-1}$ confirmed the elevated degree of plasticity of this cyanobacterium to cope with extremely high light intensities.

The *in silico* simulations were focused to investigate the spatial distribution of local light intensity in the cultivation system on the basis of the incident light intensity and the . Our model simulation allowed a careful, albeit qualitative, evaluation of the complex consequences that variations in light intensity and local light distribution can cause on the *Synechocystis* physiology within an artificially lit cultivation system. In particular, we were able to identify three distinct operative states: i) a light limited state where all the light supplied to the system is maximally exploited by the cells, a condition that is reflected in a linear relation between irradiance and *Synechocystis* physiological parameters, ii) a light optimal state where *Synechocystis* optimizes the utilization of light to support its maximal growth rate and photosynthetic activity, iii) a photo-inhibition state where the excess of incident light becomes harmful for microorganisms growth. Our model simulations suggest that regulating the incident light on the PBR, at least in a range of moderate intensities, could be used to enhance *Synechocystis* growth. Indeed, this model takes into account the formation of areas of different local light intensity within the PBR, whose extent varies as a function of the incident light intensity, and that can be

exploited by the microorganism to prevent from experiencing light-induced stress. According to our study, managing local light effects is expected to be worth careful consideration in PBR design for leveraging the microorganism exploitation.

2.5 Conclusions

The productivity of PBRs exploiting *Synechocystis* clearly depends on the photosynthetic efficiency of this microorganism. Since this efficiency largely depends on the cyanobacteria ability to manage the light collected in the cultivation apparatus, in this work we thoroughly investigated the impact of the setup of the light conditions in the PBR on *Synechocystis* growth and photosynthetic activity. Monitoring *Synechocystis* physiological state under increasing intensities of orange-red light, we found that growth rate, cell size and PSII activity were influenced by light intensity, although in slightly different ways. *Synechocystis* cells proved to be resistant to high light stress conditions, showing photoinhibition only above $800 \mu\text{mol photons m}^{-2} \text{s}^{-1}$ combined with a remarkable ability to recover from the complete state of photoinhibition experienced at $1460 \mu\text{mol photons m}^{-2} \text{s}^{-1}$ when reverting light to $200 \mu\text{mol photons m}^{-2} \text{s}^{-1}$. Considering the notable plasticity of *Synechocystis* in response to changes in light intensity, we searched for unknown features of the PBR light conditions which could leverage *Synechocystis* behavioural features to enhance the overall PBR productivity. To this end, we deemed it particularly useful to adopt also an in silico methodology by constructing a PBR model and subsequently use it to simulate the effects of increasing incident light intensities on the local light intensity distribution. Interestingly, our results indicate that the formation of areas of different light intensities could be controllable by tuning the incident light intensity on the PBR. A gain in *Synechocystis* viability is achievable by increasing the incident light intensity as far as areas of different light intensities exist to allow *Synechocystis* cells to escape from the photoinhibition state. It is useful to note that the observations herein presented are drawn from experiments and simulations carried out in turbidostat mode (constant OD730) and could vary depending on the choice of the cultivation mode. Nonetheless, our results provide useful insights in a PBR modelling perspective and, in particular, suggest that a PBR design would benefit from considering the management of local light heterogeneity to increase the microorganism photosynthetic activity, by limiting photoinhibition phenomena, to ultimately maximize the productivity.

2.6 Nomenclature

A	area, m^2
c_d	mass fraction of dispersed phase, kg kg^{-1}
C	concentration, mol m^{-3}
C_p	specific heat at constant pressure, $\text{J m}^{-3} \text{K}^{-1}$
D	diffusion coefficients, $\text{m}^2 \text{s}^{-1}$
D_{md}	turbulent dispersion coefficient, $\text{m}^2 \text{s}^{-1}$
e	enthalpy flux density, $\text{J m}^{-2} \text{s}^{-1}$
E_A	activation energy, J mol^{-1}
F	force term, $\text{kg m}^{-2} \text{s}^{-2}$
G	incident light radiation, W m^{-2}
$h_j(T)$	enthalpies heat flux densities, $\text{J m}^{-2} \text{s}^{-1}$
I	incident light intensity, W m^{-2}
I_b	black body radiation, Wm^{-2}
J	diffusion vector
k	turbulent kinetic energy, m^2s^{-3}
K_r	reaction rate constant, $\text{m}^2 \text{s}^{-1}$
m	mass of species, kg
m_{dc}	mass transfer from dispersed to continuous phase, $\text{kg m}^{-3}\text{s}^{-1}$
M	molar mass, kg mol^{-1}
n	flux density, $\text{mol m}^{-2} \text{s}^{-1}$
n_d	relative mass flux, $\text{mol m}^{-2} \text{s}^{-1}$

p	pressure, Pa
q	heat flux densities, W m^{-2}
Q	volumetric charge density, C m^{-3}
Q_r	radiative flux, W m^{-2}
R	universal gas constant, $\text{J K}^{-1} \text{mol}^{-1}$
T	temperature, K
u	velocity vector, m s^{-1}
u_c	continuous phase velocity vector, m s^{-1}
u_d	dispersed phase velocity vector, m s^{-1}
u_{slip}	slip velocity vector, m s^{-1}
V_p	the convective velocity, m s^{-1}
w	volume fraction
x	mass fraction

Greek symbols

β	extinction coefficient, m^{-1}
ε	turbulent energy dissipation, m^2s^{-3}
k_c	effective thermal conductivity coefficient, $\text{W m}^{-1} \text{K}^{-1}$
κ	absorbance coefficient, m^{-1}
μ	dynamic viscosity, kgf s m^{-2}
μ_{gr}	growth rate, h^{-1}

μ_T	turbulent viscosity,
ν	stoichiometric coefficients
ρ	density, Kg m ⁻³
σ_s	scattering coefficient, m ⁻¹
τ	turbulent stress,
ϕ_c	continuous phase fraction, -
ϕ_d	dispersed phase fraction, -
ω	rotational velocity, rad s ⁻¹

2.7 References

- Aiba S. 1982. Growth kinetics of photosynthetic microorganisms. In: Springer, Berlin, Heidelberg, 85–156. DOI: 10.1007/3540116982_3.
- Ali A. 2014. CFD Simulation of Bubbly Flow Through a Bubble Column. 5:904–910.
- Amir A. 2014. Cell size regulation in bacteria. *Physical Review Letters* 112:1–5. DOI: 10.1103/PhysRevLett.112.208102.
- Anfelt J., Hallström B., Nielsen J., Uhlén M., Hudson EP. 2013. Using transcriptomics to improve butanol tolerance of *Synechocystis* sp. strain PCC 6803. *Applied and environmental microbiology* 79:7419–27. DOI: 10.1128/AEM.02694-13.
- Angermayr SA., van Alphen P., Hasdemir D., Kramer G., Iqbal M., van Grondelle W., Hoefsloot HC., Choi YH., Hellingwerf KJ. 2016. Culturing *Synechocystis* sp. Strain PCC 6803 with N₂ and CO₂ in a Diel Regime Reveals Multiphase Glycogen Dynamics with Low Maintenance Costs. *Applied and environmental microbiology* 82:4180–9. DOI: 10.1128/AEM.00256-16.
- Angermayr SA., Gorchs Rovira A., Hellingwerf KJ. 2015. Metabolic engineering of cyanobacteria for the synthesis of commodity products. *Trends in Biotechnology* 33:352–361. DOI: 10.1016/j.tibtech.2015.03.009.
- Angermayr SA., Hellingwerf KJ., Teixeira de Mattos MJ. 2009. Energy biotechnology with cyanobacteria. *Current Opinion in Biotechnology* 20:257–263. DOI: 10.1016/J.COPBIO.2009.05.011.
- Angermayr SA., Paszota M., Hellingwerf KJ. 2012. Engineering a cyanobacterial cell factory for production of lactic acid. *Applied and Environmental Microbiology* 78:7098–7106. DOI: 10.1128/AEM.01587-12.
- Beck C., Hertel S., Rediger A., Lehmann R., Wiegard A., Kölsch A., Heilmann B., Georg J., Hess WR., Axmann IM. 2014. Daily Expression Pattern of Protein-Encoding Genes and Small Noncoding RNAs in *Synechocystis* sp. Strain PCC 6803. *Applied and Environmental Microbiology* 80:5195–5206. DOI: 10.1128/AEM.01086-14.

-
- Bird RB (Robert B., Stewart WE., Lightfoot EN. 2002. Transport phenomena. J. Wiley.
- Bumann D., Oesterhelt D. 1995. Destruction of a single chlorophyll is correlated with the photoinhibition of photosystem II with a transiently inactive donor side. *Proceedings of the National Academy of Sciences of the United States of America* 92:12195–12199. DOI: 10.1073/pnas.92.26.12195.
- Burrows EH., Wong W-K., Fern X., Chaplen FWR., Ely RL. 2009. Optimization of pH and nitrogen for enhanced hydrogen production by *Synechocystis* sp. PCC 6803 via statistical and machine learning methods. *Biotechnology Progress* 25:1009–1017. DOI: 10.1002/btpr.213.
- Červený J., Sinetova MA., Zavřel T., Los DA. 2015. Mechanisms of high temperature resistance of *Synechocystis* sp. PCC 6803: An Impact of histidine kinase 34. *Life* 5:676–699. DOI: 10.3390/life5010676.
- Chaves JE., Kirst H., Melis A. 2015. Isoprene production in *Synechocystis* under alkaline and saline growth conditions. *Journal of Applied Phycology* 27:1089–1097. DOI: 10.1007/s10811-014-0395-2.
- Chiang C-L., Lee C-M., Chen P-C. 2011. Utilization of the cyanobacteria *Anabaena* sp. CH1 in biological carbon dioxide mitigation processes. *Bioresource Technology* 102:5400–5405. DOI: 10.1016/j.biortech.2010.10.089.
- Colyer CL., Klinkade CS., Viskari PJ., Landers JP. 2005. Analysis of cyanobacterial pigments and proteins by electrophoretic and chromatographic methods. *Analytical and Bioanalytical Chemistry* 382:559–569. DOI: 10.1007/s00216-004-3020-4.
- Constant S., Eisenberg-Domovitch Y., Ohad I., Kirilovsky D. 2000. Recovery of photosystem II activity in photoinhibited *Synechocystis* cells: Light-dependent translation activity is required besides light-independent synthesis of the D1 protein. *Biochemistry* 39:2032–2041. DOI: 10.1021/bi9914154.
- Dechatiwongse P., Srisamai S., Maitland G., Hellgardt K. 2014. Effects of light and temperature on the photoautotrophic growth and photoinhibition of

nitrogen-fixing cyanobacterium *Cyanothece* sp. ATCC 51142. *Algal Research* 5:103–111. DOI: 10.1016/J.ALGAL.2014.06.004.

Du W., Jongbloets JA., Pineda Hernandez H., Bruggeman FJ., Hellingwerf KJ., Branco dos Santos F. 2016. Photonfluxostat: A method for light-limited batch cultivation of cyanobacteria at different, yet constant, growth rates. *Algal Research* 20:118–125. DOI: 10.1016/j.algal.2016.10.004.

Esteves-Ferreira AA., Inaba M., Obata T., Fort A., Fleming GTA., Araújo WL., Fernie AR., Sulpice R. 2017. A Novel Mechanism, Linked to Cell Density, Largely Controls Cell Division in *Synechocystis*. *Plant physiology* 174:2166–2182. DOI: 10.1104/pp.17.00729.

Fang L., Ge H., Huang X., Liu Y., Lu M., Wang J., Chen W., Xu W., Wang Y. 2016. Trophic Mode-Dependent Proteomic Analysis Reveals Functional Significance of Light-Independent Chlorophyll Synthesis in *Synechocystis* sp. PCC 6803. *Molecular Plant* 6803:73–85. DOI: 10.1016/j.molp.2016.08.006.

Ferrezuelo F., Colomina N., Palmisano A., Garí E., Gallego C., Csikász-Nagy A., Aldea M. 2012. The critical size is set at a single-cell level by growth rate to attain homeostasis and adaptation. *Nature communications* 3:1012. DOI: 10.1038/ncomms2015.

Gan F., Bryant DA. 2015. Adaptive and acclimative responses of cyanobacteria to far-red light. *Environmental Microbiology* 17:3450–3465. DOI: 10.1111/1462-2920.12992.

Gao Z., Zhao H., Li Z., Tan X., Lu X., Lu X., Foust TD., Hallett JP., Leak DJ., Liotta CL., Mielenz JR., Murphy R., Templer R., Tschaplinski T. 2012. Photosynthetic production of ethanol from carbon dioxide in genetically engineered cyanobacteria. *Energy Environ. Sci.* 5:9857–9865. DOI: 10.1039/C2EE22675H.

Garcia NS., Bonachela JA., Martiny AC. 2015. Growth-dependent cell size controls interactions between nutrient supply and cellular elemental stoichiometry of marine *Synechococcus*. In review:1–10. DOI: 10.1038/ismej.2016.50.

Glazer AN. 1977. Structure and molecular organization of the photosynthetic accessory pigments of cyanobacteria and red algae. *Molecular and Cellular*

Biochemistry 18:125–140. DOI: 10.1007/BF00280278.

Grima EM., Camacho FG., Pérez JAS., Sevilla JMF., Fernández FGA., Gómez AC. 1994. A mathematical model of microalgal growth in light-limited chemostat culture. *Journal of Chemical Technology AND Biotechnology* 61:167–173. DOI: 10.1002/jctb.280610212.

Hartmann P., Nikolaou A., Chachuat B., Bernard O., Nikolaou A., Chachuat B. 2013. A dynamic Model coupling Photoacclimation and Photoinhibition in Microalgae European Control Conference.

Havaux M. 2014. Carotenoid oxidation products as stress signals in plants. *The Plant Journal* 79:597–606. DOI: 10.1111/tpj.12386.

He Q., Vermaas W. 1998. Chlorophyll a availability affects psbA translation and D1 precursor processing in vivo in *Synechocystis* sp. PCC 6803. *Proceedings of the National Academy of Sciences* 95:5830–5835. DOI: 10.1073/pnas.95.10.5830.

Hernández-Prieto M a., Semeniuk TA., Giner-Lamia J., Futschik ME. 2016. The Transcriptional Landscape of the Photosynthetic Model Cyanobacterium *Synechocystis* sp. PCC6803. *Scientific reports* 6:22168. DOI: 10.1038/srep22168.

Janssen M., Tramper J., Mur LR., Wijffels RH. 2003. Enclosed outdoor photobioreactors: Light regime, photosynthetic efficiency, scale-up, and future prospects. *Biotechnology and Bioengineering* 81:193–210. DOI: 10.1002/bit.10468.

Joseph A., Aikawa S., Sasaki K., Tsuge Y., Matsuda F., Tanaka T., Kondo A. 2013. Utilization of Lactic Acid Bacterial Genes in *Synechocystis* sp. PCC 6803 in the Production of Lactic Acid. *Bioscience, Biotechnology, and Biochemistry* 77:966–970. DOI: 10.1271/bbb.120921.

Kada S., Koike H., Satoh K., Hase T., Fujita Y. 2003. Arrest of chlorophyll synthesis and differential decrease of Photosystems I and II in a cyanobacterial mutant lacking light-independent protochlorophyllide reductase. *Plant molecular biology* 51:225–35.

- Kaneko T., Sato S., Kotani H., Tanaka A., Asamizu E., Nakamura Y., Miyajima N., Hirose M., Sugiura M., Sasamoto S., Kimura T., Hosouchi T., Matsuno A., Muraki A., Nakazaki N., Naruo K., Okumura S., Shimpo S., Takeuchi C., Wada T., Watanabe A., Yamada M., Yasuda M., Tabata S. 1996. Sequence analysis of the genome of the unicellular cyanobacterium *Synechocystis* sp. strain PCC6803. II. Sequence determination of the entire genome and assignment of potential protein-coding regions. *DNA research : an international journal for rapid publication of reports on genes and genomes* 3:109–36.
- Katsuda T., Lababpour A., Shimahara K., Katoh S. 2004. Astaxanthin production by *Haematococcus pluvialis* under illumination with LEDs. *Enzyme and Microbial Technology* 35:81–86. DOI: 10.1016/J.ENZMICTEC.2004.03.016.
- Kopečna J., Komenda J., Bucinska L., Sobotka R. 2012. Long-term acclimation of the cyanobacterium *Synechocystis* PCC 6803 to high light is accompanied by an enhanced production of chlorophyll that is preferentially channeled to trimeric PSI. *Plant Physiology* 160:2239–2250. DOI: 10.1104/pp.112.207274.
- Kramer DM., Evans JR. 2011. The importance of energy balance in improving photosynthetic productivity. *Plant physiology* 155:70–8. DOI: 10.1104/pp.110.166652.
- Li M., Hu D., Liu H. 2014. Photobioreactor with ideal light-dark cycle designed and built from mathematical modeling and CFD simulation. *Ecological Engineering* 73:162–167. DOI: 10.1016/j.ecoleng.2014.09.010.
- Luengo JM., García BN., Sandoval A., Naharro GN., Olivera ER. 2003. Bioplastics from microorganisms. *Current Opinion in Microbiology* 6:251–260. DOI: 10.1016/S1369-5274(03)00040-7.
- Luo H-P., Al-Dahhan MH. 2011. Verification and validation of CFD simulations for local flow dynamics in a draft tube airlift bioreactor. *Chemical Engineering Science* 66:907–923. DOI: 10.1016/J.CES.2010.11.038.
- Mohamed A., Eriksson J., Osiewacz HD., Jansson C. 1993. Differential expression of the *psbA* genes in the cyanobacterium *Synechocystis* 6803. *MGG Molecular & General Genetics* 238:161–168. DOI: 10.1007/BF00279543.

-
- Montgomery BL. 2015. Light-dependent governance of cell shape dimensions in cyanobacteria. *Frontiers in Microbiology* 6:1–8. DOI: 10.3389/fmicb.2015.00514.
- Mulo P., Laakso S., Mäenpää P., Aro E-M. 1998. Stepwise Photoinhibition of Photosystem II. *Plant Physiology* 117:483–490. DOI: 10.1104/pp.117.2.483.
- Murata N., Takahashi S., Nishiyama Y., Allakhverdiev SI. 2007. Photoinhibition of photosystem II under environmental stress. *Biochimica et Biophysica Acta - Bioenergetics* 1767:414–421. DOI: 10.1016/j.bbabi.2006.11.019.
- Nanjo Y., Mizusawa N., Wada H., Slabas AR., Hayashi H., Nishiyama Y. 2010. Synthesis of fatty acids de novo is required for photosynthetic acclimation of *Synechocystis* sp. PCC 6803 to high temperature. *Biochimica et Biophysica Acta - Bioenergetics* 1797:1483–1490. DOI: 10.1016/j.bbabi.2010.03.014.
- Nedbal L., Trtílek M., Červený J., Komárek O., Pakrasi HB. 2008. A photobioreactor system for precision cultivation of photoautotrophic microorganisms and for high-content analysis of suspension dynamics. *Biotechnology and Bioengineering* 100:902–910. DOI: 10.1002/bit.21833.
- Ooms MD., Graham PJ., Nguyen B., Sargent EH., Sinton D. 2017. Light dilution via wavelength management for efficient high-density photobioreactors. *Biotechnology and Bioengineering* 114:1160–1169. DOI: 10.1002/bit.26261.
- Panda B., Jain P., Sharma L., Mallick N. 2006. Optimization of cultural and nutritional conditions for accumulation of poly- β -hydroxybutyrate in *Synechocystis* sp. PCC 6803. *Bioresource Technology* 97:1296–1301. DOI: 10.1016/J.BIORTECH.2005.05.013.
- Pattanaik B., Whitaker MJ., Montgomery BL. 2011. Convergence and divergence of the photoregulation of pigmentation and cellular morphology in *Fremyella diplosiphon*. *Plant Signaling & Behavior* 6:2038–2041. DOI: 10.4161/psb.6.12.18239.
- Alphen V. 2018. Physiological studies to optimize growth of the prototype biosolar cell factory. D. Phil. Thesis, Uviversity of Amsterdam

- Powles SB. 1984. Photoinhibition of Photosynthesis Induced by Visible Light. *Annual Review of Plant Physiology* 35:15–44. DOI: 10.1146/annurev.pp.35.060184.000311.
- Schuermans RM., Van Alphen P., Schuurmans JM., Matthijs HCP., Hellingwerf KJ. 2015. Comparison of the photosynthetic yield of cyanobacteria and green algae: Different methods give different answers. *PLoS ONE* 10:1–17. DOI: 10.1371/journal.pone.0139061.
- Singh AK., Bhattacharyya-Pakrasi M., Elvitigala T., Ghosh B., Aurora R., Pakrasi HB. 2009. A systems-level analysis of the effects of light quality on the metabolism of a cyanobacterium. *Plant physiology* 151:1596–608. DOI: 10.1104/pp.109.144824.
- Singh R., Parihar P., Singh M., Bajguz A., Kumar J., Singh S., Singh VP., Prasad SM. 2017. Uncovering Potential Applications of Cyanobacteria and Algal Metabolites in Biology, Agriculture and Medicine: Current Status and Future Prospects. *Frontiers in Microbiology* 8:515. DOI: 10.3389/fmicb.2017.00515.
- Solimeno A., Samsó R., Uggetti E., Sialve B., Steyer JP., Gabarró A., García J. 2015. New mechanistic model to simulate microalgae growth. *Algal Research* 12:350–358. DOI: 10.1016/j.algal.2015.09.008.
- Stanier RY., Kunisawa R., Mandel M., Cohen-Bazire G. 1971. Purification and properties of unicellular blue-green algae (Order Chroococcales). *Bacteriological reviews* 35:171–205. DOI: 10.1016/j.jbiotec.2013.07.020.
- Steiger S., Schäfer L., Sandmann G. 1999. High-light-dependent upregulation of carotenoids and their antioxidative properties in the cyanobacterium *Synechocystis* PCC 6803. *Journal of Photochemistry and Photobiology B: Biology* 52:14–18. DOI: 10.1016/S1011-1344(99)00094-9.
- Straka L., Rittmann BE. 2018. Effect of culture density on biomass production and light utilization efficiency of *Synechocystis* sp. PCC 6803. *Biotechnology and Bioengineering* 115:507–511. DOI: 10.1002/bit.26479.
- Theis J., Schroda M. 2016. Revisiting the photosystem II repair cycle. *Plant Signaling and Behavior* 11:e1218587. DOI: 10.1080/15592324.2016.1218587.

-
- Touloupakis E., Cicchi B., Benavides AMS., Torzillo G. 2016. Effect of high pH on growth of *Synechocystis* sp. PCC 6803 cultures and their contamination by golden algae (*Poterioochromonas* sp.). *Applied Microbiology and Biotechnology* 100:1333–1341. DOI: 10.1007/s00253-015-7024-0.
- Trautmann D., Beyer P., Al-Babili S. 2013. The ORF slr0091 of *Synechocystis* sp. PCC6803 encodes a high-light induced aldehyde dehydrogenase converting apocarotenals and alkanals. *FEBS Journal* 280:3685–3696. DOI: 10.1111/febs.12361.
- Triantaphylidès C., Havaux M. 2009. Singlet oxygen in plants: production, detoxification and signaling. *Trends in Plant Science* 14:219–228. DOI: 10.1016/j.tplants.2009.01.008.
- Tyytjärvi E. 2013. Photoinhibition of Photosystem II*. *International Review of Cell and Molecular Biology* 300:243–303. DOI: 10.1016/B978-0-12-405210-9.00007-2.
- Van Alphen P., Hellingwerf KJ. 2015. Sustained circadian rhythms in continuous light in *Synechocystis* sp. PCC6803 growing in a well-controlled photobioreactor. *PLoS ONE* 10. DOI: 10.1371/journal.pone.0127715.
- Varman AM., Xiao Y., Pakrasi HB., Tang YJ. 2013. Metabolic engineering of *Synechocystis* sp. Strain PCC 6803 for isobutanol production. *Applied and Environmental Microbiology* 79:908–914. DOI: 10.1128/AEM.02827-12.
- Vass I., Styring S., Hundal T., Koivuniemi a., Aro E., Andersson B. 1992. Reversible and irreversible intermediates during photoinhibition of photosystem II: stable reduced QA species promote chlorophyll triplet formation. *Proceedings of the National Academy of Sciences of the United States of America* 89:1408–1412. DOI: 10.1073/pnas.89.4.1408.
- Vatcheva I., de Jong H., Bernard O., Mars NJI. 2006. Experiment selection for the discrimination of semi-quantitative models of dynamical systems. *Artificial Intelligence* 170:472–506. DOI: 10.1016/J.ARTINT.2005.11.001.
- Vavilin D., Brune DC., Vermaas W. 2005. ¹⁵N-labeling to determine chlorophyll synthesis and degradation in *Synechocystis* sp. PCC 6803 strains lacking one

or both photosystems. *Biochimica et Biophysica Acta (BBA) - Bioenergetics* 1708:91–101. DOI: 10.1016/j.bbabi.2004.12.011.

Vavilin D., Vermaas W. 2007. Continuous chlorophyll degradation accompanied by chlorophyllide and phytol reutilization for chlorophyll synthesis in *Synechocystis* sp. PCC 6803. *Biochimica et Biophysica Acta (BBA) - Bioenergetics* 1767:920–929. DOI: 10.1016/J.BBABIO.2007.03.010.

Vermaas W. 1996. Molecular genetics of the cyanobacterium *Synechocystis* sp. PCC 6803: Principles and possible biotechnology applications. *Journal of Applied Phycology* 8:263–273.

Wang CY., Fu CC., Liu YC. 2007. Effects of using light-emitting diodes on the cultivation of *Spirulina platensis*. *Biochemical Engineering Journal* 37:21–25. DOI: 10.1016/j.bej.2007.03.004.

Wilcox DC. 2006. Turbulence modeling for CFD. DCW Industries.

Wyman M., Fay P. 1986. Underwater Light Climate and the Growth and Pigmentation of Planktonic Blue-Green Algae (Cyanobacteria) II. The Influence of Light Quality. *Proceedings of the Royal Society B: Biological Sciences* 227:381–393. DOI: 10.1098/rspb.1986.0028.

Xu H., Vavilin D., Funk C., Vermaas W. 2004. Multiple Deletions of Small Cab-like Proteins in the Cyanobacterium *Synechocystis* sp. PCC 6803. *Journal of Biological Chemistry* 279:27971–27979. DOI: 10.1074/jbc.M403307200.

Yang C., Hua Q., Shimizu K. 2002. Metabolic flux analysis in *Synechocystis* using isotope distribution from ¹³C-labeled glucose. *Metabolic engineering* 4:202–16.

Yao DCI., Brune DC., Vavilin D., Vermaas WFJ. 2012. Photosystem II component lifetimes in the cyanobacterium *Synechocystis* sp. strain PCC 6803: Small Cab-like proteins stabilize biosynthesis intermediates and affect early steps in chlorophyll synthesis. *Journal of Biological Chemistry* 287:682–692. DOI: 10.1074/jbc.M111.320994.

Yao DCI., Brune DC., Vermaas WFJ. 2012. Lifetimes of photosystem i and II proteins

in the cyanobacterium *Synechocystis* sp. PCC 6803. *FEBS Letters* 586:169–173. DOI: 10.1016/j.febslet.2011.12.010.

Yoshikawa K., Hirasawa T., Ogawa K., Hidaka Y., Nakajima T., Furusawa C., Shimizu H. 2013. Integrated transcriptomic and metabolomic analysis of the central metabolism of *Synechocystis* sp. PCC 6803 under different trophic conditions. *Biotechnology Journal* 8:571–580. DOI: 10.1002/biot.201200235.

Yu Y., You L., Liu D., Hollinshead W., Tang YJ., Zhang F. 2013. Development of *Synechocystis* sp. PCC 6803 as a Phototrophic Cell Factory. *Mar. Drugs* 11:2894–2916. DOI: 10.3390/md11082894.

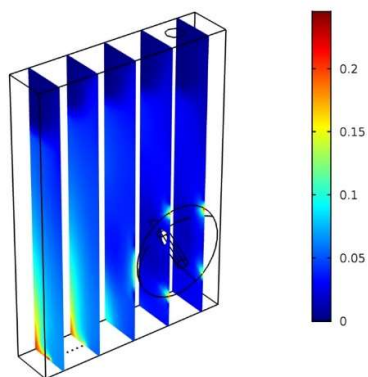
Zavřel T., Sinetova MA., Búzová D., Literáková P., Červený J. 2015. Characterization of a model cyanobacterium *Synechocystis* sp: PCC 6803 autotrophic growth in a flat-panel photobioreactor. *Engineering in Life Sciences* 15:122–132. DOI: 10.1002/elsc.201300165.

Zhang D., Dechatiwongse P., Hellgardt K. 2015. Modelling light transmission, cyanobacterial growth kinetics and fluid dynamics in a laboratory scale multiphase photo-bioreactor for biological hydrogen production. *Algal Research* 8:99–107. DOI: 10.1016/j.algal.2015.01.006.

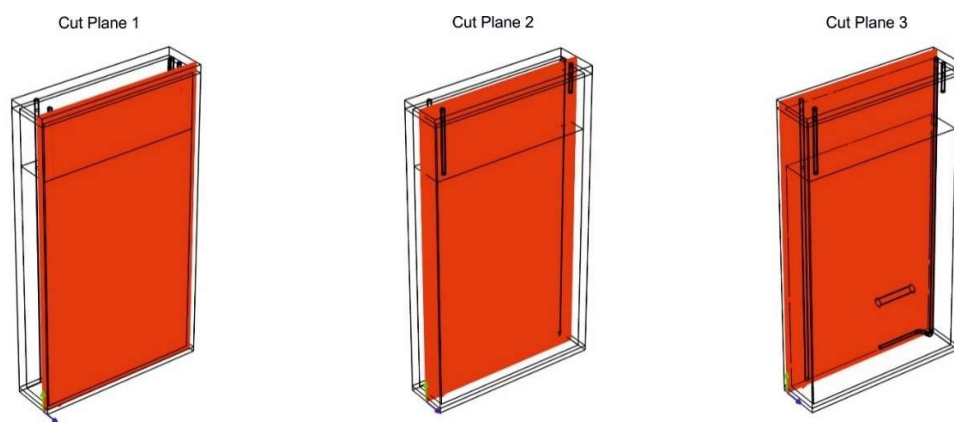
Zhang D., Xiao N., Mahbubani KT., del Rio-Chanona EA., Slater NKH., Vassiliadis VS. 2015. Bioprocess modelling of biohydrogen production by *Rhodospseudomonas palustris*: Model development and effects of operating conditions on hydrogen yield and glycerol conversion efficiency. *Chemical Engineering Science* 130:68–78. DOI: 10.1016/j.ces.2015.02.045.

Zhou J., Zhu T., Cai Z., Li Y. 2016. From cyanochemicals to cyanofactories: a review and perspective. *Microbial Cell Factories* 15. DOI: 10.1186/s12934-015-0405-3.

2.8 Supplementary information



S1 Fig. 3D slice trend of dispersed phase. The dispersed phase mixture of CO₂ and N₂ is plotted at 24 h and for incident light intensity, I_{inc} , equal to 300 $\mu\text{mol photons m}^{-2} \text{s}^{-1}$



S2 Fig. 3D visualization of three cut planes. The red planes represent the surface in which the R_I is plotted in Fig.2.5

Equation	Domain	Mathematical model
$\frac{\partial C_i}{\partial t} + \nabla \cdot C_i \mathbf{u} + \nabla \cdot \mathbf{J}_i^* = R_i$	3-4-6-7	MASS TRANSFER
$\mathbf{N}_i = \mathbf{J}_i^* + C_i \mathbf{u}$	3-4-6-7	
$\mathbf{J}_i^* = -D_i \nabla C_i$	3-4-6-7	
$\frac{\partial \rho}{\partial t} + \nabla \cdot (\rho \mathbf{u}) = 0$	3-4-6-7	FLUID-DYNAMICS
$\frac{\partial (\rho \mathbf{u})}{\partial t} + \nabla \cdot (\rho \mathbf{u} \mathbf{u}) = -\nabla p - \nabla \cdot \boldsymbol{\tau} + \rho \mathbf{g} + \mathbf{F}$	3-4-6-7	
$\boldsymbol{\tau} = -\mu [(\nabla \mathbf{u} + (\nabla \mathbf{u})^T) - \frac{2}{3} (\nabla \cdot \mathbf{u}) \mathbf{I}]$	4-6-7	
$\rho \frac{\partial k}{\partial t} + \rho \mathbf{u} \cdot \nabla k = \nabla \cdot ((\mu + \frac{\mu_T}{\sigma_k}) \nabla k) + \mathbf{P}_k - \rho \varepsilon$	4-6-7	
$\rho \frac{\partial \varepsilon}{\partial t} + \rho \mathbf{u} \cdot \nabla \varepsilon = \nabla \cdot ((\mu + \frac{\mu_T}{\sigma_\varepsilon}) \nabla \varepsilon) + C_{\varepsilon 1} \frac{\varepsilon}{k} \mathbf{P}_k - C_{\varepsilon 2} \rho \frac{\varepsilon^2}{k}$	4-6-7	
$\mathbf{P}_k = \mu_T (\nabla \mathbf{u} : (\nabla \mathbf{u} + (\nabla \mathbf{u})^T) - \frac{2}{3} (\nabla \cdot \mathbf{u})^2) - \frac{2}{3} \rho k \nabla \cdot \mathbf{u}$	4-6-7	
$\mu_T = \rho C_\mu \frac{k^2}{\varepsilon}$	4-6-7	
$\boldsymbol{\tau} = -(\mu + \mu_T) [(\nabla \mathbf{u} + (\nabla \mathbf{u})^T) - \frac{2}{3} (\nabla \cdot \mathbf{u}) \mathbf{I}] + \frac{2}{3} \rho k \mathbf{I}$	4-6-7	
$\phi_c + \phi_d = 1$	3-4-6-7	
$\mathbf{u} = \frac{\phi_c \rho_c \mathbf{u}_c + \phi_d \rho_d \mathbf{u}_d}{\rho}$	3-4-6-7	
$\rho = \phi_c \rho_c + \phi_d \rho_d$	3-4-6-7	
$\mu_{eff} = \mu_i + \mu_{i,T}$	3-4-6-7	
$\frac{\partial \phi_d}{\partial t} + \nabla \cdot (\phi_d \mathbf{u}_d) = -\frac{m_{dc}}{\rho_d}$	3-4-6-7	
$\mathbf{u}_d - \mathbf{u}_c = \mathbf{u}_{slip} - \frac{D_{md}}{(1-c_d)\phi_d} \nabla \phi_d$	3-4-6-7	
$c_d = \frac{\phi_d \rho_d}{\rho}$	3-4-6-7	

S1 Table. Model equations. The mathematical equations implemented in the software are listed and subdivided by the phenomena described, with the selection of computing domains.

Light intensity ($\mu\text{mol photons m}^{-2} \text{ s}^{-1}$)	$\text{OD}_{680}/\text{OD}_{720}$
50	1.774 ± 0.002
200	1.548 ± 0.042
300	1.518 ± 0.009
500	1.496 ± 0.022
800	1.475 ± 0.010
950	1.545 ± 0.035
1460	1.597 ± 0.041
200*	1.557 ± 0.017

S2 Table. Estimation of Chl *a* content in *Synechocystis* cells acclimated to different light intensities. Measurement by the PBR of the $\text{OD}_{680}/\text{OD}_{720}$ ratio, indicative of Chl *a* cellular content. The turbidostat-controlled cultures were grown in red-orange light under constant temperature (30°C) and pH (8.0). (*) Point of recovery at 200 $\mu\text{mol photons m}^{-2} \text{ s}^{-1}$

Domain	Element size	[m]
Reator	Height	0.1983
	Width	0.11
	Thickness	0.024
Sparger	Diameter of inlet	0.002
	Diameter of holes	0.0004
	Number of holes	7
	Lenght	0.03
Anchor	Diameter	0.006
	Lenght	0.035
Vessel	Thickness	0.0033

S3 Table. Geometry of photobioreactor.

	Gas phase	Liquid phase
Inlet velocity	150 ml/min	0
Outlet pressure	Gas outlet condition	Patm, no out
Gravity force	$g=(0,0,9.81)\text{ms}^{-2}$	
Wall conditions	No gas flux at the reactor boundary; sparger non-slip model	Wall functions
Incident light intensity	50/200/300/500/800/950/1460	

S4 Table. Boundary and operative conditions.

Chapter 3

Response of the thylakoid proteome of *Synechocystis* sp. PCC 6803 to photoinhibitory intensities of orange-red light

This chapter has been submitted as:

Alessandro Cordara, Marcello Manfredi, Pascal van Alphen, Emilio Marengo, Raffaele Pirone, Guido Saracco, Filipe Branco dos Santos, Klaas J. Hellingwerf, Cristina Pagliano.(2108). Response of the thylakoid proteome of *Synechocystis* sp. PCC 6803 to photoinhibitory intensities of orange-red light. *Plant Physiology and Biochemistry*.

Abstract

Photoautotrophic growth of *Synechocystis* sp. PCC 6803 in a flat-panel photobioreactor, run in turbidostat mode under increasing intensities of orange-red light (636 nm), showed a maximal growth rate (0.12 h^{-1}) at $300 \mu\text{mol}_{\text{photons}} \text{ m}^{-2} \text{ s}^{-1}$, whereas first signs of photoinhibition were detected above $800 \mu\text{mol}_{\text{photons}} \text{ m}^{-2} \text{ s}^{-1}$. To investigate the dynamic modulation of the thylakoid proteome in response to photoinhibitory light intensities, quantitative proteomics analyses by SWATH mass spectrometry were performed by comparing thylakoid membranes extracted from *Synechocystis* grown under low-intensity illumination (i.e. $50 \mu\text{mol}_{\text{photons}} \text{ m}^{-2} \text{ s}^{-1}$) with samples isolated from cells subjected to photoinhibitory light regimes (800 , 950 and $1460 \mu\text{mol}_{\text{photons}} \text{ m}^{-2} \text{ s}^{-1}$). We identified and quantified 126 proteins with altered abundance in all three photoinhibitory illumination regimes.

These data reveal the strategies by which *Synechocystis* responds to photoinhibitory growth irradiances of orange-red light. The accumulation of core proteins of Photosystem II and reduction of oxygen-evolving-complex subunits in photoinhibited cells revealed a different turnover and repair rates of the integral and extrinsic Photosystem II subunits with variation of light intensity. Furthermore, *Synechocystis* displayed a differentiated response to photoinhibitory regimes also regarding Photosystem I: the amount of PsaD, PsaE, PsaJ and PsaM subunits decreased, while there was an increased abundance of the PsaA, PsaB, Psak2 and PsaL proteins. Photoinhibition with 636 nm light also elicited an increased capacity for cyclic electron transport, a lowering of the amount of phycobilisomes and increase of the orange carotenoid protein content, all presumably as a photoprotective mechanism against the generation of reactive oxygen species.

3.1 Introduction

Cyanobacteria are among the most ancient prokaryotic microorganisms that appeared on Earth approximately 2.45 - 2.22 billion years ago. Their photosynthetic activity led to the accumulation of molecular oxygen in the atmosphere. *Synechocystis* forms spherical cells and its thylakoid membranes enclose a luminal space, arranged parallel to the plasma membrane and occasionally converging toward it to form biogenesis centres (Heinz et al., 2016). Differently from their plant chloroplast counterparts, in cyanobacteria the thylakoid membranes typically do not stack; rather they are uniformly sheet-like and densely packed with membrane proteins (Folea et al., 2008). The thylakoid membranes harbour the integral-membrane protein complexes of the photosynthetic electron transport chain, consisting of Photosystem (PS) II, Cytochrome *b₆f* (Cyt *b₆f*) and PSI, and also accommodate the ATP synthase (ATPase) and the majority of the respiratory electron transport complexes, amongst which are Complex I (NADH dehydrogenase I, NDH-1) and Complex II (succinate dehydrogenase, SDH). In the cyanobacterial thylakoid membrane system there is no evidence of a specific lateral distribution of those complexes; indeed a tight proximity exists especially for the two photosystems (Folea et al., 2008). Nevertheless, compartmentalized modules and supercomplexes, responsible for the formation of specific spatially separated domains and interactions, similarly to the chloroplast thylakoids of higher plants, do exist (Agarwal et al., 2010; Casella et al., 2017). In cyanobacteria, the protein complexes more represented within thylakoids are PSII, which occurs as a dimer, and PSI that is normally trimeric, differently from its higher plant counterpart that exists in a monomeric state. The most important component responsible for capturing sunlight and the subsequent transfer of excitation energy to the two PSs in cyanobacteria, is a supramolecular light harvesting system called phycobilisome (PBS). The PBS is a complex structure made up of phycobilins, water-soluble pigments strongly associated with proteins to form the brightly coloured phycobiliproteins, phycoerythrin (PE), phycocyanin (PC) and allophycocyanin (APC). Disks of phycobiliproteins, present as trimers and hexamers, are further arranged into cylinders by colourless linker proteins, and the cylinders are then assembled into PBS (Adir 2005). Thanks to the phycobiline chromophores, the PBS can adsorb visible light in the region between 500 and 670 nm, thus widening the effective absorption range of Chlorophyll *a* (Chl *a*, with absorption peaks at 435 and 680 nm) that is present - in part also with an antenna function - in the PSs (Adir 2005). The PBS interacts with the outer surface of the thylakoids and, although it transfers energy mainly to the PSII, there is evidence of its ability to channel energy directly also to PSI and to adjust its coupling to either PSII or PSI, depending on variation in illumination conditions (Rakhimberdieva et al., 2001). The energy absorbed by PBSs is transferred to the reaction centres of PSs where the photochemical reactions take place. The two PSs are connected by low-molecular-weight hydrogen/electron carriers, the plastoquinone (PQ), which

transfers electrons and protons from PSII to Cyt *b₆f*, and the plastocyanin and cytochrome *c₆*, which shuttle the electrons from Cyt *b₆f* to PSI. This linear electron flow (LEF) from PSII to PSI is accompanied by the formation of a proton gradient across the thylakoid membrane that is ultimately required to power ATP synthesis by the ATP synthase (Liu, 2016). Prolonged intense irradiation strongly reduces the photochemical efficiency of all oxygen-evolving photosynthetic organisms. Photodamage of the oxygen evolving complex (OEC) in PSII is the first event occurring in this process, which leads to the formation of reactive oxygen species (ROS) that inactivate the photochemical reaction centre of PSII, mainly at the site of the D1 protein (Tyystjärvi, 2008). Moreover, an excess of electrons coming from LEF can also cause photodamage of PSI through the formation of ROS on its donor side (Shimakawa et al., 2016). Cyanobacteria, as all the oxyphototrops, have developed mechanisms at different levels to defend themselves against photo-oxidative damage. Amongst these is the Non-Photochemical Quenching (NPQ) process, that is used to dissipate excess absorbed energy in the form of heat (Latifi et al., 2009). In cyanobacteria NPQ can be achieved via photoactivation of the orange carotenoid protein (OCP) that then, in its active form, binds to the core of the PBS and functions as energy quencher, thereby allowing the conversion of excess excitation energy into heat (Rakhimberdieva et al., 2004). Another photoprotective mechanism relies on the association of the flavodiiron (Flv) proteins Flv2/Flv4 to PSII, where they act as an electron sink at the PSII acceptor side, and allow cells to keep the PQ pool relatively oxidized. In this way Flv2/Flv4 also play an important role in photoprotection of PSII against oxidative stress (Zhang et al., 2009). Upon high light exposure, presumably to prevent photodamage to PSI, cyanobacteria overexpress the Flv1/Flv3 proteins, which divert electrons released from water-splitting by PSII directly back to O₂ by forming H₂O without production of ROS in a Mehler-like reaction (Allahverdiyeva et al., 2011). Under high light conditions, also other enzymes, such as catalases, superoxide dismutases (SOD) and peroxidases, all involved in ROS inactivation, are increasingly expressed (Tichy and Vermaas, 1999). High light stress also promotes (increased) cyclic electron flow (CEF) around PSI, in which electrons are returned from the PSI acceptor side back to the PSI donor side, thus preventing PSI photoinhibition (Thomas et al., 2001). Since CEF, in contrast to LEF, does not involve PSII, it does not result in the generation of reducing power by extraction of electrons from water, but it only produces a proton motive force that can supply additional ATP required for CO₂ fixation. In cyanobacteria, several routes for CEF exist. In one route, ferredoxin, reduced on the PSI donor side, is oxidized by the PGR5 protein that transfers electrons to the PQ pool; this electron cycle is completed by moving the electrons back to PSI via Cyt *b₆f* (Mullineaux 2014). Another route involves the thylakoid NDH-1 complex that participates in both respiratory and photosynthetic electron transport. In the latter case, reduced ferredoxin is oxidized by NDH-1, and the electrons are transferred to the PQ pool and subsequently to PSI through Cyt *b₆f* (Mullineaux 2014).

In this work, we have investigated the effects of increasing intensities (from 50 to 1460 $\mu\text{mol}_{\text{photons}} \text{m}^{-2} \text{s}^{-1}$) of incident orange-red monochromatic light of 636 nm on the steady-state growth rate of *Synechocystis*, cultivated in turbidostat mode in a laboratory scale photobioreactor (PBR). This wavelength was chosen because it allows the highest growth rate of *Synechocystis* in continuous light (Van Alphen et al., 2018), which is important from an application perspective. The constant monitoring of the cellular growth rate, used as an indicator for the physiological state of the cells, allowed detection of the threshold of light intensity that triggered photoinhibition. *Synechocystis* proved to be rather resilient to high light stress by monochromatic light of 636 nm, experiencing a state of severe photoinhibition only at intensities above 800 $\mu\text{mol}_{\text{photons}} \text{m}^{-2} \text{s}^{-1}$ (Cordara et al., in press). From cells grown under photoinhibitory light intensities of 800, 950 and 1460 $\mu\text{mol}_{\text{photons}} \text{m}^{-2} \text{s}^{-1}$ we isolated thylakoid membranes, on which then we performed an in-depth quantitative proteomic analysis, by using thylakoid membranes extracted from *Synechocystis* cells grown at 50 $\mu\text{mol}_{\text{photons}} \text{m}^{-2} \text{s}^{-1}$ as the reference. For this analysis we used SWATH-MS (sequential window acquisition of all theoretical ion spectra), an emerging label-free proteomic quantification approach that has been already used for accurate relative quantifications and large-scale identification of differentially expressed proteins in photosynthetic organisms such as plants (Albanese et al., 2016; Zhu et al., 2016) and green algae (Gao et al., 2016), but to our knowledge, not to study *Synechocystis* sp. PCC 6803 proteomics until now. This analysis allowed us to depict the dynamics of the thylakoid membrane proteome upon exposure of *Synechocystis* cells to photoinhibitory intensities of orange-red light

3.2 Material and Methods

3.2.1 Precultures

Pre-cultures of the glucose-tolerant wild-type *Synechocystis* sp. PCC6803 were prepared by growing cells in 25 mL flasks in BG11 medium supplemented with 10 mM NaHCO_3 (BG-11-PC), with a modified protocol as described in (Van Alphen and Hellingwerf, 2015). Pre-cultures were grown for 4 days at 30 °C in a shaking incubator at 120 rpm (New Brunswick Innova 44) under constant illumination with orange-red (632 nm) and blue (451 nm) light (10:1 photon ratio) at 30 $\mu\text{mol}_{\text{photons}} \text{m}^{-2} \text{s}^{-1}$, measured with a LI-250 quantum sensor (LI-COR).

3.2.2 Cell cultures

For studies of photoinhibition *Synechocystis* was grown in the commercial flat-panel PBR system FMT150.2/400 (Photon System Instruments), by inoculating 20 mL pre-culture in a final volume of approximately 380 mL. The culture medium used was BG-11-PC (Van Alphen et al., 2018).

The lid of the PBR was equipped with a combined pH/temperature probe (Mettler-Toledo) used to maintain the cell cultures at pH 8.0/30 °C, while the optical density (OD) at 720 and 680 nm was monitored with an integrated densitometer. The culture was illuminated from one side with orange-red light (636 nm, which is absorbed mainly by the phycobilisome antenna and thus favours the excitation of PSII) by high-power light emitting diodes (LEDs) providing the cells with the following light intensities: 50, 200, 300, 800, 950 and 1460 $\mu\text{mol}_{\text{photons}} \text{m}^{-2} \text{s}^{-1}$. Cells were subjected to increasing light intensity every 24 h. The CO₂ (1%, v/v in N₂) was provided by the system GMS150 (Photon Systems Instruments), coupled with a mass flow controller (Smart Mass Flow Model 5850S, Brooks Instruments) supplying a gas flow of 150 mL min⁻¹. The pH was kept in the range of 7.5 to 8.0 by adjusting the pCO₂ with gas mixing.

The PBR was run in turbidostat mode with the OD₇₂₀ measured by the integral densitometer, calibrated to a bench-top spectrophotometer OD₇₃₀ for maintaining the OD₇₃₀ at approximately 0.4 (with a maximum deviation of 3%) at 50 $\mu\text{mol}_{\text{photons}} \text{m}^{-2} \text{s}^{-1}$. In turbidostat mode, the cell density was held constant and the culture continued to grow exponentially under all tested illumination conditions.

3.2.3 Thylakoid membranes extraction

For each light intensity, at the end of the 24 h period, 90 mL of culture at the steady-state in the turbidostat was harvested, centrifuged at 2,000 g for 20 min at 4 °C and re-suspended in 4.5 mL of Buffer 1 (40 mM MES pH 6.5, 10 % (v/v) glycerol, 15 mM MgCl₂, and 15 mM CaCl₂) containing protease inhibitors (cOmplete™, Mini, EDTA-free Protease Inhibitor Cocktail). Cells at a final Chl *a* concentration of ~1.0 mg mL⁻¹ were broken with 2 passages through a high-pressure cell disruptor (One Shot, Constant system limited) and the debris were pelleted at 1,000 g for 2 min at 4 °C. The supernatant was washed with 15 mL of Buffer 1 and the thylakoids pelleted at 150,000 g for 20 min at 4 °C. The membranes were subsequently re-suspended in 2 mL of Buffer 2 (20 mM MES pH 6.5, 25% (v/v) glycerol, 10 mM MgCl₂, and 20 mM CaCl₂). It is relevant to note that in this protocol for thylakoid membrane extraction, the thylakoids were intentionally not extensively washed

during isolation, to preserve *in situ* the membrane-bound components interacting on the cytoplasmic side of the thylakoid membranes, as well as residual PBSs.

The Chl concentration was measured spectrophotometrically (Lambda25 spectrophotometer, Perkin Elmer) after extraction from membranes in 80% (v/v) acetone according to (Arnon, 1949).

3.2.4 Gel electrophoresis

The mono-dimensional sodium dodecyl sulphate polyacrylamide gel electrophoresis (SDS-PAGE) was made with 12.5% (w/v) polyacrylamide gel containing 6 M urea and the proteins were denatured and resolved following the Laemmli's protocols (Laemmli, 1970). To visualize proteins, the gel was stained by silver staining system (Switzer et al., 1979).

3.2.5 Protein precipitation and digestion

Thylakoid membranes corresponding to 150 µg Chl from three biological replicates were pooled and then precipitated in ice-cold acetone overnight at -20 °C to remove attached pigments. The thylakoid proteins were solubilized in Buffer 3 (50 mM Tris-HCl pH 8.0, 2 M thiourea, 6 M urea, 20 mM DDT) and the Bradford assay was used to determine the protein concentration (Bradford, 1976a).

Denatured proteins, 30 µg for each biological condition, at 0.3 mg mL⁻¹ concentration in Buffer 3 were incubated with 10 mM DTT for 30 min at 37 °C and, subsequently, treated for 30 min with 20 mM iodoacetamide at room temperature in darkness. Protein digestion was carried out in 100 mM ammonium bicarbonate with trypsin (Sigma, code T6567) at a final protein:protease ratio of 25:1 (w/w), followed by incubation at 37 °C overnight. Desalting of the tryptic products was performed by solid phase extraction using 30 mg Oasis HLB cartridges (Waters). The resulting eluates were mixed with approximately 1,500 femtomoles of a synthetic heavy peptide used as internal standard (Cellmano Biotech, Hefei, China), and lyophilized.

3.2.6 Mass spectrometry analysis

Peptides were analysed by a micro-LC Eksigent Technologies (Dublin, USA) system that included a micro LC200 Eksigent pump with flow module 5-50 µL coupled with a TripleTOF system 5600⁺ (AB Sciex). A Halo Fused C18 column (0.5 x 100 mm, 2.7 µm; Eksigent Technologies) was used as stationary phase. A mixture of 0.1% (v/v) formic acid in water (A) and 0.1% (v/v) formic acid in

acetonitrile (B) was used as mobile phase, eluting at a flow-rate of 15.0 $\mu\text{L min}^{-1}$ and at an increasing concentration of solvent B from 2% to 40% in 30 min. Peptides were dissolved in 30 μL of LC-MS/MS mobile phase A, and 4.0 μL samples were injected. The oven temperature was set at 40 $^{\circ}\text{C}$.

For protein identification based on the analysis of trypsin-digested peptides, the mass spectrometer worked in Data Dependent Acquisition (DDA) mode. In this type of mass spectrometric acquisition, the mass spectrometer works in a mass range of 100-1600 Da (TOF scan with an accumulation time of 0.25 s), coupled to a MS/MS product ion scan from 200 to 1250 Da (accumulation time of 5.0 ms) with the abundance threshold set at 30 cps (35 candidate ions can be monitored per cycle). The electrospray ion source was set in the positive mode with the following parameters: curtain gas (N_2) at 25 psig, nebulizer gas GAS1 at 25 psig, and GAS2 at 20 psig, ionspray floating voltage at 5000 V, source temperature at 450 $^{\circ}\text{C}$ and declustering potential at 25 V.

To perform the label free quantification, the samples undergo a cyclic data-independent analysis (DIA) SWATH of the mass spectra with a 25 Da window width (Gillet et al., 2012). The mass spectrometer was operated such that a 50 ms survey scan (TOF-MS) was performed and subsequent MS/MS experiments were carried out on all precursors. These MS/MS experiments were performed in a cyclic manner using an accumulation time of 40 ms per 25 Da SWATH (36 total SWATHs) for a total cycle time of 1.6408 s. The ions were fragmented for each MS/MS experiment in the collision cell using rolling collision energy. All MS data were acquired with Analyst TF 1.7 (AB Sciex). For each sample, two DDA runs for protein identification and three DIA runs for protein quantification were carried out.

3.2.7 Protein database search and identification

The DDA files were analysed and searched using the database search engine ProteinPilotTM v.5.0 (Sciex) and the Paragon algorithm. The following sample parameters were set: trypsin as digestion enzyme, carbamidomethylation for the cysteine alkylation and no special factors. Processing parameters were set to "Biological modification". UniProtKB database containing *Synechocystis* proteins (version 2017.05.19, with 1364 entries), through ID search effort. Only protein IDs with a ProteinPilot unused score of at least 1.3 (equivalent to a 95% confidence interval) used as cut-off threshold were accepted. The estimated local false discovery rate (FDR) was set at 1%.

3.2.8 Protein quantification

The quantification was performed by integrating the obtained ion chromatograms of all the unique ions for a specific peptide. The DDA acquisitions were used to build a peptides/proteins library. The quantification was performed with PeakView 2.0 and MarkerView 1.2. (Sciex). At least 6 peptides and 6 transitions per protein were extracted from the SWATH files. Shared peptides and peptides with modifications were excluded. Only the peptides with an FDR lower than 1% were used for the t-test performed by MarkerView.

3.3 Results and discussion

3.3.1 Physiological monitoring of cellular photoinhibition

We investigated the growth irradiances that cause photoinhibition in *Synechocystis* by monitoring the growth rate of cells cultured in PBR under increasing intensities of orange-red (636 nm) light. To this end cyanobacterial cells were grown at a constant OD₇₂₀ by running the PBR in turbidostat mode, which assures that cells continue to grow exponentially, with the maximal rate that the selected light intensity allows (Martínez et al., 2011). Therefore, the temperature and pH of the growth medium in the PBR were kept constant to assure that only the variation of the light intensity could affect *Synechocystis* growth. The growth rate, monitored at each incremental step of light intensity, revealed three different growth ranges: (i) the low-intensity range (below 50 $\mu\text{mol}_{\text{photons}} \text{m}^{-2}\text{s}^{-1}$) in which the cells were not light-stressed and increased their growth rate proportionally with light intensity; (ii) an intermediate range (around 300 $\mu\text{mol}_{\text{photons}} \text{m}^{-2}\text{s}^{-1}$) in which the cells grew close to, or at, their maximal rate; (iii) the third range ($> 1000 \mu\text{mol}_{\text{photons}} \text{m}^{-2}\text{s}^{-1}$) characterized by increasing photoinhibition with light intensity (Fig. 3.1). At 50 $\mu\text{mol}_{\text{photons}} \text{m}^{-2} \text{s}^{-1}$ *Synechocystis* showed a modest growth rate of $0.054 \pm 0.003 \text{ h}^{-1}$, while increasing the light intensity up to 200 and 300 $\mu\text{mol}_{\text{photons}} \text{m}^{-2}\text{s}^{-1}$ the generation time rapidly increased to its maximum value under the selected conditions, i.e. of $0.117 \pm 0.006 \text{ h}^{-1}$. *Synechocystis* growth started to slow-down at higher intensities, i.e. at 800 $\mu\text{mol}_{\text{photons}} \text{m}^{-2}\text{s}^{-1}$ to $0.100 \pm 0.012 \text{ h}^{-1}$ and was less than half of the maximum rate at 1460 $\mu\text{mol}_{\text{photons}} \text{m}^{-2}\text{s}^{-1}$ ($0.043 \pm 0.020 \text{ h}^{-1}$).

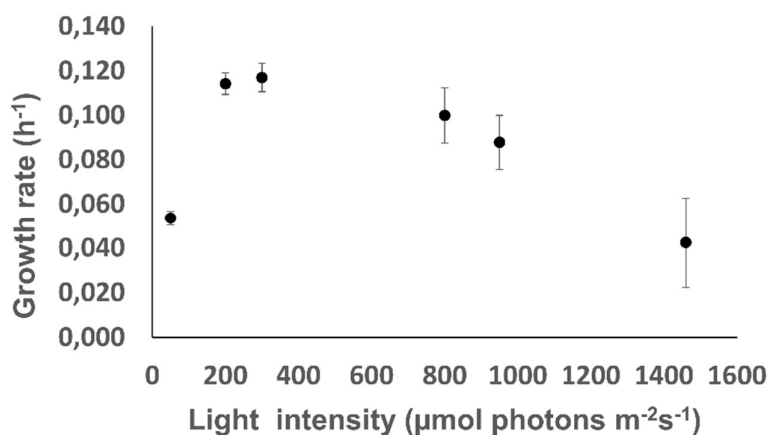


Fig 3.1. Growth of *Synechocystis* sp. PCC 6803 under increasing intensities of orange-red light. The cells, grown under turbidostat mode at constant temperature (30°C) and pH (8.0), were acclimated for 24 h at each light intensity tested (50, 200, 300, 800, 950 and 1460 $\mu\text{mol photons m}^{-2}\text{s}^{-1}$). The growth rate (h^{-1}) was calculated by linear regression of log transformed OD730 change during the growth phases in the 24 h. Values are the average and standard deviation derived from three biological replicates.

It is worth noting that *Synechocystis* showed a rather stable growth under low (50 $\mu\text{mol}_{\text{photons}}\text{ m}^{-2}\text{s}^{-1}$) and moderate (200 - 300 $\mu\text{mol}_{\text{photons}}\text{ m}^{-2}\text{s}^{-1}$) light intensities; conversely at high intensities (800, 950 and 1460 $\mu\text{mol}_{\text{photons}}\text{ m}^{-2}\text{s}^{-1}$) the growth rate became increasingly noisy (Fig. 3.1), indicative of a gradually increased stressing of the cells. The sharp increase in the cellular growth rate observed in the light step from 50 to 200 $\mu\text{mol}_{\text{photons}}\text{ m}^{-2}\text{s}^{-1}$ re-emphasized that *Synechocystis* readily (i.e. well within 24 h) adapts its metabolisms in response to increased growth irradiance up to saturating intensities (Zavřel et al., 2015). On the contrary, at the high light intensities, between 800 and 1460 $\mu\text{mol}_{\text{photons}}\text{ m}^{-2}\text{s}^{-1}$, *Synechocystis* experienced a severe slow-down in its growth rate, likely due to the photoinhibition induced by excessive irradiation that triggers oxidative stress, ultimately resulting in a variety of damages to its key cellular components (e.g., lipids, nucleic acids, pigments, proteins) (Latifi et al., 2009). **Moreover, as already pointed out in chapter 2, the increasing intensities of orange-red light influence also the PSII activity in a analogous way to the growth rate.**

3.3.2 Functional classification of differently expressed proteins in thylakoids isolated from photoinhibited cells

The dynamics of the photosynthetic apparatus in cells grown under photoinhibitory intensities of 800, 950 and 1460 $\mu\text{mol photons m}^{-2}\text{s}^{-1}$ were investigated by performing mass spectrometry analyses on thylakoid membranes isolated from high-light treated cells and compared to the control light (50 $\mu\text{mol photons m}^{-2}\text{s}^{-1}$) counterpart.

A preliminary SDS-PAGE of thylakoids extracted from *Synechocystis* cells grown under the different light intensities showed a similar protein composition, despite the relative amount of proteins varied among samples (Fig 3.2).

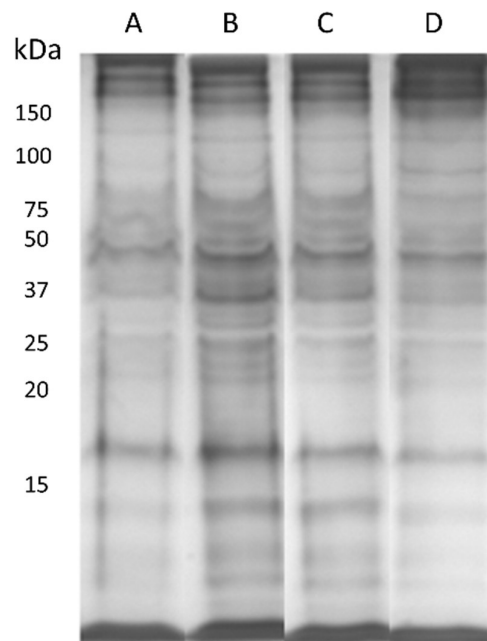


Fig 3.2. Protein composition of thylakoid membranes of *Synechocystis* grown under photoinhibitory intensities of orange-red light. Silver stained SDS-PAGE of *Synechocystis* thylakoids isolated from cells acclimated for 24 h at photoinhibitory light intensities of 800, 950 and 1460 $\mu\text{mol photons m}^{-2}\text{s}^{-1}$ compared to the low light intensity of 50 $\mu\text{mol photons m}^{-2}\text{s}^{-1}$ used as control. The same amount of Chl (3 μg) was loaded on each lane. Labels on the left indicate the molecular weight positions (Bio-Rad precision plus) A : cells growth at 50 $\mu\text{mol photons m}^{-2}\text{s}^{-1}$, B: cells growth at 800 $\mu\text{mol photons m}^{-2}\text{s}^{-1}$, C: cells growth at 950 $\mu\text{mol photons m}^{-2}\text{s}^{-1}$, D:cells growth at 1460 $\mu\text{mol photons m}^{-2}\text{s}^{-1}$

Comparing the line A (cells growth at $50 \mu\text{mol photons m}^{-2}\text{s}^{-1}$) with the lines B and C (cells growth at 800 and 950 $\mu\text{mol photons m}^{-2}\text{s}^{-1}$ respectively) it is visible how in the two photoinhibitory condition the amount of proteins is higher. From this preliminary data we can suggest that the light stress regime can induce the cells to an overexpression of some proteins needed to cope the photoinhibitory condition. Conversely, comparing the line D (cells growth under 1460 $\mu\text{mol photons m}^{-2}\text{s}^{-1}$ respectively) with line B and C, the decrease in the amount of both proteins ranged between 20 and 25 kDa and proteins below 15 kDa, resulted in an increased abundance of proteins with a molecular weight higher than 150 kDa. In this case we can suggest that the prolonged exposure of the cells to extreme light condition results in the impairment of both mechanisms the biosynthesis process and the degradation of the damaged proteins. In this last case the accumulation of fragments of the impair proteins could lead to the formation of agglomerate at high molecular weight.

The subsequent relative quantification of the thylakoid membrane proteome was carried out using the label-free SWATH-MS analysis, by comparing cells from the control light regime ($50 \mu\text{mol}_{\text{photons}} \text{m}^{-2} \text{s}^{-1}$) against those from the three photoinhibitory illumination conditions (800, 950 and 1460 $\mu\text{mol}_{\text{photons}} \text{m}^{-2} \text{s}^{-1}$). Proteins with fold changes ≥ 1.35 or ≤ 0.73 with adjusted p -values ≤ 0.05 were considered present at significantly different amounts in the samples. Accordingly, we identified 380 proteins (Supplementary Table S1), amongst which we were able to quantify 126 proteins representing the thylakoid proteome with altered abundance in samples from all three photoinhibitory illumination conditions, relative to the control regime (Supplementary Table S1). Regarding the functional distribution of the differently-expressed proteins, 25% belonged to structural proteins of the photosynthetic apparatus (ATPase, Cyt *b₆f*, proteins involved in electron transport, PSI and PSII), 26% represented auxiliary proteins of thylakoid membranes (structural and associated proteins of the PBSs, proteases, proteins involved in pigments biosynthesis, PSI and PSII assembly, cellular redox homeostasis and transporters), 43% were ribosomal or ribosome-related proteins, and 6% represented other proteins (not classifiable in the other categories, but functionally related to thylakoid membranes) (Fig. 3.3).

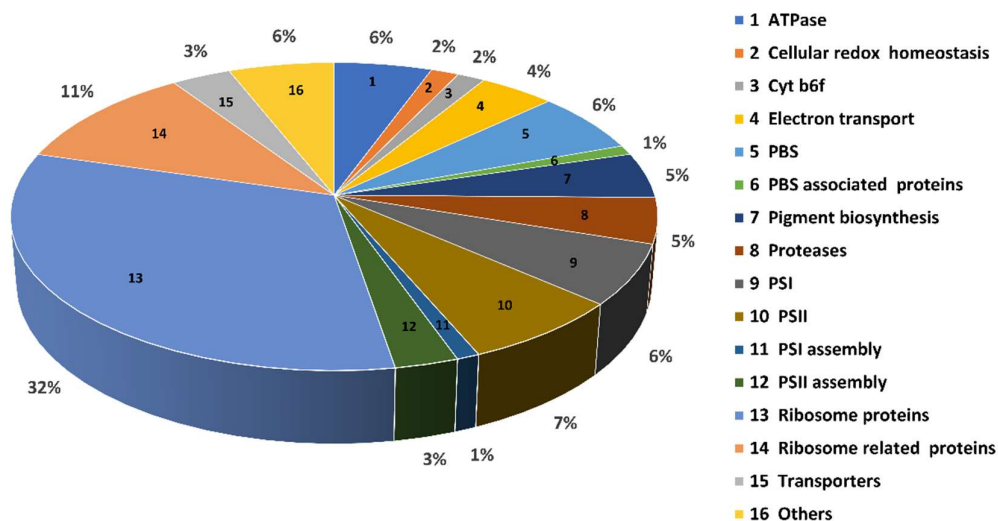


Fig 3.3. Functional classification of the proteins that represent the thylakoid proteome of *Synechocystis* which are significantly different in all the three photoinhibitory conditions with respect to the low light intensity. Graphical distribution of the 126 proteins that from relative mass spectrometry quantification are considered differentially abundant in all the three photoinhibitory conditions 800, 950 and 1460 $\mu\text{mol photons m}^{-2} \text{s}^{-1}$ when compared to 50 $\mu\text{mol photons m}^{-2} \text{s}^{-1}$ used as control. The percentage of proteins per functional category is shown.

3.3.3 Quantitation of the changes in the proteome of the thylakoid membrane of photoinhibited cells

3.3.3.1 Photosystem II

PSII is the first multi-enzymatic complex involved in the light reactions of photosynthesis occurring in the thylakoid membranes. In cyanobacteria, PSII is composed of 20 protein subunits, 35 Chl *a* molecules, 12 carotenoids and 25 lipid molecules (Umena et al., 2011). The PSII reaction centre consists of the proteins D1 (PsbA) and D2 (PsbD), connected to the CP47 (PsbB) and CP43 (PsbC) core antenna proteins and the α and β (PsbE and PsbF) subunits of cytochrome b559. Beyond the reaction centre, there are several integral low molecular mass subunits that form the PSII core. The OEC, which consists of the Mn_4CaO_5 cluster and the extrinsic proteins PsbO, PsbU and PsbV (Umena et al., 2011) (Umena et al., 2011) (Umena et al., 2011) (Umena et al., 2011) (Umena et al., 2011).

2011)(Umena et al., 2011)(Umena et al., 2011)(Umena et al., 2011)(Umena et al., 2011), is bound to the D1 and CP43 subunits of the PSII core on the luminal side of the thylakoid membrane where it catalyses water oxidation, with release of molecular oxygen.

The relative quantification of the PSII protein subunits in *Synechocystis* grown in control light with respect to photoinhibitory regimes revealed an opposite trend in the abundance of the PSII core proteins and the OEC subunits (Table 3.1). The PSII core proteins were more abundant under photoinhibitory regimes; conversely, the extrinsic proteins PsbO, PsbU and PsbV were more represented in the control illumination sample. This opposite trend can be due to different turnover rates, as well as to independent replacement of the PSII core and the OEC proteins with variation of the light intensity (Yao et al., 2011). The impairment of the OEC is the first event occurring in the process of photoinhibition (Zavafer et al., 2015); damage of the OEC leads to the production of ROS, which subsequently attack the nearby PSII core proteins. During photoinhibition, the D1 protein is the main target of oxidation by ROS and its rapid turnover (~30 minutes) is essential for prompt PSII repair (Aro et al., 1993b). The other PSII core proteins have a turnover that ranges from 3.3 to 11 hours (Yao et al., 2011); in contrast, the OEC subunits show much lower turnover rates (*i.e.*, 33 hours for PsbO) (Yao et al., 2011). Considering the high turnover of the PSII core proteins, their accumulation observed in *Synechocystis* grown under photoinhibitory regimes (Table 3.1) can be the result of a boosted PSII repair cycle. Conversely, due to their lower turnover rate, the OEC proteins are not promptly replaced, thus constitutively suffering more from the photodamage caused by progressively increased ROS formation during the photoinhibitory illumination. Another reason for the lower abundance of the OEC subunits detected under high light intensities (Table 3.1) can be the light-stress-induced down-regulation of the genes encoding these proteins (Muramatsu and Hihara, 2012). These results suggest that when the growth irradiance becomes extremely high and stressful for *Synechocystis* (*i.e.* $1460 \mu\text{mol}_{\text{photons}} \text{m}^{-2} \text{s}^{-1}$), the significant decrease observed in the cellular growth rate (Fig. 3.1) is likely related to a severe OEC damage (Table 3.1). **This hypothesis is also strengthened by the results already shown in chapter 2. Indeed, the oxygen dissolved in the medium (dO₂) decreases in a similar way to the growth rate when *Synechocystis* is grown under photoinhibitory light condition the figure (Fig. 2.3B).**

Protein name, gene	FC 50 vs 800	FC 50 vs 950	FC 50 vs 1460
Photosystem II			
Cytb559 α , <i>psbE</i>	0,59	0,54	0,61
CP47, <i>psbB</i>	0,28	0,23	0,26
CP43, <i>psbC</i>	0,31	0,26	0,33
D1, <i>psbA2</i>	0,31	0,23	0,35
D2, <i>psbD</i>	0,36	0,29	0,42
PsbH, <i>psbH</i>	0,23	0,20	0,22
PsbO, <i>psbO</i>	1,35	1,60	1,35
PsbU, <i>psbU</i>	2,95	3,13	2,45
PsbV, <i>psbV</i>	2,05	2,06	2,31
Photosystem I			
PsaA, <i>psaA</i>	0,49	0,40	0,39
PsaB, <i>psaB</i>	0,51	0,42	0,38
PsaD, <i>psaD</i>	2,30	2,41	2,01
PsaE, <i>psaE</i>	2,21	2,15	1,96
PsaK2, <i>psaK2</i>	0,35	0,30	0,37
PsaJ, <i>psaJ</i>	4,10	4,72	6,04
PsaL, <i>psaL</i>	0,59	0,46	0,42
PsaM, <i>psaM</i>	2,54	4,20	2,57
Cytochrome <i>b6f</i>			
Cytochrome b6, <i>petB</i>	0,15	0,12	0,13
Cytochrome f, <i>petA</i>	0,32	0,27	0,22
Electron transport			
Cytochrome c6, <i>petJ</i>	5,75	10,02	3,92
FNR, <i>petH</i>	0,52	0,47	0,56
NdhH, <i>ndhh</i>	0,32	0,29	0,32
NdhI, <i>ndhi</i>	0,31	0,40	0,38
NdhJ, <i>ndhj</i>	0,30	0,31	0,26
NdhK1, <i>ndhK1</i>	0,23	0,29	0,25
Plastocyanin, <i>petE</i>	3,08	3,54	2,82
ATP-synthase			
ATPase a , <i>atpB</i>	0,11	0,12	0,08
ATPase c, <i>atpE</i>	0,09	0,07	0,04
ATPase α , <i>atpA</i>	0,25	0,25	0,25
ATPase β , <i>atpD</i>	0,37	0,36	0,36
ATPase γ , <i>atpG</i>	0,47	0,38	0,44
ATPase δ , <i>atpH</i>	0,27	0,27	0,24

ATPase ϵ , <i>atpC</i>	1,55	2,21	1,69
Phycobilisome			
APC alpha subunit, <i>apcA</i>	1,70	1,76	1,60
ApcC/APC-associated linker, <i>apcC</i>	3,25	3,69	3,56
ApcE/core-membrane linker, <i>apcE</i>	0,47	0,39	0,44
APC subunit beta 18, <i>apcF</i>	1,39	1,50	1,64
C-phyocyanin alpha chain, <i>cpcA</i>	1,89	1,69	1,66
CpcC1/PC-associated linker, <i>cpcC1</i>	2,12	2,30	2,14
CpcC2/PC-associated linker, <i>cpcC2</i>	4,57	5,05	3,99
CpcD/PC rod linker, <i>cpcD</i>	5,53	5,70	5,60

Table 3.1. Relative quantification of the differentially abundant photosynthetic structural proteins of thylakoid membranes isolated from *Synechocystis* grown under photoinhibitory conditions. The fold change (FC) refers to the comparison of samples at 50 $\mu\text{mol photons m}^{-2} \text{s}^{-1}$ vs 800 $\mu\text{mol photons m}^{-2} \text{s}^{-1}$ (50 vs 800), 50 $\mu\text{mol photons m}^{-2} \text{s}^{-1}$ vs 950 $\mu\text{mol photons m}^{-2} \text{s}^{-1}$ (50 vs 950) and 50 $\mu\text{mol photons m}^{-2} \text{s}^{-1}$ vs 1460 $\mu\text{mol photons m}^{-2} \text{s}^{-1}$ (50 vs 1460).

Cells adapted to photoinhibitory irradiances accumulated an increased quantity of thylakoid membrane proteases belonging to the FtsH family (Table 3.2). *Synechocystis* possesses four FtsH isoforms, FtsH1-4, of which FtsH1 and FtsH3 are indispensable for the cell viability (Mann et al., 2000), while FtsH2 has a crucial role in the PSII repair in response to light stress (Nixon et al., 2005). Considering the direct involvement of the FtsH family in the removal of photodamaged D1 protein from the membrane and its degradation (Nixon et al., 2005), the higher amount of these proteases found in photoinhibited cells (Table 3.2) indicates their major role for sustaining the faster PSII reaction centre turnover occurring at high light regimes. In addition, we found that under photoinhibitory conditions *Synechocystis* accumulated larger amounts of the PSII auxiliary proteins Psb27 and Ycf48 with respect to the control regime (Table 3.2). Ycf48 and Psb27 are indispensable proteins for cyanobacterial growth (Jackson et al., 2014), and several studies have assessed their involvement in the recovery from photoinhibition and in the sequential steps of PSII assembly (Nowaczyk et al., 2006; Roose and Pakrasi, 2008; Komenda et al., 2008). These studies have revealed that Ycf48 participates in the prompt turnover and replacement of the photodamaged D1 protein (Komenda et al., 2008), whereas Psb27 plays a key role during PSII biogenesis (Nowaczyk et al., 2006; Roose and Pakrasi, 2008). Although Psb27 does not seem to be essential for photosynthesis in *Synechocystis* sp. PCC 6803 (Roose and Pakrasi, 2008),

knockout mutants in *T. elongatus* demonstrated its importance to increase the ability of cyanobacteria to cope with, and recover from, photodamage under photoinhibitory conditions (Nowaczyk et al., 2006). Considering the predicted function of Psb27 during PSII assembly, specifically in the insertion of the CP43 module in the non-functional PSII intermediate and in the integration of the $Mn_4Ca_1Cl_x$ cluster within the PSII complex prior to the association of the extrinsic proteins to PSII (Roose and Pakrasi, 2008), the simultaneous decrease of PsbO, PsbU and PsbV (Table 3.1) and increase of Psb27 (Table 3.2) observed in *Synechocystis* in high light suggests the existence of a concerted mechanism that finally leads to the accumulation of inactive PSII intermediates in photoinhibited cells. In contrast to Psb27 and Ycf48, Psb28 was more abundant in cells grown in the control light regime than in high light (Table 3.2). Although the exact role of Psb28 is still unclear, a regulatory function in PSII assembly was suggested for this protein, because of its preferential binding to the PSII intermediates containing CP47 and its involvement in the biogenesis of the Chl molecules utilized for the functional activation of CP47 (Dobáková et al., 2009). However, the absence of Psb28 in *Synechocystis* deletion mutants did not affect the functional properties of PSII and an accelerated turnover of the D1 protein and faster PSII repair cycle were observed with respect to the wild type (Dobáková et al., 2009). Therefore, the lower amount of Psb28 in *Synechocystis* at photoinhibitory light regimes (Table 3.2) suggests a faster operation of the PSII repair cycle, which is consistent with the observed increased amount of PSII core subunits (Table 3.1) and FtsH proteases (Table 3.2).

Protein name, gene	FC 50 vs 800	FC 50 vs 950	FC 50 vs 1460
Cellular redox homeostasis			
Superoxide dismutase [Fe], <i>sodB</i>	0,54	0,5	0,4
Thioredoxin, <i>trxA</i>	3,19	3,32	2,79
Photosystem I assembly			
Ycf4, <i>ycf4</i>	0,24	0,21	0,19
Slr 1128 protein, <i>slr1128</i>	0,32	0,34	0,22
Photosystem II assembly			
Psb27, <i>psb27</i>	0,44	0,38	0,37
Psb28, <i>psb28</i>	2,45	2,79	2,06
Ycf48-like protein, <i>slr2034</i>	0,21	0,17	0,22
Pigments biosynthesis			

Mg-chelatase subunit Chll, <i>chlI</i>	0,37	0,34	0,41
Mg-protoporphyrin IX monomethyl ester cyclase 1, <i>acsF1</i>	0,23	0,26	0,26
Delta-aminolevulinic acid dehydratase, <i>hemB</i>	0,54	0,53	0,47
Geranylgeranyl diphosphate reductase, <i>chlP</i>	0,42	0,49	0,5
Heme oxygenase 1, <i>pbsA1</i>	0,68	0,71	0,67
Porphobilinogen deaminase, <i>hemC</i>	0,36	0,31	0,31
Phycobilisome-associate proteins			
OCP, <i>slr1963</i>	0,17	0,13	0,2
Proteases			
Clp1, <i>clpP1</i>	0,51	0,53	0,59
Clp3, <i>clpP3</i>	0,36	0,27	0,4
ClpR, <i>clpR</i>	0,21	0,24	0,23
FtsH2, <i>ftsH2</i>	0,23	0,17	0,21
FtsH3, <i>ftsH3</i>	0,2	0,17	0,2
FtsH4, <i>ftsH4</i>	0,32	0,26	0,28
Transporters			
Iron uptake protein A1, <i>futA1</i>	0,12	0,11	0,22
Iron uptake protein A2, <i>futA2</i>	0,22	0,3	0,5
Na(+)/H(+) antiporters, <i>nhaS3</i>	0,15	0,12	0,1
SecY, <i>secY</i>	0,09	0,08	0,08
Others			
Glyceraldehyde-3-phosphate dehydrogenase 2, <i>gap2</i>	0,33	0,34	0,37
RuBisCO large chain, <i>cbbL</i>	0,17	0,17	0,17
Phosphoribulokinase, <i>Prk</i>	0,33	0,33	0,33
Probable RuBisCO transcriptional regulator, <i>rbcR</i>	0,2	0,2	0,2
Sll1769 protein, <i>sll1769</i>	0,51	0,51	0,51
RuBisCO small chain	0,66	0,66	0,66

Table 3.2. Relative quantification of the differentially abundant adjuvant proteins of thylakoid membranes isolated from *Synechocystis* grown under photoinhibitory conditions. The fold change (FC) refers to the comparison of samples at 50 μmol photons

$\text{m}^{-2} \text{s}^{-1}$ vs $800 \mu\text{mol photons m}^{-2} \text{s}^{-1}$ (50 vs 800), $50 \mu\text{mol photons m}^{-2} \text{s}^{-1}$ vs $950 \mu\text{mol photons m}^{-2} \text{s}^{-1}$ (50 vs 950) and $50 \mu\text{mol photons m}^{-2} \text{s}^{-1}$ vs $1460 \mu\text{mol photons m}^{-2} \text{s}^{-1}$ (50 vs 1460).

3.3.3.2 Photosystem I

PSI is a multi-enzymatic complex embedded in the thylakoid membranes responsible for the photosynthetic electron transfer from the plastocyanin/cytochrome c6 to the ferredoxin. In cyanobacteria, PSI exists mostly in trimeric form, each monomer being composed of nine transmembrane proteins, among which PsaA and PsaB form the PSI core, together with three stromal extrinsic subunits (Jordan et al., 2001).

From our data it is evident that the stromal proteins PsaD and PsaE and the intrinsic subunits PsaJ and PsaM are more abundant in cells grown under control than under photoinhibitory conditions; the opposite was found for the two core subunits PsaA/PsaB and the integral membrane proteins PsaK2 and PsaL (Table 3.1). PsaD and PsaE with PsaC form the extrinsic protein complex of PSI, which is mainly involved in binding ferredoxin and in facilitating the corresponding electron transfer. PsaM is a peculiar subunit of cyanobacteria located in the monomer/monomer interface, while PsaJ is situated on the distal part of PSI (Jordan et al., 2001). Literature shows that in *Synechocystis* PCC 6803 the thylakoid membranes contain five times more PSI than PSII under physiological growth and illumination conditions (Szabò et al., 2001), and that upon shifting cyanobacteria to high white light intensity, a selective down-regulation of PSI occurs (Muramatsu et al., 2009). Thus, it is likely that photoinhibitory orange-red light growth regimes provoke a lowering in the amount of PsaD, PsaE, PsaJ and PsaM (Table 3.1) similarly to the white light counterpart. The accumulation of PsaA/PsaB, PsaK2, PsaL (Table 3.1) as well as of the PSI assembly factor Ycf4 (Table 3.2) in the photoinhibitory regime apparently is in contradiction with the mechanism of high light induced down-regulation of PSI (Muramatsu et al., 2009); however, there is evidence that these components are necessarily abundant under specific light conditions to guarantee PSI functionality. Notably, *Synechocystis* PCC 6803 cells shifted from white to high intensity of orange light, similar to our experimental conditions, stimulated the *psaA/psaB* transcription instead of down-regulating it (Herranen et al., 2005). These results indicate that an effective light quality control of the transcription of the *psaA/psaB* genes exists, with ‘PSII-light’ (i.e., light selective for PSII) enhancing the transcription and ‘PSI-light’ (i.e., light selective for PSI) exerting an opposite effect, and that the redox poise between the two PSs might mediate the light signal to regulate the *psaA/psaB* transcription. The accumulation of PsaA and PsaB proteins observed under photoinhibitory intensities

of orange-red light (Table 3.1) indicates that the increased transcription rate of *psaA/psaB* transcripts expected in this light condition (Herranen et al., 2005) is closely paralleled by their translation rate, thus playing a major role in determining the content of functional PSI reaction centre cores at high intensities of light favouring PSII excitation. Psak2, one of the two cyanobacterial isoforms of PsaK, that is located in the periphery of PSI, is essential for energy transfer from PBS to PSI in *Synechocystis* sp. PCC 6803 grown under high light condition (Fujimori et al., 2005). Under high light, in addition to Psak2, the high light-inducible polypeptides (HLIPs) play a key role in the protection and maintenance of PSI functionality, by interacting with the Slr1128 protein and the PsaL subunit in trimeric PSI (Wang et al., 2008). Although our proteomic data did not detect the overexpression of any HLIP protein, the accumulation under photoinhibitory conditions of PsaL (Table 3.1), which is involved in biogenesis and trimerization of the PSI complex (Chitnis and Chitnis, 1993), in combination with the increase in abundance of the Slr1128 protein (Table 3.2), suggests that retaining PSI in trimeric conformation and Slr1128 is important for the fitness of cells grown under extremely high irradiances.

In excess light, on the PSI donor side, O₂ rather than ferredoxin can be reduced by electrons generated by PSII via Flv1/Flv3 proteins, thus leading to the formation of the superoxide anion radical (O²⁻) in the Mehler-like reaction (Allahverdiyeva et al., 2011). In *Synechocystis*, the Flv1/Flv3 proteins and the antioxidant enzymes superoxide dismutase (SOD) and catalase play an important role in the photoprotection of PSI from oxidative stress, minimizing the production of harmful ROS (Tichy and Vermaas, 1999; Allahverdiyeva et al., 2011). Despite the soluble nature of these proteins, whose presence in the thylakoid extracts is indicative of potential contamination of the fraction of thylakoid membrane proteins with cytoplasmic proteins, the higher amount of the FeSOD B observed in cells grown under photoinhibitory irradiance with respect to control light (Table 3.2), attests to its boosted role under high light in safeguarding PSI by scavenging O²⁻.

3.3.3.3 Electron transport chain and ATP synthase

During the photosynthetic light reactions, electrons are driven in the LEF from PSII to PSI through the Cyt *b6f*; in addition, Cyt *b6f* is also involved in the CEF pathway around PSI. Cyt *b6f* is a membrane complex that is present as a dimer, with each monomer consisting of four large subunits (Cyt *b6*, Cyt *f*, Rieske iron-sulfur protein and PetD) and four small subunits (PetG, PetL, PetM and PetN) (Baniulis et al., 2009).

Our data revealed that in photoinhibitory conditions there was an accumulation of the Cyt *b6f* components Cyt *b6* and Cyt *f*, the hydrophilic components NdhH-I-J-K1 of the NDH-1 complex and the ferredoxin-NADP⁺ reductase (FNR), which is an enzyme associated with the cytoplasmic side of the membrane via linkage to the PBSs or direct association with the membrane surface (Battchikova et al., 2011) (Table 3.1). The simultaneous accumulation of Cyt *b6f*, NDH-1 and FNR indicates that a strong activation of the capacity for CEF around PSI occurred in cells grown under photoinhibitory irradiances, via the possibility to reduce the Cyt *b6f* complex with the NDH-1 complex (Battchikova et al., 2011). Conversely, plastocyanin and Cyt *c6*, that function as electron carriers between Cyt *b6f* and PSI, were more abundant in the control sample than in high light (Table 3.1). These data are in accordance with evidence of *petJ* (coding for Cyt *c6*) / *petE* (coding for plastocyanin) suppression induced by high light intensity (Malakhov et al., 1999) and suggest that in *Synechocystis* grown under photoinhibitory regimes a LEF slow-down occurs, that may thereby prevent PSI from photoinhibition. Furthermore, our data clearly highlighted the accumulation of most of the detected ATPase subunits in cells grown under photoinhibitory regimes (Table 3.1). These results indicate that overexpressing the ATPase may be a strategy adopted by cells to increase the amount of ATP needed for recovery from photoinhibition (Thomas et al., 2001), which is fulfilled also by activating CEF rather than accelerating LEF under excessive irradiation.

3.3.3.4 Light harvesting, photoprotection and pigments biosynthesis

The PBSs are supra-molecular phycobiliprotein complexes, transiently bound to the cytosolic surface of thylakoids that in cyanobacteria serve as light harvesting antenna system, allowing an efficient energy transfer to the Chl *a*-containing PSII and PSI reaction centres (Adir et al., 2005). The PBSs are composed of two main constituents: a core structure and peripheral rods, both made of water-soluble proteins bearing different numbers of chromophores, APC in the former and PC and PE in the latter. In addition, there are colourless linker proteins that connect the rods' components, the core components, the core and rods together, and anchor the entire structure to the thylakoid membrane (Adir et al., 2005). Another family of pigments present in cyanobacteria, mainly involved in photoprotection, are the carotenoids, amongst others the ones that bind the water-soluble protein OCP (Stadnichuk et al., 2012).

From the relative quantification of PBS proteins in *Synechocystis*, we found that almost all the detected PBS components, which are the residual PBSs remained bound to the membrane during thylakoid extraction, were more abundant in control light than in photoinhibitory illumination regimes (Table 3.1). Since there is no technical reason for a light-specific detachment of different proportions of PBSs from the membranes induced by the thylakoid extraction protocol adopted, these data indicate that during exposure to strong intensities of orange-red light, that excites preferentially phycobilins but also Chl pigments, PBSs dissociate from the thylakoid membranes, likely by altering some thermo-sensitive peptides of the core and rod likers (Tamary et al., 2012), to further decrease the migration of energy to the reaction centres. Since the decrease in the number of PBS components in *Synechocystis* grown under photoinhibitory conditions vs control light (Table 3.1) was paralleled by the accumulation of the proteases Clp1, Clp3 and ClpR (Table 3.2), these data also suggest that at high intensity of orange-red light PBS degradation may occur in *Synechocystis*, likely mediated by the ClpP1/ClpR protease complex (Baier et al., 2014).

Conversely, the OCP was more abundant in cells grown under photoinhibitory light regimes than in control light (Table 3.2). The role of OCP in photoprotection from blue-green light stress is well-known (Kirilovsky and Kerfeld, 2013), however, the mechanism by which OCP functions is not easy to understand. Since this blue-light absorbing protein is not expected to be significantly activated by 636 nm light (noteworthy, we exclude any remarkable contamination of ambient light due to the design of the PBR used), the higher abundance of OCP found in photoinhibited cells suggests its overexpression that ultimately might be beneficial to protect *Synechocystis* from ROS induced by high intensities of orange-red light (Sedoud et al., 2014).

All the detected enzymes involved in pigment synthesis were related to the Chl biosynthetic pathway and were more abundant in cells grown under photoinhibitory regimes than in control light (Table 3.2). As PSI binds the majority of Chl molecules in cyanobacterial cells, it is conceivable that the mechanism controlling the PSI level is tightly associated with the Chl biosynthetic pathway. Moreover, it was established that the trimeric PSI is almost an exclusive sink for de novo-synthesized Chls in cyanobacteria, whereas PSII subunits are mostly synthesized recycling Chl molecules released during the PSII repair cycle (Kopečna et al., 2012). Our results revealed a simultaneous accumulation of both the PsaA/PsaB proteins of the PSI core complex (Table 3.1) and the enzymes catalysing the biosynthesis of Chl intermediates in cells grown under photoinhibitory regimes with respect to control light (Table 3.2). These results provide evidence of how Chl biosynthesis is

synchronized with the varying demand for Chl-binding subunits of PSI and that the acclimation of *Synechocystis* to strong orange-red light intensities is accompanied by an enhanced production of Chl, which might preferentially be channelled to trimeric PSI (Kopecna et al., 2012).

3.3.3.5 Ribosomes and associated proteins

The distribution of ribosomes in *Synechocystis* is mainly concentrated in the cytoplasm. However, there is evidence that almost 20% of the total amount of ribosomes is located close to the cytoplasmic side of the outermost thylakoid membranes, 10% is placed in between the thylakoid membrane pairs and a small amount is directly associated to the thylakoid membranes (Van De Meene et al., 2006).

Considering photoinhibitory light intensities vs control light, despite slower cell proliferation (Fig. 3.1), *Synechocystis* showed a higher content of all the detected subunits forming the ribosome (i.e., large 50S and small 30S units) and the majority of its related proteins (Table 3.3). Their abundance under high light could reflect a closer vicinity of ribosomes to the thylakoid membranes in this light regime (Tyystjärvi et al., 2001), a condition necessary to sustain the increased and fast turnover of the PSII core proteins (Table 3.1). This localization would also explain the ease of isolating ribosome-thylakoid associations and the high percentage (i.e., 43%) of ribosomal proteins observed in this study (Fig. 3.2). Under photoinhibitory light intensities, a higher content of factors involved in the initiation of translation, like IF2 and IF3, and elongation of translation, such as EF-G1, EF-Tu and EF-Ts, was observed (Table 3.3). These results clearly indicate that translational regulation might play a key role in the cellular responses to photoinhibitory growth irradiances, as demonstrated also for other environmental stresses in *Synechocystis* (Suzuki et al., 2006). In addition, cells grown under high light intensities vs control light accumulated the DnaK2 and GroL1 heat shock proteins (Table 3.3), suggesting a common response of these chaperones to heat and high light stress (Sato et al., 2007).

Protein name, gene	FC 50 vs 800	FC 50 vs 950	FC 50 vs 1460
Ribosom eproteins			
50S L2, <i>rplB</i>	0,18	0,15	0,21
50S L3, <i>rplC</i>	0,26	0,33	0,30

50S L4, <i>rplD</i>	0,28	0,18	0,19
50S L5, <i>rplE</i>	0,54	0,67	0,65
50S L6, <i>rplF</i>	0,24	0,30	0,34
50S L10, <i>rplJ</i>	0,54	0,65	0,49
50S L13, <i>rplM</i>	0,39	0,47	0,46
50S L15, <i>rplO</i>	0,25	0,23	0,25
50S L16, <i>rplP</i>	0,23	0,19	0,24
50S L17, <i>rplQ</i>	0,25	0,16	0,23
50S, L18, <i>rplR</i>	0,24	0,29	0,27
50S L19, <i>rplS</i>	0,12	0,16	0,14
50S L20, <i>rplT</i>	0,19	0,16	0,14
50S L21, <i>rplU</i>	0,52	0,69	0,52
50S L22, <i>rplV</i>	0,33	0,25	0,27
50S L23, <i>rplW</i>	0,42	0,47	0,36
50S L24, <i>rplX</i>	0,37	0,38	0,45
50S L25, <i>rplY</i>	0,47	0,65	0,57
50S L27, <i>rpmA</i>	0,42	0,37	0,42
50S L28, <i>rpmB</i>	0,22	0,24	0,29
50S L32, <i>rpmF</i>	0,37	0,54	0,37
50S L35, <i>rpmI</i>	0,2	0,19	0,22
30S S1 homolog A, <i>rps1A</i>	0,26	0,25	0,31
30S S1 homolog B, <i>rps1B</i>	0,3	0,28	0,32
30S S2, <i>rpsB</i>	0,26	0,26	0,21
30S S3, <i>rpsC</i>	0,15	0,14	0,17
30S S4, <i>rpsD</i>	0,13	0,12	0,17
30S S5, <i>rpsE</i>	0,24	0,28	0,27
30S S6, <i>rpsF</i>	0,52	0,70	0,59
30S S7, <i>rpsG</i>	0,16	0,11	0,16
30S S8, <i>rpsH</i>	0,24	0,23	0,29
30S S9, <i>rpsI</i>	0,29	0,28	0,31
30S S11, <i>rpsK</i>	0,23	0,26	0,24
30S S12, <i>rpsL</i>	0,22	0,17	0,23
30S S13, <i>rpsM</i>	0,16	0,19	0,2
30S S15, <i>rpsO</i>	0,41	0,58	0,48
30S S16, <i>rpsP</i>	0,29	0,34	0,31
30S S19, <i>rpsS</i>	0,30	0,22	0,40
30S S20, <i>rpsT</i>	0,25	0,24	0,26
30S S21, <i>rpsU</i>	0,26	0,26	0,34
PSRP-3, <i>Slr0923</i>	0,59	0,01	0,005

Ribosome associated proteins

DnaK2, <i>dnaK2</i>	0,38	0,39	0,35
Ribosome-recycling factor, <i>frr</i>	1,97	2,59	2,00
EF-G1, <i>fusA</i>	0,23	0,17	0,3
GroL1, <i>groL1</i>	0,34	0,34	0,43
GrpE, <i>grpE</i>	1,86	1,92	1,99
hibernation promotion factor, <i>Hpf</i>	1,87	2,09	1,47
IF-2, <i>infB</i>	0,22	0,15	0,23
IF-3, <i>infC</i>	0,35	0,44	0,44
Trigger factor, <i>Tig</i>	0,27	0,28	0,3
EF-Tu, <i>Tuf</i>	0,65	0,51	0,61
Ef-Ts, <i>Tsf</i>	0,37	0,45	0,48
PPlase <i>slr1251</i> , <i>slr1251</i>	0,45	0,55	0,52
Probable PPlase <i>slI0227</i> , <i>slI0227</i>	0,30	0,24	0,30

Table 3.3. Relative quantification of the differentially abundant ribosomal proteins associated with thylakoid membranes isolated from *Synechocystis* grown under photoinhibitory conditions. The fold change (FC) refers to the comparison of samples at 50 $\mu\text{mol photons m}^{-2} \text{s}^{-1}$ vs 800 $\mu\text{mol photons m}^{-2} \text{s}^{-1}$ (50 vs 800), 50 $\mu\text{mol photons m}^{-2} \text{s}^{-1}$ vs 950 $\mu\text{mol photons m}^{-2} \text{s}^{-1}$ (50 vs 950) and 50 $\mu\text{mol photons m}^{-2} \text{s}^{-1}$ vs 1460 $\mu\text{mol photons m}^{-2} \text{s}^{-1}$ (50 vs 1460).

3.4 Conclusions

Light quality and intensity are ever-changing environmental factors for cyanobacteria. Here we have shown that the saturating intensity of orange-red light for obtaining the maximal growth rate of *Synechocystis* was 300 $\mu\text{mol photons m}^{-2} \text{s}^{-1}$, whereas significant symptoms of cellular photoinhibition appeared above 800 $\mu\text{mol photons m}^{-2} \text{s}^{-1}$.

Quantitative proteomic analyses revealed multiple strategies adopted by *Synechocystis* to cope with photoinhibitory growth irradiances (800, 950, 1460 $\mu\text{mol}_{\text{photons}} \text{m}^{-2} \text{s}^{-1}$) of 636 nm light, when compared to control light (50 $\mu\text{mol}_{\text{photons}} \text{m}^{-2} \text{s}^{-1}$), amongst which the most relevant are: 1) lowering of the number of PBS antenna to reduce the excess of light absorption and accumulation of the OCP protein with a potential photoprotective function as ROS quencher; 2) accumulation of the PSII repair machinery and of thylakoid-associated ribosomes to sustain the increased turnover of the photodamaged PSII core subunits; 3) differentiated

response of PSI components, with reduction of the PsaD, PsaE, PsaJ and PsaM subunits and accumulation of the PsaA, PsaB, Psak2 and PsaL proteins suggesting a light-quality control of the expression of specific PSI subunits to sustain cells performance in high light; 4) increased CEF capacity around PSI to either counterbalance the reduced LEF capacity or sustain the accumulation of supplementary ATP, also mediated by the increased amount of ATPase. Our results provide novel insights into the response mechanisms to photoinhibition induced by high intensities of orange-red light at the thylakoid membrane level in *Synechocystis* sp. PCC6803 and may be valuable for further quantitative proteomic studies addressing photoinhibition or other environmental stresses that are currently limiting the productivity in cyanobacteria.

3.5 References

- Adir, N., 2005. Elucidation of the molecular structures of components of the phycobilisome: reconstructing a giant. *Photosynth. Res.* 85, 15–32. <https://doi.org/10.1007/s11120-004-2143-y>
- Abu-Ghosh, S., Fixler, D., Dubinsky, Z., Iluz, D., 2016. Flashing light in microalgae biotechnology. *Bioresour. Technol.* 203, 357–363. <https://doi.org/10.1016/J.BIORTECH.2015.12.057>
- Agarwal, R., Matros, A., Melzer, M., Mock, H.-P., Sainis, J.K., 2010. Heterogeneity in thylakoid membrane proteome of *Synechocystis* 6803. *J. Proteomics* 73, 976–991. <https://doi.org/10.1016/J.JPROT.2009.12.011>
- Aiba, S., 1982. Growth Kinetics of Photosynthetic Microorganisms, in: *Advances in Biochemical Engineering*. Springer, Berlin, Heidelberg, pp. 85–156. https://doi.org/10.1007/3540116982_3
- Al-Haj, L., Lui, Y., Abed, R., Gomaa, M., Purton, S., 2016. Cyanobacteria as Chassis for Industrial Biotechnology: Progress and Prospects. *Life* 6, 42. <https://doi.org/10.3390/life6040042>
- Albanese, P., Melero, R., Engel, B.D., Grinzato, A., Berto, P., Manfredi, M., Chiodoni, A., Vargas, J., Sorzano, C.Ó.S., Marengo, E., Saracco, G., Zanotti, G., Carazo, J.M., Pagliano, C., 2017. Pea PSII-LHCII supercomplexes form pairs by making connections across the stromal gap. *Sci. Rep.* 7. <https://doi.org/10.1038/s41598-017-10700-8>
- Ali, A., 2014. CFD Simulation of Bubbly Flow Through a Bubble Column 5, 904–910.
- Allahverdiyeva, Y., Ermakova, M., Eisenhut, M., Zhang, P., Richaud, P., Hagemann, M., Cournac, L., Aro, E.-M., 2011. Interplay between flavodiiron proteins and photorespiration in *Synechocystis* sp. PCC 6803. *J. Biol. Chem.* 286, 24007–14. <https://doi.org/10.1074/jbc.M111.223289>
- Allen, J.F., 2004. Cytochrome b6f: structure for signalling and vectorial metabolism. *Trends Plant Sci.* 9, 130–137. <https://doi.org/10.1016/j.tplants.2004.01.009>
- Anderson, J.M., Park, Y.-I., Chow, W.S., 1998. Unifying model for the photoinactivation of Photosystem II in vivo under steady-state photosynthesis. *Photosynth. Res.* 56, 1–13. <https://doi.org/10.1023/A:1005946808488>
- Andersson, B., Aro, E.-M., 2001. Photodamage and D1 Protein Turnover in Photosystem II, in: *Regulation of Photosynthesis*. Kluwer Academic

- Publishers, Dordrecht, pp. 377–393. https://doi.org/10.1007/0-306-48148-0_22
- Anfelt, J., Hallström, B., Nielsen, J., Uhlén, M., Hudson, E.P., 2013. Using transcriptomics to improve butanol tolerance of *Synechocystis* sp. strain PCC 6803. *Appl. Environ. Microbiol.* 79, 7419–27. <https://doi.org/10.1128/AEM.02694-13>
- Angermayr, S.A., Gorchs Rovira, A., Hellingwerf, K.J., 2015. Metabolic engineering of cyanobacteria for the synthesis of commodity products. *Trends Biotechnol.* 33, 352–361. <https://doi.org/10.1016/j.tibtech.2015.03.009>
- Angermayr, S.A., Hellingwerf, K.J., Teixeira de Mattos, M.J., 2009. Energy biotechnology with cyanobacteria. *Curr. Opin. Biotechnol.* 20, 257–263. <https://doi.org/10.1016/J.COPBIO.2009.05.011>
- Angermayr, S.A., Paszota, M., Hellingwerf, K.J., 2012. Engineering a cyanobacterial cell factory for production of lactic acid. *Appl. Environ. Microbiol.* 78, 7098–7106. <https://doi.org/10.1128/AEM.01587-12>
- Angermayr, S.A., van Alphen, P., Hasdemir, D., Kramer, G., Iqbal, M., van Grondelle, W., Hoefsloot, H.C., Choi, Y.H., Hellingwerf, K.J., 2016. Culturing *Synechocystis* sp. Strain PCC 6803 with N₂ and CO₂ in a Diel Regime Reveals Multiphase Glycogen Dynamics with Low Maintenance Costs. *Appl. Environ. Microbiol.* 82, 4180–9. <https://doi.org/10.1128/AEM.00256-16>
- Arnon, D.I., 1949. Copper Enzymes in Isolated Chloroplasts. Polyphenoloxidase in *Beta Vulgaris*. *Plant Physiol.* 24, 1–15. <https://doi.org/10.1104/pp.24.1.1>
- Aro, E.M., Virgin, I., Andersson, B., 1993a. Photoinhibition of Photosystem II. Inactivation, protein damage and turnover. *BBA - Bioenerg.* 1143, 113–134. [https://doi.org/10.1016/0005-2728\(93\)90134-2](https://doi.org/10.1016/0005-2728(93)90134-2)
- Aro, E.M., Virgin, I., Andersson, B., 1993b. Photoinhibition of Photosystem II. Inactivation, protein damage and turnover. *BBA - Bioenerg.* 1143, 113–134. [https://doi.org/10.1016/0005-2728\(93\)90134-2](https://doi.org/10.1016/0005-2728(93)90134-2)
- Baier, A., Winkler, W., Korte, T., Lockau, W., Karradt, A., 2014. Degradation of phycobilisomes in *synechocystis* sp. pcc6803 evidence for essential formation of an nbla1/nbla2 heterodimer and its codegradation by a clp protease complex. *J. Biol. Chem.* 289, 11755–11766. <https://doi.org/10.1074/jbc.M113.520601>
- Bailey, S., Grossman, A., 2008. Photoprotection in cyanobacteria: Regulation of light harvesting. *Photochem. Photobiol.* 84, 1410–1420. <https://doi.org/10.1111/j.1751-1097.2008.00453.x>
- Baniulis, D., Yamashita, E., Whitelegge, J.P., Zatsman, A.I., Hendrich, M.P., Hasan,

- S.S., Ryan, C.M., Cramer, W.A., 2009. Structure-Function, Stability, and Chemical Modification of the Cyanobacterial Cytochrome b6f Complex from *Nostoc* sp. PCC 7120. *J. Biol. Chem.* 284, 9861–9. <https://doi.org/10.1074/jbc.M809196200>
- Barber, J., 2016. “Photosystem II: the water splitting enzyme of photosynthesis and the origin of oxygen in our atmosphere.” *Q. Rev. Biophys.* 49, e14. <https://doi.org/10.1017/S0033583516000093>
- Barsanti, L., Gualtieri, P., 2006. *Algae, Anatomy, Biochemistry, and Biotechnology.* <https://doi.org/10.1017/CBO9781107415324.004>
- Battchikova, N., Aro, E.M., 2007. Cyanobacterial NDH-1 complexes: Multiplicity in function and subunit composition. *Physiol. Plant.* 131, 22–32. <https://doi.org/10.1111/j.1399-3054.2007.00929.x>
- Battchikova, N., Eisenhut, M., Aro, E.M., 2011. Cyanobacterial NDH-1 complexes: Novel insights and remaining puzzles. *Biochim. Biophys. Acta - Bioenerg.* 1807, 935–944. <https://doi.org/10.1016/j.bbabi.2010.10.017>
- Beck, C., Hertel, S., Rediger, A., Lehmann, R., Wiegard, A., Kölsch, A., Heilmann, B., Georg, J., Hess, W.R., Axmann, I.M., 2014. Daily Expression Pattern of Protein-Encoding Genes and Small Noncoding RNAs in *Synechocystis* sp. Strain PCC 6803. *Appl. Environ. Microbiol.* 80, 5195–5206. <https://doi.org/10.1128/AEM.01086-14>
- Berz, G.A., 1997. Natural Disasters and the Greenhouse Effect: Impact on the Insurance Industry and Possible Countermeasures. *Geneva Pap. Risk Insur. - Issues Pract.* 22, 501–514. <https://doi.org/10.1057/gpp.1997.35>
- Bird, B.R., Stewart, W.E., Lightfoot, E.N., 2006. *Transport Phenomena.* J. Wiley.
- Blubaugh, D.J., Atamian, M., Babcock, G.T., Golbeck, J.H., Cheniae, G.M., 1991. Photoinhibition of hydroxylamine-extracted photosystem II membranes: identification of the sites of photodamage. *Biochemistry* 30, 7586–97.
- Blubaugh, D.J., Cheniae, G.M., 1990. Kinetics of photoinhibition in hydroxylamine-extracted photosystem II membranes: relevance to photoactivation and sites of electron donation. *Biochemistry* 29, 5109–18.
- Boyer, P.D., 1997. THE ATP SYNTHASE—A SPLENDID MOLECULAR MACHINE. *Annu. Rev. Biochem.* 66, 717–749. <https://doi.org/10.1146/annurev.biochem.66.1.717>
- Bradford, M.M., 1976a. A rapid and sensitive method for the quantitation of microgram quantities of protein utilizing the principle of protein-dye binding. *Anal. Biochem.* 72, 248–254. [https://doi.org/10.1016/0003-2697\(76\)90527-3](https://doi.org/10.1016/0003-2697(76)90527-3)

-
- Bradford, M.M., 1976b. A rapid and sensitive method for the quantitation of microgram quantities of protein utilizing the principle of protein-dye binding. *Anal. Biochem.* 72, 248–254. [https://doi.org/10.1016/0003-2697\(76\)90527-3](https://doi.org/10.1016/0003-2697(76)90527-3)
- Bumann, D., Oesterhelt, D., 1995a. Destruction of a single chlorophyll is correlated with the photoinhibition of photosystem II with a transiently inactive donor side. *Proc. Natl. Acad. Sci. U. S. A.* <https://doi.org/10.1073/pnas.92.26.12195>
- Bumann, D., Oesterhelt, D., 1995b. Destruction of a single chlorophyll is correlated with the photoinhibition of photosystem II with a transiently inactive donor side. *Proc. Natl. Acad. Sci. U. S. A.* 92, 12195–12199. <https://doi.org/10.1073/pnas.92.26.12195>
- Burrows, E., Wong, W., 2009. Optimization of pH and nitrogen for enhanced hydrogen production by *Synechocystis* sp. pcc 6803 via statistical and machine learning methods. *Biotechnol.* <https://doi.org/10.1021/bp.213>
- Callahan, F.E., Becker, D.W., Cheniae, G.M., 1986. Studies on the Photoactivation of the Water-Oxidizing Enzyme: II. Characterization of Weak Light Photoinhibition of PSII and Its Light-Induced Recovery. *Plant Physiol.* 82, 261–9. <https://doi.org/10.1104/PP.82.1.261>
- Campbell, D., Clarke, A.K., Gustafsson, P., Oquist, G., 1996. D1 exchange and the Photosystem II repair cycle in the cyanobacterium *Synechococcus*. *iENCE ELSEVIER Plant Sci. IS* 183–190.
- Cardona, T., Sedoud, A., Cox, N., Rutherford, A.W., 2012. Charge separation in Photosystem II: A comparative and evolutionary overview. *Biochim. Biophys. Acta - Bioenerg.* 1817, 26–43. <https://doi.org/10.1016/j.bbabi.2011.07.012>
- Carvalho, A.P., Meireles, L.A., Malcata, F.X., 2006. Microalgal reactors: A review of enclosed system designs and performances. *Biotechnol. Prog.* 22, 1490–1506. <https://doi.org/10.1021/bp060065r>
- Chang, L., Liu, X., Li, Y., Liu, C.-C., Yang, F., Zhao, J., Sui, S.-F., 2015. Structural organization of an intact phycobilisome and its association with photosystem II. *Cell Res.* 25, 726–737. <https://doi.org/10.1038/cr.2015.59>
- Chaumont, D., 1993. Biotechnology of algal biomass production: a review of systems for outdoor mass culture. *J. Appl. Phycol.* 5, 593–604. <https://doi.org/10.1007/BF02184638>
- Chaves, J.E., Kirst, H., Melis, A., 2015. Isoprene production in *Synechocystis* under alkaline and saline growth conditions. *J. Appl. Phycol.* 27, 1089–1097. <https://doi.org/10.1007/s10811-014-0395-2>
- Chen, G.X., Kazimir, J., Cheniae, G.M., 1992. Photoinhibition of hydroxylamine-

- extracted photosystem II membranes: studies of the mechanism. *Biochemistry* 31, 11072–11083. <https://doi.org/10.1021/bi00160a017>
- Chiang, C.-L., Lee, C.-M., Chen, P.-C., 2011. Utilization of the cyanobacteria *Anabaena* sp. CH1 in biological carbon dioxide mitigation processes. *Bioresour. Technol.* 102, 5400–5405. <https://doi.org/10.1016/j.biortech.2010.10.089>
- Chisti, Y., 2016. *Algae Biotechnology*. <https://doi.org/10.1007/978-3-319-12334-9>
- Chitnis, V.P., Chitnis, P.R., 1993. PsaL subunit is required for the formation of photosystem I trimers in the cyanobacterium *Synechocystis* sp. PCC 6803. *FEBS Lett.* 336, 330–334. [https://doi.org/10.1016/0014-5793\(93\)80831-E](https://doi.org/10.1016/0014-5793(93)80831-E)
- Chow, W.S., Aro, E.-M., 2005. Photoinactivation and Mechanisms of Recovery, in: *Photosystem II*. Springer-Verlag, Berlin/Heidelberg, pp. 627–648. https://doi.org/10.1007/1-4020-4254-X_28
- Colyer, C.L., Klinkade, C.S., Viskari, P.J., Landers, J.P., 2005. Analysis of cyanobacterial pigments and proteins by electrophoretic and chromatographic methods. *Anal. Bioanal. Chem.* 382, 559–569. <https://doi.org/10.1007/s00216-004-3020-4>
- Constant, S., Eisenberg-Domovitch, Y., Ohad, I., Kirilovsky, D., 2000. Recovery of photosystem II activity in photoinhibited *Synechocystis* cells: Light-dependent translation activity is required besides light-independent synthesis of the D1 protein. *Biochemistry* 39, 2032–2041. <https://doi.org/10.1021/bi9914154>
- Curtis, S.E., 1988. Structure, organization and expression of cyanobacterial ATP synthase genes. *Photosynth Res* 18, 223–244.
- De Las Rivas, J., Andersson, B., Barber, J., 1992. Two sites of primary degradation of the D1-protein induced by acceptor or donor side photo-inhibition in photosystem II core complexes. *FEBS Lett.* 301, 246–252. [https://doi.org/10.1016/0014-5793\(92\)80250-K](https://doi.org/10.1016/0014-5793(92)80250-K)
- De Las Rivas, J., Balsera, M., Barber, J., 2004. Evolution of oxygenic photosynthesis: Genome-wide analysis of the OEC extrinsic proteins. *Trends Plant Sci.* 9, 18–25. <https://doi.org/10.1016/j.tplants.2003.11.007>
- Dechatiwongse, P., Srisamai, S., Maitland, G., Hellgardt, K., 2014. Effects of light and temperature on the photoautotrophic growth and photoinhibition of nitrogen-fixing cyanobacterium *Cyanothece* sp. ATCC 51142. *Algal Res.* 5, 103–111. <https://doi.org/10.1016/J.ALGAL.2014.06.004>
- Derks, A., Schaven, K., Bruce, D., 2015. *Biochimica et Biophysica Acta* Diverse mechanisms for photoprotection in photosynthesis . Dynamic regulation of

- photosystem II excitation in response to rapid environmental change. *BBA - Bioenerg.* 1847, 468–485. <https://doi.org/10.1016/j.bbabi.2015.02.008>
- Dobáková, M., Sobotka, R., Tichý, M., Komenda, J., 2009. Psb28 Protein Is Involved in the Biogenesis of the Photosystem II Inner Antenna CP47 (PsbB) in the Cyanobacterium *Synechocystis* sp. PCC 6803. *Plant Physiol.* 149, 1076–1086. <https://doi.org/10.1104/pp.108.130039>
- Du, W., Jongbloets, J.A., Pineda Hernández, H., Bruggeman, F.J., Hellingwerf, K.J., Branco dos Santos, F., 2016. Photonfluxostat: A method for light-limited batch cultivation of cyanobacteria at different, yet constant, growth rates. *Algal Res.* 20, 118–125. <https://doi.org/10.1016/j.algal.2016.10.004>
- Eckert, H.-J., Geiken, B., Bernarding, J., Napiwotzki, A., Eichler, H.-J., Renger, G., 1991. Two sites of photoinhibition of the electron transfer in oxygen evolving and Tris-treated PS II membrane fragments from spinach. *Photosynth. Res.* 27, 97–108. <https://doi.org/10.1007/BF00033249>
- Esteves-Ferreira, A.A., Inaba, M., Obata, T., Fort, A., Fleming, G.T.A., Araújo, W.L., Fernie, A.R., Sulpice, R., 2017. A Novel Mechanism, Linked to Cell Density, Largely Controls Cell Division in *Synechocystis*. *Plant Physiol.* 174, 2166–2182. <https://doi.org/10.1104/pp.17.00729>
- Fang, L., Ge, H., Huang, X., Liu, Y., Lu, M., Wang, J., Chen, W., Xu, W., Wang, Y., 2016. Trophic Mode-Dependent Proteomic Analysis Reveals Functional Significance of Light-Independent Chlorophyll Synthesis in *Synechocystis* sp. PCC 6803. *Mol. Plant* 6803, 73–85. <https://doi.org/10.1016/j.molp.2016.08.006>
- Ferreira, K.N., Iverson, T.M., Maghlaoui, K., Barber, J., Iwata, S., 2004. Architecture of the photosynthetic oxygen-evolving center. *Science* 303, 1831–8. <https://doi.org/10.1126/science.1093087>
- Folea, I.M., Zhang, P., Aro, E.-M., Boekema, E.J., 2008. Domain organization of photosystem II in membranes of the cyanobacterium *Synechocystis* PCC6803 investigated by electron microscopy. <https://doi.org/10.1016/j.febslet.2008.04.044>
- Fork, D.C., Herbert, S.K., 1993. Electron transport and photophosphorylation by Photosystem I in vivo in plants and cyanobacteria. *Photosynth. Res.* 36, 149–168. <https://doi.org/10.1007/BF00033035>
- Friso, G., Giacometti, G.M., Barber, J., Barbato, R., 1993. Evidence for concurrent donor and acceptor side photoinduced degradation of the D1-protein in isolated reaction centres of Photosystem II. *BBA - Bioenerg.* 1144, 265–270. [https://doi.org/10.1016/0005-2728\(93\)90110-2](https://doi.org/10.1016/0005-2728(93)90110-2)

- Fromme, P., Melkozernov, A., Jordan, P., Krauss, N., 2003. Structure and function of photosystem I: Interaction with its soluble electron carriers and external antenna systems. *FEBS Lett.* 555, 40–44. [https://doi.org/10.1016/S0014-5793\(03\)01124-4](https://doi.org/10.1016/S0014-5793(03)01124-4)
- Fujimori, T., Hihara, Y., Sonoike, K., 2005. PsaK2 subunit in photosystem I is involved in state transition under high light condition in the cyanobacterium *Synechocystis* sp. PCC 6803. *J. Biol. Chem.* 280, 22191–22197. <https://doi.org/10.1074/jbc.M500369200>
- Gan, F., Bryant, D.A., 2015. Adaptive and acclimative responses of cyanobacteria to far-red light. *Environ. Microbiol.* 17, 3450–3465. <https://doi.org/10.1111/1462-2920.12992>
- Gantt, E., 1980. Structure and Function of Phycobilisomes: Light Harvesting Pigment Complexes in Red and Blue-Green Algae, *International Review of Cytology*. [https://doi.org/10.1016/S0074-7696\(08\)61971-3](https://doi.org/10.1016/S0074-7696(08)61971-3)
- Gao, Z., Zhao, H., Li, Z., Tan, X., Lu, X., Lu, X., Foust, T.D., Hallett, J.P., Leak, D.J., Liotta, C.L., Mielenz, J.R., Murphy, R., Templer, R., Tschaplinski, T., 2012. Photosynthetic production of ethanol from carbon dioxide in genetically engineered cyanobacteria. *Energy Environ. Sci.* 5, 9857–9865. <https://doi.org/10.1039/C2EE22675H>
- Gillet, L.C., Navarro, P., Tate, S., Röst, H., Selevsek, N., Reiter, L., Bonner, R., Aebersold, R., 2012. Targeted Data Extraction of the MS/MS Spectra Generated by Data-independent Acquisition: A New Concept for Consistent and Accurate Proteome Analysis. *Mol. Cell. Proteomics* 11, O111.016717. <https://doi.org/10.1074/mcp.O111.016717>
- Glazer, A.N., 1977. Structure and molecular organization of the photosynthetic accessory pigments of cyanobacteria and red algae. *Mol. Cell. Biochem.* 18, 125–140. <https://doi.org/10.1007/BF00280278>
- Glazer, A.N., Gindt, Y.M., Chan, C.F., Sauer, K., 1994. Selective disruption of energy flow from phycobilisomes to Photosystem I. *Photosynth. Res.* 40, 167–173. <https://doi.org/10.1007/BF00019333>
- Goh, C.H., Ko, S.M., Koh, S., Kim, Y.J., Bae, H.J., 2012. Photosynthesis and Environments: Photoinhibition and Repair Mechanisms in Plants. *J. Plant Biol.* 55, 93–101. <https://doi.org/10.1007/s12374-011-9195-2>
- Grima, E.M., Camacho, F.G., Pérez, J.A.S., Sevilla, J.M.F., Fernández, F.G.A., Gómez, A.C., 1994. A mathematical model of microalgal growth in light-limited chemostat culture. *J. Chem. Technol. Biotechnol.* 61, 167–173. <https://doi.org/10.1002/jctb.280610212>

- Grotjohann, I., Fromme, P., 2005. Structure of cyanobacterial Photosystem I. *Photosynth. Res.* 85, 51–72. <https://doi.org/10.1007/s11120-005-1440-4>
- Guedes, A.C., Katkam, N.G., Varela, J., Malcata, F.X., 2013. Photobioreactors for cyanobacterial culturing. *Cyanobacteria An Econ. Perspect.* 270–292. <https://doi.org/10.1002/9781118402238.ch17>
- Guo, X., Kristal, B.S., 2012. The use of underloaded C18 solid-phase extraction plates increases reproducibility of analysis of tryptic peptides from unfractionated human plasma. *Anal. Biochem.* 426, 86–90. <https://doi.org/10.1016/j.ab.2012.04.003>
- Hai, T., Ahlers, H., Gorenflo, V., Steinbüchel, A., 2000. Axenic cultivation of anoxygenic phototrophic bacteria, cyanobacteria, and microalgae in a new closed tubular glass photobioreactor. *Appl. Microbiol. Biotechnol.* 53, 383–9.
- Hartmann, P., Nikolaou, A., Chachuat, B., Bernard, O., Nikolaou, A., Chachuat, B., 2013. A dynamic Model coupling Photoacclimation and Photoinhibition in Microalgae A dynamic Model coupling Photoacclimation and Photoinhibition in Microalgae A Dynamic Model coupling Photoacclimation and Photoinhibition in Microalgae. *Eur. Control Conf.*
- Hasan, S.S., Yamashita, E., Baniulis, D., Cramer, W.A., 2013. Quinone-dependent proton transfer pathways in the photosynthetic cytochrome b6f complex. *Proc. Natl. Acad. Sci.* 110, 4297–4302. <https://doi.org/10.1073/pnas.1222248110>
- Havaux, M., 2014. Carotenoid oxidation products as stress signals in plants. *Plant J.* 79, 597–606. <https://doi.org/10.1111/tpj.12386>
- Hedges, S.B., Chen, H., Kumar, S., Wang, D.Y., Thompson, A.S., Watanabe, H., 2001. A genomic timescale for the origin of eukaryotes. *BMC Evol. Biol.* 1, 4. <https://doi.org/10.1186/1471-2148-1-4>
- Heinz, S., Liauw, P., Nickelsen, J., Nowaczyk, M., 2016. Analysis of photosystem II biogenesis in cyanobacteria. *Biochim. Biophys. Acta - Bioenerg.* 1857, 274–287. <https://doi.org/10.1016/j.bbabi.2015.11.007>
- Herbert, S.K., Martin, R.E., Fork, D.C., 1995. Light adaptation of cyclic electron transport through Photosystem I in the cyanobacterium *Synechococcus* sp. PCC 7942. *Photosynth. Res.* 46, 277–285. <https://doi.org/10.1007/BF00020441>
- Hihara, Y., Kamei, A., Kanehisa, M., Kaplan, A., Ikeuchi, M., 2001. DNA microarray analysis of cyanobacterial gene expression during acclimation to high light. *Plant Cell* 13, 793–806. <https://doi.org/10.1105/TPC.13.4.793>
- HILL, R., BENDALL, F., 1960. Function of the Two Cytochrome Components in

- Chloroplasts: A Working Hypothesis. *Nature* 186, 136–137. <https://doi.org/10.1038/186136a0>
- Horton, P., 2012. Optimization of light harvesting and photoprotection: molecular mechanisms and physiological consequences. *Philos. Trans. R. Soc. Lond. B. Biol. Sci.* 367, 3455–65. <https://doi.org/10.1098/rstb.2012.0069>
- Huang, W., Yang, Y.-J., Zhang, S.-B., Liu, T., 2018. Cyclic Electron Flow around Photosystem I Promotes ATP Synthesis Possibly Helping the Rapid Repair of Photodamaged Photosystem II at Low Light. *Front. Plant Sci.* 9, 239. <https://doi.org/10.3389/fpls.2018.00239>
- Ikeuchi, M., Tabata, S., 2001. *Synechocystis* sp. PCC 6803 - a useful tool in the study of the genetics of cyanobacteria. *Photosynth. Res.* 70, 73–83. <https://doi.org/10.1023/A:1013887908680>
- IPCC, 2007. Climate Change 2007 Synthesis Report. Intergov. Panel Clim. Chang. [Core Writ. Team IPCC 104. <https://doi.org/10.1256/004316502320517344>
- Jackson, S.A., Hervey, J.R.D., Dale, A.J., Eaton-Rye, J.J., 2014. Removal of both Ycf48 and Psb27 in *Synechocystis* sp. PCC 6803 disrupts Photosystem II assembly and alters QA-oxidation in the mature complex. *FEBS Lett.* 588, 3751–3760. <https://doi.org/10.1016/j.febslet.2014.08.024>
- Janssen, M., Tramper, J., Mur, L.R., Wijffels, R.H., 2003. Enclosed outdoor photobioreactors: Light regime, photosynthetic efficiency, scale-up, and future prospects. *Biotechnol. Bioeng.* 81, 193–210. <https://doi.org/10.1002/bit.10468>
- Jegerschöld, C., Virgin, I., Styring, S., 1990. Light-dependent degradation of the D1 protein in photosystem II is accelerated after inhibition of the water splitting reaction. *Biochemistry* 29, 6179–86.
- Jordan, P., Fromme, P., Witt, H.T., Klukas, O., Saenger, W., Krauß, N., 2001. Three-dimensional structure of cyanobacterial photosystem I at 2.5 Å resolution. *Nature* 411, 909–917. <https://doi.org/10.1038/35082000>
- JOSEPH, A., AIKAWA, S., SASAKI, K., TSUGE, Y., MATSUDA, F., TANAKA, T., KONDO, A., 2013. Utilization of Lactic Acid Bacterial Genes in *Synechocystis* sp. PCC 6803 in the Production of Lactic Acid. *Biosci. Biotechnol. Biochem.* 77, 966–970. <https://doi.org/10.1271/bbb.120921>
- Jung, J., Kim, H.-S., 1990. THE CHROMOPHORES AS ENDOGENOUS SENSITIZERS INVOLVED IN THE PHOTOGENERATION OF SINGLET OXYGEN IN SPINACH THYLAKOIDS. *Photochem. Photobiol.* 52, 1003–1009. <https://doi.org/10.1111/j.1751-1097.1990.tb01817.x>
- Kada, S., Koike, H., Satoh, K., Hase, T., Fujita, Y., 2003. Arrest of chlorophyll

- synthesis and differential decrease of Photosystems I and II in a cyanobacterial mutant lacking light-independent protochlorophyllide reductase. *Plant Mol. Biol.* 51, 225–35.
- Kale, R., Hebert, A.E., Frankel, L.K., Sallans, L., Bricker, T.M., Pospíšil, P., 2017. Amino acid oxidation of the D1 and D2 proteins by oxygen radicals during photoinhibition of Photosystem II. *Proc. Natl. Acad. Sci.* 114, 2988–2993. <https://doi.org/10.1073/pnas.1618922114>
- Kallas, T., 1994. The Cytochrome b6f Complex, in: *The Molecular Biology of Cyanobacteria*. Springer Netherlands, Dordrecht, pp. 259–317. https://doi.org/10.1007/978-94-011-0227-8_9
- Kaneko, T., Sato, S., Kotani, H., Tanaka, A., Asamizu, E., Nakamura, Y., Miyajima, N., Hirosawa, M., Sugiura, M., Sasamoto, S., Kimura, T., Hosouchi, T., Matsuno, A., Muraki, A., Nakazaki, N., Naruo, K., Okumura, S., Shimpo, S., Takeuchi, C., Wada, T., Watanabe, A., Yamada, M., Yasuda, M., Tabata, S., 1996. Sequence analysis of the genome of the unicellular cyanobacterium *Synechocystis* sp. strain PCC6803. II. Sequence determination of the entire genome and assignment of potential protein-coding regions. *DNA Res.* 3, 109–36.
- Katsuda, T., Lababpour, A., Shimahara, K., Katoh, S., 2004. Astaxanthin production by *Haematococcus pluvialis* under illumination with LEDs. *Enzyme Microb. Technol.* 35, 81–86. <https://doi.org/10.1016/J.ENZMICTEC.2004.03.016>
- Kettunen, R., Tyystjärvi, E., Aro, E.-M., 1996. Degradation pattern of photosystem II reaction center protein D1 in intact leaves. *Plant Physiol.* 111, 1183–1190. <https://doi.org/10.1104/pp.111.4.1183>
- Kim, J.-D., Lee, C.-G., 2005. Systemic optimization of microalgae for bioactive compound production. *Biotechnol. Bioprocess Eng.* 10, 418–424. <https://doi.org/10.1007/BF02989824>
- Kirilovsky, D., 2015. Modulating energy arriving at photochemical reaction centers: Orange carotenoid protein-related photoprotection and state transitions. *Photosynth. Res.* 126, 3–17. <https://doi.org/10.1007/s11120-014-0031-7>
- Kirilovsky, D., Kerfeld, C.A., 2013. The Orange Carotenoid Protein: a blue-green light photoactive protein. *Photochem. Photobiol. Sci.* 12, 1135. <https://doi.org/10.1039/c3pp25406b>
- Koivuniemi, A., Aro, E.-M., Andersson, B., 1995. Degradation of the D1-and D2-Proteins of Photosystem II in Higher Plants Is Regulated by Reversible Phosphorylation1. *Biochemistry* 34, 16022–16029.

- Komenda, J., Rg Nickelsen, J., Tich, M., Prášil, O., Eichacker, L.A., Nixon, P.J., 2008. The Cyanobacterial Homologue of HCF136/YCF48 Is a Component of an Early Photosystem II Assembly Complex and Is Important for Both the Efficient Assembly and Repair of Photosystem II in *Synechocystis* sp. PCC 6803 * □ S. <https://doi.org/10.1074/jbc.M801917200>
- Kopečna, J., Komenda, J., Bucinska, L., Sobotka, R., 2012. Long-term acclimation of the cyanobacterium *Synechocystis* PCC 6803 to high light is accompanied by an enhanced production of chlorophyll that is preferentially channeled to trimeric PSI. *Plant Physiol.* 160, 2239–2250. <https://doi.org/10.1104/pp.112.207274>
- Kramer, D.M., Evans, J.R., 2011. The importance of energy balance in improving photosynthetic productivity. *Plant Physiol.* 155, 70–8. <https://doi.org/10.1104/pp.110.166652>
- Krieger-Liszskay, A., Fufezan, C., Trebst, A., 2008. Singlet oxygen production in photosystem II and related protection mechanism. *Photosynth. Res.* 98, 551–564. <https://doi.org/10.1007/s11120-008-9349-3>
- Kusama, Y., Inoue, S., Jimbo, H., Takaichi, S., Sonoike, K., Hihara, Y., Nishiyama, Y., 2014. Zeaxanthin and echinenone protect the repair of Photosystem II from inhibition by singlet oxygen in *synechocystis* sp. PCC 6803. *Plant Cell Physiol.* 56, 906–916. <https://doi.org/10.1093/pcp/pcv018>
- LAEMMLI, U.K., 1970. Cleavage of Structural Proteins during the Assembly of the Head of Bacteriophage T4. *Nature* 227, 680–685. <https://doi.org/10.1038/227680a0>
- Latifi, A., Ruiz, M., Zhang, C.-C., L, G., TM, L., E, C., ND, C., HC, M., L, F., A, G., 2009. Oxidative stress in cyanobacteria. *FEMS Microbiol. Rev.* 33, 258–278. <https://doi.org/10.1111/j.1574-6976.2008.00134.x>
- Lee, Y.-K., Ding, S.-Y., Low, C.-S., Chang, Y.-C., Forday, W.L., Chew, P.-C., 1995. Design and performance of an α -type tubular photobioreactor for mass cultivation of microalgae. *J. Appl. Phycol.* 7, 47–51. <https://doi.org/10.1007/BF00003549>
- Li, H., Li, D., Yang, S., Xie, J., Zhao, J., 2006. The state transition mechanism—simply depending on light-on and -off in *Spirulina platensis*. <https://doi.org/10.1016/j.bbabi.2006.08.009>
- Li, M., Hu, D., Liu, H., 2014. Photobioreactor with ideal light-dark cycle designed and built from mathematical modeling and CFD simulation. *Ecol. Eng.* 73, 162–167. <https://doi.org/10.1016/j.ecoleng.2014.09.010>
- Liu, H., Zhang, H., Niedzwiedzki, D.M., Prado, M., He, G., Gross, M.L., Blankenship,

- R.E., 2013. Phycobilisomes Supply Excitations to Both Photosystems in a Megacomplex in Cyanobacteria. *Science* (80-.). 342, 1104–1107. <https://doi.org/10.1126/science.1242321>
- Liu, L.-N., 2016. Distribution and dynamics of electron transport complexes in cyanobacterial thylakoid membranes. *Biochim. Biophys. Acta* 1857, 256–65. <https://doi.org/10.1016/j.bbabi.2015.11.010>
- Liu, L.N., 2016. Distribution and dynamics of electron transport complexes in cyanobacterial thylakoid membranes. *Biochim. Biophys. Acta - Bioenerg.* 1857, 256–265. <https://doi.org/10.1016/j.bbabi.2015.11.010>
- Los, D.A., Zorina, A., Sinetova, M., Kryazhov, S., Mironov, K., Zinchenko, V. V., 2010. Stress sensors and signal transducers in cyanobacteria. *Sensors* 10, 2386–2415. <https://doi.org/10.3390/s100302386>
- Luengo, J.M., García, B.N., Sandoval, A., Naharro, G.N., Olivera, E.R., 2003. Bioplastics from microorganisms. *Curr. Opin. Microbiol.* 6, 251–260. [https://doi.org/10.1016/S1369-5274\(03\)00040-7](https://doi.org/10.1016/S1369-5274(03)00040-7)
- Luo, H.-P., Al-Dahhan, M.H., 2011. Verification and validation of CFD simulations for local flow dynamics in a draft tube airlift bioreactor. *Chem. Eng. Sci.* 66, 907–923. <https://doi.org/10.1016/J.CES.2010.11.038>
- Martínez, L., Redondas, V., García, A.I., Morán, A., 2011. Optimization of growth operational conditions for CO₂ biofixation by native *Synechocystis* sp. J. *Chem. Technol. Biotechnol.* 86, 681–690. <https://doi.org/10.1002/jctb.2568>
- Materna, A.C., Sturm, S., Kroth, P.G., Lavaud, J., 2009. First induced plastid genome mutations in an alga with secondary plastids: *psbA* mutations in the diatom *Phaeodactylum tricornutum* (bacillariophyceae) reveal consequences on the regulation of photosynthesis 1. *J. Phycol.* 45, 838–846. <https://doi.org/10.1111/j.1529-8817.2009.00711.x>
- Matthews, H.D., Solomon, S., Pierrehumbert, R., 2012. Cumulative carbon as a policy framework for achieving climate stabilization. *Philos. Trans. A. Math. Phys. Eng. Sci.* 370, 4365–79. <https://doi.org/10.1098/rsta.2012.0064>
- McCarty, R.E., Hammes, G.G., 1987. Molecular architecture of chloroplast coupling factor 1. *Trends Biochem. Sci.* 12, 234–237. [https://doi.org/10.1016/0968-0004\(87\)90116-2](https://doi.org/10.1016/0968-0004(87)90116-2)
- Merchant, S., Sawaya, M.R., 2005. The light reactions: a guide to recent acquisitions for the picture gallery. *Plant Cell* 17, 648–63. <https://doi.org/10.1105/tpc.105.030676>
- Metz, J., Nixon, P., Diner, B., 1990. Nucleotide sequence of the *psbA3* gene from the cyanobacterium *Synechocystis* PCC 6803. *Nucleic Acids Res.* 18, 6715.

- Mimuro, M., Kikuchi, H., Murakami, A., 1999. Structure and function of phycobilisomes. *Photosynth. Photomorphogenes.* 104–135.
- Monod, C., Takahashi, Y., Goldschmidt-Clermont, M., Rochaix, J.D., 1994. The chloroplast *ycf8* open reading frame encodes a photosystem II polypeptide which maintains photosynthetic activity under adverse growth conditions. *EMBO J.* 13, 2747–54.
- Montgomery, B.L., 2015. Light-dependent governance of cell shape dimensions in cyanobacteria. *Front. Microbiol.* 6, 1–8. <https://doi.org/10.3389/fmicb.2015.00514>
- Montgomery, B.L., 2014. The Regulation of Light Sensing and Light-Harvesting Impacts the Use of Cyanobacteria as Biotechnology Platforms. *Front. Bioeng. Biotechnol.* 2, 22. <https://doi.org/10.3389/fbioe.2014.00022>
- Mullineaux, C.W., Kirchhoff, H., Schneider, D., 2014. Electron transport and light-harvesting switches in cyanobacteria THE ENVIRONMENT IN AND AROUND CYANOBACTERIAL THYLAKOID MEMBRANES 18, 44–1. <https://doi.org/10.3389/fpls.2014.00007>
- Mulo, P., Laakso, S., Mäenpää, P., Aro, E.-M., 1998. Stepwise Photoinhibition of Photosystem II. *Plant Physiol.* 117, 483–490. <https://doi.org/10.1104/pp.117.2.483>
- Mulo, P., Tyystjärvi, T., Tyystjärvi, E., Govindjee, Mäenpää, P., Aro, E.M., 1997. Mutagenesis of the D-E loop of photosystem II reaction centre protein D1. Function and assembly of photosystem II. *Plant Mol. Biol.* 33, 1059–1071. <https://doi.org/10.1023/A:1005765305956>
- Munekage, Y., Hojo, M., Meurer, J., Endo, T., Tasaka, M., Shikanai, T., 2002. PGR5 Is Involved in Cyclic Electron Flow around Photosystem I and Is Essential for Photoprotection in Arabidopsis. *Cell* 110, 361–371. [https://doi.org/10.1016/S0092-8674\(02\)00867-X](https://doi.org/10.1016/S0092-8674(02)00867-X)
- Muramatsu, M., Hihara, Y., 2012. Acclimation to high-light conditions in cyanobacteria: from gene expression to physiological responses. *J. Plant Res.* 125, 11–39. <https://doi.org/10.1007/s10265-011-0454-6>
- Muramatsu, M., Sonoike, K., Hihara, Y., 2009. Mechanism of downregulation of photosystem I content under high-light conditions in the cyanobacterium *Synechocystis* sp. PCC 6803. *Microbiology* 155, 989–996. <https://doi.org/10.1099/mic.0.024018-0>
- Murata, N., Takahashi, S., Nishiyama, Y., Allakhverdiev, S.I., 2007. Photoinhibition of photosystem II under environmental stress. *Biochim. Biophys. Acta - Bioenerg.* 1767, 414–421. <https://doi.org/10.1016/j.bbabi.2006.11.019>

- Nanjo, Y., Mizusawa, N., Wada, H., Slabas, A.R., Hayashi, H., Nishiyama, Y., 2010. Synthesis of fatty acids de novo is required for photosynthetic acclimation of *Synechocystis* sp. PCC 6803 to high temperature. *Biochim. Biophys. Acta - Bioenerg.* 1797, 1483–1490. <https://doi.org/10.1016/j.bbabi.2010.03.014>
- Napiwotzki, A., Bergmann, A., Decker, K., Legall, H., Eckert, H.-J., Eichle, H.-J., Renger, G., 1997. Acceptor side photoinhibition in PS II: On the possible effects of the functional integrity of the PS II donor side on photoinhibition of stable charge separation. *Photosynth. Res.* 52, 199–213. <https://doi.org/10.1023/A:1005897503276>
- Nedbal, L., Trtílek, M., Červený, J., Komárek, O., Pakrasi, H.B., 2008. A photobioreactor system for precision cultivation of photoautotrophic microorganisms and for high-content analysis of suspension dynamics. *Biotechnol. Bioeng.* 100, 902–910. <https://doi.org/10.1002/bit.21833>
- Nelson, N., 2011. Photosystems and global effects of oxygenic photosynthesis. *Biochim. Biophys. Acta - Bioenerg.* 1807, 856–863. <https://doi.org/10.1016/j.bbabi.2010.10.011>
- Nelson, N., Ben-Shem, A., 2004. The complex architecture of oxygenic photosynthesis. *Nat. Rev. Mol. Cell Biol.* 5, 971–982. <https://doi.org/10.1038/nrm1525>
- Nguyen, K., Bruce, B.D., 2014. Growing green electricity: Progress and strategies for use of Photosystem I for sustainable photovoltaic energy conversion. *Biochim. Biophys. Acta - Bioenerg.* 1837, 1553–1566. <https://doi.org/10.1016/j.bbabi.2013.12.013>
- Nickelsen, J., Rengstl, B., 2013. Photosystem II Assembly: From Cyanobacteria to Plants. *Annu. Rev. Plant Biol.* 64, 609–635. <https://doi.org/10.1146/annurev-arplant-050312-120124>
- Nishiyama, Y., Allakhverdiev, S.I., Murata, N., 2006. A new paradigm for the action of reactive oxygen species in the photoinhibition of photosystem II. *Biochim. Biophys. Acta - Bioenerg.* <https://doi.org/10.1016/j.bbabi.2006.05.013>
- Nishiyama, Y., Yamamoto, H., Allakhverdiev, S.I., Inaba, M., Yokota, A., Murata, N., 2001. Oxidative stress inhibits the repair of photodamage to the photosynthetic machinery. *EMBO J.* 20, 5587–94. <https://doi.org/10.1093/emboj/20.20.5587>
- Nixon, P.J., Barker, M., Boehm, M., De Vries, R., Komenda, J., 2005. FtsH-mediated repair of the photosystem II complex in response to light stress. *J. Exp. Bot.* 56, 357–363. <https://doi.org/10.1093/jxb/eri021>
- Nixon, P.J., Mullineaux, C.W., n.d. Regulation of Photosynthetic Electron

- Transport, in: Regulation of Photosynthesis. Kluwer Academic Publishers, Dordrecht, pp. 533–555. https://doi.org/10.1007/0-306-48148-0_30
- Nowaczyk, M.M., Hebel, R., Schlodder, E., Meyer, H.E., Warscheid, B., Rogner, M., 2006. Psb27, a Cyanobacterial Lipoprotein, Is Involved in the Repair Cycle of Photosystem II. *Plant Cell Online* 18, 3121–3131. <https://doi.org/10.1105/tpc.106.042671>
- Ohnishi, N., Kashino, Y., Satoh, K., Ozawa, S.I., Takahashi, Y., 2007. Chloroplast-encoded polypeptide PsbT is involved in the repair of primary electron acceptor QA of photosystem II during photoinhibition in *Chlamydomonas reinhardtii*. *J. Biol. Chem.* 282, 7107–7115. <https://doi.org/10.1074/jbc.M606763200>
- Ooms, M.D., Graham, P.J., Nguyen, B., Sargent, E.H., Sinton, D., 2017. Light dilution via wavelength management for efficient high-density photobioreactors. *Biotechnol. Bioeng.* 114, 1160–1169. <https://doi.org/10.1002/bit.26261>
- Ort, D.R., Melis, A., Melis, A., 2011. Optimizing antenna size to maximize photosynthetic efficiency. *Plant Physiol.* 155, 79–85. <https://doi.org/10.1104/pp.110.165886>
- Panda, B., Jain, P., Sharma, L., Mallick, N., 2006. Optimization of cultural and nutritional conditions for accumulation of poly- β -hydroxybutyrate in *Synechocystis* sp. PCC 6803. *Bioresour. Technol.* 97, 1296–1301. <https://doi.org/10.1016/J.BIORTECH.2005.05.013>
- Pattanaik, B., Whitaker, M.J., Montgomery, B.L., 2011. Convergence and divergence of the photoregulation of pigmentation and cellular morphology in *Fremyella diplosiphon*. *Plant Signal. Behav.* 6, 2038–2041. <https://doi.org/10.4161/psb.6.12.18239>
- Pcc, S., Alphen, V., 2018. UvA-DARE (Digital Academic Repository) Physiological studies to optimize growth of the prototype biosolar cell factory.
- Peretó, J., 2011. Oxygenic Photosynthesis, in: *Encyclopedia of Astrobiology*. Springer Berlin Heidelberg, Berlin, Heidelberg, pp. 1209–1209. https://doi.org/10.1007/978-3-642-11274-4_1721
- Pohl, P., Kohlhase, M., Martin, M., 1988. Photobioreactors for the axenic mass cultivation of microalgae. *Algal Biotechnol.* / Ed. by T. Stadler ... [et al.].
- Porankiewicz, J., Schelin, J., Clarke, A.K., 1998. The ATP-dependent Clp protease is essential for acclimation to UV-B and low temperature in the cyanobacterium *Synechococcus*. *Mol. Microbiol.* 29, 275–83.
- Powles, S.B., 1984. Photoinhibition of Photosynthesis Induced by Visible Light. *Annu. Rev. Plant Physiol.* 35, 15–44.

<https://doi.org/10.1146/annurev.pp.35.060184.000311>

- Quan, Y., Pehkonen, S.O., Ray, M.B., 2004. Evaluation of Three Different Lamp Emission Models Using Novel Application of Potassium Ferrioxalate Actinometry. *Ind. Eng. Chem. Res.* 43, 948–955. <https://doi.org/10.1021/ie0304210>
- Rakhimberdieva, M.G., Boichenko, V.A., Karapetyan, N. V., Stadnichuk, I.N., 2001. Interaction of Phycobilisomes with Photosystem II Dimers and Photosystem I Monomers and Trimers in the Cyanobacterium *Spirulina platensis* †. *Biochemistry* 40, 15780–15788. <https://doi.org/10.1021/bi010009t>
- Rakhimberdieva, M.G., Stadnichuk, I.N., Elanskaya, I. V., Karapetyan, N. V, Bakh, A.N., 2004. Carotenoid-induced quenching of the phycobilisome fluorescence in photosystem II-deficient mutant of *Synechocystis* sp. <https://doi.org/10.1016/j.febslet.2004.07.087>
- Ravnikar, P.D., Sevnck, R. debus, J., Saetaert, P., McIntosh, L., 1989. Nucleotide sequence of a second *psbA* gene from the unicellular cyanobacterium *Synechocystis* 6803. *Nucleic Acids Res.* 17, 3991. <https://doi.org/10.1093/nar/17.10.3991>
- RENGER, G., VÖLKER, M., ECKERT, H.J., FROMME, R., HOHM-VEIT, S., GRÄBER, P., 1989. ON THE MECHANISM OF PHOTOSYSTEM II DETERIORATION BY UV-B IRRADIATION. *Photochem. Photobiol.* 49, 97–105. <https://doi.org/10.1111/j.1751-1097.1989.tb04083.x>
- Richmond, A., Cheng-Wu, Z., 2001. Optimization of a flat plate glass reactor for mass production of *Nannochloropsis* sp. outdoors. *J. Biotechnol.* 85, 259–69.
- Roach, T., Krieger-Liszkay, A., 2014. Regulation of photosynthetic electron transport and photoinhibition. *Curr. Protein Pept. Sci.* 15, 351–362. <https://doi.org/10.2174/1389203715666140327105143>
- Roose, J.L., Pakrasi, H.B., 2008. The *Psb27* protein facilitates manganese cluster assembly in photosystem II. *J. Biol. Chem.* 283, 4044–4050. <https://doi.org/10.1074/jbc.M708960200>
- Salih, G.F., Jansson, C., 1997. Activation of the silent *psbA1* gene in the cyanobacterium *Synechocystis* sp strain 6803 produces a novel and functional D1 protein. *Plant Cell* 9, 869–878. <https://doi.org/10.1105/tpc.9.6.869>
- Sánchez Mirón, A., García Camacho, F., Contreras Gómez, A., Grima, E.M., Chisti, Y., 2000. Bubble-column and airlift photobioreactors for algal culture. *AIChE J.* 46, 1872–1887. <https://doi.org/10.1002/aic.690460915>
- Saroussi, S.I., Wittkopp, T.M., Grossman, A.R., 2016. The Type II NADPH

- Dehydrogenase Facilitates Cyclic Electron Flow, Energy-Dependent Quenching, and Chlororespiratory Metabolism during Acclimation of *Chlamydomonas reinhardtii* to Nitrogen Deprivation. *Plant Physiol.* 170, 1975–1988. <https://doi.org/10.1104/pp.15.02014>
- Sato, M., Nimura-Matsune, K., Watanabe, S., Chibazakura, T., Yoshikawa, H., 2007. Expression analysis of multiple *dnaK* genes in the cyanobacterium *Synechococcus elongatus* PCC 7942. *J. Bacteriol.* 189, 3751–8. <https://doi.org/10.1128/JB.01722-06>
- Scherer, S., 1990. Do photosynthetic and respiratory electron transport chains share redox proteins? *Trends Biochem. Sci.* 15, 458–462. [https://doi.org/10.1016/0968-0004\(90\)90296-N](https://doi.org/10.1016/0968-0004(90)90296-N)
- Schopf, J.W., 2000. The Fossil Record: Tracing the Roots of the Cyanobacterial Lineage, in: *The Ecology of Cyanobacteria*. Kluwer Academic Publishers, Dordrecht, pp. 13–35. https://doi.org/10.1007/0-306-46855-7_2
- Schreiber, U., 2004. Pulse-Amplitude-Modulation (PAM) Fluorometry and Saturation Pulse Method: An Overview, in: *Chlorophyll a Fluorescence*. Springer Netherlands, Dordrecht, pp. 279–319. https://doi.org/10.1007/978-1-4020-3218-9_11
- Schröder, W.P., Åkerlund, H.-E., 1986. H₂O₂ accessibility to the Photosystem II donor side in protein-depleted inside-out thylakoids measured as flash-induced oxygen production. *Biochim. Biophys. Acta - Bioenerg.* 848, 359–363. [https://doi.org/10.1016/0005-2728\(86\)90211-2](https://doi.org/10.1016/0005-2728(86)90211-2)
- Schuurmans, R.M., Van Alphen, P., Schuurmans, J.M., Matthijs, H.C.P., Hellingwerf, K.J., 2015. Comparison of the photosynthetic yield of cyanobacteria and green algae: Different methods give different answers. *PLoS One* 10, 1–17. <https://doi.org/10.1371/journal.pone.0139061>
- Seibert, M., Toon, S., Govindjee, O'Neil, M.P., Wasielewski, M.R., 1992. Primary charge separation in isolated photosystem II reaction centers. *Res. Photosynth. II* 41–44.
- Sherbinin, A. de, Carr, D., Cassels, S., Jiang, L., 2007. Population and Environment. *Annu. Rev. Environ. Resour.* 32, 345–373. <https://doi.org/10.1146/annurev.energy.32.041306.100243>
- Shevchenko, A., Wilm, M., Vorm, O., Mann, M., 1996. Mass spectrometric sequencing of proteins from silver-stained polyacrylamide gels. *Anal. Chem.* 68, 850–858. <https://doi.org/10.1021/ac950914h>
- Shimakawa, G., Shaku, K., Miyake, C., 2016. Oxidation of P700 in Photosystem I Is Essential for the Growth of Cyanobacteria. *Plant Physiol.* 172, 1443–1450.

<https://doi.org/10.1104/pp.16.01227>

- Shipton, C.A., Barber, J., 1991. Photoinduced degradation of the D1 polypeptide in isolated reaction centers of photosystem II: evidence for an autoproteolytic process triggered by the oxidizing side of the photosystem. *Proc. Natl. Acad. Sci. U. S. A.* 88, 6691–6695. <https://doi.org/10.1073/pnas.88.15.6691>
- Silva, P., Thompson, E., Bailey, S., Kruse, O., Mullineaux, C.W., Robinson, C., Mann, N.H., Nixon, P.J., 2003. FtsH is involved in the early stages of repair of photosystem II in *Synechocystis* sp PCC 6803. *Plant Cell* 15, 2152–2164. <https://doi.org/10.1105/tpc.012609.tivity>
- Singh, A.K., Bhattacharyya-Pakrasi, M., Elvitigala, T., Ghosh, B., Aurora, R., Pakrasi, H.B., 2009a. A systems-level analysis of the effects of light quality on the metabolism of a cyanobacterium. *Plant Physiol.* 151, 1596–608. <https://doi.org/10.1104/pp.109.144824>
- Singh, A.K., Bhattacharyya-Pakrasi, M., Elvitigala, T., Ghosh, B., Aurora, R., Pakrasi, H.B., 2009b. A systems-level analysis of the effects of light quality on the metabolism of a cyanobacterium. *Plant Physiol.* 151, 1596–608. <https://doi.org/10.1104/pp.109.144824>
- Singh, N.K., Sonani, R.R., Rastogi, R.P., Madamwar, D., 2015. The phycobilisomes: an early requisite for efficient photosynthesis in cyanobacteria. *EXCLI J.* 14, 268–89. <https://doi.org/10.17179/excli2014-723>
- Singh, R., Parihar, P., Singh, M., Bajguz, A., Kumar, J., Singh, S., Singh, V.P., Prasad, S.M., 2017. Uncovering Potential Applications of Cyanobacteria and Algal Metabolites in Biology, Agriculture and Medicine: Current Status and Future Prospects. *Front. Microbiol.* 8, 515. <https://doi.org/10.3389/fmicb.2017.00515>
- Singh, R.N., Sharma, S., 2012. Development of suitable photobioreactor for algae production – A review. *Renew. Sustain. Energy Rev.* 16, 2347–2353. <https://doi.org/10.1016/j.rser.2012.01.026>
- Solimeno, A., Samsó, R., Uggetti, E., Sialve, B., Steyer, J.P., Gabarró, A., García, J., 2015. New mechanistic model to simulate microalgae growth. *Algal Res.* 12, 350–358. <https://doi.org/10.1016/j.algal.2015.09.008>
- Stanier, R.Y., Kunisawa, R., Mandel, M., Cohen-Bazire, G., 1971. Purification and properties of unicellular blue-green algae (Order Chroococcales). *Bacteriol. Rev.* 35, 171–205. <https://doi.org/10.1016/j.jbiotec.2013.07.020>
- Steiger, S., Schäfer, L., Sandmann, G., 1999. High-light-dependent upregulation of carotenoids and their antioxidative properties in the cyanobacterium *Synechocystis* PCC 6803. *J. Photochem. Photobiol. B Biol.* 52, 14–18.

[https://doi.org/10.1016/S1011-1344\(99\)00094-9](https://doi.org/10.1016/S1011-1344(99)00094-9)

- Straka, L., Rittmann, B.E., 2018. Effect of culture density on biomass production and light utilization efficiency of *Synechocystis* sp. PCC 6803. *Biotechnol. Bioeng.* 115, 507–511. <https://doi.org/10.1002/bit.26479>
- Styring, S., Virgin, I., Ehrenberg, A., Andersson, B., 1990. Strong light photoinhibition of electrontransport in Photosystem II. Impairment of the function of the first quinone acceptor, QA. *Biochim. Biophys. Acta - Bioenerg.* 1015, 269–278. [https://doi.org/10.1016/0005-2728\(90\)90031-X](https://doi.org/10.1016/0005-2728(90)90031-X)
- Sukenik, A., Zohary, T., Padisák, J., 2009. Cyanoprokaryota and Other Prokaryotic Algae, in: *Encyclopedia of Inland Waters*. Elsevier, pp. 138–148. <https://doi.org/10.1016/B978-012370626-3.00133-2>
- Switzer, R.C., Merrill, C.R., Shifrin, S., 1979. A highly sensitive silver stain for detecting proteins and peptides in polyacrylamide gels. *Anal. Biochem.* 98, 231–237. [https://doi.org/10.1016/0003-2697\(79\)90732-2](https://doi.org/10.1016/0003-2697(79)90732-2)
- Szabò, I., Rigoni, F., Bianchetti, M., Carbonera, D., Pierantoni, F., Seraglia, R., Segalla, A., Giacometti, G.M., 2001. Isolation and characterization of photosystem II subcomplexes from cyanobacteria lacking photosystem I. *Eur. J. Biochem.* 268, 5129–5134. <https://doi.org/10.1046/j.0014-2956.2001.02441.x>
- Takahashi, S., Murata, N., 2008. How do environmental stresses accelerate photoinhibition? *Trends Plant Sci.* 13, 178–182. <https://doi.org/10.1016/j.tplants.2008.01.005>
- Takahashi, S., Murata, N., 2005. Interruption of the Calvin cycle inhibits the repair of Photosystem II from photodamage. *Biochim. Biophys. Acta - Bioenerg.* 1708, 352–361. <https://doi.org/10.1016/j.bbabi.2005.04.003>
- Tamary, E., Kiss, V., Nevo, R., Adam, Z., Bernát, G., Rexroth, S., Rögner, M., Reich, Z., 2012a. Structural and functional alterations of cyanobacterial phycobilisomes induced by high-light stress. *BBA - Bioenerg.* 1817, 319–327. <https://doi.org/10.1016/j.bbabi.2011.11.008>
- Tamary, E., Kiss, V., Nevo, R., Adam, Z., Bernát, G., Rexroth, S., Rögner, M., Reich, Z., 2012b. Structural and functional alterations of cyanobacterial phycobilisomes induced by high-light stress. *Biochim. Biophys. Acta - Bioenerg.* 1817, 319–327. <https://doi.org/10.1016/j.bbabi.2011.11.008>
- Theis, J., Schroda, M., 2016. Revisiting the photosystem II repair cycle. *Plant Signal. Behav.* 11, e1218587. <https://doi.org/10.1080/15592324.2016.1218587>
- Thomas, D.J., Thomas, J., Youderian, P.A., Herbert, S.K., 2001. Photoinhibition and Light-Induced Cyclic Electron Transport in *ndhB*– and *psaE*– Mutants of

- Synechocystis sp. PCC 6803. *Plant Cell Physiol.* 42, 803–812. <https://doi.org/10.1093/pcp/pce104>
- Toole, C.M., Plank, T.L., Grossman, A.R., Anderson, L.K., 1998. Bilin deletions and subunit stability in cyanobacterial light-harvesting proteins. *Mol. Microbiol.* 30, 475–486. <https://doi.org/10.1046/j.1365-2958.1998.01082.x>
- Tóth, T.N., Chukhutsina, V., Domonkos, I., Knoppová, J., Komenda, J., Kis, M., Lénárt, Z., Garab, G., Kovács, L., Gombos, Z., Van Amerongen, H., 2015. Carotenoids are essential for the assembly of cyanobacterial photosynthetic complexes. *Biochim. Biophys. Acta - Bioenerg.* 1847, 1153–1165. <https://doi.org/10.1016/j.bbabi.2015.05.020>
- Touloupakis, E., Cicchi, B., Benavides, A.M.S., Torzillo, G., 2016. Effect of high pH on growth of *Synechocystis* sp. PCC 6803 cultures and their contamination by golden algae (*Poterioochromonas* sp.). *Appl. Microbiol. Biotechnol.* 100, 1333–1341. <https://doi.org/10.1007/s00253-015-7024-0>
- Trautmann, D., Beyer, P., Al-Babili, S., 2013. The ORF slr0091 of *Synechocystis* sp. PCC6803 encodes a high-light induced aldehyde dehydrogenase converting apocarotenals and alkanals. *FEBS J.* 280, 3685–3696. <https://doi.org/10.1111/febs.12361>
- Tredici, M.R., n.d. Mass Production of Microalgae: Photobioreactors, in: *Handbook of Microalgal Culture*. Blackwell Publishing Ltd, Oxford, UK, pp. 178–214. <https://doi.org/10.1002/9780470995280.ch9>
- Triantaphylidès, C., Havaux, M., 2009. Singlet oxygen in plants: production, detoxification and signaling. *Trends Plant Sci.* 14, 219–228. <https://doi.org/10.1016/j.tplants.2009.01.008>
- Tyystjärvi, E., 2013. Photoinhibition of Photosystem II*. *Int. Rev. Cell Mol. Biol.* 300, 243–303. <https://doi.org/10.1016/B978-0-12-405210-9.00007-2>
- Tyystjärvi, E., 2008. Photoinhibition of Photosystem II and photodamage of the oxygen evolving manganese cluster. *Coord. Chem. Rev.* 252, 361–376. <https://doi.org/10.1016/j.ccr.2007.08.021>
- Tyystjärvi, E., Aro, E.M., 1996. The rate constant of photoinhibition, measured in lincomycin-treated leaves, is directly proportional to light intensity. *Proc. Natl. Acad. Sci. U. S. A.* 93, 2213–2218. <https://doi.org/10.1073/pnas.93.5.2213>
- Tyystjärvi, T., Herranen, M., Aro, E.M., 2001. Regulation of translation elongation in cyanobacteria: Membrane targeting of the ribosome nascent-chain complexes controls the synthesis of D1 protein. *Mol. Microbiol.* 40, 476–484. <https://doi.org/10.1046/j.1365-2958.2001.02402.x>

- Umena, Y., Kawakami, K., Shen, J.-R., Kamiya, N., 2011. Crystal structure of oxygen-evolving photosystem II at a resolution of 1.9 Å. *Nature* 473, 55–60. <https://doi.org/10.1038/nature09913>
- UNFCCC. Conference of the Parties (COP), 2015. Paris Climate Change Conference- November 2015, COP 21. Adopt. Paris Agreement. Propos. by Pres. 21932, 32. <https://doi.org/FCCC/CP/2015/L.9/Rev.1>
- Van Alphen, P., Hellingwerf, K.J., 2015. Sustained circadian rhythms in continuous light in *Synechocystis* sp. PCC6803 growing in a well-controlled photobioreactor. *PLoS One* 10. <https://doi.org/10.1371/journal.pone.0127715>
- Van De Meene, A.M.L., Hohmann-Marriott, M.F., Vermaas, W.F.J., Roberson, R.W., 2006. The three-dimensional structure of the cyanobacterium *Synechocystis* sp. PCC 6803. *Arch. Microbiol.* 184, 259–270. <https://doi.org/10.1007/s00203-005-0027-y>
- Varman, A.M., Xiao, Y., Pakrasi, H.B., Tang, Y.J., 2013. Metabolic engineering of *Synechocystis* sp. Strain PCC 6803 for isobutanol production. *Appl. Environ. Microbiol.* 79, 908–914. <https://doi.org/10.1128/AEM.02827-12>
- Vass, I., Styring, S., Hundal, T., Koivuniemi, a, Aro, E., Andersson, B., 1992a. Reversible and irreversible intermediates during photoinhibition of photosystem II: stable reduced QA species promote chlorophyll triplet formation. *Proc. Natl. Acad. Sci. U. S. A.* 89, 1408–1412. <https://doi.org/10.1073/pnas.89.4.1408>
- Vass, I., Styring, S., Hundal, T., Koivuniemi, a, Aro, E., Andersson, B., 1992b. Reversible and irreversible intermediates during photoinhibition of photosystem II: stable reduced QA species promote chlorophyll triplet formation. *Proc. Natl. Acad. Sci. U. S. A.* 89, 1408–1412. <https://doi.org/10.1073/pnas.89.4.1408>
- Vatcheva, I., de Jong, H., Bernard, O., Mars, N.J.I., 2006. Experiment selection for the discrimination of semi-quantitative models of dynamical systems. *Artif. Intell.* 170, 472–506. <https://doi.org/10.1016/J.ARTINT.2005.11.001>
- Vavilin, D., Brune, D.C., Vermaas, W., 2005. 15N-labeling to determine chlorophyll synthesis and degradation in *Synechocystis* sp. PCC 6803 strains lacking one or both photosystems. *Biochim. Biophys. Acta - Bioenerg.* 1708, 91–101. <https://doi.org/10.1016/j.bbabi.2004.12.011>
- Vavilin, D., Vermaas, W., 2007. Continuous chlorophyll degradation accompanied by chlorophyllide and phytol reutilization for chlorophyll synthesis in *Synechocystis* sp. PCC 6803. *Biochim. Biophys. Acta - Bioenerg.* 1767, 920–

929. <https://doi.org/10.1016/J.BBABIO.2007.03.010>
- Vermaas, W., 1996. Molecular genetics of the cyanobacterium *Synechocystis* sp. PCC 6803: Principles and possible biotechnology applications. *J. Appl. Phycol.* 8, 263–273.
- Walker, J.E., Tybulewicz, V.L.J., 1985. Comparative genetics and biochemistry of light-driven ATP synthases.
- Wang, C.Y., Fu, C.C., Liu, Y.C., 2007. Effects of using light-emitting diodes on the cultivation of *Spirulina platensis*. *Biochem. Eng. J.* 37, 21–25. <https://doi.org/10.1016/j.bej.2007.03.004>
- Wang, Q., Jantaro, S., Lu, B., Majeed, W., Bailey, M., He, Q., 2008. The high light-inducible polypeptides stabilize trimeric photosystem I complex under high light conditions in *Synechocystis* PCC 6803. *Plant Physiol.* 147, 1239–50. <https://doi.org/10.1104/pp.108.121087>
- Whitmarsh, J., Govindjee, M., 2002. Photosystem II. *Encycl. Life Sci.* 6, 1–13. <https://doi.org/10.1002/9780470015902.a0022548>
- Whitton, B.A., Potts, M., 2012. Introduction to the cyanobacteria, in: *Ecology of Cyanobacteria II: Their Diversity in Space and Time*. Kluwer Academic Publishers, Dordrecht, pp. 1–13. https://doi.org/10.1007/978-94-007-3855-3_1
- Wijffels, R.H., Kruse, O., Hellingwerf, K.J., 2013. Potential of industrial biotechnology with cyanobacteria and eukaryotic microalgae. *Curr. Opin. Biotechnol.* 24, 405–413. <https://doi.org/10.1016/j.copbio.2013.04.004>
- Wilcox, D.C., 1993. Turbulence modeling for CFD, Aiaa. DCW Industries. <https://doi.org/0963605151>
- Wilson, A., Punginelli, C., Gall, A., Bonetti, C., Alexandre, M., Routaboul, J.-M., Kerfeld, C.A., van Grondelle, R., Robert, B., Kennis, J.T.M., Kirilovsky, D., 2008. A photoactive carotenoid protein acting as light intensity sensor. *Proc. Natl. Acad. Sci.* 105, 12075–12080. <https://doi.org/10.1073/pnas.0804636105>
- Wyman, M., Fay, P., 1986. Underwater Light Climate and the Growth and Pigmentation of Planktonic Blue-Green Algae (Cyanobacteria) II. The Influence of Light Quality. *Proc. R. Soc. B Biol. Sci.* 227, 381–393. <https://doi.org/10.1098/rspb.1986.0028>
- Xu, H., Vavilin, D., Funk, C., Vermaas, W., 2004. Multiple Deletions of Small Cab-like Proteins in the Cyanobacterium *Synechocystis* sp. PCC 6803. *J. Biol. Chem.* 279, 27971–27979. <https://doi.org/10.1074/jbc.M403307200>
- Yang, C., Hua, Q., Shimizu, K., 2002. Metabolic flux analysis in *Synechocystis* using

isotope distribution from ¹³C-labeled glucose. *Metab. Eng.* 4, 202–16.

- Yao, D.C.I., Brune, D.C., Vavilin, D., Vermaas, W.F.J., 2011. Photosystem II Component Lifetimes in the Cyanobacterium *Synechocystis* sp. Strain PCC 6803 SMALL Cab-LIKE PROTEINS STABILIZE BIOSYNTHESIS INTERMEDIATES AND AFFECT EARLY STEPS IN CHLOROPHYLL SYNTHESIS * □ S. <https://doi.org/10.1074/jbc.M111.320994>
- Yao, D.C.I., Brune, D.C., Vermaas, W.F.J., 2012. Lifetimes of photosystem i and II proteins in the cyanobacterium *Synechocystis* sp. PCC 6803. *FEBS Lett.* 586, 169–173. <https://doi.org/10.1016/j.febslet.2011.12.010>
- Yoshikawa, K., Hirasawa, T., Ogawa, K., Hidaka, Y., Nakajima, T., Furusawa, C., Shimizu, H., 2013. Integrated transcriptomic and metabolomic analysis of the central metabolism of *Synechocystis* sp. PCC 6803 under different trophic conditions. *Biotechnol. J.* 8, 571–580. <https://doi.org/10.1002/biot.201200235>
- Yu, Y., You, L., Liu, D., Hollinshead, W., Tang, Y.J., Zhang, F., 2013a. Development of *Synechocystis* sp. PCC 6803 as a Phototrophic Cell Factory. *Mar. Drugs* 11, 2894–2916. <https://doi.org/10.3390/md11082894>
- Yu, Y., You, L., Liu, D., Hollinshead, W., Tang, Y.J., Zhang, F., 2013b. Development of *Synechocystis* sp. PCC 6803 as a Phototrophic Cell Factory. *Mar. Drugs* 11, 2894–2916. <https://doi.org/10.3390/md11082894>
- Zakar, T., Laczko-Dobos, H., Toth, T.N., Gombos, Z., 2016. Carotenoids Assist in Cyanobacterial Photosystem II Assembly and Function. *Front. Plant Sci.* 7, 1–7. <https://doi.org/10.3389/fpls.2016.00295>
- Zavafer, A., Cheah, M.H., Hillier, W., Chow, W.S., Takahashi, S., 2015. Photodamage to the oxygen evolving complex of photosystem II by visible light. *Sci. Rep.* 5, 16363. <https://doi.org/10.1038/srep16363>
- Zavřel, T., Sinetova, M.A., Búzová, D., Literáková, P., Červený, J., 2015. Characterization of a model cyanobacterium *Synechocystis* sp: PCC 6803 autotrophic growth in a flat-panel photobioreactor. *Eng. Life Sci.* 15, 122–132. <https://doi.org/10.1002/elsc.201300165>
- Zhang, D., Dechatiwongse, P., Hellgardt, K., 2015. Modelling light transmission, cyanobacterial growth kinetics and fluid dynamics in a laboratory scale multiphase photo-bioreactor for biological hydrogen production. *Algal Res.* 8, 99–107. <https://doi.org/10.1016/j.algal.2015.01.006>
- Zhang, D., Xiao, N., Mahbubani, K.T., del Rio-Chanona, E.A., Slater, N.K.H., Vassiliadis, V.S., 2015. Bioprocess modelling of biohydrogen production by *Rhodospseudomonas palustris*: Model development and effects of operating

conditions on hydrogen yield and glycerol conversion efficiency. *Chem. Eng. Sci.* 130, 68–78. <https://doi.org/10.1016/j.ces.2015.02.045>

Zhang, H., Liu, H., Blankenship, R.E., Gross, M.L., 2016. Isotope-Encoded Carboxyl Group Footprinting for Mass Spectrometry-Based Protein Conformational Studies. *J. Am. Soc. Mass Spectrom.* 27, 178–81. <https://doi.org/10.1007/s13361-015-1260-5>

Zhang, P., Eisenhut, M., Brandt, A.-M., Carmel, D., Silén, H.M., Vass, I., Allahverdiyeva, Y., Salminen, T.A., Aro, E.-M., 2012. Operon flv4-flv2 provides cyanobacterial photosystem II with flexibility of electron transfer. *Plant Cell* 24, 1952–71. <https://doi.org/10.1105/tpc.111.094417>

Zhou, J., Zhu, T., Cai, Z., Li, Y., 2016. From cyanochemicals to cyanofactories: a review and perspective. *Microb. Cell Fact.* 15. <https://doi.org/10.1186/s12934-015-0405-3>

3.6Supplementary

Identified proteins list (with a ProteinPilot unused score of at least 1.3 and FDR 1%)

N	Unused score	Total score	% Cov (95)	Description	Species	Peptides(95%)
1	140,13	140,13	93,7	60 kDa chaperonin	SYNY3	114
2	113,97	113,67	65,7	Phycobiliprotein ApcE	SYNY3	62
3	93,89	104,55	91,9	60 kDa chaperonin 2	SYNY3	67
4	86,34	86,3	87,7	Elongation factor Tu	SYNY3	76
5	82,68	83,29	75,5	Ribulose biphosphate carboxylase large chain	SYNY3	77
6	81,8	81,8	70,1	Chaperone protein dnaK2	SYNY3	51
7	80,99	81,4	34,1	DNA-directed RNA polymerase subunit beta'	SYNY3	38
8	69,06	69,58	76,7	ATP synthase subunit alpha	SYNY3	55
9	64,65	64,87	93	ATP synthase subunit beta	SYNY3	62
10	62,53	62,79	36,2	DNA-directed RNA polymerase subunit beta	SYNY3	31
11	60,75	60,83	58,9	Elongation factor G 1	SYNY3	30
12	58,83	58,79	72	30S ribosomal protein S1 homolog A	SYNY3	36
13	54,7	54,71	44,4	Polyribonucleotide nucleotidyltransferase	SYNY3	28
14	52,19	52,19	95,7	C-phycoyanin alpha chain	SYNY3	95
15	51,26	51,31	88,2	Ketol-acid reductoisomerase (NADP(+))	SYNY3	35
16	49,56	50,57	93	C-phycoyanin beta chain	SYNY3	99
17	48,57	49,56	31,4	Translation initiation factor IF-2	SYNY3	24
18	47,19	47,24	65,3	Phosphoglycerate kinase	SYNY3	29
19	46,73	46,77	82,8	Transcription regulator LexA	SYNY3	32
20	46,42	46,75	79	50S ribosomal protein L1	SYNY3	27
21	45,72	45,79	74,2	Glyceraldehyde-3-phosphate dehydrogenase 2	SYNY3	32
22	45,17	45,36	57,5	Trigger factor	SYNY3	22
23	43,39	43,43	73,1	Iron uptake protein	SYNY3	23
24	42,25	42,94	58,3	D-3-phosphoglycerate dehydrogenase	SYNY3	22
25	42,1	42,11	75,5	Fructose-bisphosphate aldolase class 2	SYNY3	32
26	42,03	42,34	41,8	Photosystem II CP47 reaction center protein	SYNY3	24
27	40,99	41,79	95	Allophycocyanin beta chain	SYNY3	56
28	40,26	40,91	57,3	Glutamine synthetase	SYNY3	23
29	39,74	40,05	43,5	ATP-dependent zinc metalloprotease FtsH 3	SYNY3	26
30	39,3	39,36	56,2	Ferredoxin--NADP reductase	SYNY3	21
31	38,89	38,82	95,7	Allophycocyanin alpha chain	SYNY3	49
32	38,68	38,8	63,9	Phosphoribulokinase	SYNY3	25
33	38,22	38,42	71,5	Adenosylhomocysteinase	SYNY3	30
34	38,1	38,23	93,8	50S ribosomal protein L7/L12	SYNY3	28
35	38,04	38,15	63,4	DNA-directed RNA polymerase subunit alpha	SYNY3	19
36	37,78	38,12	48,4	Enolase	SYNY3	21
37	37,48	39,51	62,3	Phycobilisome 32.1 kDa linker polypeptide	SYNY3	26

37	37,48	39,51	62,3	Phycobilisome 32.1 kDa linker polypeptide	SYNY3	26
38	36,86	37,02	34,7	DNA-directed RNA polymerase subunit gamma	SYNY3	19
39	36,48	36,58	67,4	50S ribosomal protein L2	SYNY3	22
40	36,47	36,49	40,9	Photosystem II CP43 reaction center protein	SYNY3	22
41	36,38	36,55	62,3	Nitrate transport protein NrtA	SYNY3	21
42	36,28	38,27	74,2	30S ribosomal protein S3	SYNY3	22
43	35,9	39,22	66,3	Phycobilisome 32.1 kDa linker	SYNY3	26
44	35,71	36	40,9	Nitrate transport ATP-binding protein NrtC	SYNY3	19
45	35,51	35,76	61	30S ribosomal protein S2	SYNY3	26
46	33,62	33,67	72,6	Orange carotenoid-binding protein	SYNY3	23
47	33,37	33,46	55,4	D-fructose 1,6-bisphosphatase class 2/sedoheptulose 1,7-bisphosphatase	SYNY3	22
48	32,14	32,86	96,5	Allophycocyanin subunit beta-18	SYNY3	32
49	31,87	32,03	23,3	Photosystem I P700 chlorophyll a apoprotein A1	SYNY3	22
50	31,69	31,76	80,3	50S ribosomal protein L3	SYNY3	19
51	30,93	31,04	80	50S ribosomal protein L5	SYNY3	16
52	30,76	30,79	88,4	Nitrogen regulatory protein P-II	SYNY3	20
53	30,39	30,9	45,5	Geranylgeranyl diphosphate reductase	SYNY3	15
54	30,28	30,38	71,7	30S ribosomal protein S13	SYNY3	16
55	30,14	31,41	28,4	Ribonuclease J	SYNY3	16
56	29,97	30,12	78,2	50S ribosomal protein L6	SYNY3	17
57	29,01	29,07	22,2	Photosystem I P700 chlorophyll a apoprotein A2	SYNY3	19
58	28,93	29,13	75,7	Putative peroxiredoxin sll1621	SYNY3	19
59	28,42	28,46	96,4	Carbon dioxide-concentrating mechanism protein CcmK homolog 1	SYNY3	20
60	28,18	28,63	78,7	Photosystem I reaction center subunit II	SYNY3	23
61	27,88	27,95	91,3	10 kDa chaperonin	SYNY3	23
62	27,7	27,94	50,9	Iron uptake protein A2	SYNY3	14
63	27,28	27,37	66,1	Elongation factor Ts	SYNY3	15
64	27,03	27,24	81,8	Photosystem II manganese-stabilizing polypeptide	SYNY3	26
65	26,91	27,17	55,2	Putative thylakoid lumen peptidyl-prolyl cis-trans isomerase sll0408	SYNY3	15
66	26,66	26,81	80	DNA-binding protein HU	SYNY3	20
67	26,59	26,92	79,6	50S ribosomal protein L9	SYNY3	17
68	26,27	27,01	50,5	30S ribosomal protein S4	SYNY3	16
69	25,89	30,08	35,6	ATP-dependent zinc metalloprotease FtsH 2	SYNY3	19
70	25,6	25,81	72,5	Ribosome-recycling factor	SYNY3	13
71	25,11	25,11	93,2	50S ribosomal protein L29	SYNY3	17
72	25,04	26,23	58,6	50S ribosomal protein L4	SYNY3	14
73	24,7	24,64	70,5	30S ribosomal protein S5	SYNY3	18
74	24,54	24,79	48,3	Argininosuccinate synthase	SYNY3	14

75	23,84	23,99	22,4	Sulfite reductase [ferredoxin]	SYNY3	11
76	23,57	26,06	65	ATP synthase gamma chain	SYNY3	15
77	23,19	23,18	87,6	Allophycocyanin subunit alpha-B	SYNY3	11
78	23,11	23,27	39,4	Magnesium-protoporphyrin IX monomethyl ester [oxidative] cyclase	SYNY3	13
79	22,54	22,59	56,4	Photosystem I reaction center subunit III	SYNY3	15
80	22,04	22,29	56,9	Uncharacterized protein slr0617	SYNY3	16
81	22,03	22,11	89,2	Adenylate kinase 1	SYNY3	12
82	21,95	21,96	99,1	Nucleoid-associated protein slr1847	SYNY3	12
83	21,65	21,73	71,8	30S ribosomal protein S7	SYNY3	15
84	21,49	21,87	30,8	S-adenosylmethionine synthase	SYNY3	11
85	21,47	21,94	37,8	Porphobilinogen deaminase	SYNY3	11
86	21,4	21,41	70,2	50S ribosomal protein L13	SYNY3	12
87	21,34	21,43	78,2	50S ribosomal protein L21	SYNY3	13
88	21,03	21,16	48,5	Cytochrome f	SYNY3	14
89	20,84	20,89	57,4	Protein GrpE	SYNY3	11
90	20,81	20,9	70,5	50S ribosomal protein L10	SYNY3	12
91	20,79	20,94	71,4	30S ribosomal protein S10	SYNY3	11
92	20,73	22,09	65,7	ATP synthase subunit b'	SYNY3	16
93	20,58	20,77	31,7	6-phosphogluconate dehydrogenase, decarboxylating	SYNY3	11
94	20,33	20,45	84,2	50S ribosomal protein L23	SYNY3	14
95	20,06	20,3	89	ATP synthase epsilon chain	SYNY3	13
96	19,96	20,1	71,8	Uncharacterized protein slr1894	SYNY3	10
97	19,92	20,14	72,1	50S ribosomal protein L14	SYNY3	19
98	19,72	20,59	50,3	ATP synthase subunit b	SYNY3	12
99	19,42	19,77	73,1	Cytochrome c-550	SYNY3	15
100	19,41	19,71	69,9	30S ribosomal protein S8	SYNY3	10
101	19,3	19,39	95,2	Phycobilisome 8.9 kDa linker polypeptide, phycocyanin-associated, rod	SYNY3	13
102	19,29	19,59	27,6	RNA helicase CrhR	SYNY3	10
103	19,06	19,18	16,1	1,4-alpha-glucan branching enzyme GlgB	SYNY3	10
104	18,97	19,07	47,7	Ribose-5-phosphate isomerase A	SYNY3	10
105	18,84	19,28	25,1	Dihydrolipoyl dehydrogenase	SYNY3	10
106	18,78	18,93	65,6	50S ribosomal protein L19	SYNY3	14
107	18,65	18,87	70,2	Photosystem II 12 kDa extrinsic protein	SYNY3	13
108	18,62	18,75	47,4	Ribulose-phosphate 3-epimerase	SYNY3	10
109	18,16	18,24	72	30S ribosomal protein S16	SYNY3	11
110	18,15	18,17	82,9	Superoxide dismutase [Fe]	SYNY3	13
111	18,02	18,31	97,4	Ribulose biphosphate carboxylase small chain	SYNY3	22
112	18	18,01	46,7	Cytochrome b6-f complex iron-sulfur subunit 2	SYNY3	13
113	17,87	18,18	49,1	Inorganic pyrophosphatase	SYNY3	15
114	17,71	17,85	62	Peptidyl-prolyl cis-trans isomerase slr1251	SYNY3	10
115	17,51	19,92	83,1	30S ribosomal protein S18	SYNY3	12
116	17,42	17,49	26,9	NAD(P)H-quinone oxidoreductase subunit H	SYNY3	9

117	17,28	17,35	83,9	Carbon dioxide-concentrating mechanism protein CcmK homolog 4	SYNY3	10
118	17,22	17,33	69,2	30S ribosomal protein S11	SYNY3	10
119	17,21	17,56	57,8	Hydroperoxy fatty acid reductase gpx2	SYNY3	10
120	17,15	17,39	83,2	30S ribosomal protein S6	SYNY3	11
121	17,1	17,15	68,1	Ribosome hibernation promotion factor	SYNY3	9
122	17,03	17,25	83	50S ribosomal protein L11	SYNY3	12
123	16,95	17,12	32,9	Uroporphyrinogen decarboxylase	SYNY3	8
124	16,72	16,82	44,4	GTP cyclohydrolase 1	SYNY3	9
125	16,67	17,16	30,9	Serine hydroxymethyltransferase	SYNY3	10
126	16,66	16,87	28,7	Uncharacterized protein slr1128	SYNY3	8
127	16,38	16,59	27,7	Sulfate adenylyltransferase	SYNY3	9
128	16,31	16,54	93,3	Probable thylakoid lumen protein slr11769	SYNY3	9
129	16,23	17,49	41,5	Oxygen-dependent coproporphyrinogen-III oxidase	SYNY3	10
130	16,04	16,13	76,9	50S ribosomal protein L15	SYNY3	9
131	16,04	16,09	23,1	Ycf48-like protein	SYNY3	8
132	15,89	16,12	42,4	Transcription termination/antitermination protein NusG	SYNY3	9
133	15,7	15,75	25,3	Photosystem II D2 protein	SYNY3	10
134	15,38	15,43	27	Glutamate-1-semialdehyde 2,1-aminomutase	SYNY3	9
135	15,32	15,45	75,1	ATP synthase subunit delta	SYNY3	8
136	15,06	15,07	64,4	50S ribosomal protein L27	SYNY3	8
137	15,04	15,17	31,5	Ribose-phosphate pyrophosphokinase	SYNY3	9
138	14,81	15,55	62	30S ribosomal protein S9	SYNY3	10
139	14,8	14,9	93,2	Photosystem I reaction center subunit IV	SYNY3	21
140	14,79	14,82	50,6	30S ribosomal protein S17	SYNY3	7
141	14,61	14,72	62,5	50S ribosomal protein L18	SYNY3	9
142	14,52	14,8	14,4	Ribonuclease E/G-like protein	SYNY3	8
143	14,44	14,67	21,2	Glucose-1-phosphate adenylyltransferase	SYNY3	9
144	14,24	14,33	24,3	Adenylosuccinate synthetase	SYNY3	10
145	14,1	14,35	48,3	Nucleoside diphosphate kinase	SYNY3	9
146	14,1	14,11	37,3	Putative ATP-dependent Clp protease	SYNY3	7
147	14,07	14,08	38,3	Heme oxygenase 1	SYNY3	7
148	14,06	14,08	58,7	30S ribosomal protein S19	SYNY3	10
149	14	14,01	61,7	Thioredoxin	SYNY3	8
150	14	14	95,5	Probable 30S ribosomal protein PSRP-3	SYNY3	8
151	13,48	13,83	26,9	DNA polymerase III subunit beta	SYNY3	15
152	13,46	13,66	30,7	NAD(P)H-quinone oxidoreductase subunit K 1	SYNY3	7
153	13,43	13,62	66,3	30S ribosomal protein S15	SYNY3	7
154	13,41	14,09	51	30S ribosomal protein S14	SYNY3	9
155	13,36	13,72	50,4	50S ribosomal protein L22	SYNY3	7
156	13,23	13,38	48,5	30S ribosomal protein S20	SYNY3	9
157	13,19	13,4	37,8	NAD(P)H-quinone oxidoreductase subunit I	SYNY3	7
158	13,06	13,26	50,2	Aldehyde decarboxylase	SYNY3	7

159	13,06	13,17	41	Protein DrgA	SYNY3	9
160	12,86	12,93	21,9	1-deoxy-D-xylulose-5-phosphate synthase	SYNY3	8
161	12,59	12,71	16,2	Uncharacterized protein sll1526	SYNY3	8
162	12,56	12,7	26,3	Protein RecA	SYNY3	6
163	12,5	12,92	17,2	RNA polymerase sigma factor SigA	SYNY3	8
164	12,38	12,64	46,3	Probable adenylyl-sulfate kinase	SYNY3	8
165	12,36	12,45	79,8	UPF0296 protein ssl2874	SYNY3	6
166	12,35	12,37	75	Photosystem II reaction center Psb28 protein	SYNY3	9
167	12	20,92	96,1	Carbon dioxide-concentrating mechanism protein CcmK homolog 2	SYNY3	17
168	11,99	12,14	53	50S ribosomal protein L24	SYNY3	7
169	11,87	11,95	97	Thylakoid-associated protein slr0729	SYNY3	8
170	11,72	12,07	48,3	50S ribosomal protein L17	SYNY3	9
171	11,56	11,63	55,5	Uncharacterized thylakoid-associated protein sll0982	SYNY3	8
172	11,48	12,02	10,1	Chaperone protein ClpB 2	SYNY3	7
173	11,41	11,94	11,1	GTP-binding protein TypA/BipA homolog	SYNY3	5
174	11,36	12,94	11,7	Glucose-6-phosphate isomerase	SYNY3	6
175	11,13	11,21	37,9	Delta-aminolevulinic acid dehydratase	SYNY3	6
176	11,07	11,16	24,6	Probable branched-chain-amino-acid aminotransferase	SYNY3	6
177	10,74	10,81	44,6	Putative RNA-binding protein RbpA	SYNY3	8
178	10,68	11,45	52,1	50S ribosomal protein L20	SYNY3	8
179	10,63	10,8	22,6	LL-diaminopimelate aminotransferase	SYNY3	7
180	10,54	12,46	34,1	30S ribosomal protein S1 homolog B	SYNY3	7
181	10,37	10,88	10,7	Putative methyl-accepting chemotaxis protein sll0041	SYNY3	8
182	10,35	10,43	26,8	Orotate phosphoribosyltransferase	SYNY3	5
183	10,14	10,21	21	Isoaspartyl peptidase/L-asparaginase	SYNY3	5
184	10,08	10,32	77,6	50S ribosomal protein L25	SYNY3	10
185	10,05	10,05	21,1	Photosystem II protein D1 2	SYNY3	9
186	10,01	10,01	32,8	Photosystem I biogenesis protein BtpA	SYNY3	7
187	10	10	60	30S ribosomal protein S21	SYNY3	5
188	9,91	10	47,8	50S ribosomal protein L35	SYNY3	5
189	9,87	10,3	15,5	Putative serine protease HhoA	SYNY3	5
190	9,83	9,9	45,2	Photosystem I reaction center subunit XI	SYNY3	8
191	9,82	9,96	50	Photosystem II lipoprotein Psb27	SYNY3	5
192	9,79	10,36	23,4	Aspartate-semialdehyde dehydrogenase	SYNY3	6
193	9,73	9,8	82,9	DNA-directed RNA polymerase subunit omega	SYNY3	5
194	9,57	9,74	51,6	30S ribosomal protein S12	SYNY3	7
195	9,49	10,19	52,6	Bacterioferritin	SYNY3	8
196	9,06	9,11	40,3	Cell division protein SepF	SYNY3	8
197	8,97	9,06	79,2	NAD(P)H-quinone oxidoreductase subunit O	SYNY3	5
198	8,78	9,04	9,1	Acetazolamide conferring resistance protein zam	SYNY3	6
199	8,63	8,82	13,3	Phosphomethylpyrimidine synthase	SYNY3	5

200	8,6	8,84	13,7	Pyruvate kinase 2	SYNY3	5
201	8,39	8,46	42,3	50S ribosomal protein L28	SYNY3	4
202	8,23	8,37	34,5	Translation initiation factor IF-3	SYNY3	5
203	8,14	8,35	15,7	Chaperone protein DnaJ 1	SYNY3	6
204	8,13	8,21	15,4	Magnesium-chelatase subunit ChII	SYNY3	5
205	8,04	8,05	48,3	Cytochrome c6	SYNY3	8
206	8,03	8,1	30,2	NAD(P)H-quinone oxidoreductase subunit J	SYNY3	5
207	8,01	8,03	14,1	3-isopropylmalate dehydrogenase	SYNY3	4
208	8	8,06	15,4	N-acetyl-gamma-glutamyl-phosphate reductase	SYNY3	4
209	8	8	39,4	Flavodoxin	SYNY3	5
210	7,52	7,56	25,8	Tryptophan synthase alpha chain	SYNY3	4
211	7,49	7,52	24,3	Cytochrome b6	SYNY3	5
212	7,48	7,51	52,4	Carbon dioxide-concentrating mechanism protein CcmK homolog 3	SYNY3	4
213	7,37	7,45	34,7	Photosystem I assembly protein Ycf3	SYNY3	5
214	7,36	7,41	33,3	Thylakoid-associated single-stranded DNA-binding protein slr1034	SYNY3	4
215	7,28	7,33	42,9	Ycf54-like protein	SYNY3	7
216	7,28	7,32	45,2	Plastocyanin	SYNY3	6
217	7,17	7,22	53,7	Phycobilisome 7.8 kDa linker polypeptide	SYNY4	6
218	7,07	7,3	19,2	Glyceraldehyde-3-phosphate dehydrogenase 1	SYNY3	5
219	7,04	7,29	2,9	Ferredoxin-dependent glutamate synthase 2	SYNY3	5
220	6,92	6,97	22,5	Elongation factor P	SYNY3	5
221	6,89	6,98	37,3	Translation initiation factor IF-1	SYNY3	3
222	6,65	6,95	4,3	Phenylalanine--tRNA ligase beta subunit	SYNY3	4
223	6,51	6,6	21,5	3-oxoacyl-[acyl-carrier-protein] reductase	SYNY3	4
224	6,5	7,37	42,5	50S ribosomal protein L16	SYNY3	6
225	6,43	6,86	3	DNA gyrase subunit B	SYNY3	3
226	6,43	6,58	5,4	Aconitate hydratase B	SYNY3	4
227	6,28	6,37	17,9	Carbonic anhydrase	SYNY3	3
228	6,26	6,29	13,6	Tryptophan synthase beta chain	SYNY3	4
229	6,22	6,33	71	Photosystem I reaction center subunit XII	SYNY3	6
230	6,19	6,3	19,3	Cell division protein FtsZ	SYNY3	4
231	6,13	6,23	21,5	Triosephosphate isomerase	SYNY3	4
232	6,06	6,08	23,9	ATP synthase subunit a	SYNY3	4
233	6,04	6,36	13,4	Acetolactate synthase small subunit	SYNY3	3
234	6,03	6,1	5,4	Glycine--tRNA ligase beta subunit	SYNY3	3
235	6,01	6,09	24,8	Enoyl-[acyl-carrier-protein] reductase [NADH] FabI	SYNY3	4
236	6	6,14	26,7	Adenine phosphoribosyltransferase	SYNY3	3
237	6	6,03	26,1	Universal stress protein SII1654	SYNY3	4
238	6	6,01	7,5	UDP-N-acetylmuramoyl-L-alanyl-D-glutamate--2,6-diaminopimelate ligase	SYNY3	4
239	6	6	46,9	Cytochrome b559 subunit alpha	SYNY3	4

240	6	6	56,3	Putative pterin-4-alpha-carbinolamine dehydratase	SYNY3	3
241	5,92	6,01	20,9	Chromophore lyase CpcT/CpeT	SYNY3	4
242	5,79	5,94	29,6	50S ribosomal protein L31	SYNY3	4
243	5,79	5,87	19,2	ATP-dependent Clp protease proteolytic subunit 1	SYNY3	3
244	5,76	5,84	20,2	Putative sulfur carrier protein slr0821	SYNY3	5
245	5,72	6,07	9,3	Aspartate--tRNA(Asp/Asn) ligase	SYNY3	4
246	5,67	5,95	7,7	Transaldolase	SYNY3	3
247	5,65	5,8	5,2	Protein translocase subunit SecA	SYNY3	3
248	5,59	5,64	13,2	Pyridoxine 5'-phosphate synthase	SYNY3	3
249	5,5	5,67	25,6	Single-stranded DNA-binding protein 1	SYNY3	3
250	5,48	5,54	53,3	Ferredoxin-thioredoxin reductase, variable chain	SYNY3	3
251	5,47	5,52	38,8	Uncharacterized protein ssr3122	SYNY3	3
252	5,46	5,62	13,4	Probable peptidyl-prolyl cis-trans isomerase slr0227	SYNY3	3
253	5,43	5,64	11,6	Chorismate synthase	SYNY3	4
254	5,4	5,55	50	Urease subunit gamma	SYNY3	3
255	5,4	5,47	29,6	Photosystem I iron-sulfur center	SYNY3	4
256	5,31	5,42	8,6	Acetyl-coenzyme A carboxylase carboxyl transferase subunit alpha	SYNY3	3
257	5,22	5,39	7,8	Glycogen synthase 1	SYNY3	3
258	5,12	5,21	19,2	Cyanophycinase	SYNY3	3
259	5,08	5,3	17,9	Thylakoid membrane protein slr1796	SYNY3	4
260	5,01	5,13	23,6	Membrane-associated protein slr1513	SYNY3	3
261	5	5,1	8,4	Light-dependent protochlorophyllide reductase	SYNY3	3
262	4,89	5,04	35,5	UPF0367 protein ssl1972	SYNY3	4
263	4,88	4,96	28	Carbon dioxide concentrating mechanism protein CcmL	SYNY3	3
264	4,85	5,08	5,5	DNA gyrase subunit A	SYNY3	4
265	4,74	4,83	9,6	Peptide chain release factor 1	SYNY3	3
266	4,66	4,81	5,9	Zeta-carotene desaturase	SYNY3	3
267	4,46	4,6	4,1	GMP synthase [glutamine-hydrolyzing]	SYNY3	2
268	4,45	4,48	21,2	Glutamyl-tRNA(Gln) amidotransferase subunit C	SYNY3	2
269	4,44	4,53	16,6	Hydroperoxy fatty acid reductase gpx1	SYNY3	2
270	4,43	4,52	16,5	NAD(P)H-quinone oxidoreductase subunit M	SYNY3	2
271	4,37	4,43	6,7	Adenylosuccinate lyase	SYNY3	2
272	4,3	4,43	13,5	Septum site-determining protein MinD	SYNY3	3
273	4,29	4,38	4,7	Membrane protein insertase YidC	SYNY3	2
274	4,27	4,35	6,4	2,3-bisphosphoglycerate-independent phosphoglycerate mutase	SYNY3	2
275	4,23	4,33	9,1	Uncharacterized tRNA/rRNA methyltransferase slr0955	SYNY3	2
276	4,19	4,41	7,6	Acyl-[acyl-carrier-protein]-UDP-N-acetylglucosamine O-acyltransferase	SYNY3	2

277	4,14	9,24	9,9	ATP-dependent zinc metalloprotease FtsH 4	SYNY3	7
278	4,13	4,18	8,9	Phosphate acyltransferase	SYNY3	2
279	4,08	4,1	18,1	Cyanate hydratase	SYNY3	2
280	4,06	4,23	8,7	Phosphoribosylaminoimidazole- succinocarboxamide synthase	SYNY3	2
281	4,04	10,13	10,1	Chaperone protein ClpB 1	SYNY3	7
282	4,02	4,1	11,5	Putative biopolymer transport protein ExbB-like 2	SYNY3	3
283	4,01	4,29	6,8	Threonine synthase	SYNY3	2
284	4,01	4,06	13,5	Uridylate kinase	SYNY3	3
285	4	4,09	20	Urease subunit beta	SYNY3	2
286	4	4,05	5,1	1-deoxy-D-xylulose 5-phosphate reductoisomerase	SYNY3	2
287	4	4,01	4,7	Metalloprotease slr1322	SYNY3	2
288	4	4,01	27,8	Arsenate reductase ArsI1	SYNY3	2
289	4	4	21,1	Thioredoxin-like protein slr1139	SYNY3	2
290	3,86	4,13	47,4	50S ribosomal protein L32	SYNY3	3
291	3,82	4,08	8,5	Amidophosphoribosyltransferase	SYNY3	4
292	3,82	3,89	20,8	Acyl carrier protein	SYNY3	3
293	3,8	3,98	12,2	Photosystem I assembly protein Ycf4	SYNY3	3
294	3,74	4,14	9,9	Cysteine synthase	SYNY3	3
295	3,7	3,77	7,8	1-(5-phosphoribosyl)-5-[(5- phosphoribosylamino)methylideneamino] imidazole-4-carboxamide isomerase	SYNY3	2
296	3,67	3,85	6,7	4-hydroxy-3-methylbut-2-en-1-yl diphosphate synthase (ferredoxin)	SYNY3	2
297	3,61	3,74	12,6	Uncharacterized sugar kinase slr0537	SYNY3	3
298	3,6	3,68	12,4	NAD(P)H-quinone oxidoreductase subunit N	SYNY3	2
299	3,57	3,65	21,1	Uncharacterized protein slI1735	SYNY3	2
300	3,53	3,72	13,6	Probable RuBisCO transcriptional regulator	SYNY3	3
301	3,51	3,67	12,4	Probable ATP-dependent Clp protease proteolytic subunit 3	SYNY3	2
302	3,44	3,64	13,1	Cytochrome b6-f complex subunit 4	SYNY3	3
303	3,42	3,5	11,6	3-hydroxyacyl-[acyl-carrier-protein] dehydratase FabZ	SYNY3	2
304	3,37	4,9	6,5	Aspartyl/glutamyl-tRNA(Asn/Gln) amidotransferase subunit B	SYNY3	3
305	3,36	3,65	6,7	Isocitrate dehydrogenase [NADP]	SYNY3	2
306	3,29	3,36	3,7	Bifunctional protein ThiO/ThiG	SYNY3	2
307	3,27	3,66	11,4	Arginine biosynthesis bifunctional protein ArgJ	SYNY3	4
308	3,19	3,25	59,3	ATP synthase subunit c	SYNY3	5
309	3,12	3,19	23,6	Phasin PhaP	SYNY3	2
310	3,1	3,2	5,2	Glutamate--tRNA ligase	SYNY3	2
311	3,05	3,12	9,1	6,7-dimethyl-8-ribityllumazine synthase	SYNY3	2
312	3	3,15	3,3	DNA topoisomerase 1	SYNY3	2

313	2,9	3,01	4,4	UDP-N-acetylmuramoylalanine--D-glutamate ligase	SYNY3	2
314	2,88	2,95	6,3	NAD(P)H-quinone oxidoreductase chain 5	SYNY3	3
315	2,83	2,89	13,3	6-phosphogluconolactonase	SYNY3	2
316	2,8	2,93	2,2	Probable cytosol aminopeptidase	SYNY3	1
317	2,74	2,87	3,6	Dihydroxy-acid dehydratase	SYNY3	2
318	2,68	2,76	7,2	3-oxoacyl-[acyl-carrier-protein] synthase 2	SYNY3	2
319	2,67	2,73	9,6	Acetylornithine aminotransferase	SYNY3	2
320	2,66	2,73	27,7	Uncharacterized protein ssl0461	SYNY3	3
321	2,63	3,04	3,6	Elongation factor G 2	SYNY3	2
322	2,6	2,68	7,3	Citrate synthase	SYNY3	2
323	2,6	2,64	3,2	Protein translocase subunit SecY	SYNY3	2
324	2,55	2,67	11,9	Ferredoxin-thioredoxin reductase, catalytic chain	SYNY3	2
325	2,47	2,53	12,6	Malonyl CoA-acyl carrier protein transacylase	SYNY3	2
326	2,46	2,59	7,6	Nitrate transport permease protein NrtB	SYNY3	3
327	2,32	2,37	1,5	UDP-N-acetylmuramoyl-tripeptide--D-alanyl-D-alanine ligase	SYNY3	2
328	2,29	2,33	3,5	Bifunctional purine biosynthesis protein PurH	SYNY3	2
329	2,19	2,21	3,6	Uncharacterized WD repeat-containing protein slr1410	SYNY3	1
330	2,16	2,24	2,5	Biotin synthase	SYNY3	1
331	2,15	2,22	2,6	Carbamoyl-phosphate synthase small chain	SYNY3	1
332	2,14	2,21	2,5	D-alanine--D-alanine ligase	SYNY3	1
333	2,14	2,17	2,9	Bifunctional protein GlmU	SYNY3	1
334	2,1	2,16	8,6	N utilization substance protein B homolog OS=Synechocystis sp. (strain PCC 6803 / Kazusa) GN=nusB PE=3 SV=2	SYNY3	1
335	2,08	2,18	6,6	Probable ATP-dependent transporter slr0075 OS=Synechocystis sp. (strain PCC 6803 / Kazusa) GN=slr0075 PE=3 SV=1	SYNY3	1
336	2,08	2,09	3,9	Sirohydrochlorin cobaltochelataze	SYNY3	1
337	2,07	2,11	3	2-isopropylmalate synthase	SYNY3	1
338	2,07	2,08	9,2	Urease accessory protein UreG	SYNY3	1
339	2,07	2,08	3,4	Sulfate-binding protein	SYNY3	1
340	2,06	2,12	5,4	3-phosphoshikimate 1-carboxyvinyltransferase OS=Synechocystis sp. (strain PCC 6803 / Kazusa) GN=aroA PE=3 SV=1	SYNY3	2
341	2,05	2,07	5,2	Ferrochelataze	SYNY3	1
342	2,04	2,05	19,7	Uncharacterized protein sll1783	SYNY3	2
343	2,02	2,74	5,4	Probable 2-phosphosulfolactate phosphatase OS=Synechocystis sp. (strain PCC 6803 / Kazusa) GN=comB PE=3 SV=1	SYNY3	2
344	2,02	2,07	2,2	High-affinity Na(+)/H(+) antiporter NhaS3	SYNY3	1
345	2,02	2,04	4,9	Putative ammonium transporter sll0108	SYNY3	1

346	2,02	2,03	4,1	Histidinol dehydrogenase 1	SYNY3	2
347	2,01	2,15	3,5	NADP-specific glutamate dehydrogenase	SYNY3	2
348	2,01	2,05	1,1	Probable phosphoketolase	SYNY3	1
349	2,01	2,03	22	Fluorescence recovery protein	SYNY3	1
350	2,01	2,02	15,7	UPF0426 protein ssl0294	SYNY3	1
351	2,01	2,01	21,9	Photosystem II reaction center protein H	SYNY3	1
352	2	2,19	7,1	Thylakoid membrane protein slr0575	SYNY3	1
353	2	2,12	4,3	Uncharacterized protein sll0400	SYNY3	1
354	2	2,04	2,2	ATP-dependent Clp protease ATP-binding subunit ClpX	SYNY3	1
355	2	2,02	1,8	Dihydroorotase	SYNY3	1
356	2	2,02	11,8	Ycf51-like protein	SYNY3	1
357	2	2,01	5,1	Bifunctional protein Foid	SYNY3	1
358	2	2,01	5,6	Putative biopolymer transport protein ExbD	SYNY3	1
359	2	2,01	12,2	Uncharacterized protein sll1483	SYNY3	1
360	2	2,01	9	Large-conductance mechanosensitive channel	SYNY3	1
361	2	2	2,6	Probable glycogen synthase 2	SYNY3	1
362	2	2	11,1	Photosystem I reaction center subunit PsaK 2	SYNY3	1
363	2	2	22,5	Photosystem I reaction center subunit IX	SYNY3	1
364	2	2	4,6	Agmatinase 1	SYNY3	1
365	2	2	38,6	Cytochrome b559 subunit beta	SYNY3	1
366	1,96	2	4,2	Putative serine protease HtrA	SYNY3	1
367	1,87	2,22	3,3	Serine--tRNA ligase	SYNY3	2
368	1,86	2,02	2,7	Glycogen phosphorylase	SYNY3	2
369	1,86	1,96	2,4	Glucose-6-phosphate 1-dehydrogenase	SYNY3	1
370	1,83	1,93	48,7	Photosystem II protein Y	SYNY3	2
371	1,81	1,94	2,6	Iron-sulfur cluster carrier protein	SYNY3	1
372	1,8	1,89	5,6	Uncharacterized monothiol glutaredoxin ycf64-like	SYNY3	1
373	1,66	1,83	28,9	50S ribosomal protein L34	SYNY3	2
374	1,54	1,69	5,2	Acetyl-coenzyme A carboxylase carboxyl transferase subunit beta	SYNY3	2
376	1,43	1,7	3,2	Probable signal peptidase I-2	SYNY3	1
377	1,42	1,55	1,4	Phosphoenolpyruvate carboxylase	SYNY3	1
378	1,38	1,5	4,3	Diaminopimelate decarboxylase	SYNY3	1
379	1,37	1,62	4,7	Thylakoid membrane protein slr1949	SYNY3	1
380	1,33	1,41	19,8	Uncharacterized protein ssr3402	SYNY3	1

Chapter 4

Short term photoinhibition

4.1 Introduction

The Photosystem II (PSII) is the first multi enzymatic complex involved in the light dependent reaction of the oxygenic photosynthesis. The PSII, present in thylakoid membrane of plant, algae and cyanobacteria, use the light energy to oxidize the water and transfer the electrons to the plastoquinone (Whitmarsh and Govindjee, 2002). It is composed of two parts: the PSII core, where the catalytic reactions take place, and the peripheral light harvesting system. At exception of some extrinsic proteins, PSII core is a very conserved complex among the different photosynthetic organisms, while, the peripheral antenna systems are very different between eukaryotic and prokaryotes (Albanese et al., 2017). The inhibition of the photochemical electron transfer activity of PSII under strong light condition is a phenomenon known as photoinhibition (Aro et al., 1993a);(Goh et al., 2012);(Tyystjärvi, 2013); (Zavafer et al., 2015). The first event of the photoinhibitory process is the photodamage of the PSII, with the D1 as main target. In agreement with (Tyystjärvi and Aro, 1996) the photo degradation of the D1 polypeptide is directly proportional to the light intensity provided to the microorganism for growing. Two different process are involved in the photoinactivation of the PSII base to its initial site of damage: the acceptor and the donor side photoinhibition. The acceptor-side mechanism is due to a sequence of events where the double reduced quinone Q_A can not work as an electron carrier. The subsequent recombination of Q_A with the primary radical pair $P680^+ Pheo^-$ leads to the formation of the triplet state of the P680, which can react with molecular oxygen leading to generation of the reactive form of oxygen (ROS) singlet oxygen (1O_2) (Mulo et al., 1998);(Vass et al., 1992b). Since its extremely short lifetime, the ROS mainly impairs the protein closely to their site of production, with D1 as primary target (Triantaphylidès and Havaux, 2009). The donor-side photoinhibition is due to inactivation of the oxygen-evolving system (OEC).The impairment of electron transfer from water to the Chlorophyll P680 leads to an extended life time of the radicals $TyrZ^+$ and $P680^+$ that work as strong oxidants damaging the D1 polypeptide and its surrounding proteins. (Bumann and Oesterhelt, 1995b). From literature is known that the two different mechanisms of photoinhibition lead to a different pattern of fragmentation of the D1 protein. The acceptor side photo damage result in cleavage of D1 in the DE stromal loop generate the 23 kDa N-terminal and 10 C-terminal fragments. Conversely, donor side photoinhibition result in the formation of N-terminal and C-terminal fragments with a weight of 10kDa and 24kDa respectively (De Las Rivas et al., 1992). Moreover, in (Kettunen et al., 1996). suggest that the protein D1 is also cleavage in the luminal

CD loop breaking the protein in half. *Shynechocystis*, as different photosynthetic microorganisms, when are growth under photoinhibitory condition activate a repair cycle needed to replace the photodamaged D1 and restore the normal PSII activity. The PSII repair cycle counts different step- process: (I) phosphorylation of the PSI core, partial disassembling of the PSII, (ii) Proteolytic degradation of the D1 protein, (iii) replace of the of the damaged D1 protein with the new synthesized copy, (iv) reassembly of the PSII. When the rate of the PSII photoinhibitory state overcome the rate of repair, a severe photoinhibition take place, leading to the death of the photosynthetic organisms.

In the present work we have examined the effect of the photoinhibition on the activity of the PSII trying to better understand the process involved in the short term photoinhibition and in the photodamage of the protein D1.

4.2 Material and Methods

4.2.1 Isolation and photoinhibition of PSII monomer

Stacked thylakoids membranes, with a final concentration of 1mg mL⁻¹, were solubilized with 20 mM n-dodecyl- β -D-maltoside (β -DDM) for 1 minutes in dark condition at 4 °C. In the solution was added also 500m Phenylmethylsulphonylfluoride (PMSF) to prevent the protease activity. The samples were subsequently centrifuged for 10 minutes at 21.000g at 4 °C and. The supernatant (400 μ l) were loaded on the top of a linear sucrose gradient. The sucrose gradient was created by thawing ultracentrifuge tubes filled with a solution of 25 mM Mes, 10 mM NaCl, 5mM NaCl₂, 5 M sucrose 0,5 Betaine and 0,03% β -DM (*n-Dodecyl β -D-maltoside*). The centrifugation was performed at 39000g for 18h at 4°C.

The band containing the PSII monomer was subsequently harvested using a syringe. The sample was then concentrated with Amicon with 100kDa cut-off devices and stored at -80°C.

The photoinhibition of the PSII reaction centers was performed as mentioned in (Shipton and Barber, 1991). Briefly, the PSII monomers were maintained in a plastic cuvette under constant stirring at 4 °C under. The PSII monomers, in a concentration of 100 μ g [Chl]/ ml, was mixed in a buffer with 50 mM Tris-HCl (pH 8), 2 mM dodecyl- β maltoside and 0.2 mM of the electron acceptors 2,6-Dichloro-1,4 benzoquinone 98% (DCBQ). The photoinhibition was induced maintaining the

sample under the constant illumination in white light by optic fibre at a light intensity of $6000 \mu\text{mol photon m}^{-2} \text{ s}^{-1}$ for 1 h.

4.2.2 *Synechocystis* growth condition

Synechocystis precultures was used to inoculate the flat panel photobioreactor (PBR). The experiments were carried on growing the cells in red-orange light (627 nm) in the commercial flat panel photobioreactor FMT150/1000 Photon System Instruments (Nedbal et al., 2008) in a final volume approximately of 380ml. The culture was grown in a modified BG-11 medium described by (Van Alphen and Hellingwerf, 2015) supplemented with 10 mM of NaCOH_3 . The PBR was provided of pH/temperature probe (Mettler-Toledo) and a densitometer that allow the measurement of the optical density (OD) of the culture at 720 and 680 nm (see chapter 2). The cells were grown at $50 \mu\text{mol photons m}^{-2} \text{ s}^{-1}$ and the photoinhibition was induced setting the light at $1460 \mu\text{mol photons m}^{-2} \text{ s}^{-1}$. The light intensity, in the end, was set again at $50 \mu\text{mol photons m}^{-2} \text{ s}^{-1}$ to induce the cell to recover from the photoinhibitory condition. The culture was grown at constant temperature (30°C) and the pH was maintained at 8.0 by pCO_2 automatically adjusted by gas mixing system GMS150 (Photon Systems Instruments). The cells suspension was fluxed with CO_2 (1%) mixed with N_2 (99%) with a gas flow of 150 ml/min. The OD of the culture suspension was kept approximately constant at 0.4 calibrating the OD_{720} , measured by the PBR densitometer, with OD_{730} measured by the bench top spectrophotometer.

4.2.3 SDS-page and Western blot

The polypeptides come from Thylakoids (10ug Chl), PSII monomer dark adapted (8ug Chl) and PSII light treated (8 ug Chl) were separated by a SDS-PAGE gradient gels (10-17%) containing 6Murea using the Leammli's system(LAEMMLI, 1970) The SDS-PAGE gels were either stained by the silver staining method compatible for mass spectrometry analysis, as described in (Shevchenko et al., 1996) or transferred onto PVDF membrane and immunodetected with the specific antibodies against the C-term and the whole D1 protein (Agrisera, catalogue number AS05 084).

4.2.4 Mass spectrometry analysis

The PSII monomers were centrifuged at 20,000g for 10 minutes at 4°C and the pellet was subsequently resuspended in 10mM HEPES pH7.5. The protein were

precipitated and maintained over night at -20 in pre-cooled pure acetone to remove attached pigments. The solution was centrifuged a 20.000 g for 20 minutes at 4 °C, and the proteins were denatured in buffer with 6M urea, 2M thiourea and 5mM 1,4 dithiothreitol (DTT) until the complete solubilization. The solubilized solution was subsequently centrifuged at 15,000g for 10 minutes at room temperature, and the the insoluble material was discard. The Bradford assay (Bradford, 1976b) was carried on to define the protein concentration . Protein at a concentration of 0.1 mg ml⁻¹ were further denatured and reduced in a solution of pure 2,2,2-Trifluoroethanol (TFE), 100mM ammonium bicarbonate and 200mM DTT for 45 minutes at 60° C, alkylated with 200mM iodoacetamide for 40 minutes at room temperature in the dark, followed by another step of reduction with 200mM DTT for 40 minutes at 37 °C. The digestion of the protein was conducted by adding Trypsin (sigma code T6567) at a final protein: protease ratio of 20:1 (w/w) and maintaining the digestion solution overnight at 37°C. the salts present in the peptides solution were removed by a desalting step performed by a solid phase extraction as described in (Guo and Kristal, 2012) using 30 mg Oasis HLB cartridges (Waters, MA, USA). In the end the peptides were dried and then dissolved in 30 µl of LC-MS/MS mobile phase A (water containing 0.1% (v/v) formic acid). A Liquid chromatography coupled to tandem mass spectrometry(LC-MS/MS) instrument was used for the experiments. The mass spectrometry analyses were carried on by a micro-LC Eksigent Technologies (Dublin, USA) system, using a Halo Fused C18 column (0.5 x 100 mm, 2.7 µm; Eksigent Technologies Dublin, USA) as stationary phase. The mobile phase was composed of a mixture of 0.1% (v/v) formic acid in water (solvent A) and 0.1% (v/v) formic acid in acetonitrile (solvent B). The elution was performed with a flow rate of 15.0 µL min⁻¹ with a constant incrementation of the solvent B from 2 to 40% in 30 minutes. Each analysis was conducted on 4.0 µl of sample. The LC system was connected with a 5600⁺ TripleTOF™ system (AB Sciex, Concord, Canada) provided with DuoSpray™ Ion Source and CDS (Calibrant Delivery System). The analysis with the mass spectrometer were performed in information dependent acquisition (IDA) mode.

The IDA analysis was operated in a mass range of 100-1600 Da (TOF scan with an accumulation time of 100.0 ms), followed by a MS/MS product ion scan from 200 to 1250 Da (accumulation time of 5.0 ms) with the abundance threshold set at 30 cps. The electrospray ion source was set in positive mode in the follow way curtain gas (N₂) at 25 psig, nebulizer gas GAS1 at 25 psig, and GAS2 at 20 psig, ionspray floating voltage (ISFV) at 5000 V, source temperature at 450 °C and declustering potential at 25 V. MS data were acquired with Analyst TF 1.7 (AB

SCIEX, Concord, Canada). ProteinPilot™ v.5.0.1.0, 4895 (AB Sciex, Concord, Canada) with the Paragon algorithm v.5.0.1.0, 4874 was used for analyzing the raw data files. The processing of the data were carried on using the following parameters: Trypsin/Lys-C digestion, cysteine alkylation set to carbamidomethylation and no special factor. All data files were searched, thorough ID search effort, using UniProtKB/TrEMBL database containing Viridiplantae proteins, concatenated with a reversed “decoy” version of the “forward” database. After searching, we accepted protein IDs that had a ProteinPilot Unused Score of at least 1.3 (equivalent to a 95% confidence interval) as a cutoff threshold and an estimated local false discovery rate (FDR) not higher than 1%.

4.2.5 PSI activity in short term photoinhibition assay by mini-PAM

The yield of the Chlorophyll (Chl) fluorescence was evaluated retain the cells of *Synechocystis* on glass microfiber filters (Wathman). The photosynthetic activity was measured by MINI-PAM-II (Heinz Walz, Effeltrich, Germany) setting the instrument in according with the online manual (Fig 4.1). The instrument was provided of a light guide fiber which was adapted in a stopper of the Multiple vacuum filtration system (Millipore 1225).

The cells were grown as previously mentioned in the flat pannel phothobioreactor FMT150/1000.

The light at 50 $\mu\text{mol photons m}^{-2} \text{ s}^{-1}$ was set as control light. The photoinhibition was induced switching the light from 50 to 1460 $\mu\text{mol photons m}^{-2} \text{ s}^{-1}$. The photoinhibitory condition was maintained for 60 minutes, evaluating the quantum yield of PSII photochemistry at the times 5, 10,15,30,45 and 60 minutes. The recovery phase was induced setting the light back to 50 $\mu\text{mol photons m}^{-2} \text{ s}^{-1}$ and checking the PSII the quantum yield of PSII photochemistry at 75,90,120 and 150 minutes. The photosynthetic yield estimation was performed sampling 2.5 ml of culture with a sterile syringe at each established time. The cells suspension was left on the filters in the Multiple vacuum filtration system and the rubber stopper was rapidly exchange with the Mini-PAM adapted fiber. For each sample the value of minimal fluorescence level of illuminated sample (F_0'), maximal fluorescence level of illuminated sample (F_m') were determined. With the F_0' and F_m' values the variable fluorescence F_v and the quantum yield of PSII ($\phi = F_v / F_m'$) were calculated.



Fig 4.1 Pulse-amplituted modulated (PAM) and filtration system .

4.3 Result and discussion

4.3.1 Short term photoinhibition in vitro (PSII monomer)

In this work we have tried to identify the pattern of D1 fragmentation when the Photosystem II core complex (PSII core) is illuminated by a strong irradiance source. To focus our attention in the study of the donor side photoinhibition, the OEC functionality was prevented by suspending the PSII core in a buffer Tris ph 8 with no addition of the CaCl₂ in presence of DCBQ as electron acceptor as described in (De Las Rivas et al., 1992).

In Fig 4.2A is shown a gradient gel (10-17% acrilammide) of the polypeptides separation from Thylakoid (T), dark adapted PSII core (D) and PSII core light treated (L).

Comparing the lines D and L it was evident how the protein D1 is subjected at damage when the PSII core is adapted in high light intensity. In the line L the band of the D1 protein is almost disappeared and it was possible to see some additional bands at lower weight not present in the line D. This result in according with an extensive publication in literature (Tyystjärvi, 2008 and the reference therein)

confirm that the D1 is the main protein damaged in the PSII reaction center under photoinhibitory light conditions.

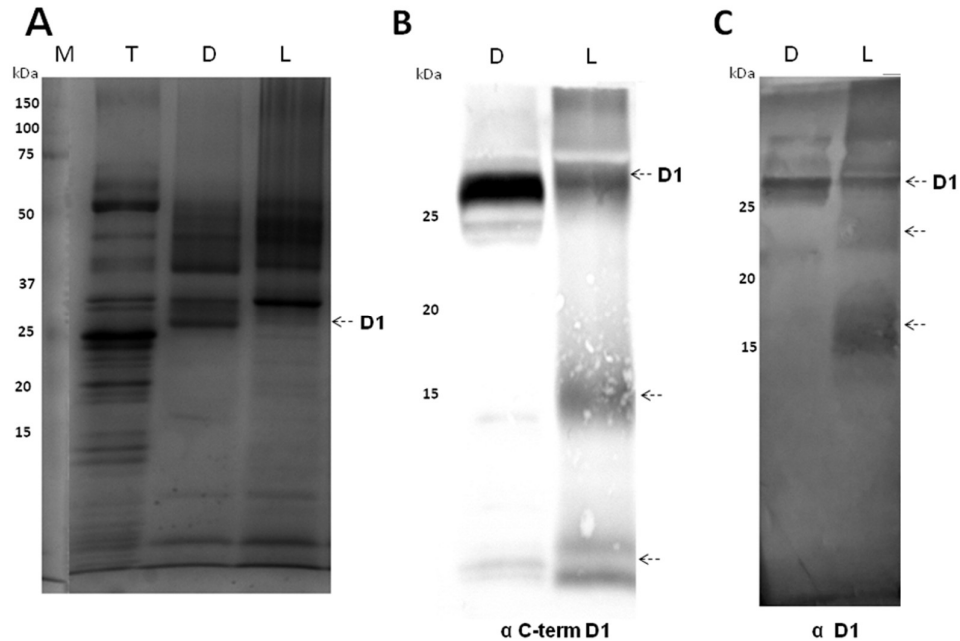


Fig 4.2 Photo-degradation of D1 protein and identification of its degradation products in PSII monomer extracted by thylakoid isolated from control light treated plants. (A) SDS-PAGE gradient gel (10-17%) of polypeptides from Thylakoids (10ug Chl, T), PSII monomer dark adapted (8ug Chl,D) and PSII light treated (8 Chl ug, L), the arrow show the different amount of D1 protein between dark adapted and light treated samples; (B and C) Immunoblots of D1 fragments identified in D and L samples using anti-C-term D1 and anti- D1 respectively; the arrows underline the presence of a double fragmentation of D1 protein. In either case in the lane L is present a main fragmentation at approximately 16 kDa; in (B) is visible a second fragmentation on the bottom of western blot, while in (C) the second fragmentation is present on the top of western blot, close to D1 protein band. In both case in the lane D is shown the quite totally absence of D1 fragments.

The Fig 4.2B and C shown the immunoblot of the PSII dark adapted (line D) and light adapted (line L) detected by the use of the antibodies anti-C term D1 and anti-D1 respectively. In both of them the line L is characterized by a decreased amount of the whole D1 protein with the formation of a D1 fragmentation pattern. The use

of the anti-C terminal D1 has highlighted the formation of two additional bands with an apparent molecular weight of 16-18 kDa and approximately 10 kDa. Conversely, the use of anti-D1 has revealed the formation of fragments at 24 kDa and 16-18 kDa. Our data suggest that the photoinhibitory process lead to the fragmentation of the protein D1 in two different points, with the tendency to break the D1 polypeptide mainly in the middle. In this last case the fragmentation lead to the formation of two fragments with similar weight (16 kDa N-terminal fragment and 17 kDa C-terminal fragment) which are not discernible by western blot. Conversely, the second point of break in D1 leads to the formation of two D1 fragments with a clear different molecular weight: 24 kDa n-terminal fragment and 10 kDa C-term fragment. In accordance with (Kettunen et al., 1996) and (De Las Rivas et al., 1992) the pattern of fragmentation that we have obtained is similar to the acceptor side photoinhibition. As observed in literature both donor side and acceptor side photoinhibitory are involved in the D1 damage when the PSII is subject to strong illumination (Zavafer et al., 2015). Moreover, in agreement with (Friso et al., 1993), it is suggested that in *in vitro* experimental design the concentration of the electron acceptor can affect the balance between the two photoinhibitory processes, where its concentration of 0.25 mM is needed to exclude the acceptor side.

4.3.2 Proteomic analysis of the PSII photoinhibited

In order to study in deep the light induced fragmentation of D1 mass spectrometry analysis of the dark adapted PSII and the light adapted PSII were performed. Indeed, a polypeptide visible only in the light treated sample and not belonging to the typical tryptic pattern fragmentation looked for. In addition, mass spectrometry analysis was used to get more information about other possible proteins in PSII affected by strong light. The label free SWATH-MS analysis (Gillet et al., 2012), processing the ion product (MS2) chromatograms of the peptides derived from the protein analysed was performed. The peptides with a fold change ≥ 2 or ≤ 0.5 which correspond to log2 fold change of $1 \geq$ or ≤ -1 are used as cut-off to discriminate which protein suffered a significant effect in photoinhibitory conditions. In the Table 4.1 the peptides with statistical differences between dark adapted and light adapted conditions are showed. Only three peptides of the protein D1 were detected with a significant decreasing of their amount in the light treated sample compared to the dark adapted one was observed. All

fragments detected were situated to the C-terminal with a typical tryptic pattern of fragmentation.

ID	Proteins	Peptides	L Vs. D	
			Fold change	p-value
sp P05037 ATPB_PEA	AtpB	GIYPAVDPLDSTSTMLQPR	0,11	0
sp Q85V24 ATPB_BARJA	AtpB	GMEVLDTGAALSVPVGGATLGR	0,47	0.0005
sp P06004 PSBC_PEA	Cp43	SPTGEVIFGGETMR	0,07	0
sp P06004 PSBC_PEA	Cp43	LKKDIQPWQER	0,39	0
sp P06004 PSBC_PEA	Cp43	GIDRDFEPVLSMTPLN	0,1	0
sp P06004 PSBC_PEA	Cp43	DFEPVLSMTPLN	0,07	0
sp A0A315 PSBA_COFAR	D1	VINTWADIINRANLGMVMHER	0,08	0
sp A0A315 PSBA_COFAR	D1	ANLGMVMHER	0,06	0
sp A0A315 PSBA_COFAR	D1	NAHNFLDLA	0,04	0
sp P06006 PSBD_PEA	D2	NILLNEGIRAWMATQDQPENLIFPEEVLPR	0,36	0
sp P06006 PSBD_PEA	D2	AWMATQDQPENLIFPEEVLPR	0,2	0
sp P31336 PST2_GOSHI	PsbT	KAYAPVCVTMPTAR	0,41	0
			0,11	0

Table 4.1 Relative quantification of PSII monomer proteins isolated from pea plants.

The fold change (FC) was based on the analysis of the MS2 scan. While comparing high light adapted samples and dark adapted samples (L and D respectively), peptides with a fold change ≥ 2 or ≤ 0.5 used as cut-off with adjusted p-values ≤ 0.05 were considered differentially abundant

From this results was not possible to determinate any natural point of degradation in the protein D1. However, the experimental data suggest a fragmentation of the D1 polypeptide around the amino acid 300 which can lead to the formation of the 10 kDa fragment as observed also in western blot (Fig 4.2B). From the mass spectrometry analysis different fragments of the proteins D2, CP43 and PsbT resulted more abundant in the PSII adapted to strong light intensity. The proteins D1 and D2 lying at the core of the photosystem creating a heterodimer that bind the chlorophyll P680. Under photoinhibitory conditions the chlorophyll P680 play a important role in the damage of PSII. Indeed, in the acceptor side process, P680 is involved in the development of reactive form of oxygen (ROS) (Bumann and Oesterhelt, 1995b), while in the donor side photoinhibitory process itself works as strong oxidant (Mulo et al., 1998) damaging all the proteins surrounding it. Since the intimately association with D1, we can suggest that also D2 is strongly susceptible to the photodamage but, in accordance with (Koivuniemi et al., 1995); (Kale et al., 2017) it suffer a lesser extend effect.

The polypeptide CP43 is one of the chlorophyll binding protein present in the PSII core. In accordance with (Yamamoto Y. and Alasko T. 1995) during the donor side photoinhibition CP43 is also degraded. Since it is not directly involved in the electron transport of the PSII we point out the degradation of CP43 as result of its proximity to the strong oxidant present in the PSII.

The low molecular weight protein PsbT is associated with the D1/D2 heterodimer in the PSII and. In accordance with (Monod et al., 1994), PsbT is not essential for the stability and the functionality of the PSII. Conversely, it has a possible role for an efficient post- translational repair of the PSII in high light stress conditions (Ohnishi et al., 2007). Since, we have conducted an in vitro experiment, the damage observed in the experimental data was probably due to its strong association with the D1 protein.

In the Table 4.1 is showed that also two peptide of the ATP synthase subunit beta (AtpB) resulted more abundant in the high light treated sample. Since the experiment were conducted on the PSII monomer extracted from pea thylakoids, the presence of this protein is probably due to a contamination verify during the PSII extraction.

4.3.3 Short term photoinhibition *in vivo* (*Synechocystis*)

In order to better understand the mechanisms involved in the short term photoinhibition and pointing out a possible D1 photoinhibitory marker, in vivo experiments on the model organism *Synechocystis* were conducted. In *Synechocystis* three genes for the expression of D1 protein are present (psbAI, psbAII and psbAIII). In accordance to (Ravnikar et al., 1989) and (Metz et al., 1990) the coding region of psbAI and psbAIII share the 99% of nucleotide identity decoding for the same D1 isoform, while the gene psbAI, which is considered silent (Salih and Jansson, 1997), encodes for a divergent protein called D1'.

In literature (Materna et al., 2009) was already observed a strong conservation of the D1 protein among photosynthetic organisms with different evolutionary origins.

In S1 Fig. the alignment between the protein sequences of D1 from Pea plant and *Synechocystis* showed a identity of 86% was observed, highlighting how the protein D1 is strongly preserved in this two different photosynthetic organisms. *Synechocystis* was grown in a semi-continuous regime by running the flat panel photobioreactor (PBR) in turbidostat mode. In this operative conditions the cells were kept in exponential phase in a constant range of OD. Maintaining constant

the temperature of the medium, the pH and the OD of the culture it was assumed that only the light could influence the culturing. The cells were grown at $50 \mu\text{mol photons m}^{-2}\text{s}^{-1}$, the photoinhibitory state was induced growing the cells at $1460 \mu\text{mol photons m}^{-2}\text{s}^{-1}$ for one h and the recovery was evaluated by reverting the incident light intensity to $50 \mu\text{mol photons m}^{-2}\text{s}^{-1}$ for 1.30 h. The photochemical efficiency of the PSII was detected by PAM fluorescence in order to evaluate the decrease of the PSII activity over the time when the cells are grown under strong light condition and the time needed to PSII for its complete recovery.

In Fig 4.3 the PSII quantum yield was calculated as $\phi\text{PSII} = (F_M' - F_0') / F_M'$ (Van Kooten O. et al., 1990). At time 0 the initial PSII efficiency was 0.41 ± 0.012 . When the light was increased to $1460 \mu\text{mol photons, m}^{-2} \text{s}^{-1}$ (red panel) the ϕPSII sharply decreased to 0.2 ± 0.00 after only 10 minutes reaching the lowest value of 0.02 ± 0.010 after 45 minutes (0.75h) and it remains constant after 60 minutes (1h). Reverting the light intensity to $50 \mu\text{mol photons m}^{-2}\text{s}^{-1}$ (green panel), the PSII activity recovered from the photoinhibitory state increasing up to 0.16 ± 0.00 after 15 minutes (1.25 h) and almost a complete recovery (0.33 ± 0.019) was attested after 90 minutes (2.30h).

Our data suggest that the PSII activity is dramatically affected from the light and, when *Synechocystis* is grown under strong light irradiance, the PSII is completely inactivated after 45 minutes. These results are in accordance with (Mulo et al., 1997) and (Mulo et al., 1998), where the growth of *Synechocystis* under light stress condition results in a severe decrease of the PSII activity after 60 minutes and the half-time ($T_{1/2}$) of the D1 protein was attested around 30 minutes. The prompt recovery of the PSII observed by reverting the light to $50 \mu\text{mol photons m}^{-2}\text{s}^{-1}$ pointed out a prompt activation of the PSII repair mechanism aimed to substitute the damaged D1 protein in the multi-enzymatic complex with a newly synthesized form. Moreover, from our data (Fig 4.3 green panel) we can suggest that the protein synthesis and the incorporation of the newly synthesized protein in the thylakoids is activated during light recovering condition and the process continues for at least 1.30h, as observed also in (Constant et al., 2000).

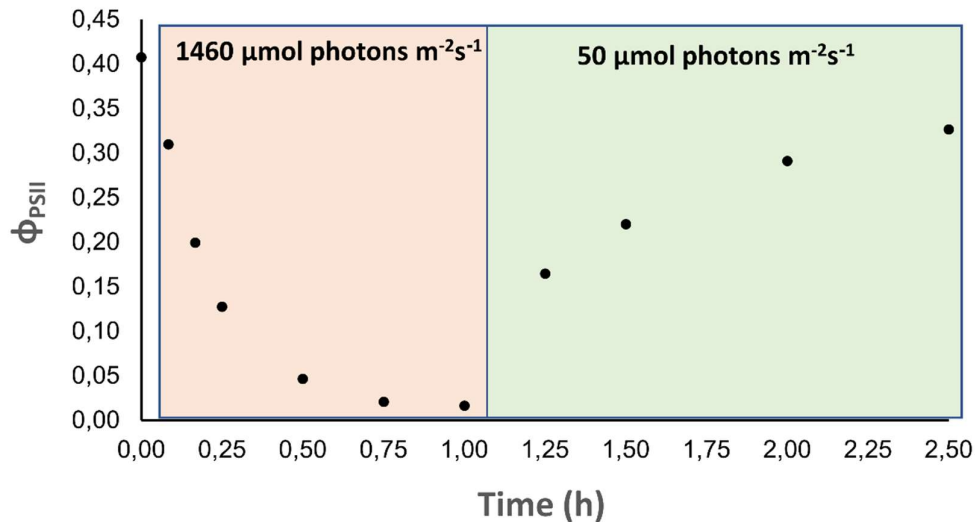


Fig 4.3 Measurement of fluorescence yield in short term photoinhibition experiment with a pulse-amplitude modulated (PAM) fluorescence in wild type *Synechocystis* sp. PCC 6803. ϕ_{PSII} , quantum yield of PSII calculated with F_o' and F_m' ($F_m' - F_o' / F_m'$). The value at time = 0 is taken growing the cells under control light of $50 \mu\text{mol photons m}^{-2} \text{s}^{-1}$. In the red square is shown the decreasing of ϕ_{PSII} value keeping the cells 1h minutes under photoinhibitory condition. In the green square are shown the value of ϕ_{PSII} during the recovery phase, growing the cells for 1.30h minutes at $50 \mu\text{mol photons m}^{-2} \text{s}^{-1}$.

In order to prevent the new synthesis of the protein D1 the protein synthesis inhibitor lincomycin was added to the *Synechocystis* culture. Under such growth conditions it was possible to observe how the suppression of the PSII repair cycle could affect the recover of *Synechocystis* from the photoinhibitory state. In figure 4.4 (red panel) is showed the decreasing of the PSII quantum yield of *Synechocystis* growth for 1h at $1460 \mu\text{mol photons m}^{-2} \text{s}^{-1}$ in presence of lincomycin. In this case the loss of activity of the PSII results sharper compared to culture without lincomycin (Fig 4.3).

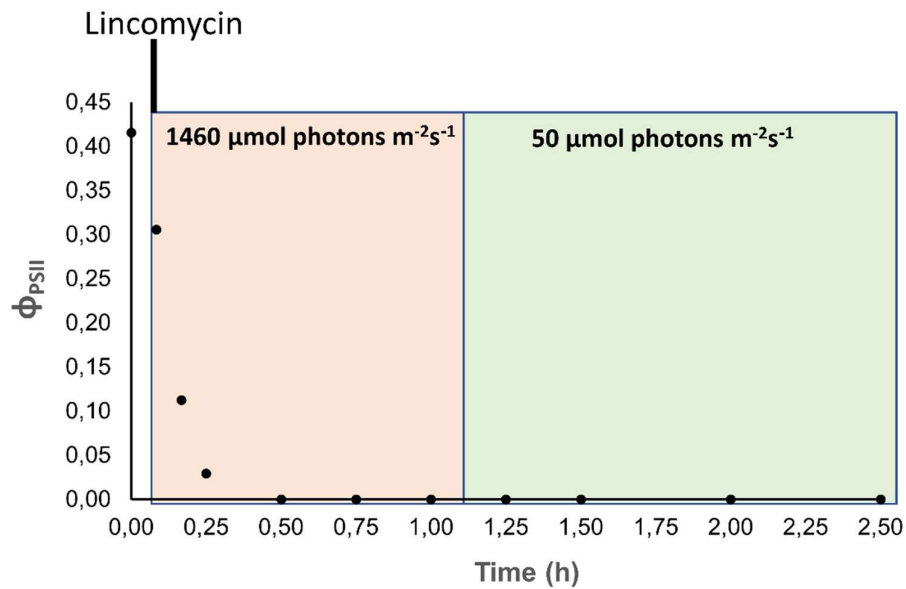


Fig 4.4 Measurement of PSII fluorescence yield in short-term photoinhibition experiment, after the addition of lincomycin, with a pulse-amplitude modulated (PAM) fluorescence in wild type *Synechocystis*. ϕ_{PSII} , quantum yield of PSII calculated with F_o' and F_m' ($F_m' - F_o' / F_m'$). The value at time = 0 is taken growing the cells under control light of $50 \mu\text{mol photons m}^{-2} \text{s}^{-1}$. Before to switch the light intensity to $1460 \mu\text{mol photons m}^{-2} \text{s}^{-1}$, $400 \mu\text{g mL}^{-1}$ of Lincomycin was added. In the red square is shown the decreasing of ϕ_{PSII} value keeping the cells 1h minutes under photoinhibitory condition. In the green square are shown the value of ϕ_{PSII} during the recovery phase, growing the cells for 1.30h minutes at $50 \mu\text{mol photons m}^{-2} \text{s}^{-1}$.

Indeed, after 15 minutes (0.25h) the PSII efficiency was decreased almost to 0 and after 30 minutes (0.50h) the total absence of the PSII activity was evidenced. Reverting the light regime to $50 \mu\text{mol photons m}^{-2} \text{s}^{-1}$, the cells were not able to recover from the photoinhibitory phase highlighting how the inhibition of the protein repair mechanism led the cells under an irreversible state of photoinhibition.

4.4 Conclusions

In this chapter we studied in deep the photo-induced fragmentation of the D1 protein and we have widen the knowledge on the short term photoinhibitory process by studying the photoinactivation of the PSII. Two typologies of experiments are conducted: i) *in vitro*, where the photoinhibition of the PSII extracted from thylakoid of pea was performed, ii) *in vivo*, where the photosynthetic microorganism model *Synechocystis* was growth in a flat panel photobioreactor.

The photoinhibition of the PSII isolated from thylakoids pea, shown that the photo-induced fragmentation of the protein D1 lead to the formation of four peptides: 23 kDa N-terminal, 10 kDa C-terminal, 17 kDa N-terminal and 16kDa C-terminal fragments. Moreover, from the proteomics analysis, we have concluded that also the surrounding D1 proteins D2, Cp43 and psbT, are damaged by the strong oxidant formed under photoinhibitory light conditions.

Growing *Synechocystis* in a fully controlled reactor system under strong light intensity and in absence of lincomycin we observed that the complete inactivation of the PSII occurs after 45 minute, ϕ_{PSII} 00.02. Conversely, a notably ability of the PSII to restore from the photinhibitory conditions was detected when *Synechocystis* was growth under light recovery regime with the almost total recover of the PSII photosynthetic efficiency in 1.30h. From this data we can conclude that a prompt activation of the PSII repair cycle occurs when the microorganism was further adapted at $50 \mu\text{mol photons m}^{-2}\text{s}^{-1}$, and it continued for at least 1.30h. The introduction of the lincomycin in the *Synechocystis* culture has highlighted how the abolishment of the PSII repair cycle can dramatically affect the ability of *Synechocystis* to cope to light stress condition.

4.6 References

- Albanese, P., Melero, R., Engel, B.D., Grinzato, A., Berto, P., Manfredi, M., Chiodoni, A., Vargas, J., Sorzano, C.Ó.S., Marengo, E., Saracco, G., Zanotti, G., Carazo, J.M., Pagliano, C., 2017. Pea PSII-LHCII supercomplexes form pairs by making connections across the stromal gap. *Sci. Rep.* 7. <https://doi.org/10.1038/s41598-017-10700-8>
- Alphen, P. Van, Hellingwerf, K.J., 2015. Sustained Circadian Rhythms in Continuous Light in *Synechocystis* sp . PCC6803 Growing in a Well-Controlled Photobioreactor. <https://doi.org/10.1371/journal.pone.0127715>
- Aro, E.M., Virgin, I., Andersson, B., 1993. Photoinhibition of Photosystem II. Inactivation, protein damage and turnover. *BBA - Bioenerg.* 1143, 113–134. [https://doi.org/10.1016/0005-2728\(93\)90134-2](https://doi.org/10.1016/0005-2728(93)90134-2)
- Bradford, M.M., 1976. A rapid and sensitive method for the quantitation of microgram quantities of protein utilizing the principle of protein-dye binding. *Anal. Biochem.* 72, 248–254. [https://doi.org/10.1016/0003-2697\(76\)90527-3](https://doi.org/10.1016/0003-2697(76)90527-3)
- Bumann, D., Oesterhelt, D., 1995. Destruction of a single chlorophyll is correlated with the photoinhibition of photosystem II with a transiently inactive donor side. *Proc. Natl. Acad. Sci. U. S. A.* 92, 12195–12199. <https://doi.org/10.1073/pnas.92.26.12195>
- Constant, S., Eisenberg-Domovitch, Y., Ohad, I., Kirilovsky, D., 2000. Recovery of photosystem II activity in photoinhibited *Synechocystis* cells: Light-dependent translation activity is required besides light-independent synthesis of the D1 protein. *Biochemistry* 39, 2032–2041. <https://doi.org/10.1021/bi9914154>
- De Las Rivas, J., Andersson, B., Barber, J., 1992. Two sites of primary degradation of the D1-protein induced by acceptor or donor side photo-inhibition in photosystem II core complexes. *FEBS Lett.* 301, 246–252. [https://doi.org/10.1016/0014-5793\(92\)80250-K](https://doi.org/10.1016/0014-5793(92)80250-K)
- Friso, G., Giacometti, G.M., Barber, J., Barbato, R., 1993. Evidence for concurrent donor and acceptor side photoinduced degradation of the D1-protein in isolated reaction centres of Photosystem II. *BBA - Bioenerg.* 1144, 265–270. [https://doi.org/10.1016/0005-2728\(93\)90110-2](https://doi.org/10.1016/0005-2728(93)90110-2)
- Gillet, L.C., Navarro, P., Tate, S., Röst, H., Selevsek, N., Reiter, L., Bonner, R., Aebersold, R., 2012. Targeted Data Extraction of the MS/MS Spectra Generated by Data-independent Acquisition: A New Concept for Consistent and Accurate Proteome Analysis. *Mol. Cell. Proteomics* 11, O111.016717. <https://doi.org/10.1074/mcp.O111.016717>
- Goh, C.H., Ko, S.M., Koh, S., Kim, Y.J., Bae, H.J., 2012. Photosynthesis and Environments: Photoinhibition and Repair Mechanisms in Plants. *J. Plant*

- Biol. 55, 93–101. <https://doi.org/10.1007/s12374-011-9195-2>
- Guo, X., Kristal, B.S., 2012. The use of underloaded C18 solid-phase extraction plates increases reproducibility of analysis of tryptic peptides from unfractionated human plasma. *Anal. Biochem.* 426, 86–90. <https://doi.org/10.1016/j.ab.2012.04.003>
- Kale, R., Hebert, A.E., Frankel, L.K., Sallans, L., Bricker, T.M., Pospíšil, P., 2017. Amino acid oxidation of the D1 and D2 proteins by oxygen radicals during photoinhibition of Photosystem II. *Proc. Natl. Acad. Sci.* 114, 2988–2993. <https://doi.org/10.1073/pnas.1618922114>
- Kettunen, R., Tyystjärvi, E., Aro, E.-M., 1996. Degradation pattern of photosystem II reaction center protein D1 in intact leaves. *Plant Physiol.* 111, 1183–1190. <https://doi.org/10.1104/pp.111.4.1183>
- Koivuniemi, A., Aro, E.-M., Andersson, B., 1995. Degradation of the D1-and D2-Proteins of Photosystem II in Higher Plants Is Regulated by Reversible Phosphorylation. *Biochemistry* 34, 16022–16029.
- LAEMMLI, U.K., 1970. Cleavage of Structural Proteins during the Assembly of the Head of Bacteriophage T4. *Nature* 227, 680–685. <https://doi.org/10.1038/227680a0>
- Materna, A.C., Sturm, S., Kroth, P.G., Lavaud, J., 2009. First induced plastid genome mutations in an alga with secondary plastids: psbA mutations in the diatom *Phaeodactylum tricorutum* (bacillariophyceae) reveal consequences on the regulation of photosynthesis I. *J. Phycol.* 45, 838–846. <https://doi.org/10.1111/j.1529-8817.2009.00711.x>
- Metz, J., Nixon, P., Diner, B., 1990. Nucleotide sequence of the psbA3 gene from the cyanobacterium *Synechocystis* PCC 6803. *Nucleic Acids Res.* 18, 6715.
- Monod, C., Takahashi, Y., Goldschmidt-Clermont, M., Rochaix, J.D., 1994. The chloroplast ycf8 open reading frame encodes a photosystem II polypeptide which maintains photosynthetic activity under adverse growth conditions. *EMBO J.* 13, 2747–54.
- Mulo, P., Laakso, S., Mäenpää, P., Aro, E.-M., 1998. Stepwise Photoinhibition of Photosystem II. *Plant Physiol.* 117, 483–490. <https://doi.org/10.1104/pp.117.2.483>
- Mulo, P., Tyystjärvi, T., Tyystjärvi, E., Govindjee, Mäenpää, P., Aro, E.M., 1997. Mutagenesis of the D-E loop of photosystem II reaction centre protein D1. Function and assembly of photosystem II. *Plant Mol. Biol.* 33, 1059–1071. <https://doi.org/10.1023/A:1005765305956>
- Murata, N., Takahashi, S., Nishiyama, Y., Allakhverdiev, S.I., 2007. Photoinhibition of photosystem II under environmental stress. *Biochim. Biophys. Acta - Bioenerg.* 1767, 414–421. <https://doi.org/10.1016/j.bbabi.2006.11.019>

- Nedbal, L., Trtílek, M., Červený, J., Komárek, O., Pakrasi, H.B., 2008. A photobioreactor system for precision cultivation of photoautotrophic microorganisms and for high-content analysis of suspension dynamics. *Biotechnol. Bioeng.* 100, 902–910. <https://doi.org/10.1002/bit.21833>
- Ohnishi, N., Kashino, Y., Satoh, K., Ozawa, S.I., Takahashi, Y., 2007. Chloroplast-encoded polypeptide PsbT is involved in the repair of primary electron acceptor QA of photosystem II during photoinhibition in *Chlamydomonas reinhardtii*. *J. Biol. Chem.* 282, 7107–7115. <https://doi.org/10.1074/jbc.M606763200>
- Ravnikar, P.D., Sevnck, R., debus, J., Saetaert, P., McIntosh, L., 1989. Nucleotide sequence of a second psbA gene from the unicellular cyanobacterium *Synechocystis* 6803. *Nucleic Acids Res.* 17, 3991. <https://doi.org/10.1093/nar/17.10.3991>
- Salih, G.F., Jansson, C., 1997. Activation of the silent psbA1 gene in the cyanobacterium *Synechocystis* sp strain 6803 produces a novel and functional D1 protein. *Plant Cell* 9, 869–878. <https://doi.org/10.1105/tpc.9.6.869>
- Shevchenko, A., Wilm, M., Vorm, O., Mann, M., 1996. Mass spectrometric sequencing of proteins from silver-stained polyacrylamide gels. *Anal. Chem.* 68, 850–858. <https://doi.org/10.1021/ac950914h>
- Shipton, C.A., Barber, J., 1991. Photoinduced degradation of the D1 polypeptide in isolated reaction centers of photosystem II: evidence for an autoproteolytic process triggered by the oxidizing side of the photosystem. *Proc. Natl. Acad. Sci. U. S. A.* 88, 6691–6695. <https://doi.org/10.1073/pnas.88.15.6691>
- Triantaphylidès, C., Havaux, M., 2009. Singlet oxygen in plants: production, detoxification and signaling. *Trends Plant Sci.* 14, 219–228. <https://doi.org/10.1016/j.tplants.2009.01.008>
- Tyystjärvi, E., 2013. Photoinhibition of Photosystem II*. *Int. Rev. Cell Mol. Biol.* 300, 243–303. <https://doi.org/10.1016/B978-0-12-405210-9.00007-2>
- Tyystjärvi, E., 2008. Photoinhibition of Photosystem II and photodamage of the oxygen evolving manganese cluster. *Coord. Chem. Rev.* 252, 361–376. <https://doi.org/10.1016/j.ccr.2007.08.021>
- Tyystjärvi, E., Aro, E.M., 1996. The rate constant of photoinhibition, measured in lincomycin-treated leaves, is directly proportional to light intensity. *Proc. Natl. Acad. Sci. U. S. A.* 93, 2213–2218. <https://doi.org/10.1073/pnas.93.5.2213>
- Vass, I., Styring, S., Hundal, T., Koivuniemi, a, Aro, E., Andersson, B., 1992. Reversible and irreversible intermediates during photoinhibition of photosystem II: stable reduced QA species promote chlorophyll triplet formation. *Proc. Natl. Acad. Sci. U. S. A.* 89, 1408–1412. <https://doi.org/10.1073/pnas.89.4.1408>
- Whitmarsh, J., Govindjee, M., 2002. Photosystem II. *En cycl. Life Sci.* 6, 1–13.

<https://doi.org/10.1002/9780470015902.a0022548>

Zavafer, A., Cheah, M.H., Hillier, W., Chow, W.S., Takahashi, S., 2015. Photodamage to the oxygen evolving complex of photosystem II by visible light. *Sci. Rep.* 5, 16363. <https://doi.org/10.1038/srep163>

4.7 Supporting information

Score	Expect	Method	Identities	Positives	Gaps
632 bits(1631)	0.0	Compositional matrix adjust.	295/344(86%)	326/344(94%)	0/344(0%)
Syne	1	MTAILERRDSENLWGRFCNWIITSTENRLYIGWFGVLMIPITLLTATSVFIIAFIAAPPVDI			60
Pea	1	MT L++R+S +LW +FC W+IST NR+Y+GWFG LMIPTLLTAT+ FIIAFIAAPPVDI			60
Syne	61	DGIREPVSGLLYGNIIISGAIIPISAAIGLHFYPIWEAASVDEWLYNGGPLYELIVLHFL			120
Pea	61	DGIREPV+GSLLYGNIIISGA++P+S AIGLHFYPIWEAAS+DEWLYNGGPLY+L+V HFL			120
Syne	121	LGVACYMGREWELSFRLGMRPWIAVAYSAPVAAATAVFLIYPIGQGSFSDGMPLGISGTF			180
Pea	121	+G+ CYMGR+WELS+RLGMRPWI VAYSAPV+AAATAVFLIYPIGQGSFSDGMPLGISGTF			180
Syne	181	NFMIVFQAEHNILMHPFHMLGVAGVFGGSLFSAMHGSLVTSSSLIRETTENESANEGYRFG			240
Pea	181	NFMIVFQAEHNILMHPFHMLGVAGVFGGSLFSAMHGSLVTSSSLVRETTEVESQNYGYKFG			240
Syne	241	QEEETYNIVAAHGYFGRLIFQYASFNNSRSLHFFLAANPVGIVWFTALGISTMAFNLNGF			300
Pea	241	QEEETYNIVAAHGYFGRLIFQYASFNNSRSLHFFL ANPV+GIWFTA+G+STMAFNLNGF			300
Syne	301	NFNQSVVDSQGRVINTWADIINRANLGMVEMHERNAHNFPDLA		344	
Pea	301	NFNQSVVDSQGRVINTWADIINRANLGMVEMHERNAHNFPDLA		344	

S1 Fig Alignment of D1 protein sequences from Pea plant (Pea) and Synchocystis (Syne)

Chapter 5

Conclusions

The increased demand of energy occurred in the last decades has promote an always more exploitation of the fossil fuels with dramatic consequences for the climatic changes. Even though, different studies has provided that the photosynthetic microorganisms such as *Synechocystis* (Angermayr et al., 2015) can be used to recycle the CO₂ into energy carriers and chemicals by the exploitation of the abundant energy provided by the sun, our current economy still rely in the fossil reserves. This is mainly due to two reasons: i) the current biocatalysts (i.e. engineered photosynthetic microorganisms) are still not optimized for a competitive production compared to the amount of product obtained from fossil reserves, ii) the photobioreactors are not yet optimized for their fully efficient growth of the photosynthetic microorganisms such *Synechocystis*. The main disadvantages of the photobioreactors concern the inadequate systems for a suitable use of the light needed to the microorganisms to grow. Indeed, one of the primary problem is due to the low light penetration of the inside the reactor while, the excess of the light provided to the reactors induce the photosynthetic microorganisms in photoinhibitions. This project aimed to improve our knowledge on the photoinhibitory process that occur in *Synechocystis* when is grown under light stress conditions. Our results can be considerate a starting point for making more productive the growth of *Synechocystis* in photobioreactors.

In this thesis we have looked into the influence of the different light distribution inside the PBR at increased light irradiance on *Synechocystis* photosynthetic efficiency [chapter 2]. In order to correlate the effect of the photoinhibition and the *Synechocystis* growth in PBR, quantitative mass spectrometry analysis was performed, comparing the proteome of thylakoids extracted from cells grown under control light and photoinhibitory light regimes [chapter 3]. Finally, a preliminary study on the effect of the short term photoinhibition on the protein D1 of the PSII, both in vitro and in vivo experimental set up [chapter 4].

Here, the conclusions of the different chapters will be summarized in order to give an overview of the project.

The project started up with the study of the local light distribution inside the vessel at increased incident light intensity to better understand how it can affect the growth rate and the morphology of *Synechocystis* [chapter 2]. The physiological state of *Synechocystis* was monitored under increasing intensity of orange-red light ranging between 50-1460 $\mu\text{mol photons m}^{-2} \text{s}^{-1}$. We found that the growth rate, the PSII activity and the cell size are clearly affected, although in slightly different ways, by the light provided to the PBR. The maximum growth rate and amount of oxygen dissolved in the medium of $0.117 \pm 0.006 \text{ h}^{-1}$ and 2.56 ± 0.12 , respectively.

Synechocystis showed to be resistant to light stress condition until $800 \mu\text{mol photons m}^{-2} \text{ s}^{-1}$ achieving the maximal state of photoinhibition at $1460 \mu\text{mol photons m}^{-2}\text{s}^{-1}$. *Synechocystis* showed a prompt recover by reverting the light to lower intensity. Since the notable plasticity of *Synechocystis* observed in response of the light changes, we studied features of the PBR lightening conditions not experimentally detectable which could affect the *Synechocystis* behaviour.

Thus, we have reproduced a PBR model where the effects of increasing incident light intensities on the local light distribution within the vessel was investigated. From the analysis resulted that the coexistences of lower and higher local light area inside the vessel are controllable by tuning the incident light intensity. The iridescence of the light can be increased to improve the *Synechocystis* growth rate and the PSII efficiency as far as the cells have the opportunity to make experience of lower and higher local light area, preventing the photoinhibitory state. Despite our consideration are based on experiments and simulation concerning the turbidostat mode, this result suggest that the PBR design should considering the management of local light inhomogeneity to prevent the photoinhibition phenomena.

Then we focused our study on the long term photoinhibitory process [chapter 3]. *Synechocystis* was grown in PBR in turbidostat mode and adapted to different intensity of orange-red light for 24 h. The constant decrease of *Synechocystis* growth rate at the light irradiance of 800, 950 and $1460 \mu\text{mol photons m}^{-2} \text{ s}^{-1}$ was investigated by the mass spectrometry analysis comparing the proteome of thylakoids extracted from cells grown under control light ($50 \mu\text{mol photons m}^{-2} \text{ s}^{-1}$) and photoinhibitory light regimes. Our data shown a high sensitivity of the PSII to the high light. Indeed, the strong down regulation of the proteins PsbO, PsbU and PsbV suggest a possible impairment of the OEC system due to the progressive increment of the ROS species. Conversely, the up regulation of the other protein forming PSII, among which the main photoinhibitory target D1, clearly show an accelerated metabolism of the microorganism for replacing the damaged PSII core proteins. The down regulation of most of the subunits present in the PSI was attributed to the physiological decrease of the PSI amount observed in several photoautotrophic organisms under light stress. Conversely, the over expression of the PSI subunits PsaA/B, PsaK2, PsaL and the Slr128 protein, was suggest to be necessary for protecting the PSI functionality when the cells were cultured under photoinhibitory condition. Furthermore, the higher presences of polypeptides involved in both NPQ and enzymatic mechanisms of defences (SODs) combined with the up regulation of the proteins involved in the cyclic electron flow around

the PSI (NDH-1, Cytb6f and ATPase) clearly show the ability of *Synechocystis* to use different strategies to preserve the functionality of the photosynthetic apparatus. Moreover the higher presence of the ribosomal proteins and the ribosomal associated proteins in the cells growth under photoinhibitory condition is barely indicative of an increased protein biosynthesis needed to *Synechocystis* for a prompt PSII repair.

This work was then concluded with a preliminary studies on the PSII photodamage in short time photoinhibition[chapter 4].

From our it was observed that a strong light treatment for 1h in vitro of the PSII lead to photodegradation of the D1 protein. The fragmentation of D1 in 23 kDa N-terminal , 10 kDa C-terminal, 17 kDa N-terminal and 16kDa C-terminal fragments was observed by western blot analysis performed on light and dark adapted samples. Despite the evidence of the protein degradation, from mass spectrometry analysis, it was not possible to determine the aminoacidic sequences of the D1 fragments. Moreover, it was pointed out how the photo-oxidative stress of the PSII lead also to the photodamage of other proteins present in the multi-enzymatic complex core as : D2, Cp43 and psbT. The further, growth of *Synechocystis* in a fully controlled reactor system get us more information about the effect of the short term photoinhibition in vivo. The exploitation of the PAM system was used for monitoring the photosynthetic efficiency of the PSII. After 45 minutes of treatment under high light condition ($1460\mu\text{mol photons m}^{-2}\text{s}^{-1}$) almost a total inactivation of the multi-enzymatic complex was observed with a ϕPSII drop to 0. Taken together this data pointing out how the strong susceptibility of the D1 protein to the high light can affect the PSII activity. On the other side, when light provided to *Synechocystis* was reverted to $50\mu\text{mol photon}$ the photosynthetic efficiency of the PSII show a total recover in 1.30 h. Conversely, in presence of the lincomycin protein synthesis inhibitor the photosynthetic efficiency of the PSII did not show any recover. This result suggests a key role of the D1 repair cycle to cope the photoinhibitory condition and for a prompt reactivation of the PSII.

5.1 Future plan

In this work I have faced three different topics aimed to study the influences of the light intensity on the photoinhibitory process of the cyanobacterium *Synechocystis*. The research presented has risen some interesting question which can be used for program future interesting works.

In chapter 2 it was suggested that a different distribution of the light inside the vessel could lead to some benefit in the growth of *Synechocystis* in turbidostat mode.

In order better investigate the effective light experiences of the cells inside the reactor energized with different intensity of light, a further work on the cells particle tracking can be carried on.

Indeed, beside the growth rate, the oxygen dissolved in the medium and the dry weight, further experimental data could be performed on the study of the fluid dynamic within the vessel. The evaluation of the turbulence inside the reactor related to the different light distribution observed in this study could be used for evaluating the effective amount of light experienced by *Synechocystis* during the time. Moreover, by the experimental detection of the I_{out} beside the I_{in} values, growth rate, and dry weight values could be used to calculate experimentally the photosynthetic efficiency of *Synechocystis* growth under different light incident condition as calculated in Shurmans et al., 2015.

In chapter 4 a preliminary study of the effect of the strong light on the PSII activity and the D1 turnover was done. This work will be further investigated by performing mass spectrometry analysis of the cells growth in both absence and presence of lincomycin. In the first case the thylakoids proteome of the samples harvested at time 0, the cells growth at $1460 \mu\text{mol photons m}^{-2}\text{s}^{-1}$ for 15 minutes (maximum slope in the photoinhibition curve), and 60 minutes (maximum state of photoinhibition) will be compared. The proteomic differences amongst samples will be related to the photosynthetic efficiency revealed by PAM. In this way it will be possible to better understand the protective processes that take place during the short term photoinhibition. On the other hand, comparing the thylakoid proteome of cells harvested at time 0, 60 minutes (maximum state of photoinhibition), 90 minutes (maximum slope in the recovery curve) and 150 minute we can get insight in the physiological process which lead the PSII to recover at its maximal efficiency.

Conversely, the quantitative mass spectrometry analysis on the cells thylakoids proteome treated with lincomycin could be really valuable to point out the fragmentation pattern of the D1 photodamaged, which was just hypnotized from previous works (Kettunen et al., 1996).

The identification of one or more fragment sequences of the photodamage D1 could be used as biochemical photoinhibitory marker to follow the state of degradation of the protein at different light conditions.

Overall, in this work several interesting new results on the behaviour of *Synechocystis* growth under light stress conditions have been found. The influence of the increased light regimes observed on the cells morphology and growth rate related to the different light distribution inside the reactor and the deep study of the cells thylakoids proteome can be an extremely useful base for improving the photosynthetic microorganisms growth in PBR systems. Moreover, our results provide useful insights for a future photobioreactor design which better exploit the light request of the microorganisms.

Acknowledgment

Dopo un percorso così lungo è sempre difficile fare i ringraziamenti, semplicemente perché le persone da ringraziare sono tante, e tu sai benissimo che alla fine non c'è qualcuno più importante di qualcun'altro. Tutti in qualche modo hanno contribuito al tuo accrescimento sia professionale che umano.

Da qualche parte però bisogna pure iniziare, perciò inizierei a ringraziare tutto il gruppo DISAT e il Biosolar Lab per il supporto ottenuto durante il mio dottorato.

Nello specifico vorrei ringraziare il Prof. Pirone per il suo sostegno nei vari momenti complicati e cruciali che si sono presentati nell'arco di questi anni risultando sempre una persona di riferimento.

Vorrei ringraziare la Dr. Cristina Pagliano (in realtà dovrei spendere pagine intere per ringraziarti ma spero che queste poche righe possano bastare). Ti ringrazio perché mi hai introdotto in un campo scientifico totalmente nuovo per me dandomi gli strumenti per poterci lavorare in modo competente. Ti ringrazio perché nei vari momenti difficili della vita da laboratorio e anche quando i risultati faticavano ad arrivare hai sempre avuto una parola di conforto e un ottimismo che spesso è risultato fondamentale. Anche se negli anni possiamo avere avuto confronti o delle discussioni ho sempre considerato questi momenti come spunti per una mia crescita personale oltre che professionale.

Vorrei ringraziare Pascal Ablanese per essere stato uno straordinario collega al Biosolar Lab, sempre fonte di saggi e utili consigli. Ringrazio di cuore anche Niccolò Vasile per il lavoro svolto e il suo enorme contributo nel raggiungere importanti risultati presenti in questa tesi e Angela Re per la sua supervisione nella stesura di tali risultati.

Inoltre, vorrei ringraziare l'ISALIT e nello specifico Marcello Manfredi per suo grande supporto e lavoro fatto durante la nostra collaborazione.

Continuerei i miei ringraziamenti esprimendo la mia enorme gratitudine a tutto il SILS group dell'università di Amsterdam.

In particolare vorrei ringraziare il Prof. Klaas Hellingwerf per avermi accolto nel suo gruppo di ricerca, interessandosi al mio progetto e dandomi validi consigli non solo durante la mia permanenza ad Amsterdam ma anche nei mesi successivi.

Vorrei ringraziare il Prof. Filipe Branco dos Santos per la sua estrema disponibilità e per la sua capacità di dare nuovi stimoli e idee riguardanti il mio lavoro.

Ringrazio enormemente Pascal Van Alphen per la sua enorme pazienza nel seguire il mio lavoro per un anno intero. Ti sei sempre dimostrato un modello da seguire come ricercatore e un amico al di fuori del laboratorio.

Un ringraziamento a Mara che con la sua gentilezza si è sempre dimostrata una valida amica.

Ringrazio inoltre Davide e Federico per aver trovato in loro due validi compagni sempre disponibili e sinceri con cui condividere tante esperienze e affrontare valide discussioni.

Un ringraziamento SPECIALE a PARSÀ che si è dimostrato più di un amico, ma un vero e proprio fratello durante la mia permanenza in Olanda.

Un secondo ringraziamento SPECIALE ad Andrea, il fratellino più piccolo oltre che compagno di tante avventure sia in Olanda che in Italia.

Un terzo ringraziamento SPECIALE a Valentina, con la quale ormai condivido una stima e un'amicizia profonda che ci lega da tanti anni e che per me è sempre grande fonte d'ispirazione e orgoglio.

Un ringraziamento super speciale a Beatrice, la mia sorellina all'interno del politecnico, la tua positività e la tua saggezza mi sono sempre stati di enorme conforto la tua volontà un esempio da seguire.

Un grandissimo ringraziamento alla mia famiglia e a mia mamma che con i suoi insegnamenti e i suoi sacrifici mi ha reso l'uomo che sono.

In fine, ma sicuramente non per ordine di importanza, un ringraziamento al Prof. Guido Saracco. L'ho lasciata per ultimo perchè in realtà dovrei ringraziarla per veramente così tante cose che non saprei da dove iniziare.

La ringrazio per aver creduto in me, come persona e come ricercatore, dandomi l'opportunità di lavorare nel suo gruppo di ricerca. La ringrazio perchè mi ha dato la possibilità di accrescere le mie competenze professionali, permettendomi di svolgere un periodo di attività all'estero. La ringrazio perchè nonostante i suoi numerosi impegni ha sempre trovato del tempo da dedicarmi o un consiglio da darmi.